Dipl.-Ing. Judith Radebner, BSc

Germanium and Tin Based Photoinitiators

DISSERTATION

zur Erlangung des akademischen Grades

Doktorin der technischen Wissenschaften

eingereicht an der

Technischen Universität Graz

Betreuer

Ao. Univ. Prof. Dipl.-Ing. Dr. techn. Harald Stüger

Institut für Anorganische Chemie

Fakultät für Technische Chemie, Verfahrenstechnik und Biotechnologie

Graz, März 2018

EIDESSTATTLICHE ERKLÄRUNG

Ich erkläre an Eides statt, dass ich die vorliegende Arbeit selbstständig verfasst, andere als die angegebenen Quellen/Hilfsmittel nicht benutzt, und die den benutzten Quellen wörtlich und inhaltlich entnommenen Stellen als solche kenntlich gemacht habe. Das in TUGRAZonline hochgeladene Textdokument ist mit der vorliegenden Dissertation identisch.

Datum

Unterschrift

Oma und Opa, in Erinnerung gewidmet

Remember to look up at the stars
and not down at your feet.Try to
make sense to what you see and
wonder about what makes the
universe exist. Be curious. And
however difficult life may seem,
there is always something you can
do and succeed at.

It matters that you don’t just give up.

(Stephen Hawking)

DANKSAGUNG

Allen voran gilt mein Dank meinem Betreuer, Herrn Professor Harald Stüger, für die interessante Aufgabenstellung und Betreuung während meiner Zeit am Institut.

Meinen Bachelorstudenten möchte ich hiermit für ihre Mithilfe und ihr Engagement danken. Dado, Marlene, Nina, Paul, Tanja und Thomas ihr habt dafür gesorgt, dass ich immer gerne an die Zeit am Institut zurückdenken werde.

Ich bedanke mich auch bei dir Janine für deine tatkräftige Unterstützung im Labor am Beginn meiner Dissertation, ebenso wie bei Markus, dass du mich auch am Ende noch großartig unterstützt hast.

Danken möchte ich auch der Arbeitsgruppe, Lukas, Michael S., Thomas und Viktor für die Zusammenarbeit, die lustigen Mittagspausen und die ehrliche und lockere Atmosphäre im Labor.

Für die Aufklärung der unzähligen Kristallstrukturen möchte ich mich bei Frau Dr. Ana Torvisco Gomez und Herrn Professor Roland Fischer bedanken.

Michi H. und Mario, ich freue mich, dass wir als Trio im und fernab vom Labor über Acylgermane philosophieren konnten. Auch wenn ihr in Australien und Amerika seid, danke ich euch für eure fachliche und mentale Unterstützung fortwährend meiner Zeit hier am Institut.

Liebe Resi, ich danke auch dir, dass du so eine gute Seele bist und immer ein offenes Ohr für mich hattest.

Nicht nur in Zeiten, wo die Motivation auf sich warten ließ, warst du immer wieder eine gesuchte Stütze hier an der Uni, liebe Indira (und mittlerweile auch dein kleiner Sonnenschein Sara), ich danke dir, dass du immer zu mir gehalten hast und du mir durch Sara auch gezeigt hast, wie relativ die Sorgen des Laboralltags sind, wenn ich bei euch zu Besuch war.

Ich möchte mich auch bei Philipp, Flo und den anderen Trainingsbuddies bedanken. Der Tag an der Uni konnte noch so lange sein, aber mit euch konnte ich mich immer wieder zu neuen Leistungen pushen und vor allem die Gedanken an missglückte Synthesen hinter mir lassen.

Dominik, ich denke du kennst deinen Beitrag zum Entstehen dieser Arbeit. Ich danke dir so sehr für deine unbeugsame Geduld mir zuzuhören und deine Unterstützung in allen Lebenslagen. Auch wenn hin und wieder Zweifel auftraten, konntest du mich überzeugen, den Blick auf das Wesentlich nicht zu verlieren.

Mein größter Dank gilt meinen Eltern, die mir die Freiheit und Möglichkeit gaben dieses Studium zu beginnen. Ich danke euch für das Vertrauen und die Geduld, mit der ihr mich fortwährend unterstützt. Ebenso danke ich meiner Schwester, dass du immer wieder die richtigen Worte im richtigen Moment findest.

ABSTRACT

In the last decades the demand and application of high performance photochemically produced polymers has been immensely growing. Nowadays, their use is no longer restricted to the manufacture of micro-electronic devices, coatings, adhesives, inks, printing plates, optical waveguides but also emerges fields of medicine (dental filling materials, artificial tissue, heart valves etc.) and fabrication of 3D objects. The design and synthesis of photoinitiators (PIs) are challenging, since they have to be tailored to fulfill specific requirements. Among promising PI systems, mono- and bisacylgermanes have become interesting radical precursors generating acyl- and germyl-centered radicals upon irradiation, which add very rapidly to double bonds of various monomers. Compared to frequently applied phosphorus-based PIs, they offer the advantage of significantly red-shifted absorption bands and reduced toxicity.

Commercially available Ge-based photoinitiators, such as bis(4-methoxybenzoyl)diethylgermane (Ivocerin), evolved in the last couple of years as advantageous PI for dental composites. However, Ivocerin still suffers from inefficient curing depth at wavelengths >500 nm. Additionally, it is prepared via a tedious multi-step procedure (Corey-Seebach Umpolung) and the related purification steps cause Ivocerin to be a high-priced compound.

In this respect, we were able to develop a facile one-pot synthesis towards the long sought-after tetra-substituted acylgermanes, completing the spectrum from mono-to tetraacylgermanes. The robust synthetic protocol allowed the preparation of various differently substituted tetraacylgermanes.

In close collaboration with Prof. Gescheidt we investigated the PI properties of tetraacylgermanes by time-resolved EPR measurements, chemically induced dynamic nuclear polarization (CIDNP) spectroscopy, laser-flash photolysis (LFP) and steady-state photolysis (SSP)

The performance of tetraacylgermanes as radical source was tested by the preparation of dental composites and methacrylate resins in cooperation with Prof. Moszner.

As tetraacylgermanes carry the highest number of photo-cleavable bonds per molecule, we examined the possibility of multiple-photocleavage. These experiments were conducted in collaboration with Prof. Barner-Kowollik.

Besides of these results, we were able to extend the scope of the established reaction sequence to prepare and isolate for the first time tetraacylstannanes, which are unexpectedly stable under ambient conditions.

KURZZUSAMMENFASSUNG

In den letzten Jahrzehnten hat die Nachfrage und Anwendung von photochemisch hergestellten Polymeren mit hoher Leistung immens zugenommen. Heute beschränkt sich ihr Einsatz nicht mehr ausschließlich auf die Herstellung von mikroelektronischen Geräten, Beschichtungen, Klebstoffen, Tinten, Druckplatten, Lichtwellenleitern, sondern auch auf Gebiete der Medizin (Zahnfüllungsmaterialien, künstliche Gewebe, Herzklappen etc.) und der Herstellung von 3D-Objekten. Das Design und die Synthese von Photoinitiatoren (PIn) sind eine Herausforderung, da sie auf spezifische Anforderungen zugeschnitten sein müssen. Unter den vielversprechenden PI-Systemen sind Mono- und Bisacylgermane zu interessanten Radikalvorläufern geworden, die bei Bestrahlung Acyl- und Germyl-zentrierte Radikale erzeugen, die sich sehr schnell an Doppelbindungen verschiedener Monomere addieren. Im Vergleich zu den häufig verwendeten phosphorbasierten PIn bieten sie den Vorteil von deutlich rotlichtverschobenen Absorptionsbanden und reduzierter Toxizität.

Kommerziell erhältliche Ge-basierte Photoinitiatoren, wie Bis(4-methoxybenzoyl)diethylgerman (Ivocerin), entwickelten sich in den letzten Jahren als vorteilhafter PI für Dentalkomposite. Ivocerin weist jedoch immer noch ineffiziente Durchhärtungstiefen bei Wellenlängen > 500 nm auf. Zusätzlich basiert die Synthese auf einem langwierigen mehrstufigen Verfahren (Corey-Seebach-Umpolung). Die damit verbundenen Reinigungsschritte führen dazu, dass Ivocerin eine hochpreisige Chemikalie ist.

In diesem Zusammenhang konnten wir eine einfache Eintopfsynthese hin zu den lang angestrebten tetrasubstituierten Acylgermanen entwickeln, die das Spektrum von Mono- bis Tetraacylgermanen vervollständigen. Das robuste Syntheseprotokoll erlaubte die Herstellung verschiedener, unterschiedlich substituierter Tetraacylgermane.

In enger Zusammenarbeit mit Prof. Gescheidt untersuchten wir die PI-Eigenschaften von Tetraacylgermanen durch zeitaufgelöste EPR-Messungen, chemisch induzierte dynamische Kernpolarisations- (CIDNP) –Spektroskopie, Laser-Flash-Photolyse (LFP) und Steady-State Photolyse (SSP). Die Leistungsfähigkeit von Tetraacylgermanen als Radikalquelle wurde in Zusammenarbeit mit Prof. Moszner durch die Herstellung von Dentalkompositen und Methacrylatharzen getestet. Da Tetraacylgermane die höchste Anzahl an photospaltbaren Bindungen pro Molekül tragen, untersuchten wir die Möglichkeit einer Mehrfachspaltung. Diese Experimente wurden in Zusammenarbeit mit Prof. Barner-Kowollik durchgeführt.

Neben diesen Ergebnissen konnten wir die entwickelte Synthese ausweiten, um erstmals Tetraacylstannane herzustellen, die unter Umgebungsbedingungen unerwartet stabil sind.

TABLE OF CONTENTS

ABSTRACT I

KURZZUSAMMENFASSUNG II

TABLE OF CONTENTS III

1 INTRODUCTION 1

2 LITERATURE OVERVIEW 3

2.1 Acylgermanes 3
2.1.1 Introduction 3
2.1.2 Synthesis of Acylgermanes 4
2.1.3 Spectroscopic Properties of Acylgermanes 7
2.1.4 Reactivity of Acylgermanes 8
2.1.5 Acylgermanes as photoinitiators 8

2.2 Acylstannanes 13
2.2.1 Introduction 13
2.2.2 Synthesis of Acylstannanes 13
2.2.3 Spectroscopic Properties of Acylstannanes 14
2.2.4 Reactivity of Acylstannanes 16
2.2.5 Acylstannanes as photoinitiators 16

2.3 References 17

3 PUBLICATIONS 19

3.1 Tetraacylgermanes: Highly Efficient Photoinitiators for Visible-Light-Induced Free-Radical Polymerization 20
3.1.1 Abstract 20
3.1.2 Introduction 21
3.1.3 Results and Discussion 21
3.1.4 Conclusion 29
3.1.5 Experimental Section 29
3.1.6 References 36

3.2 Synthesis, Spectroscopic Behavior, and Photoinduced Reactivity of Tetraacylgermanes 38
3.2.1 Abstract 38
3.2.2 Introduction 39
3.2.3 Results and Discussion 41
3.2.4 Conclusion 49
3.2.5 Experimental Section 49
3.2.6 References 56

3.3 From Mono- to Tetraacylgermanes: Extending the Scope of Visible Light Photoinitiators 58
3.3.1 Abstract 58
3.3.2 Introduction 59
3.3.3 Results and Discussion 60
3.3.4 Conclusion 72

3.3.5 Experimental Section 73
3.3.6 References 76

3.4 Tetraacylgermanes as Highly Efficient Photoinitiators for Visible Light Cured Dimethacrylate Resins and Dental Composites 77
3.4.1 Abstract 77
3.4.2 Introduction 78
3.4.3 Results and Discussion 80
3.4.4 Conclusion 89
3.4.5 Experimental Section 90
3.4.6 References 92

3.5 A Priori Prediction of Mass Spectrometric Product Patterns of Photoinitiated Polymerizations 93
3.5.1 Abstract 93
3.5.2 Introduction 94
3.5.3 Results and Discussion 94
3.5.4 Conclusion 101
3.5.5 References 102

3.6 Recent Advances in Germanium-Based Photoinitiator Chemistry 103
3.6.1 Abstract 103
3.6.2 Introduction 104
3.6.3 The Beginning of Acylgermanium Chemistry 106
3.6.4 Synthesis of Germanium-Based PIs 106
3.6.5 Spectroscopic Properties of Germanium-Based PIs 109
3.6.6 PI Performance 113
3.6.7 Conclusion 116
3.6.8 Outlook 116
3.6.9 References 117

3.7 Breaking Borders: Tetraacylstannanes as Long-Wavelength Visible-Light Photoinitiators with Intriguing Low Toxicity 119
3.7.1 Abstract 119
3.7.2 Introduction 120
3.7.3 Results and Discussion 121
3.7.4 Conclusion 127
3.7.5 Experimental Section 128
3.7.6 References 133

4 CONCLUSION AND OUTLOOK 135

CURRICULUM VITAE 142

1 INTRODUCTION

For decades the synthesis and photochemical properties of acylsilanes were intensively studied by various working groups.[1] Due to the photochemical behavior of acylsilanes, these derivatives were exploited for the generation of silicon-carbon double bonds.[2] Along with acylsilanes, acylgermanes were investigated as higher group 14 congeneres.[3]

Contrary to acylsilanes, which undergo a 1,3 silyl-shift upon irradiation (i.e. Brook Rearrangement) giving rise to a Si=C bond, acylgermanes form radicals upon homolytic scission of the Ge-C(O) bond (Chart 1).[4]

Chart 1. Photochemical Behavior of Acylsilanes and Acylgermanes.

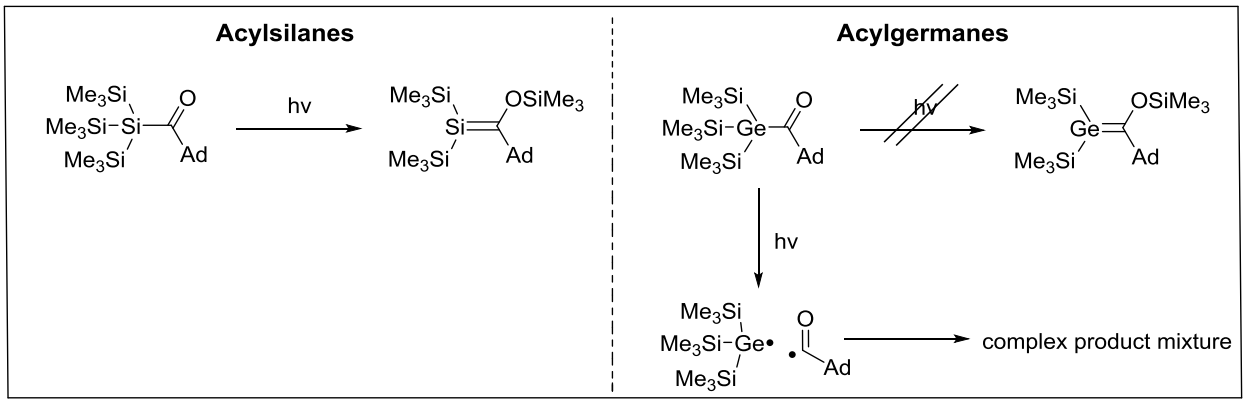

Owing to the unique property of acylgermanes, this compound class experienced a resurgence of interest in the last few years. In 2008 mono- and bisacylgermanes have first been reported as advantageous radical sources adding readily to a double bond. Since then, substantial efforts have been made by several working groups to elucidate the photoreactivity and preparation of acylgermanes.[5] So far, only synthetic methods towards mono-, bis-, and trisacylgermanes were known completely lacking of strategies towards the tetra-substituted acylgermanes.

In this context, we were able to develop a synthetic approach towards tetraacylgermanes, bearing the highest number of photo-cleavable bonds within one molecule. Thus, the major objective of the presented thesis was to improve the newly elaborated synthetic approach towards the long-sought after tetraacylgermanes and to test the found methodology with respect to its group tolerance. Additionally, the obtained products should be investigated in terms of their photochemical properties by various spectroscopic methods.

References

[1] H.-J. Zhang, D. L. Priebbenow, C. Bolm, *Chem. Soc. Rev.* **2013**, *42*, 8540.

[2] A. G. Brook, H. J. Wessely, *Organometallics* **1985**, *4*, 1487.

[3] a) R. E. Bruns, P. Kuznesof, *J. Organomet. Chem.* **1973**, *56*, 131; b) M. Wakasa, K. Mochida, Y. Sakaguchi, J. Nakamura, H. Hayashi, *J. Phys. Chem.* **1991**, *95*, 2241; c) K. Mochida, K. Ichikawa, S. Okui, Y. Sakaguchi, H. Hayashi, *Chem. Lett.* **1985**, *14*, 1433; d) A. Alberti, G. Seconi, G. F. Pedulli, A. Degl'innocenti, *J. Organomet. Chem.* **1983**, *253*, 291.

[4] A. G. Brook, F. Abdesaken, H. Söllradl, *J. Organomet. Chem.* **1986**, *299*, 9.

[5] a) W. Feuerstein, S. Höfener, W. Klopper, I. Lamparth, N. Moszner, C. Barner-Kowollik, A.-N. Unterreiner, *Chemphyschem* **2016**, *17*, 3460; b) Y. Catel, U. Fischer, P. Faessler, N. Moszner, *Macromol. Chem. Phys.* **2016**, *217*, 2686; c) D. Neshchadin, A. Rosspeintner, M. Griesser, B. Lang, S. Mosquera-Vazquez, E. Vauthey, V. Gorelik, R. Liska, C. Hametner, B. Ganster, R. Saf, N. Moszner, G. Gescheidt, *J. Am. Chem. Soc.* **2013**, *135*, 17314; d) J. Lalevée, X. Allonas, J. P. Fouassier, *Chem. Phys. Lett* **2009**, *469*, 298.

2 LITERATURE OVERVIEW

2.1 Acylgermanes

2.1.1 Introduction

The preparation, spectral properties and chemical behavior of acylgermanes were previously reviewed.[1] Historically speaking, synthetic efforts towards acylgermanes were mainly initiated to provide substrates for spectroscopic studies of acyl group 14 metal analogues.[1a] This has continued to be the driving force in this area until the early 21st century.[2]

Among the pioneering works of A. Brook on the chemistry of acylsilanes, he was also the first to prepare acylgermanes and to explore their reactivity in 1957 (**1**, Chart 1).[3]

Chart 1. First Examples of Monoacylgermanes.

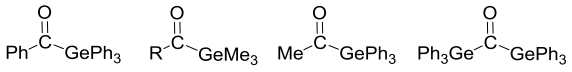

1 **2** **3** **4**

R = Aryl

Unlike acylsilanes, which tend to undergo Brook-type rearragements,[4] a different photochemical behavior of acylgermanes was found. The spectral properties and photochemical behavior of germanium-containing organometallic keto-derivatives (**1**-**4**, Chart 1) were studied more than 30 years ago by Mochida and coworkers.[2b,2c] Upon irradiation, this compound class is capable of radical formation.[5] Due to this substance property researchers recently drew their attention to acylgermanes and their application as photoinitiators (PIs).[6]

In 2008, benzoyl germanium derivatives **2** and bisacylgermanes **5** (Chart 2) were introduced as PIs for visible-light curing by Moszner and coworkers.[7]

Chart 2. First Examples of Bisacylgermanes.

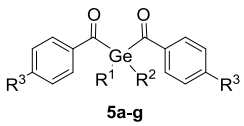

5a-g

5a: $R^1 = R^2 = -C_2H_5$, $R^3 = -H$
5b: $R^1 = CH_3$ $R^2 = -CH_3$, $R^3 = -H$
5c: $R^1 = R^2 = -C_4H_9$, $R^3 = -H$
5d: $R^1 = R^2 = -C_2H_5$, $R^3 = -OCH_3$
5e: $R^1 = R^2 = -C_5H_{10}$, $R^3 = -H$
5f: $R^1 = CH_3$ $R^2 = -Ph$, $R^3 = -H$
5g: $R^1 = R^2 = -C_2H_5$, $R^3 = -OH$

Since then, substantial efforts have been made to elucidate the photoreactivity of acylgermanes. Lalevée and coworkers reported on the excited state processes and reactivity of acylgermanes in 2009.[6] In 2013, Gescheidt and coworkers investigated the reactivity of the Ge-centered radicals by time-resolved EPR

spectroscopy and by photo-chemically induced dynamic nuclear polarization techniques.[8] Unterreiner and coworkers studied the substitution effects on the photo-physical properties of various para-substituted monoacylgermanes in 2016.[9] In the same year, Catel and coworkers disclosed the high PI efficiency of **5d** for the polymerization of vinylcyclopropanes.[10]

2.1.2 Synthesis of Acylgermanes

Concerning the synthetic methods towards mono-, bis-, and trisacylgermanes, several methods were reported throughout the last decades. However, researchers were still missing approaches towards the long-sought-after tetra substituted acylgermanes.

2.1.2.1 Monoacylgermanes

The first synthesis of monoacylgermanes achieved by Brook *et al*. proceeds via hydrolysis of α,α-dibromoalkylgermanes (equation 1).[11]

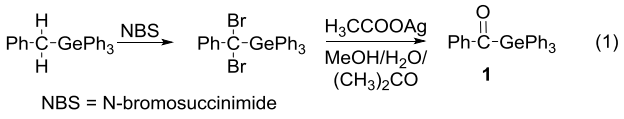

(1)

The most common method for acylgermane synthesis is the salt metathesis reaction of metallogermanes with carboxylic acid derivatives, i.e. acid chlorides[12], amides[13] and esters (equation 2).[14]

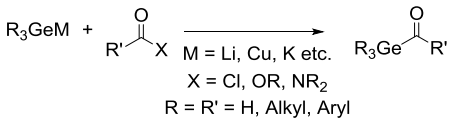

(2)

Yamamoto et al. achieved the synthesis of monoacylgermanes **2** from hexamethyldigermane and the respective acid chlorides in the presence of a Pd-catalyst and triethyl phosphite (equation 3).[15]

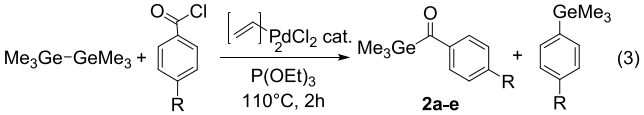

(3)

2a: R = -H
2b: R = -OMe
2c: R = -F
2d: R = -CN
2e: R = $-NO_2$

yield: 17 - 78 %

Brook's synthetic approach via hydrolysis of α,α-dibromoalkylgermanes was superseded by treating trialkylchlorogermanes with carbanions derived from 1,3-dithiane compounds followed by hydrolysis (equation 4).[11]

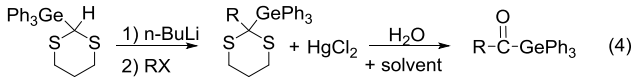

The problems arising from the use of dithiane masked derivatives were circumvented by employing 1,3-dioxanes[16] or O,S-acetales[17] as alternative carbonyl masking groups (equation 5).

Another method for the preparation of monoacylgermanes is the hydrolysis of germyl enol ethers, giving α,β-unsaturated acylgermanes (equation 6).[18]

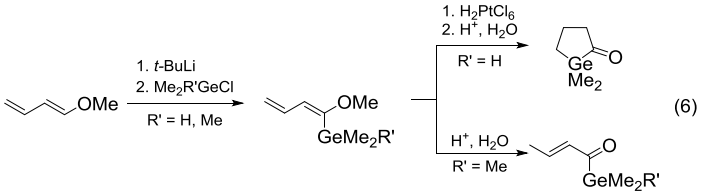

The reaction of aldehydes with trialkylgermyllithium species results in the formation of α-hydroxyalkylgermanes. These derivatives can be converted to acylgermanes by oxidation under Swern conditions or chromic acid (equation 7).

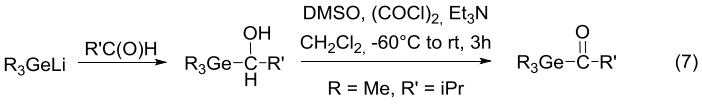

The synthesis of bisgermyl derivative **4** was accomplished by the oxidation of bis(triphenylgermyl)methanol with dicyclohexylcarbodiimide/pyridinium trifluoroacetate in DMSO (equation 8).[19]

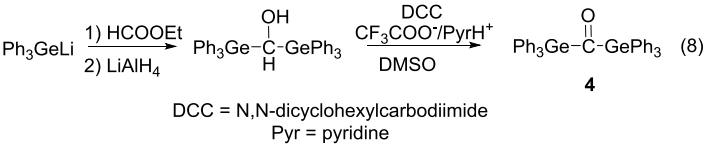

2.1.2.2 Bisacylgermanes

In analogy to monoacylgermanes, bisacylgermanes were synthesized by the reaction of aryl acid chlorides with germyllithiums of the form Ar_2HGeLi[20] or ArH_2GeLi (equation 9).[21]

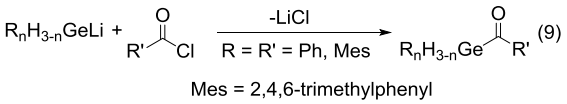

Bisacylgermanium derivatives **5a**-**g** were synthesized by a Corey-Seebach type reaction, which was adapted for higher homologues of carbon by A. Brook (equation 10).[7b–d,11]

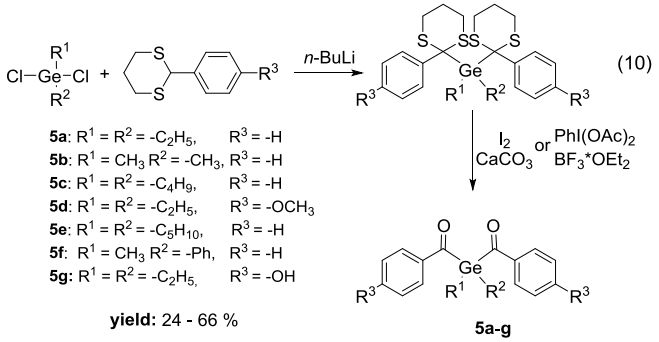

In the case of the sterically demanding bisacylgermane **5h** the dithiane route failed. Thus, compound **5h** was alternatively prepared by the acylation of diphenylgermane though the low yield prevented complete characterization (equation 11).[7d]

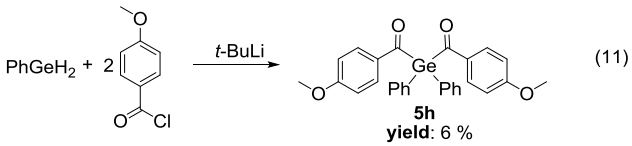

2.1.2.3 Trisacylgermanes

The only reported trisacylgermane derivative was prepared form PhH_2GeLi (equation 12).[21]

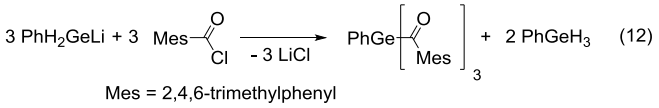

2.1.3 Spectroscopic Properties of Acylgermanes

2.1.3.1 Infrared Spectroscopy

In general acylgermanes feature a strong carbonyl stretching at around 1620 cm^{-1}.[7d] Similar carbonyl stretching bands for acylsilanes (~1645 cm^{-1}) were reported.[22] Reported carbonyl stretching bands of selected mono- and bisacylgermanes are listed in Table 1.

Table 1. IR Carbonyl Stretching of Selected Acylgermanes.

IR carbonyl stretching in cm^{-1}			
2a	1622	**5d**	1616
5a	1616	**5e**	1622
5b	1622	**5f**	1624
5c	1616	**5h**	1615

2.1.3.2 UV-Vis Spectroscopy

Contrary to the colorless carbon analogues, acylgermanes are bright yellow compounds. Therefore, the UV-Vis spectral properties were intensively studied. The longest-wavelength absorption bands were assigned to a n-π* transition.[22] Table 2 shows λ_{max} values and extinction coefficients for the longest wavelength absorption bands of all reported acylgermanes.

Table 2. λ_{max} Values and Extinction Coefficients for the Longest Wavelength Absorption Bands of Monoacylgermanes **2a**-**e**,[9,7b] Bisacylgermanes **5a**-**5h**,[7d].

	λ_{max}/ ε [L·mol^{-1}·cm^{-1}]		**λ_{max}/ ε [L·mol^{-1}·cm^{-1}]**		**λ_{max}/ ε [L·mol^{-1}·cm^{-1}]**
Monoacylgermanes					
2a	411.5/ 137	**2c**	405/ [a]	**2e**	429/ [a]
2b	397/ [a]	**2d**	425/ [a]		
Bisacylgermanes					
5a	418.5/ 490	**5d**	408.2/ 724	**5g**	406.2/ 686
5b	417.6/ 511	**5e**	418.1/ 568	**5h**	402.5/ 570
5c	418.5/ 529	**5f**	418.8/ 549		

[a] not published

2.1.3.3 NMR-Spectroscopy

It was shown that the carbonyl ^{13}C resonance line of acylgermanes is significantly downfield shifted compared to ketones.[3,7] All reported shifts appear around 230 ppm. Similar observations were also found for cyclic acylgermanes.[23] Table 3 summarizes ^{13}C resonance lines of the carbonyl C-atom of selected acylgermanes.

Table 3. ^{13}C NMR Shifts of Ge-CO of Selected Acylgermanes.

^{13}C NMR δ [ppm] of Ge-CO ($CDCl_3$)			
2a	234.39	**5d**	227.4
5a	230.22	**5e**	229.0
5b	229.1	**5f**	227.2
5c	230.8	**5h**	222.8

2.1.4 Reactivity of Acylgermanes

Contrary to acylsilanes, the germanium analogues tend to cleave via Norrish-type I pathways upon UV irradiation. Thus, acylgermanes undergo homolytic bond cleavage when exposed to a light source, generating a germyl and an acyl centered radical pair (Chart 3).

Chart 3. Mechanism of Norrish Type I and Norrish Type II Reaction.

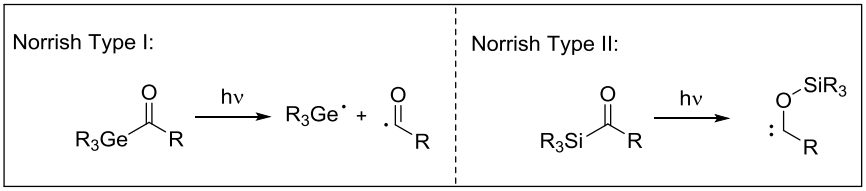

Due to this photochemical behavior, acylgermanes have evolved over the last view years as promising radical precursors for visible-light induced free radical polymerization.[24]

Apart from their photochemical behavior, the reactivity of acylgermanes was not yet investigated.

2.1.5 Acylgermanes as photoinitiators

In 2008, Moszner and coworkers and Liska and coworkers successfully reinvestigated acylgermanes. They showed that among the promising PI systems, mono- and bisacylgermanes act as suitable radical precursors generating acyl and germyl centered radicals upon irradiation, which add very rapidly to double bonds of various monomers.[6,7b–d,8,10,25]

Due to the significantly red-shifted absorption bands of acylgermanes, Liska et al. reported on the advantageous usage of a monoacylgermane (**2a**: benzoyltrimethylgermane) as PI system for LED-based dental filling materials. The so far applied PI systems, such as bisacylphosphine oxides (BAPOs) lack of sufficient light absorption in the visible region, prohibiting their application in this field (cf. Figure 1).[26]

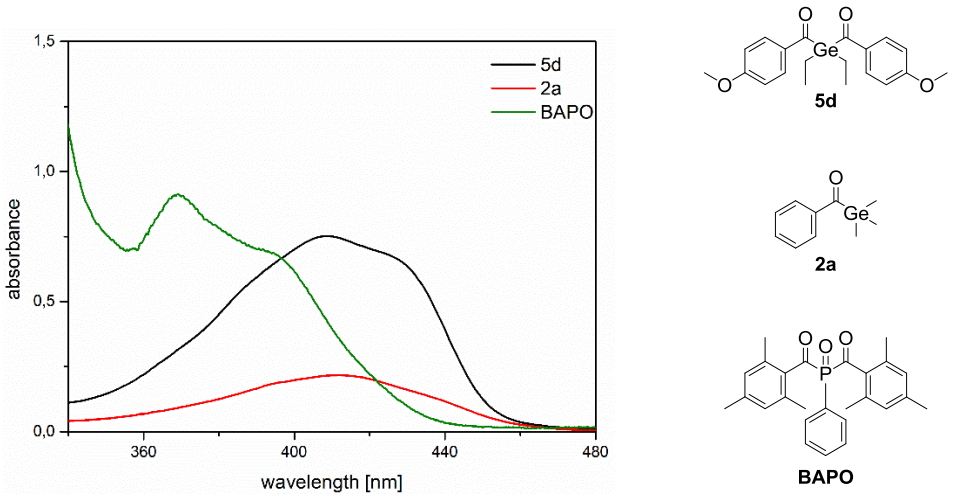

Figure 1. UV-Vis Absorption of Ivocerin **5d**, Benzoyltrimethylgerman **2a**, and BAPO.

Furthermore, their use in biomedical applications is often prohibited due to the high toxicity of most BAPOs.[27] In this context, Moszner and coworkers reported on the toxicity of **2a** and related acylgermanes. The cytotoxicity test was shown to be negative, as well as the bacterial reverse mutation test, i.e. the AMES test, proved that these compounds do not induce gene mutation, which supported their application in biomedical applications.[7d,28]

The bimolecular PI system consisting of campherquinone (CQ) and ethyl-4-dimethylaminobenzoate (DMAB) is the state-of-the art PI for dental primer and restorative composites (cf. Chart 4). To a large extend, the dental formulations are still based on the combination of CQ with suitable tertiary amines as coinitiators. CQ shows a broad absorption spectrum between 400 and 500 nm (λ_{max} = 468 nm).[29] They show a good photobleaching effect that allows the curing of relatively thick layers. The disadvantages of CQ/A PIs concern the toxicity of the used amines and the yellowing of the cured materials caused by oxidation of amine impurities. Moreover, in CQ/A PIs as two-component PI system, the interaction of the partners is strongly dictated by the viscosity of the medium.[7d] A further considerable drawback of this system is their low reactivity, especially in water-based formulations.[30]

Liska and coworkers were the first to highlight the beneficial properties of monoacylgermanes as PIs for dental filling materials. Apart from the low toxicity, they indicated the high reactivity of the radicals derived from acylgermanes and could prove the enhanced photobleaching behavior of this compound class when compared to the CQ/amine system.[7a]

Chart 4. Acylgermanes **2a**, **5a** and Reference PIs.

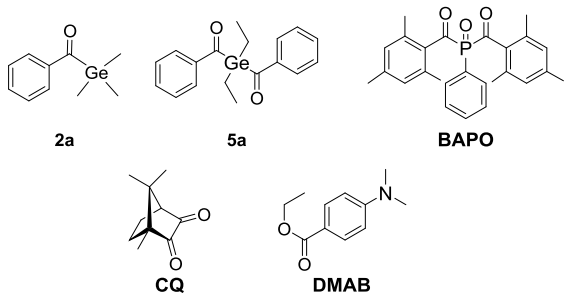

Almost concurrently with the introduction of monoacylgermanes as promising PIs, bisacylgermanes were studied by Moszner and coworkers and Liska and coworkers.[7c,7d] A series of novel bisacylgermanes was prepared and tested for their curing efficiency of dimethacrylate resin-based composites in comparison with a CQ/A PI system. Moszner and coworkers concluded a higher photocuring activity compared to the CQ/A system, which was explained by the more intense absorption in the VL region (400 – 450 nm) than CQ. Furthermore, for the photodecomposition of bisacylgermane (**5a**: Dibenzoyldiethylgermane) a quantum yield of 0.85[7d] was found, which was significantly higher than that of CQ (~0.07).[31]

In 2009, Lalevée and coworkers reinvestigated and contributed on the understanding of excited state processes and reactivity of acylgermanes as scarce data was available on the Ge-radical chemistry.

Steady-state photolysis was carried out a long time ago by Brook and coworkers.[32] The fluorescence properties and T_1 state reactivity of acylgermanes (benzoyltriphenylgermane **1**, benzoyltrimethylgermane **2a** and benzoyldimethylphenylgermane) were studied by Mochida et *al*. and Hayashi et *al*. in 1983 and 1991 respectively.[2b,33] The formation and spectral characterization of Ge-radical was provided but the reactivity was not investigated.[34]

Lalevée and coworkers conducted laser-flash photolysis (LFP) experiments to validate the kinetics of the $Ph_3Ge\bullet$ radical. Strikingly, they found higher addition rate constants than for classical carbon centered radicals, which were already considered as reactive structures.[35] For Ge-centered radicals they stated an addition rate constant of $10^7\ M^{-1}s^{-1}$, being two orders of magnitude higher as compared to acyl radicals ($10^5\ M^{-1}s^{-1}$).[6]

These investigations were followed by studies on the acylgermane **5a** conducted by Gescheidt and coworkers in 2013.[8] In this contribution they established the mechanism of the primary cleavage of **5a** and investigated the properties of the formed Ge-centered radicals.

Scheme 1. Reaction Scheme of the Relevant Photophysical Processes of **5a** upon Laser Excitation, The Boxes Refer to the Processes Observable with the Respective Experimental Techniques.

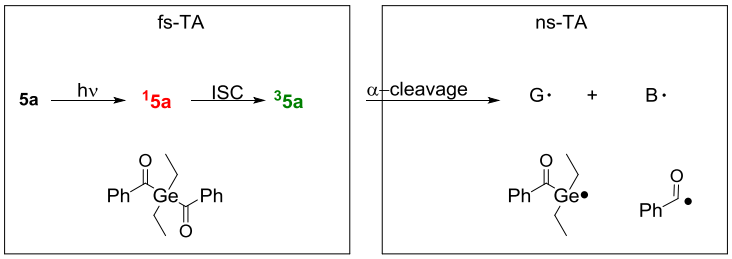

The photo-physical experiments gave information on the time scale of the formation of the Ge-centered radical. The obtained a transient absorption (TA) spectrum, with a maximum around 470 nm, which could be attributed to the singlet excited state of ^{1}**5a**. This species disappeared within picoseconds ((6 ± 2) 10^{7} s^{-1}) and gave rise to the triplet state of ^{3}**5a** (cf. Scheme 1) which decayed within ~15 ns. A new band at 500 nm was observed thereby. This absorption was ascribed to the Ge-centered radical G•, as B• radicals do not absorb in the region between 400 – 700 nm.[36]

By time-resolved EPR spectroscopy Gescheidt and coworkers could also show that the primary formed radicals can be clearly assigned to the G• and B•radicals (Scheme 1).

Through time-resolved CIDNP techniques they investigated radical follow-up reaction pathways of G• and B• and reported typical photoproducts (benzaldehyde, benzil the respective digermane [2+2] and [2+4] cycloaddition products).[8]

The LFP experiments and obtained addition rate constants were presented by Gescheidt and coworkers. Table 4 summarizes all reported literature on this topic.

Table 4. Experimentally Established Rate Constants for the Addition of the Radicals G• to Butyl Acrylate and Ph_3G• to Methyl Acrylate.

Radical	Solvent	k_{add} [$M^{-1} s^{-1}$]	Ref
G•	Toluene	$(1.2 \pm 0.1) \cdot 10^8$	8
G•	Acetonitrile	$(3.2 \pm 0.2) \cdot 10^8$	8
Ph_3G•	Acetonitrile	$2.2 \cdot 10^8$	6
B•	Acetonitrile	$2.7 \cdot 10^5$ (± 10%)	36

For the first time, the kinetics of the germanium-centered radical were studied. Lalevée and coworkers and Gescheidt and coworkers showed that the addition of such is ∼1 order of magnitude faster than related phosphorus-based radicals.[37]

In 2016, Unterreiner and coworkers reported on the photo-physical properties of benzoylgermane and para-substituted derivatives (Chart 5). They investigated the influence of substitution at the aryl moiety on the electronic transition.[9]

Chart 5. Investigated Acylgermanes.

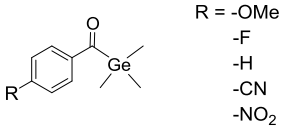

R = -OMe
-F
-H
-CN
$-NO_2$

They concluded that electron-withdrawing cyano and nitro groups can stabilize the lowest excited singlet and triplet states, in contrast to the methoxy- and fluoro substituents. As the electron-pushing groups (OMe or F) are not able to stabilize the negative charge via resonance, inductive effects or polarizability the transition state barriers are lower when compared to the cyano or nitro substituted derivatives.[9] Therefore, ISC (intersystem crossing) from ^1S into ^1T (i.e. radical formation) of acylgermanes substituted with electron-withdrawing groups is less favored than for derivatives with electron-pushing substituents.

In the same year, Catel and coworkers successfully applied the bisacylgermane **5d** to photocure vinylcyclopropanes. They compared the PI performance of CQ/amine system with that of **5d**. Under the same polymerization conditions it appeared that the Ge-based PI shows significantly higher polymerization rates. A 92% conversion of the polymerizable double bonds was achieved after 120 seconds. Due to the promising performance of **5d**, Catel and coworkers prepared dental composites solely based on vinylcyclopropanes and **5d**. The prepared composites convinced with their good mechanical properties.[10]

2.2 Acylstannanes

2.2.1 Introduction

Due to their acute toxicity, organotin compounds have been used in a very restrictive manner in chemical synthesis and related research activities have gradually diminished over time. Hitherto, the interest in acylstannane-chemistry remained modest because of a lack of suitable synthetic methods towards such. For a long time they were virtually unknown and believed to be extremely labile.[38] For the sake of completeness, the acylated tin derivatives were mentioned as a side note when reporting on acylsilanes and acylgermanes.[1a,39]

Exposure to dioxygen rapidly converts acylstannanes into the corresponding acyloxystannanes.[40] Consequently, purification and storage of these compounds are difficult undoubtedly restricting the application of acylstannanes in synthesis.[38] However, there are few reports on the successful synthesis of acylstannanes.

2.2.2 Synthesis of Acylstannanes

In 1968, Peddle and coworkers reported on the preparation and properties of α-tin ketones. These compounds were prepared from Ph_3SnLi and acid chlorides (equation 13).[39a]

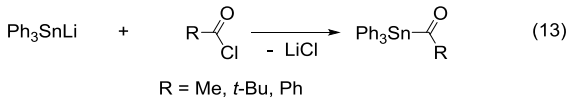

(13)

In 1987, Kosugi et *al*. and Migita et *al*. contributed to the synthesis of acylstannanes. They reported yields of 12 to 15% when reacting Bu_3SnLi and acid chlorides (equation 14).[39c]

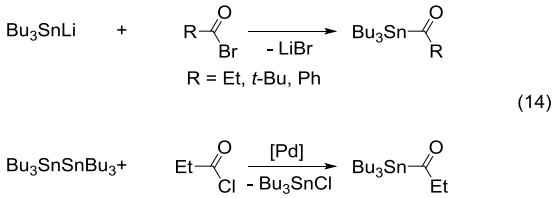

(14)

In 1989, Degl'Innocenti and coworkers published a general synthetic access to acylstannanes (equation 15). They found that trialkylstannyllithium reacts with a variety of electrophiles, such as acid chlorides, ethyl carboxylates, and thioesters to afford the corresponding acylstannanes.[39b]

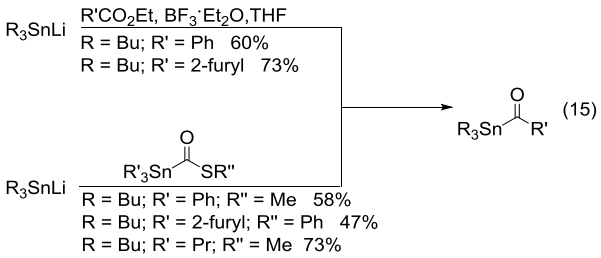

Reactions in which ethyl esters were employed as acylating agents were more successful, the reactions were performed in the presence of excess of boron trifluoide-diethyl ether complex (equation 15).

Alternatively, they used thioesters for the acylation to circumvent the use of boron trifluoride. Thus, the isolation of the sensitive acylstannanes was easier to accomplish.[38]

So far, no further reaction pathways towards monoacylstannanes were reported. Literature completely lacks reports on bis, tris- or tetraacylstannanes.

2.2.3 Spectroscopic Properties of Acylstannanes

2.2.3.1 Infrared Spectroscopy

Characteristic of acylgermanes is the strong carbonyl stretching at around 1620 cm^{-1}.[7d] Similar carbonyl stretching bands for acylsilanes (~1645 cm^{-1}) were reported and are comparable with those of acylstannanes (cf. Table 5).[22]

Table 5. IR Carbonyl Stretching of Selected Acylstannanes and Metalloid Ketones.[1a]

IR carbonyl stretching in cm^{-1}	
$Ph_3SnC(O)Me$	1670
$Ph_3SnC(O)tBu$	1655
$Ph_3SnC(O)Ph$	1627

M =	**C**	**Si**	**Ge**
$Ph_3MC(O)Ph$	1692	1618	1629

2.2.3.2 UV-Vis Spectroscopy

Acylstannanes were also investigated with respect to their absorption properties. Due to the instability of the compounds the extinction coefficients were neither determined nor reported. However, the longest-wavelength absorption bands of all prepared acylstannanes were measured and are summarized in Table 6. Compared to analogues Si- or Ge- acyl derivatives, (e.g. $Ph_3SiC(O)Ph$, λ_{max} = 424 nm;[1a] $Ph_3GeC(O)Ph$, λ_{max} = 417 nm)[1a] bathochromic values for λ_{max} were reported.

Table 6. λ_{max} [nm] Values for the Longest Wavelength Absorption Bands of Reported Acylstannanes.[1a,39c]

	λ_{max} [nm]
$Ph_3SnC(O)Me$	363, 375, 391
$Ph_3SnC(O)tBu$	376
$Ph_3SnC(O)Ph$	435
$Bu_3SnC(O)Et$	385, 370
$Bu_3SnC(O)iPr$	390, 375
$Bu_3SnC(O)Ph$	440

2.2.3.3 NMR-Spectroscopy

It was shown that the C=O ^{13}C resonance line of acylstannanes is significantly downfield shifted compared to ketones.[38] Similar behavior was found for acylgermanes.[3,7] All reported shifts appear around 240 ppm. Table 7 summarizes ^{13}C resonance lines of the carbonyl C-atom and ^{119}Sn shifts of all reported acylstannanes.

Table 7. ^{13}C NMR Shifts of Sn-CO and ^{119}Sn NMR Shifts of Reported Acylstannanes.[1a,39b]

	^{13}C NMR δ(C=O) [ppm]	**^{119}Sn NMR δ [ppm]**
$Bu_3SnC(O)Et$	250.1	
$Bu_3SnC(O)iPr$	249.8	
$Bu_3SnC(O)Ph$	244	-84
$Me_3SnC(O)Ph$	239.5	-80
$Bu_3SnC(O)$-3-tolyl	230	-84
$Me_3SnC(O)$-2-furyl	234	-87
$Bu_3SnC(O)$-2-furyl	236	-89
$Bu_3SnC(O)$-2-thionyl	249	-90.5

2.2.4 Reactivity of Acylstannanes

Kosugi and coworkers and Migita and coworkers were mainly focusing on the synthesis of acylstannanes. In 1987, they reported that acylstannanes are fairly stable in the dark under inert gas atmosphere and can be stored for months.[39c] They stated the high reactivity of acylstannanes towards molecular oxygen resulting in the quantitative formation of tributyltin carboxylates. Upon addition of 10% of galvinoxyl, which is a commercially available free radical inhibitor, the oxidation was inhibited. Whereas, upon addition of AIBN (azobisisobutyronitrile), the decomposition was slightly accelerated. Kosugi and coworkers and Migita and coworkers suggested a free radical chain mechanism (cf. equation 16)

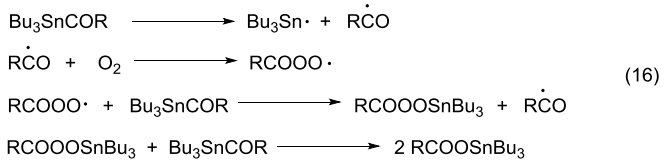

(16)

2.2.5 Acylstannanes as photoinitiators

To date, no application of acylstannanes as PIs are reported.

2.3 References

[1] a) A. G. Brook in *Advances in Organometallic Chemistry, 7* (Eds.: F. G. A. Stone, R. West), Elsevier, Burlington, **1969**, pp. 95–153; b) A. C. Spivey, C. M. Diaper in *Science of synthesis*. *Houben-Weyl Methods of Molecular Transformations*. Category 1: Organometallics (Ed.: M. G. Moloney), Thieme, Stuttgart, **2003**, pp. 109–112.

[2] a) R. E. Bruns, P. Kuznesof, *J. Organomet. Chem.* **1973**, *56*, 131; b) M. Wakasa, K. Mochida, Y. Sakaguchi, J. Nakamura, H. Hayashi, *J. Phys. Chem.* **1991**, *95*, 2241; c) K. Mochida, K. Ichikawa, S. Okui, Y. Sakaguchi, H. Hayashi, *Chem. Lett.* **1985**, *14*, 1433; d) A. Alberti, G. Seconi, G. F. Pedulli, A. Degl'innocenti, *J. Organomet. Chem.* **1983**, *253*, 291; e) K. Mochida, K. Yamamoto, *Bull. Chem. Soc. Jpn.* **1988**, *61*, 2933; f) V. Y. Vitkovskii, D. A. Bravo-Zhivotovskii, S. D. Pigarev, O. A. Vyazankina, N. S. Vyazankin, *Russ Chem Bull* **1984**, *33*, 2172.

[3] A. G. Brook, F. Abdesaken, H. Söllradl, *J. Organomet. Chem.* **1986**, *299*, 9.

[4] A. G. Brook, *Acc. Chem. Res.* **1974**, *7*, 77.

[5] A. G. Brook, M. A. Quigley, G. J. D. Peddle, N. V. Schwartz, C. M. Warner, *J. Am. Chem. Soc.* **1960**, *82*, 5102.

[6] J. Lalevée, X. Allonas, J. P. Fouassier, *Chem. Phys. Lett* **2009**, *469*, 298.

[7] a) B. Ganster, U. K. Fischer, N. Moszner, R. Liska, *Macromol. Rapid Comm.* **2008**, *29*, 57; b) N. Moszner, U. K. Fischer, B. Ganster, R. Liska, V. Rheinberger, *Dent. Mater.* **2008**, *24*, 901; c) B. Ganster, U. K. Fischer, N. Moszner, R. Liska, *Macromolecules* **2008**, *41*, 2394; d) N. Moszner, F. Zeuner, I. Lamparth, U. K. Fischer, *Macromol. Mater. Eng.* **2009**, *294*, 877.

[8] D. Neshchadin, A. Rosspeintner, M. Griesser, B. Lang, S. Mosquera-Vazquez, E. Vauthey, V. Gorelik, R. Liska, C. Hametner, B. Ganster, R. Saf, N. Moszner, G. Gescheidt, *J. Am. Chem. Soc.* **2013**, *135*, 17314.

[9] W. Feuerstein, S. Höfener, W. Klopper, I. Lamparth, N. Moszner, C. Barner-Kowollik, A.-N. Unterreiner, *Chemphyschem* **2016**, *17*, 3460.

[10] Y. Catel, U. Fischer, P. Faessler, N. Moszner, *Macromol. Chem. Phys.* **2016**, *217*, 2686.

[11] A. G. Brook, J. M. Duff, P. F. Jones, N. R. Davis, *J. Am. Chem. Soc.* **1967**, *89*, 431.

[12] a) D. A. Nicholson, A. L. Allred, *Inorg. Chem.* **1965**, *4*, 1747; b) U. Iserloh, D. P. Curran, *J. Org. Chem.* **1998**, *63*, 4711; c) E. Piers, R. Lemieux, *Organometallics* **1995**, *14*, 5011; d) M. Nanjo, K. Matsudo, K. Mochida, *Chem. Lett.* **2001**, *30*, 1086.

[13] D. A. Bravo-Zhivotovskii, S.D. Pigarev, I. D. Kalikhman, O. A. Vyazankina, N. S. Vyazankin, *J. Organomet. Chem.* **1983**, *248*, 51.

[14] S. Kiyooka, A. Miyauchi, *Chem. Lett.* **1985**, *12*, 1829.

[15] K. Yamamoto, A. Hayashi, S. Suzuki, J. Tsuji, *Organometallics* **1987**, *6*, 974.

[16] a) K. J. H. Kruithof, R. F. Schmitz, G. W. Klumpp, *J. Chem. Soc., Chem. Commun.* **1983**, 239; b) K. J. H. Kruithof, R. F. Schmitz, G. W. Klumpp, *Tetrahedron* **1983**, *39*.

[17] R. Johannesen, T. Benneche, *J. Chem. Soc., Perkin Trans. 1* **2000**, 2677.

[18] a) J. A. Soderquist, A. Hassner, *J. Am. Chem. Soc.* **1980**, *102*, 1577; b) J. A. Soderquist, A. Hassner, *Tetrahedron Lett.* **1988**, *29*, 1899.

[19] A. G. Brook, P. F. Jones, G. J. D. Peddle, *Can. J. Chem.* **1968**, *46*, 2119.

[20] A. Castel, P. Rivière, J. Satgé, H. Y. Ko, *Organometallics* **1990**, *9*, 205.

[21] A. Castel, P. Rivière, J. Satgé, D. Desor, *J. Organomet. Chem.* **1992**, *433*, 49.

[22] F. G. A. Stone, R. West (Eds.) *Advances in Organometallic Chemistry, 7*, Elsevier, Burlington, **1969**.

[23] M. Haas, M. Leypold, D. Schnalzer, A. Torvisco, H. Stueger, *Organometallics* **2015**, *34*, 5291.

[24] J. P. Fouassier, J. Lalevée in *Photoinitiators for Polymer Synthesis*, Wiley-VCH Verlag GmbH & Co. KGaA, Weinheim, Germany, **2012**.

[25] V. Y. Lee, A. Sekiguchi in *Organometallic compounds of low-coordinate Si, Ge, Sn and Pb*. *From phantom species to stable compounds*, Wiley, Oxford, **2010**.

[26] a) R. Guggenberger, Lechner, G.: Weinmann, W., *Am. Chem. Soc., Div. Polym. Chem., Polym. Prepr.* **1997**, *38*, 105; b) N. D. Richards, S. H. Dickkens, J. M. Antonucci, *Am. Chem. Soc., Div. Polym. Chem., Polym. Prepr.* **2004**, *45*, 362.

[27] Safety Data sheet of Phenylbis(2,4,6-trimethylbenzoyl)phosphine oxide.

[28] Safety Data sheet of Bis(4-methoxybenzoyl)diethylgermane.

[29] N. B. Cramer, J. W. Stansbury, C. N. Bowman, *J. Dent. Res.* **2011**, *90*, 402.

[30] G. Ullrich, B. Ganster, U. Salz, N. Moszner, R. Liska, *J. Polym. Sci. A Polym. Chem.* **2006**, *44*, 1686.

[31] Y.-C. Chen, J. L. Ferracane, S. A. Prahl, *Dent. Mater.* **2007**, *23*, 655.

[32] A. G. Brook, P. J. Dillon, R. Pearce, *Can. J. Chem.* **1971**, *49*, 133.

[33] H. Hayashi, K. Mochida, *Chem. Phys. Lett* **1983**, *101*, 307.

[34] a) C. Chatgilialoglu, K. U. Ingold, J. Lusztyk, A. S. Nazran, J. C. Scaiano, *Organometallics* **1983**, *2*, 1332; b) K. Mochida, K. Ichikawa, S. Okui, Sakaguchi Y., H. Hayashi, *Chem. Lett.* **1985**, 1433.

[35] H. Fischer, L. Radom, *Angew. Chem. Int. Ed.* **2001**, *40*, 1340.

[36] C. S. Colley, D. C. Grills, N. A. Besley, S. Jockusch, P. Matousek, A. W. Parker, M. Towrie, N. J. Turro, P. M. W. Gill, M. W. George, *J. Am. Chem. Soc.* **2002**, *124*, 14952.

[37] A. Eibel, M. Schmallegger, M. Zalibera, A. Huber, Y. Bürkl, H. Grützmacher, G. Gescheidt, *Eur. J. Inorg. Chem.* **2017**, *2017*, 2469.
[38] P. B. Wyatt in *Science of synthesis*. *Houben-Weyl Methods of Molecular Transformations*. Category 1: Organometallics (Ed.: M. G. Moloney), Thieme, Stuttgart, **2003**, pp. 423–431.
[39] a) G.J.D. Peddle, *J. Organomet. Chem.* **1968**, *14*, 139; b) A. Capperucci, A. Degl'innocenti, C. Faggi, G. Reginato, A. Ricci, *J. Org. Chem.* **1989**, *54*, 2966; c) M. Kosugi, H. Naka, H. Sano, T. Migita, *Bull. Chem. Soc. Jpn.* **1987**, *60*, 3462.
[40] P. C.-M. Chan, J. M. Chong, *J. Org. Chem.* **1988**, *53*, 5584.

3 PUBLICATIONS

The following sections cover the publications submitted during this thesis. The first part deals with the very first literature report on the synthesis of tetraacylgermanes, followed by a publication on the versatility (high group tolerance) of the newly developed synthetic route and highlights the found structure-property relationship. The third publication illustrates the photochemical properties and reactivities of this new compound class and stresses their superior potential as highly efficient long-wavelength visible-light photoinitiators (PIs) when compared to commercially available PIs, which was accomplished under collaborative work with Prof. Gescheidt and Anna Eibel. Our cooperation company Ivoclar Vivadent AG tested the efficiency of tetraacylgermanes as radical sources. The results are demonstrated in the fourth publication that features the preparation of dimethacrylate resins and dental composites using these novel PIs.

Tetraacylgermanes carry the highest number of photo-cleavable bonds per molecule. The possibility of multiple bond cleavage was investigated by Prof. Barner-Kowollik and coworkers. The results are summarized in section **3.5**.

The work finally climaxes in a minireview on the development and recent advances of germanium-based photoinitiator chemistry.

Finally, the section is rounded off with the first report on the synthesis and photochemical reactivity of tetraacylstannanes.

3.1 Tetraacylgermanes: Highly Efficient Photoinitiators for Visible-Light-Induced Free-Radical Polymerization

Judith Radebner,[a] Anna Eibel,[b] Mario Leypold,[a] Christian Gorsche,[c] Lukas Schuh,[a] Roland Fischer,[a] Ana Torvisco,[a] Dmytro Neshchadin,[b] Roman Geier,[b] Norbert Moszner,[d] Robert Liska,[c] Georg Gescheidt,[b,*] Michael Haas[a,*] and Harald Stueger[a,*]

[a] Institute of Inorganic Chemistry,Technische Universität Graz, Austria

[b] Institute of Physical and Theoretical Chemistry, Technische Universität Graz, Austria

[c] Institute of Applied Synthetic Chemistry and Christian Doppler Laboratory for Photopolymers in Digital and Restorative Dentistry, Technische Universität Wien, Austria

[d] Ivoclar Vivadent AG, Liechtenstein

published in *Angewandte Chemie Int. Ed.*, **2017**, 56, 3103-3107.

(and in *Angewandte Chemie*, **2017**, 129, 3150-3154.)

Graphical Abstract:

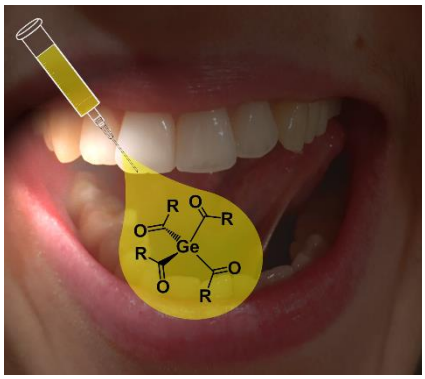

3.1.1 Abstract

In this contribution a convenient synthetic method to obtain tetraacylgermanes $Ge[(CO)R]_4$ (R = mesityl (**1a**), phenyl (**1b**), a previously unknown class of highly efficient Ge-based photoinitiators, is described. Tetraacylgermanes are easily accessible via a one-pot synthetic protocol in >85% yields, as confirmed by NMR spectroscopy, mass spectrometry and X-ray crystallography. Their performance as photoinitiators is demonstrated in photobleaching (UV-Vis), time-resolved EPR (CIDEP) and NMR/CIDNP investigations as well as by photo-DSC studies. Remarkably, the tetraacylgermanes **1** exceed the performance of currently known long-wavelength visible-light photoinitiators for free-radical polymerization.

3.1.2 Introduction

Photoinitiators (PIs) play an essential role in a broad range of industrial processes (coatings, adhesives, dental filling materials, micro-electronics or the manufacture of 3D-objects). The design and the syntheses of PIs are challenging, since they have to be tailored to fulfill very specific requirements.[1] Among promising PI systems, mono- and bisacylgermanes can act as suitable radical precursors generating acyl and germyl centered radicals upon irradiation, which add very rapidly to double bonds of various monomers.[2] Moreover, they offer the advantages of significantly red-shifted absorption bands and reduced toxicity compared to the frequently applied phosphorus-based PIs.[3,4] Commercially available Ge-based photoinitiators, such as (bis(4-methoxybenzoyl)diethylgermane (Ivocerin®),[2f] still suffer from inefficient curing depth at wavelengths > 500 nm.[2d] Furthermore, it is highly desirable to replace the multi-step synthesis of Ivocerin® (based on the Corey-Seebach reaction) by simplified synthetic approaches.[5]

3.1.3 Results and Discussion

Herein, we present a facile synthesis and the characterization of the novel tetraacylgermanes **1a**,**b** and report their superior potential as a novel class of long wavelength PIs for visible-light induced free-radical polymerization. The synthetic protocols A and B depicted in Scheme 1 represent a robust and easy-to-perform reaction sequence and, therefore, outperform the synthetic methods used for the synthesis of state-of-the-art PIs.[2d]

Scheme 1. Synthesis of Tetraacylgermanes **1a**,**b** and Tris(trimethylsilyl)acylgermanes **3a**,**b**.

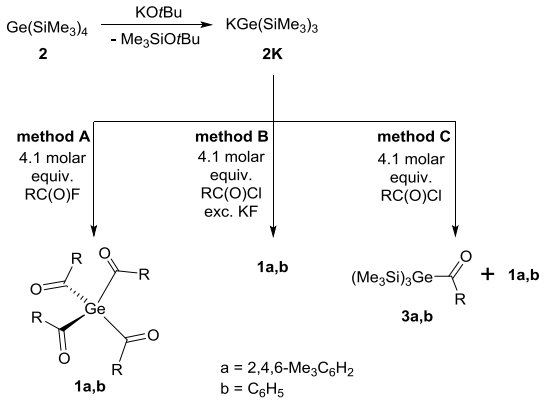

Following the results obtained by Marschner *et al.* concerning multiple abstraction of silyl groups from $(Me_3Si)_3SiK$ by fluorinated reagents,[6] we discovered that the reaction of potassium germanide **2K**[7] with 4.1 molar equiv. of acid fluorides F-C(O)R (R = aryl) leads to the formation of tetraacylgermanes **1** in >85% yields (method A, crystallized from acetone). The drawback of method A is the high price and the limited availability of acid fluorides. Hence, we developed method B, where **2K** is added to a DME solution of 4.1 molar equiv. of the corresponding acid chloride and an excess of KF. Likewise, the fast and selective formation of **1** (complete conversion after one hour, monitored by NMR spectroscopy) possibly via intermediate formation of the respective acid fluoride could be observed. In the absence of KF, **2K** and acid chlorides reacted to tris(trimethylsilyl)acylgermanes **3** as the major products along with merely minor amounts of **1**.

The analytical data for **1a**,**b** (see *Supporting Information*) are consistent with the proposed structures. Particularly striking are the structural differences between **1a** and **1b**, obtained by single-crystal X-ray diffraction analyses, with respect to the relative orientation of the four aryl rings in the molecules (Figure 1 and 2). The structure of **1a** shows two pairs of aryl rings, each arranged in a coplanar fashion with a distance of 3.98 Å between the ring planes (intramolecular π-π stacking) and relatively large dihedral angles γ between the C=O groups and the aromatic ring planes of around 70°. Compound **1b**, on the other hand, exhibits a random arrangement of the sterically less demanding phenyl ring planes and much smaller values for γ. Moreover, the mean Ge-C bond distances (2.023 (**1b**) and 2.036 Å (**1a**)), which are cleaved in the photolytic process, are considerably elongated relative to the average Ge–C bond length of 1.97 Å.[8] Similar structural features for the bond lengths and torsion angles have been observed for acylphosphanes.[3]

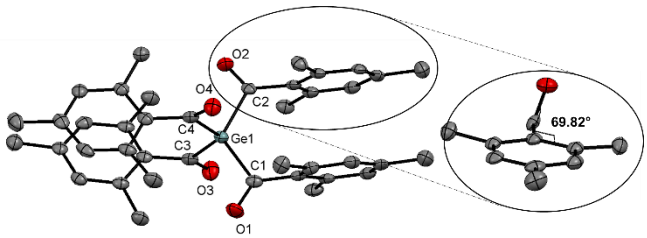

Figure 1. ORTEP Representation of **1a**. Thermal ellipsoids are drawn at the 50% probability level. Hydrogen atoms are omitted for clarity. The crystals contain two independent molecules with insignificantly different structural parameters in the asymmetric unit (compare *Supporting Information*). Selected experimental and {calculated} bond lengths [Å] and angles [°] with estimated standard deviations: Ge(1)-C(1) 2.042(3), Ge(1)-C(2) 2.040(3), Ge(1)-C(3) 2.040(3), Ge(1)-C(4) 2.025(3), {Ge(1)-C(O) (mean) 2.045}; C-O (mean) 1.214 {1.222}; C-Ge-C (mean) 109.5; O-C-C_{aryl}-C_{aryl} (mean) 69.9.

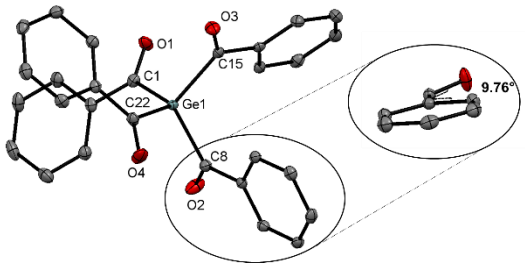

Figure 2. ORTEP Representation of **1b**. Thermal ellipsoids are drawn at the 50% probability level. Hydrogen atoms are omitted for clarity. Selected bond experimental and {calculated} lengths [Å] and bond and torsional angles [°] with estimated standard deviations: Ge(1)-C(1) 2.026(2), Ge(1)-C(8) 2.020(2), Ge(1)-C(15) 2.023(1), Ge(1)-C(22) 2.023(2), {Ge(1)-C(O) (mean) rotamer 1: 2.013, rotamer 2: 2.012}; C-O(mean) 1.217 {rotamer 1: 1.223, rotamer 2: 1.221};C-Ge-C(mean) 109.5; O-C-C_{aryl}-C_{aryl} (mean) 11.6.

In line with the observations for method A, we propose that the initial step of the mechanism is a salt metathesis reaction where KF, trimethylsilyl-*tert*-butylether **4** and tris(trimethylsilyl)acylgermane **3** are formed. The following nucleophilic attack of the fluoride ion on **4** *in situ* generates Me_3SiF **5** and tBuO$^-$, which further reacts with **3** to form the germenolate **6**. Accordingly, **4** and **5** could be detected by NMR spectroscopy in the reaction mixture (δ^{29}Si = 30.3 ppm and 6.97 ppm, respectively).[9] Subsequently the applied excess of acid fluoride immediately reacts with **6** to the respective bisacylgermane **7** upon release of KF and **4**. Acylation proceeds until all trimethylsilyl-groups have been abstracted and the final product **1** is formed (Scheme 2).

Scheme 2. Proposed Mechanism for the Synthesis of Tetraacylgermanes (Method A). (R: a = 2,4,6-$Me_3C_6H_2$; b = C_6H_5)

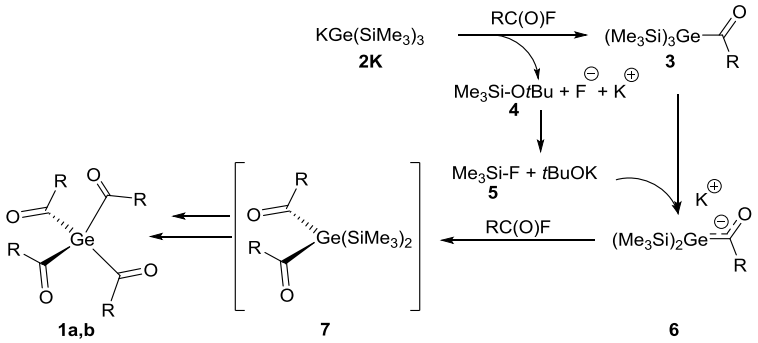

To verify the intermediate formation of the germenolate **6**, **3a** was reacted with 1.05 molar equiv. of KOtBu in THF or in toluene solution in the presence of 1.05 molar equiv. of 18-crown-6 at -70°C. We observed the facile and quantitative formation of **6a** as indicated by a ~33 ppm downfield shift of the ^{13}C resonance for the C=O group. The molecular structure of **6a** as determined by single-crystal X-ray crystallography and the complete set of consistent NMR data obtained for **6a** can be found in the *Supporting Information*.

The chemical shift values are in accordance with the ones observed earlier for structurally related cyclic acylgermenolates.[10]

As many applications of free radical photoinitiators require long excitation wavelengths (e.g. dental fillings), UV-Vis absorption spectra of **1a**,**b** were recorded and compared to structurally related monoacylgermanes **3a**, **3b**, benzoyltrimethylgermane **8** and dibenzoyldiethylgermane **9**. Experimental and calculated data depicted in Figure 3 are in agreement (for detail see *Supporting Information*, Table S1).[11]

All compounds show long-wavelength absorption bands with λ_{max} values between 363 and 419 nm tailing well into the visible region. These bands were computationally assigned to the HOMO-LUMO transition and show considerable charge transfer character. Upon excitation, electron density is displaced from the n(C=O)/σ(Ge-C) bonding HOMO to the π*(C=O/Aryl) antibonding LUMO (compare Figure 4), which results in the population of an orbital with antibonding character between the Ge-C bond (Figure 4 right side). In analogy with bisacylgermanes[12] and related ketones,[13] homolytic bond cleavage occurs upon intersystem crossing via the excited triplet state. In line with literature data of structurally related acylsilanes λ_{max} values significantly vary with the nature of the aryl group attached to the C=O moiety.[14] The bathochromic shift observed in the order **1a** ~ **3a** ⟶ **1b** ~ **3b** roughly correlates with the torsion angle γ between the plane of the phenyl ring and the C=O moiety, which is significantly smaller in the phenyl derivatives for steric reasons (compare Figures 1 and 2). This correlation is conclusive because smaller values of γ enhance phenyl/C=O π-π conjugation thus reducing the HOMO-LUMO gap and shifting the corresponding UV maximum to the red. Otherwise nearly identical λ_{max} values were measured for the phenyl substituted mono-, bis- and tetraacylgermanes. However, tetraacylgermanes show considerably increased band intensities due to the presence of four RC=O chromophores, which results in much more effective light absorption of **1a,b** in the visible region between 400 and 450 nm as compared to **3**, **8** and **9**.

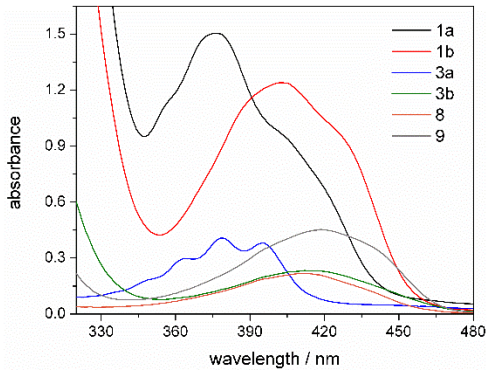

Figure 3. UV-Vis absorption spectra of **1a**,**b**, **3a**,**b**, **8**, **9** (acetonitrile solution, c = 10^{-3} mol·L^{-1}).

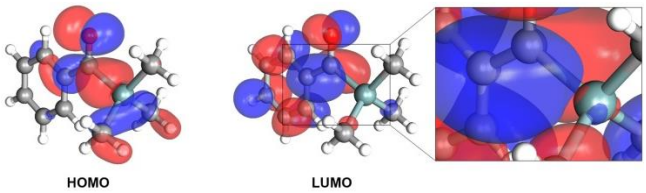

Figure 4. HOMO (left), LUMO (middle) and magnified part of the LUMO (right, Iso-Value = 0.010) of benzoyltrimethylgermane **8**.[15]

To determine the efficiency of our PIs we have investigated the photoreactivity of **1a** and **1b** using steady-state photolysis (SSP),[2d] time-resolved EPR (CIDEP)[2b,16] and NMR/CIDNP spectroscopy[17] as well as photo-DSC measurements.[2d] Steady-state photolysis using LEDs (385, 430 and 470 nm) monitored by UV-Vis showed efficient photobleaching for **1a** and **1b**. Figures 5a,b exhibit the corresponding spectra at 470 nm for **1b** and for the reference Ivocerin®, respectively. The (normalized) decay of the absorbance versus time monitored at the band maximum of the parent compounds is depicted in Figures 5c,d. While the reference Ivocerin® slightly outperforms initiator **1b** in the photobleaching performance at 385 nm and 430 nm, **1b** bleaches significantly faster than Ivocerin® upon irradiation at 470 nm. This is remarkable, since irradiation with high-wavelength visible light is desired for many applications of radical photo-polymerization, especially in dental applications. From the SSP experiments it can also be perceived that no photoproducts absorbing in the visible range of the spectrum are observable.

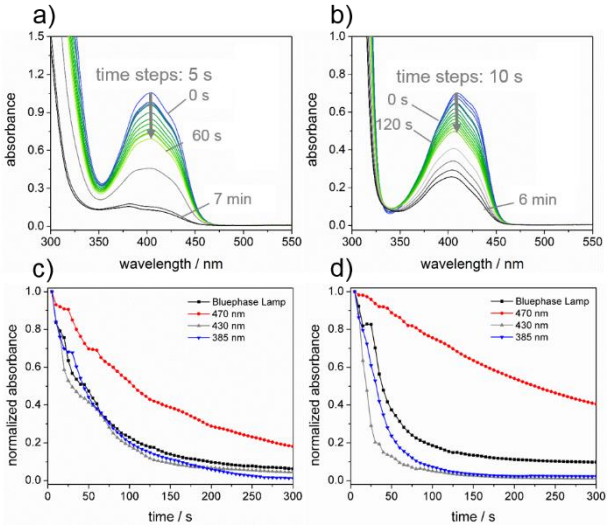

Figure 5. SSP at 470 nm of (a) tetrabenzoylgermane **1b** and (b) bisacylgermane Ivocerin® and plots of the normalized absorbance at the absorption maximum versus time for (c) **1b** (monitoring wavelength: 404 nm) and (d) Ivocerin® (monitoring wavelength: 410 nm).

TR-EPR (CIDEP) [time resolution of ~50 ns] is ideally suited to study primary radicals formed upon irradiation.[18] Laser-flash photolysis (355 nm) of **1b** leads to the TR-EPR spectrum shown in Figure 6. It consists of two overlapping signals, attributed to the benzoyl radical **B•** (g = 2.000) and the germanium-centered radical **G(1b)•** (g = 2.001) revealing α cleavage of **1b** (after intersystem crossing from the excited singlet to the excited triplet state, see Scheme 3).

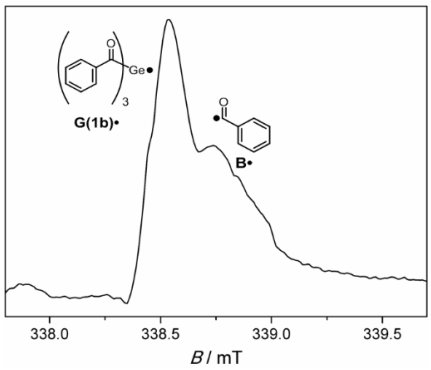

Figure 6. TR-EPR spectrum of **1b** in toluene, taken 300 – 400 ns after the laser flash (355 nm), showing two different EPR signals: **B•** (g = 2.000) and **G(1b)•** (g = 2.001).

Scheme 3. α-Cleavage of tetraacylgermane derivatives **1a**,**b**, leading to the formation of Ge-centered radicals **G•** and benzoyl radical **B•**.

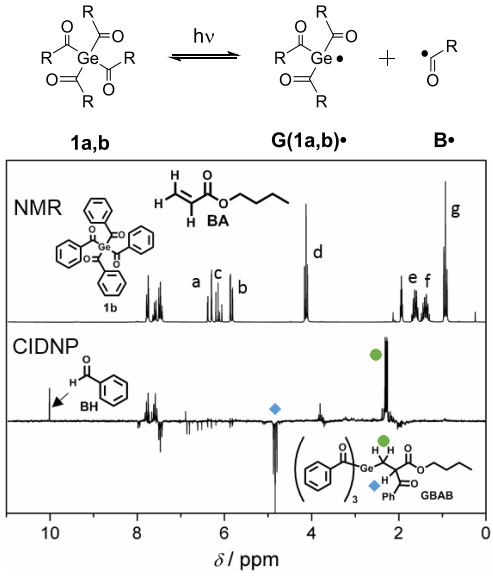

Figure 7. ^{1}H-NMR and CIDNP spectra of **1b** (10 mM solution in acetonitrile-d_3) taken in presence of butyl acrylate (50 mM).

To investigate the reaction pathways of radicals **G•** and **B•** ^{1}H-CIDNP spectroscopy was applied. Figure 7 shows the ^{1}H-NMR and CIDNP spectrum of **1b** in the presence of butyl acrylate monomer (see *Supporting*

Information for the corresponding CIDNP spectrum of **1a**). The characteristic signal at δ = 10.01 ppm corresponds to the benzaldehyde **BH**, formed via a disproportionation reaction (β-hydrogen transfer) between the benzoyl radical and radicals, which are able to donate hydrogen atoms (growing polymer chain).[17b]

The triplet at 4.83 ppm appearing in emission and the strongly polarized absorptive signals at 2.29 ppm are provisionally assigned to the methylene protons of the addition product of **G(1b)•** and butyl acrylate, which is terminated with a benzoyl radical (**GBAB**). CIDNP spectra of **1a**,**b** recorded in the absence of monomers show polarized signals of the parent compounds (see *Supporting Information).* This can be attributed to the (cage) reformation of **1a**,**b** indicating partially reversible α-cleavage.

Photo-DSC experiments can be viewed as an ideal characterization methodology for PI performance. Here, the photocuring of a crosslinking monomer (1,6-hexanediol diacrylate, HDDA) with **1a,b** has been investigated by means of photo-DSC. The previously reported monoacylgermane **8** and bisacylgermane **9** were investigated as reference compounds. From the resulting photo-DSC plots characteristic parameters such as time to reach the maximum heat flow (t_{max}), maximum rate of polymerization (R_{pmax}), time to reach 95% of final conversion ($t_{95\%}$) and final double bond conversion (DBC) can be derived. The obtained DSC parameters can be found in the *Supporting Information*. Photo-DSC and conversion plots are depicted in Figure 8.

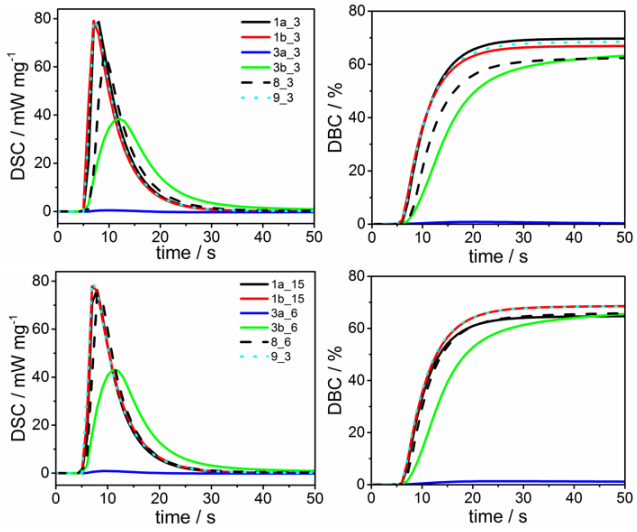

Figure 8. Photo-DSC (left) and conversion plots (right) for photopolymerization of HDDA with 0.3 mol% PI (top) and PI concentration with equimolar amounts of radically cleavable groups (bottom).

For the comparison of PI performance it has to be taken into consideration that **1a**,**b** can potentially generate four germyl radicals upon scission of the Ge-C bonds while the monoacylgermanes **3a**,**b** and **8** only contain one photocleavable Ge-C bond. When comparing equal molar PI concentrations (0.30 mol%) the tetrafunctional PIs **1a**,**b** exhibited photoreactivities comparable to the state-of-the-art long-wavelength PI **9** (Figure 8, top) with a t_{max} < 3 s and an R_{pmax} > 0.45 mol L^{-1} s^{-1}. The final DBC of photopolymers cured with **1a**,**b** was close to 70% and also lies in the range of the photopolymer cured with **9**. As expected, the monofunctional PIs **3a**,**b** and **8** showed lower photoreactivities than **1a,b**. The superior performance of the tetrafunctional PIs **1a**,**b** is clearly demonstrated by the experiment conducted with equimolar amounts of radically cleavable groups (0.15 mol% for **1a**,**b**; 0.6 mol% for **3a**,**b** and **8**; 0.3 mol% for **9**) (Figure 8, bottom). Although only half of the molar concentration was used, **1a**,**b** showed nearly identical photoreactivity compared to **9** (t_{max} < 3 s; R_{pmax} > 0.45 mol L^{-1} s^{-1}; DBC ~ 70%) while the photopolymerization tends to reach full conversion even slightly faster ($t_{95\%}$ < 18 s). This confirms that for PIs **1a**,**b** much lower molar concentrations can be employed without negative effects on the observed photoreactivity.

3.1.4 Conclusion

In conclusion we present the first tetraacylgermanes **1** obtained by a facile one-pot synthetic protocol. Their low toxicity and fast photobleaching, even upon irradiation with high wavelength visible light demonstrate their superior potential as highly efficient photoinitiators for free radical polymerization, especially for the use as PIs in dental filling materials. We continue to explore the chemistry of **1** including its photochemistry, which may lead to new germanium compounds with further enhanced photo-induced reactivity.

3.1.5 Experimental Section

3.1.5.1 General Considerations

All experiments were performed under a nitrogen atmosphere using standard Schlenk techniques. Solvents were dried using a column solvent purification system.[19] Commercial KO*t*Bu (97%), ClCOMes (99%), ClCOPh (99%) were used without any further purification. 1,6-Hexanediol diacrylate (HDDA) was purchased from Alfa Aesar and the photoinitiator bis(4-methoxybenzoyl)diethylgermanium (Ivocerin®)[2f] was provided by Ivoclar Vivadent AG.

^{1}H (299.95 MHz), ^{13}C (75.43 MHz) and ^{29}Si (59.59 MHz) NMR spectra were recorded on a Varian INOVA 300 spectrometer in C_6D_6 or $CDCl_3$ solution and referenced versus TMS using the internal ^{2}H-lock signal of the solvent. Tetrakis(trimethylsilyl)germane was prepared according to published procedures[7a]. CIDNP experiments were carried out on a 200 MHz Bruker AVANCE DPX spectrometer equipped with a custom-made CIDNP probe head. A Quantel Nd-YAG Brilliant B Nd:YAG laser (355 nm, ~40 mJ/pulse, pulse length ~8−10 ns) operating at 20 Hz served as the light source. The typical CIDNP timing sequence consists of the following parts: composite pulse presaturation, laser flash, 90° radiofrequency detection pulse (2.2 µs), and FID. Chemical shifts (δ) are reported in ppm relative to tetramethylsilane (TMS) using the residual deuterated solvent signals as an internal reference (CDCN, δH = 1.94 ppm).

HRMS spectra were run on a Kratos Profile mass spectrometer. Infrared spectra were obtained on a Bruker Alpha-P Diamond ATR Spectrometer from the solid sample. Melting points were determined using a Buechi 535 apparatus and are uncorrected. Elemental analyses were carried out on a Hanau Vario Elementar EL apparatus.

UV absorption spectra were recorded on a Perkin Elmer Lambda 5 spectrometer. Photobleaching experiments (steady state photolysis, SSP) were performed on a TIDAS UV-VIS spectrometer (J&M, Germany). 1 mM samples of the photoinitiator in acetonitrile were irradiated from the side in a quartz

cuvette (1 cm x 1 cm) while UV-VIS spectra were recorded. As irradiation light sources, light emitting diodes (LEDs, Roithner Lasertechnik, Vienna) at 470 nm (3.8 cd output power at 20 mA, 30 nm half width), 430 nm (22 mW at 20 mA, 20 nm half width) and 385 nm (11 mW at 20 mA, 15 nm half width) as well as a Bluephase Dentist Lamp (Ivoclar Vivadent, 1200 mW cm^{-2}, λ_{max} at 410 nm and 470 nm).

TR-EPR (Chemically Induced Dynamic Electron Polarization; CIDEP) Spectroscopy was performed using light pulses (355 nm, ~10 mJ/pulse, pulse length ~8 ns) from a InnoLas Spitlight 400 Nd:YAG laser, operating at 20 Hz. A Bruker ESP 300E X-band spectrometer with unmodulated static magnetic field and a LeCroy 9400 dual 125 MHz digital oscilloscope were used to acquire the TR-EPR spectra. Spectra were recorded by acquiring the accumulated (50-100 accumulations) time responses to the incident laser pulses at each magnetic field value of the chosen field range (field steps: 0.1 G). The experimental setup was controlled using fsc2, software developed and kindly provided by J. Toerring (Berlin). Argon-saturated solutions of the samples in toluene (~ 10 mM in photoinitiator concentration) were pumped through a quartz tube (inner diameter 2 mm) positioned in the cavity of the EPR spectrometer using a flow system (flow rate: 2-3 mL min^{-1}). The data were analyzed using the Matlab software.were applied.

Photo DSC measurements were conducted using a Netzsch DSC 204 F1 with autosampler. The monomer HDDA was combined with the respective amounts of photoinitiator (0.15 and 0.30 mol% for **1a,b**; 0.3 and 0.6 mol% for **3a,b** and **8**; 0.3 mol% for **9**) and then the formulations were mixed in an ultra-sonic bath for 30 min at ambient temperature. The prepared formulations were loaded into a photo-DSC and irradiated (~ 20 mW cm^{-2}, 400-500 nm) at 25 °C under inert atmosphere (N_2-flow = 20 mL min^{-1}). All formulations were analyzed in triplicate and each sample was weighed into an open aluminum pan (~ 10 ± 1 mg). After an equilibration phase (4 min) the samples were irradiated for 5 min with filtered UV-light (400-500 nm) from an Exfo OmniCureTM series 2000 at 25 °C under constant nitrogen flow (20 mL min^{-1}). The light intensity was set to 1 W cm^{-2} at the tip of the light guide (~20 mW cm^{-2} on the surface of the sample) and the heat flow of the polymerization reaction was recorded as a function of time. From the theoretical heat of polymerization of the monomer HDDA ($\Delta H_{0,HDDA}$ = 761.92 J g^{-1} or 172.4 kJ mol^{-1}, determined from 86.2 kJ mol^{-1} per acrylate unit[S3]) the double bond conversion (DBC) was calculated by dividing the measured heat of polymerization ΔH through $\Delta H_{0,HDDA}$. The maximum rate of polymerization $R_{p,max}$ was determined using equation 1, with h as the height of the exothermic polymerization signal in mW mg^{-1} and ρ = 1010 g L^{-1} as the density for HDDA at 25 °C.[20]

$$R_{P,max} = \frac{h \cdot \rho}{\Delta H_{0,HDDA}} \qquad (1)$$

3.1.5.2 Synthesis of 1a:

Method A

A solution of $(Me_3Si)_3GeK$ in 10 mL of DME was freshly prepared from 1.00 g $Ge(SiMe_3)_4$ (2.74 mmol) and 0.34 g KO*t*Bu (3.01 mmol) and slowly added to a solution of 2.05 g (11.2 mmol) 2,4,6-trimethylbenzoylfluoride in 15 mL DME. The mixture was stirred for another 12 h. After aqueous work up with 3% sulfuric acid the organic layer was separated, dried over Na_2SO_4 and the solvents evaporated under reduced pressure. The crude product was recrystallized from acetone, giving yellow crystals of **1a**. Yield: 1.6 g (90%) of analytically pure **1b** as yellow crystals.

Method B

A solution of $(Me_3Si)_3GeK$ in 10 mL of DME was freshly prepared from 1.00 g $Ge(SiMe_3)_4$ (2.74 mmol) and 0.34 g KO*t*Bu (3.01 mmol) and slowly added to a 0°C cooled solution of 2.05 g (11.2 mmol) 2,4,6-methylbenzoylchloride and an excess of KF in 15 mL DME. The mixture was stirred for another 12 h. After aqueous work up with 3% sulfuric acid the organic layer was separated, dried over Na_2SO_4 and the solvents evaporated under reduced pressure. The **1a** was recrystallized from acetone. Yield: 1.5 g (83%) of analytically pure **1a** as yellow crystals.

Method C

A solution of $(Me_3Si)_3GeK$ in 20 mL of DME was freshly prepared from 2.77 g $Ge(SiMe_3)_4$ (7.58 mmol) and 0.94 g KO*t*Bu (8.38 mmol) and slowly added to a solution of 1.66 g (0.91 mmol) 2,4,6-trimethylbenzoylchloride in 15 mL DME. The mixture was stirred for another 12 h. After aqueous work up with 3% sulfuric acid the organic layer was separated, dried over Na_2SO_4 and the solvents evaporated under reduced pressure to obtain a product mixture of **1a** and **3a**. **1a** and **3a** were separated by column chromatography (solvent gradient: heptane→toluene). Both products were recrystallized from acetone. Yield: 1.92 g (58%) **3a** and 1.58 g (24%) **1a**.

mp: 198-199 °C. Anal. Found: C, 72.33; H, 6.60 % Calc.: C, 72.64; H, 6.71 %. ^{13}C-NMR ($CDCl_3$, TMS, ppm): 233.40 (*C*=O); 141.60, 139.26, 132.88, 128.53 (Mes-*C*); 21.15, 19.13 (Mes-*C*H_3).^{1}H-NMR ($CDCl_3$, TMS, ppm): 6.57 (s, 2H, Mes-*H*); 2.24 (s, 3H, Mes-C*H*$_3$); 2.06 (s, 6H, Mes-C*H*$_3$). IR (neat): ν(C=O) = 1639, 1608 cm^{-1}. HRMS: calc. 647.2227 for (M^+) found: 647.2192. UV-VIS: λ [nm] (ε [L mol^{-1} cm^{-1}]) = 288 (17428), 376 (1475).

3.1.5.3 Synthesis of 1b:

The procedure followed was that used for **1a** (Method B) with 3.00 g (8.21 mmol) of tetrakis(trimethylsilyl)germane, 1.01 g KO*t*Bu (9.03 mmol) and 4.18 g (33.7 mmol) benzoyl fluoride. Yield: 3.8 g (85%) of analytically pure **1b** as yellow crystals.

mp: 82.5-83 °C. Anal. Found: C, 68.45; H, 4.15 % Calc.: C, 68.20; H, 4.09 %. ^{13}C-NMR (C_6D_6, TMS, ppm): 222.01 (*C*=O); 140.57, 133.81, 129.15, 128.77 (Ph-*C*). ^{1}H-NMR ($CDCl_3$, TMS, ppm): 7.99-7.96 (m, 2H, Ph-*H*); 6.84-6.82 (m, 3H, Ph-*H*). IR (neat): ν(C=O) = 1639, 1617 cm^{-1}. HRMS: calc. 494.0580 for (M^+) found: 494.0534. UV-VIS: λ [nm] (ε [L mol^{-1} cm^{-1}]) = 403 (1240), 419 (1050).

3.1.5.4 Synthesis 3a:

3a was prepared according to Method A with 2.77 g (7.58 mmol) of tetrakis(trimethylsilyl)germane, 0.94 g KO*t*Bu (8.38 mmol) and 1.66 g (9.09 mmol) 2,4,6-trimethyl benzoyl chloride. Yield: 1.92 g of analytically pure **3a (58%)** as yellow crystals.

mp: 83-84 °C. Anal. Found: C, 51.60; H, 8.74 % Calc.: C, 51.94; H, 8.72 %. ^{29}Si-NMR ($CDCl_3$, TMS, ppm): -5.06 (*Si*Me_3). ^{13}C-NMR ($CDCl_3$, TMS, ppm): 247.83 (*C*=O), 147.22, 137.39, 130.15, 128.52 (Mes-*C*), 20.98, 19.32 (Mes-*C*H_3). ^{1}H-NMR ($CDCl_3$, TMS, ppm): 6.75 (s, 3H, Ph-*H*), 2.25 (s, 3H, Mes-C*H*$_3$), 2.15 (s, 6H, Mes-C*H*$_3$), 0.21 (s, 27H, Si(C*H*$_3$)$_3$). IR (neat): ν(C=O) = 1623, 1609. HRMS: calc. 436.1473 for (M^+) found: 436.1476. UV-VIS: λ [nm] (ε [L mol-1 cm-1]) = 363 (296), 378 (407), 396 (382).

3.1.5.5 Synthesis 3b:

3b was prepared according to Method A with 0.74 g (2.03 mmol) of tetrakis(trimethylsilyl)germane, 0.25 g KO*t*Bu (2.23 mmol) and 0.34 g (2.43 mmol) benzoyl chloride. Yield: 0.42 g (52%) of analytically pure **3b** as yellow oil.

Anal. Found: C, 48.42; H, 8.10 % Calc.: C, 48.37; H, 8.12 %. ^{29}Si-NMR ($CDCl_3$, TMS, ppm): -5.12 (*Si*Me_3). ^{13}C-NMR ($CDCl_3$, TMS, ppm): 235.72 (*C*=O), 143.71, 132.40, 128.24, 127.69 (Ph-*C*), 2.06 (Si(*C*H_3)$_3$). ^{1}H-NMR ($CDCl_3$, TMS, ppm): 7.72 (d, 2H, J=8.47, Ph-*H*), 7.45 (m, 3H, Ph-*H*), 0.29 (s, 27H, Si(C*H*$_3$)$_3$). IR (neat): ν(C=O) = 1619, 1591. HRMS: calc. 398.0973 for (M^+) found 398.0932. UV-VIS: λ [nm] (ε [L mol-1 cm-1]) = 414 (236).

3.1.5.6 Steady-State Photolysis (SSP) / UV-Vis Spectroscopy.

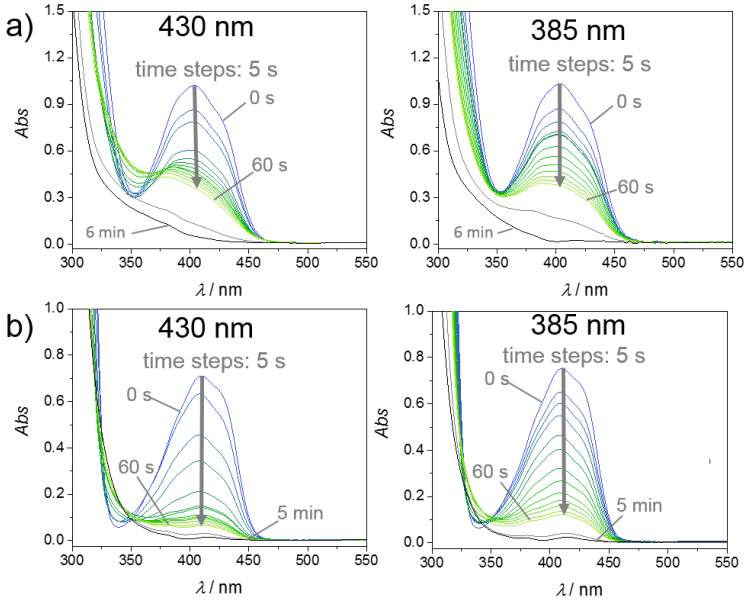

Figure 9. a) SSP of tetrabenzoylgermane **1b** at 430 nm and 385 nm; b) SSP of bisacylgermane Ivocerin® at 430 nm and 385 nm.

3.1.5.7 CIDNP Spectroscopy

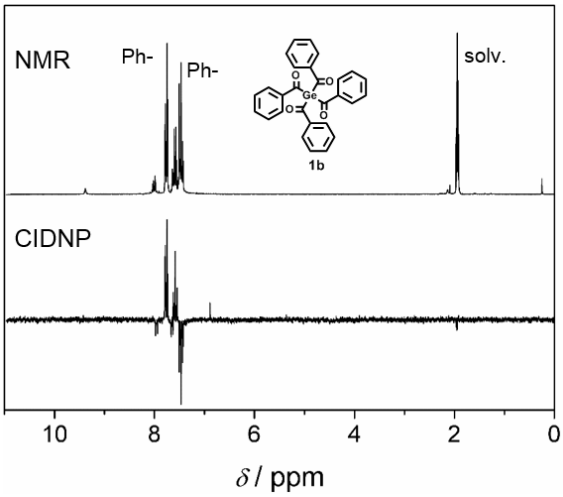

Figure 10. ^{1}H-NMR and CIDNP spectra of **1b** (10 mM solution in acetonitrile-d_3). The signals of the aromatic protons (δ = 7.43-7.82 ppm) of **1b** are polarized; this can be attributed to the (cage) re-formation of **1b**, indicating a partly reversible α-cleavage.

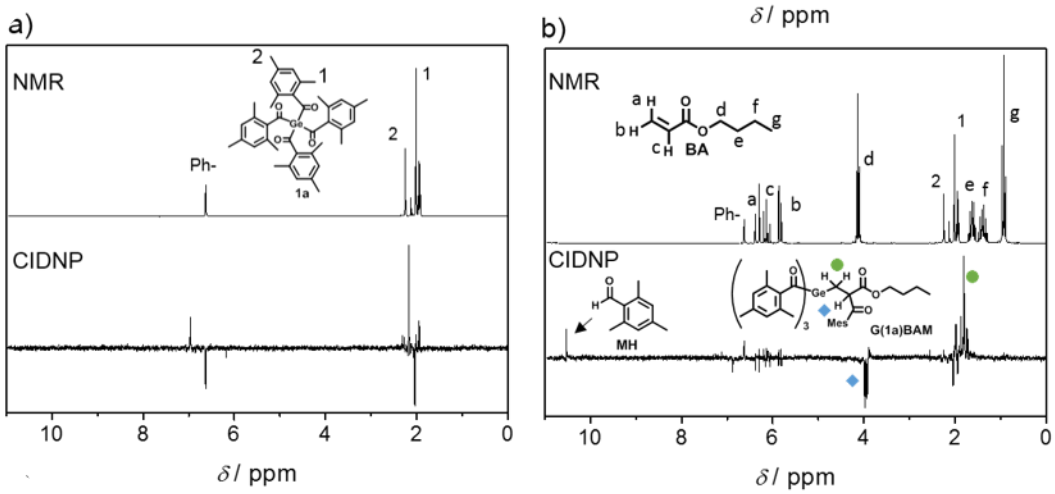

Figure 11. ^{1}H-CIDNP spectra of **1a** (10 mM solution in acetonitrile-d_3) taken in absence (a) and in the presence (b) of butyl acrylate (50 mM).

3.1.5.8 X-ray Crystallography

For X-ray structure analysis suitable crystals were mounted onto the tip of glass fibres using mineral oil. Data collection was performed on a Bruker Kappa Apex II CCD diffractometer at 100 K using graphite-monochromated Mo Kα= 0.71073 Å radiation. The SHELX version 6.1 program package was used for the structure solution and refinement.[21] Absorption corrections were applied using the SADABS program.[22] All non-hydrogen atoms were refined with anisotropic displacement parameters. Hydrogen atoms were included in the refinement at calculated positions using a riding model as implemented in the SHELXTL program. All nonhydrogen atoms of the disordered parts were refined anisotropically and hydrogen atoms were placed on calculated positions. The solvent of crystallization for compound 6a was removed from the refinement by using the "squeeze" option available in the PLATON program suite.[23] Crystallographic data (excluding structure factors) have been deposited with the Cambridge Crystallographic Data Centre as supplementary publications CCDC-1518469 (**1a**), CCDC-1518470 (**1b**), CCDC-1518471 (**6a**). Copies of the data can be obtained free of charge on application to The Director, CCDC, 12 Union Road, Cambridge CB2 1EZ, UK (fax (internat.) +44-1223/336-033; e-mail: deposit@ccdc.cam.ac.uk).

3.1.5.9 Computational Section

All computational studies were executed on a computing cluster with blade architecture using the Gaussian09 software package.[24] Geometry optimizations were performed in the gas phase with B3LYP as hydride density functional[25] together with the 6-31G(d) split-valence basis set for all atoms.[26] Minimum structures were characterized by harmonic frequency calculations, yielding none imaginary frequency. Vertical excitations were calculated via time-dependent DFT (TD-DFT) at the CAM-B3LYP/def2-TZVP level of theory[27] and solvent effects were considered by applying the polarized continuum model (PCM).[28] Acetonitrile (MeCN) was used as a solvent with a dielectric constant of ε = 35.688. All gained vertical excitation energies were manually corrected by 3 %, as PCM(MeCN) TD-DFT CAM-B3LYP/def2-TZVP//B3LYP/6-31G(d) overestimated the excitation energies for this substance class systematically.[11] If not explicitly mentioned, all structures and molecular orbitals (isovalues of 0.025) were plotted using the Gabedit software package.[29]

3.1.6 References

[1] a) J.-P. Fouassier, F. Morlet-Savary, J. Lalevée, X. Allonas, C. Ley, *Materials (Basel, Switzerland)* **2010**, *3*, 5130; b) Y. Yagci, S. Jockusch, N. J. Turro, *Macromolecules* **2010**, *43*, 6245; c) K. Dietliker in *A compilation of photoinitiators*. *Commercially available for UV today*, SITA Technology Ltd, Edinbergh, London, **2002**; d) K. Dietliker, T. Jung, J. Benkhoff, H. Kura, A. Matsumoto, H. Oka, D. Hristova, G. Gescheidt, G. Rist, *Macromol. Symp.* **2004**, *217*, 77; e) J. P. Fouassier, J. F. Rabek in *Radiation curing in polymer science and technology*, Elsevier Applied Science, London, **1993**; f) J. P. Fouassier, J. Lalevée in *Photoinitiators for Polymer Synthesis*, Wiley-VCH Verlag GmbH & Co. KGaA, Weinheim, Germany, **2012**.

[2] a) V. Y. Lee, A. Sekiguchi in *Organometallic compounds of low-coordinate Si, Ge, Sn and Pb*. *From phantom species to stable compounds*, Wiley, Oxford, **2010**; b) D. Neshchadin, A. Rosspeintner, M. Griesser, B. Lang, S. Mosquera-Vazquez, E. Vauthey, V. Gorelik, R. Liska, C. Hametner, B. Ganster, R. Saf, N. Moszner, G. Gescheidt, *J. Am. Chem. Soc.* **2013**, *135*, 17314; c) J. Lalevée, X. Allonas, J. P. Fouassier, *Chem. Phys. Lett* **2009**, *469*, 298; d) B. Ganster, U. K. Fischer, N. Moszner, R. Liska, *Macromolecules* **2008**, *41*, 2394; e) N. Moszner, U. K. Fischer, B. Ganster, R. Liska, V. Rheinberger, *Dent. Mater.* **2008**, *24*, 901; f) N. Moszner, F. Zeuner, I. Lamparth, U. K. Fischer, *Macromol. Mater. Eng.* **2009**, *294*, 877; g) Y. Catel, U. Fischer, P. Faessler, N. Moszner, *Macromol. Chem. Phys.* **2016**, *217*, 2686.

[3] a) H. Grützmacher, J. Geier, D. Stein, T. Ott, H. Schönberg, R. H. Sommerlade, S. Boulmaaz, J.-P. Wolf, P. Murer, T. Ulrich, *Chimia* **2008**, *62*, 18; b) L. Gonsalvi, M. Peruzzini, *Angew. Chem. Int. Ed.* **2012**, *51*, 7895; c) W. Feuerstein, S. Höfener, W. Klopper, I. Lamparth, N. Moszner, C. Barner-Kowollik, A.-N. Unterreiner, *Chemphyschem* **2016**, *17*, 3460; d) R. Appel, G. Haubrich, F. Knoch, *Chem. Ber.* **1984**, *117*, 2063.

[4] a) Safety Data sheet of Phenylbis(2,4,6-trimethylbenzoyl)phosphine oxide.; b) Safety Data sheet of Bis(4-methoxybenzoyl)diethylgermane.

[5] E. J. Corey, D. Seebach, *Angew. Chem. Int. Ed.* **1965**, *4*, 1075.

[6] J. Hlina, C. Mechtler, H. Wagner, J. Baumgartner, C. Marschner, *Organometallics* **2009**, *28*, 4065.

[7] a) A. G. Brook, F. Abdesaken, H. Söllradl, *J. Organomet. Chem.* **1986**, *299*, 9; b) J. Fischer, J. Baumgartner, C. Marschner, *Organometallics* **2005**, *24*, 1263.

[8] a) M. L. Amadoruge, C. S. Weinert, *Chem. Rev.* **2008**, *108*, 4253; b) K. M. Baines, W. G. Stibbs, *Coord. Chem. Rev.* **1995**, *145*, 157.

[9] a) B. K. Hunters, L. W. Reeves, *Can. J. Chem.* **1968**, *46*, 1399; b) J. Schraml, V. Chvalovsky, H. Jancke, G. Engelhardt, *Org. Magn. Reson.* **1977**, *9*, 237.

[10] M. Haas, M. Leypold, D. Schnalzer, A. Torvisco, H. Stueger, *Organometallics* **2015**, *34*, 5291.

[11] T. M. Maier, H. Bahmann, A. V. Arbuznikov, M. Kaupp, *J. Chem. Phys.* **2016**, *144*, 074106/1-074106/14.

[12] S. Jockusch, I. V. Koptyug, P. F. McGarry, G. W. Sluggett, N. J. Turro, D. M. Watkins, *J. Am. Chem. Soc.* **1997**, *119*, 11495.

[13] S. Jockusch, M. S. Landis, B. Freiermuth, N. J. Turro, *Macromolecules* **2001**, *34*, 1619.

[14] M. Haas, L. Schuh, A. Torvisco, H. Stueger, C. Grogger, *Phosphorus, Sulfur, and Silicon Relat. Elem.* **2016**, *191*, 638.

[15] For the sake of clarity the relatively simple HOMO and LUMO of 8 were chosen. Compounds 1, 3, and 9 have frontier orbitals with identical character (see the Supporting Information).

[16] I. Gatlik, P. Rzadek, G. Gescheidt, G. Rist, B. Hellrung, J. Wirz, K. Dietliker, G. Hug, M. Kunz, J.-P. Wolf, *J. Am. Chem. Soc.* **1999**, *121*, 8332.

[17] a) U. Kolczak, G. Rist, K. Dietliker, J. Wirz, *J. Am. Chem. Soc.* **1996**, *118*, 6477; b) M. Griesser, D. Neshchadin, K. Dietliker, N. Moszner, R. Liska, G. Gescheidt, *Angew. Chem. Int. Ed.* **2009**, *48*, 9359.

[18] A. Yurkovskaya, O. Morozova, G. Gescheidt in *Encyclopedia of Radicals in Chemistry, Biology, and Materials* (Eds.: C. Chatgilialoglu, A. Studer), John Wiley & Sons, Chichester, West Sussex, Hoboken, N.J., **2012**.

[19] A. B. Pangborn, M. A. Giardello, R. H. Grubbs, R. K. Rosen, F. J. Timmers, *Organometallics* **1996**, *15*, 1518.

[20] G. Ullrich, B. Ganster, U. Salz, N. Moszner, R. Liska, *J. Polym. Sci. A Polym. Chem.* **2006**, *44*, 1686.

[21] SHELX and SHELXL PC: VERSION 5.03, Bruker AXS, Inc., Madson, WI, 1994.

[22] Bruker AXS in *SADABS: Area-Detection Absorption Correction*, **1995**.

[23] a) P. van der Sluis, A. L. Spek, *Acta Cryst.* **1990**, *46*, 194; b) A. L. Spek, *Acta crystallographica. Section C, Structural chemistry* **2015**, *71*, 9.

[24] M. J. Frisch, G. W. Trucks, H. B. Schlegel, G. E. Scuseria, M. A. Robb, J. R. Cheeseman, G. Scalmani, V. Barone, B. Mennucci, G. A. Petersson, H. Nakatsuji, M. Caricato, X. Li, H. P. Hratchian, A. F. Izmaylov, J. Bloino, G. Zheng, J. L. Sonnenberg, M. Hada, M. Ehara, K. Toyota, R. Fukuda, J. Hasegawa, M. Ishida, T. Nakajima, Y. Honda, O. Kitao, H. Nakai, T. Vreven, Montgomery, Jr. J., A., J. E. Peralta, F. Ogliaro, M. Bearpark, J. J. Heyd, E. Brothers, K. N. Kudin, N. Staroverov, T. V. Keith, R. Kobayashi, J. Normand et al. in *Gaussian 09, Revision D.01, Gaussian, Inc.: Wallingford, CT*, **2013**.

[25] a) A. D. Becke, *J. Chem. Phys.* **1993**, *98*, 1372; b) C. Lee, W. Yang, R. G. Parr, *Phys. Rev. B: Condens. Matter Mater. Phys.* **1988**, *37*, 785.

[26] a) P. C. Hariharan, J. A. Pople, *Theoret. Chim. Acta* **1973**, *28*, 213; b) W. J. Hehre, R. Ditchfield, J. A. Pople, *J. Chem. Phys.* **1972**, *56*, 2257; c) R. Ditchfield, W. J. Hehre, J. A. Pople, *J. Chem. Phys.* **1971**, *54*, 724.

[27] a) T. Yanai, D. P. Tew, N. C. Handy, *Chem. Phys. Lett* **2004**, *393*, 51; b) F. Weigend, R. Ahlrichs, *Phys. Chem. Chem. Phys.* **2005**, *7*, 3297.
[28] J. Tomasi, B. Mennucci, R. Cammi, *Chem. Rev.* **2005**, *105*, 2999.
[29] A.-R. Allouche, *J. Comput. Chem.* **2011**, *32*, 174.

3.2 Synthesis, Spectroscopic Behavior, and Photoinduced Reactivity of Tetraacylgermanes

Judith Radebner,† Mario Leypold,† Anna Eibel,‡ Janine Maier,† Lukas Schuh,† Ana Torvisco,† Roland Fischer,† Norbert Moszner,§ Georg Gescheidt,‡ Harald Stueger,† Michael Haas†*

†Institute of Inorganic Chemistry and ‡Institute of Physical and Theoretical Chemistry, Graz University of Technology, Stremayrgasse 9, A-8010 Graz, Austria

§Ivoclar Vivadent AG, Bendererstraße 2, FL-9494 Schaan, Liechtenstein

published in *Organometallics*, **2017**, 36, 3624-3632.

Graphical Abstract:

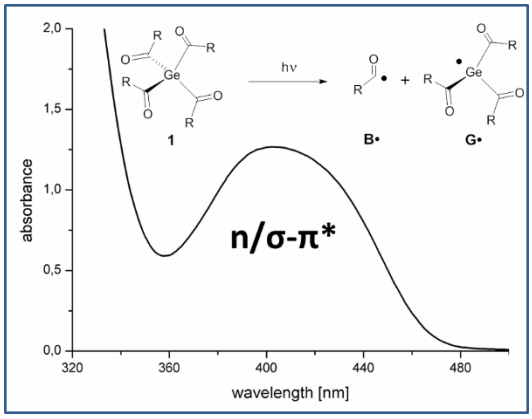

3.2.1 Abstract

Acylgermanes have been subject of great interest recently because of their low toxicity and the applicability as sources for germanium-centered radical for visible-light induced free radical polymerization processes. We report on a novel and versatile method for the synthesis of tetraacylgermanes allowing the preparation of various tetra-substituted acylgermanes **1a**-**m**. The formation of these derivatives was confirmed by NMR spectroscopy, mass spectrometry, and X-ray crystallography. UV-Vis absorption spectra of the prepared compounds reveal absorption in the visible region. This transition was assigned by TD-DFT calculations. It enabled a general screening of the influence of different substitution patterns on the absorption properties. The radical formation upon irradiation was confirmed by TR-EPR spectroscopy.

3.2.2 Introduction

Over the past few years acylgermanes have emerged as promising scaffolds for radical photo-polymerization processes.[1] Contrary to acylsilanes, the germanium analogues tend to cleave via Norrish type-I pathways, opening up possible applications as germanium-centered radical acceptor synthons (see Chart 1).[2,3]

Chart 1. Mechanism of Norrish Type I and Norrish Type II Reaction.

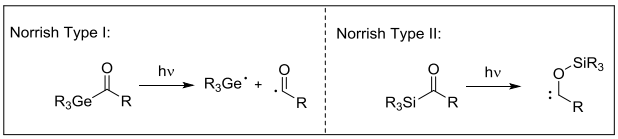

Historically speaking, the preparation of acylgermanes was mainly triggered by the need of substrates for spectroscopic studies on acyl-group 14 metal compounds.[4] Thus, the number of literature reports on acylgermanes remained modest. The most common method for acylgermane synthesis is the reaction of metallogermanes with carboxylic acid derivatives, i.e. acid chlorides[5], amides[6] and esters (Chart 2, method A).[7] The first synthesis of acylgermanes achieved by Brook *et al*. proceeded via hydrolysis of α,α-dibromoalkylgermanes.[8] Based on the findings of Corey and Seebach this approach was revised by exploiting the hydrolysis of 1,3-dithiane masked carbonyl systems to generate monoacylgermanes (Chart 2, method B) .[9,10] Yamamoto et. al. achieved the synthesis of acylgermanes via a Pd-catalyzed acylation of hexamethyldigermane (Chart 2, method C).[11] Another common method is the hydrolysis of germyl enol ethers, giving α,β-unsaturated acylgermanes (Chart 2, method D).[12] In analogy to monoacylgermanes, di- and triacylgermanes are synthesized by the reaction of aryl acid chlorides with germyllithiums of the form Ar_2HGeLi[13] or ArH_2GeLi (Chart 2, method A).[14] Only a few years ago, Moszner *et al*. adapted Brook's dithiane route in order to prepare diacylgermanes (Chart 2, method B).[15] Recently our group reported on the preparation of the – so far – unknown tetraacylgermanes.[16]

Chart 2. Synthetic Methods Towards Acylgermanes.

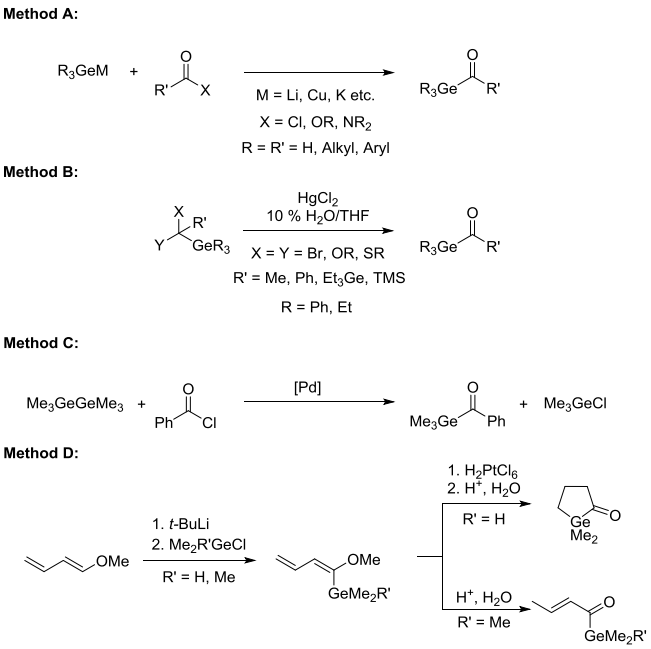

Promoted by their outstanding optical absorption properties and the ability to undergo efficient homolytic bond cleavage upon irradiation, tetraacylgermanes have become of substantial interest in the field of photoinitiating systems.[16] Supported by the low toxicity and sufficient absorption in the visible region, tetraacylgermanes are highly promising alternatives to the frequently applied phosphorus-based photoinitiator (PI) systems (for the preparation of dental fillings, 3D-printing or coatings). Herein, we report on the synthesis and characterization of a series of previously unknown tetraacylgermanes **1a**-**m**. The aim of this study was to induce a more pronounced bathochromic shift of the longest wavelength absorption (n/σ-π* transition) upon targeted functionalization. Moreover, detailed experimental and computational studies of the UV absorption properties are presented along with time-resolved EPR investigations of selected molecules.

3.2.3 Results and Discussion

3.2.3.1 Synthesis of Tetraacylgermanes

The reaction sequence used for the preparation of the tetraacylgermanes **1a**-**m** is depicted in Scheme 1. The air-stable, yellow and crystalline target compounds were obtained in isolated yields >80% when $KGe(SiMe_3)_3$ (**2K**) was reacted with 4.1 molar equivalents of the corresponding acid fluoride. **2K** is easily accessible from $Ge(SiMe_3)_4$ and KO*t*Bu as previously reported.[17]

Scheme 1. Synthesis of tetraacylgermanes **1a**-**m**.

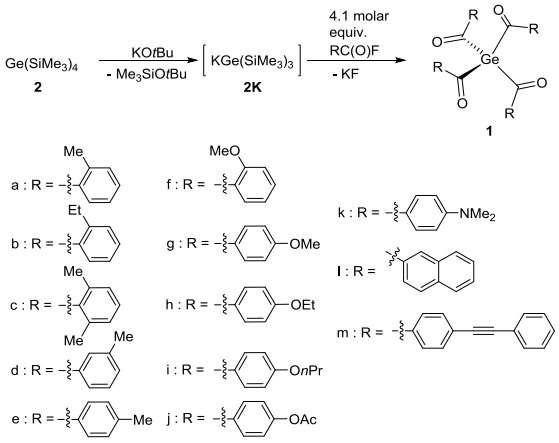

The multiple abstraction of silyl groups from **2K** by fluorinated reagents was observed by Marschner *et al*. and later by our group.[18] In this context, we now report on a series of tetraacylgermanes. So far, the method turns out to be restricted to derivatives containing either unsubstituted aromatic rings or aryl groups with electron-donating (EDG) substituents. Up to now, we have not observed tetraacylgermane formation when acid fluorides carrying electron-withdrawing (EWG; e.g. bromo-, chloro-, iodo- and cyano-substituted acid fluorides) groups at the aromatic ring were used.

This restriction arises from the impact of the substituents on the electronic nature of the carbonyl C-atom. In contrast to electron-donating groups, electron-withdrawing groups reduce the electron density at the carbonyl C-atom, which is also reflected in the Hammett parameters.[19] Hence, the decreased electron density at the carbonyl C-atom most probably enables the concurring nucleophilic attack of either *tert*-butanolate or fluoride anion, which leads to the degradation of the intermediary formed tetraacylgermane.

3.2.3.2 NMR-Spectroscopy

Analytical and spectroscopic data obtained for **1a**-**m** are consistent with the proposed structures. NMR spectra and detailed assignments are provided in the Experimental Section and in the *Supporting Information*. All derivatives show very similar ^{13}C chemical shifts for the carbonyl C-atom between δ = 219.3 and 233.1 ppm, which is characteristic for carbonyl groups directly linked to a germanium atom.[16,20]

3.2.3.3 X-ray-Crystallography

Crystals suitable for single-crystal X-ray diffraction analysis were obtained for compounds **1a**-**c** and **1e-l**. Table 1 summarizes selected bond lengths and bond angles along with the torsion angles between the C=O groups and the aromatic ring planes. As two representative examples, the molecular structures of **1c** (large torsion angle) and **1e** (small torsion angle) are depicted in Figures 1 and 2. All other structures are included in the *Supporting Information*.

Table 1. Selected bond lengths d [Å], bond angles and torsion angles [deg] of compounds **1a**-**c**,**e**-**l**.

	d Ge-C (mean)	d C-O (mean)	∠C-Ge-C (mean)	∠O-C-C_{Ph}-C_{Ph}
1a	2.035	1.214	108.11	37.2
1b	2.030	1.214	106.85	37.8
1c	2.050	1.211	111.65	61.6
1e	2.021	1.219	104.75	15.3
1f	2.011	1.227	112.89	17.4
1g	2.012	1.227	104.79	15.5
1h	2.018	1.227	100.38	17.4
1i	2.021	1.216	110.68	10.9
1j	2.011	1.214	105.00	3.2
1k	2.023	1.231	104.51	3.2
1l	2.019	1.221	108.18	4.8

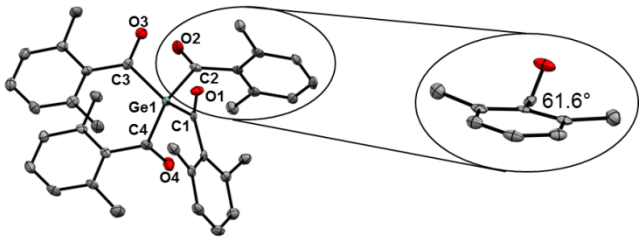

Figure 1. ORTEP representation of **1c**. Thermal ellipsoids are depicted at the 50% probability level. Hydrogen atoms are omitted for clarity. The torsion angle (mean value) between the C=O group and the aromatic ring plane is shown in the magnified part.

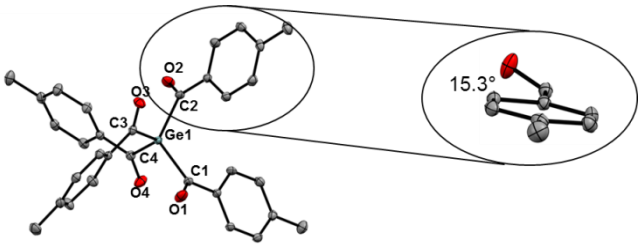

Figure 2. ORTEP representation of **1e**. Thermal ellipsoids are depicted at the 50% probability level. Hydrogen atoms are omitted for clarity. The torsion angle (mean value) between the C=O group and the aromatic ring plane is shown in the magnified part.

Structural data are in accordance with literature values of other acyl germanium compounds.[16,20,21] The mean Ge-C bond distances are considerably elongated relative to the average Ge-C bond length of 1.97 Å.[22] Likewise, the mean C=O bond lengths between 1.21-1.23 Å are also slightly elongated compared to the average C=O double bond length of 1.19 Å.[23] This deviation originates probably from steric repulsion effects.

3.2.3.4 UV/Vis Spectroscopy

To further elucidate substituent effects on the absorption behavior of tetraacylgermanes UV−Vis absorption spectra of **1a**-**m** were recorded. They exhibit the longest-wavelength absorptions between 374 and 407 nm (ε ~1500 mol·L^{-1}·cm^{-1}) tailing well into the visible region, as well as additional bands in the UV region with much higher intensity. Similar absorption properties were observed earlier for other aryl acylsilanes and -germanes.[24] Comparable but strongly blue shifted absorptions were also observed for simple aryl ketones.[25] Comparison of the extinction coefficients, furthermore, demonstrates that the absorption of the silyl- and germyl-derivatives is by far the more intense.

The longest wavelength absorption band together with its energetically ensuing were computationally assigned via PCM(MeCN) TD-DFT CAM-B3LYP/def2-TZVP//B3LYP/6-31+G(d,p). We observed that the absorption bands of mono- and tetraacylgermanes do not vary significantly.[16] Therefore, we used acyltrimethylgermanes instead of tetraacylgermanes to reduce the complexity of the simulated system.

The experimental values for **1a**-**m** and computational data of the respective trimethylgermanes are summarized in Table 2 and show reasonable agreement. The longest wavelength absorption bands feature HOMO/LUMO (**1a-f**, **1j**) or HOMO-1/LUMO transition (**1g-i**, **1k-m**), respectively, with considerable charge transfer character. Upon excitation, electron density is displaced from the n(C=O)/σ(Ge-C) bonding orbital (either HOMO or HOMO-1) into the π*(C=O/Aryl) antibonding LUMO. Consecutive bands were computationally assigned as π/π^* transitions. Herein, electron density is displaced from the π (C=O/Aryl) (either HOMO, HOMO-1 or HOMO-2) into the π^*(C=O/Aryl) (either LUMO or LUMO+1)

depending on the functional group that is attached to the aromatic ring system. Depicted π / π^* transitions are summarized in Table 2. In addition, simulations of the calculated UV/Vis spectra can be found in the *Supporting Information*.

n/σ-π* Transition. The experimental UV-Vis absorption spectra of **1a**-**m** are depicted in Figures 3-6. For better clarity, the UV-Vis spectra of 1a-m are separated according to the substitution pattern at the aromatic system. Figure 3 shows all alkyl-substituted tetraacylgermanes. Figure 4 illustrates all alkoxy-substituted derivatives. In comparison to alkoxy-substitution, alkyl-substitution results in a decreased extinction coefficient and a more pronounced tailing of the absorption band into the visible region. Di-*ortho*-substitution induces a significant hypsochromic shift confirming the close relationship between bathochromic shift of λ_{max} and the torsion angle γ. The absorption band for **1j** deviates from all other compounds as the acetoxy-substituent is a weaker electron-donating group than alkyl- and alkoxy substituents leading to a bathochromic shift and a significantly decreased extinction coefficient.

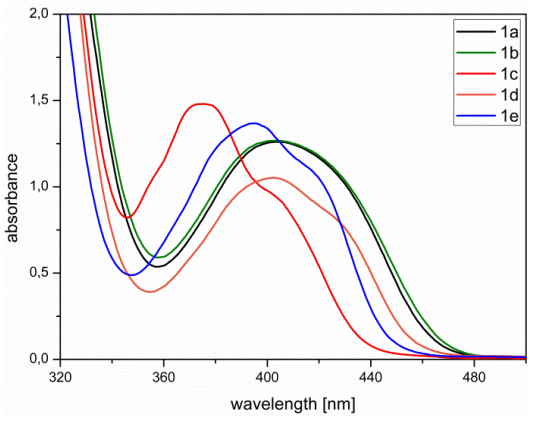

Figure 3. UV-Vis absorption spectra of **1a**-**e** (acetonitrile solution, c = 10^{-3} mol•L^{-1})

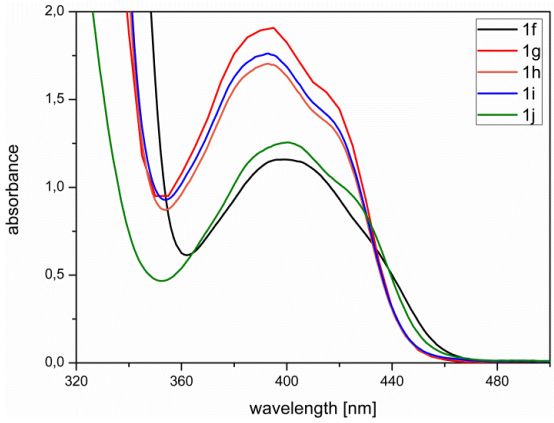

Figure 4. UV-Vis absorption spectra of **1f**-**j** (acetonitrile solution, c = 10^{-3} mol•L^{-1})

The most striking feature associated with the n/σ-π* transition in substituted tetracylgermanes is the shift of the absorption edge. The *ortho*-alkyl substituted compounds **1a**,**b** show a significant bathochromic shift of the absorption edge compared to *meta*-(**1d**) and *para*-(**1e**). We assume that *ortho* substitution reduces the symmetry within the molecule giving more fine structures. Consequently, a broadening of the n/σ-π* absorption band is observed (Figure 5). The same holds true for *meta*- substitution but due to a lower extinction coefficient the effect is not as pronounced. Regarding the possible applications as visible light photoinitiators of **1**, this tailing of the absorption is crucial. The pushing of the "edge" enables effective photopolymerization with **1a**,**b** upon irradiation with conventional LED sources emitting at 450 nm.

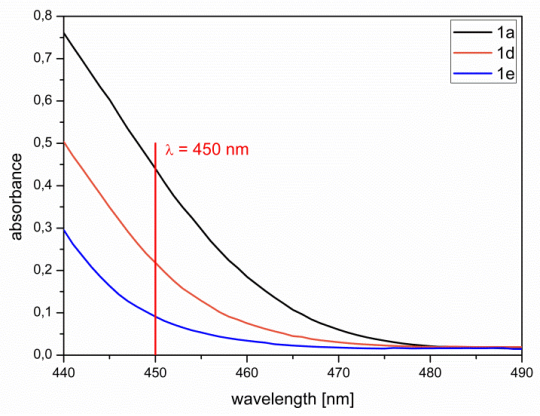

Figure 5. Tailing into visible region of **1a**,**d** and **e** (acetonitrile solution, c = 10^{-3} mol•L^{-1}). Red line resembles harmless light source for curing processes emitting at 450 nm.

In Figure 6 two selected examples of tetraacylgermanes with an elongated π-system and one amino-substituted derivative are shown. A common feature of **1k**-**m** is the overlapping of the π/π* transition with the n/σ-π* transition. Thus, the experimental values for λ_{max} cannot be determined. In order to illustrate both transitions, two different concentrations are depicted. From the tailing of the absorption bands into the visible region (dashed lines), one can state that λ_{max} is red-shifted in comparison to **1a-j**. This experimental observation is also confirmed by the results of TD-DFT calculations and the fact that elongated π-systems lead to a bathochromic shifted absorption. Notably, the amino-functionality, which can be regarded as a strong electron-donating group, causes a significant bathochromic shift of the π/π*-transition, resulting in a nearly complete overlap of these two transitions. Thus, we also examined the π/π*-transition in detail.

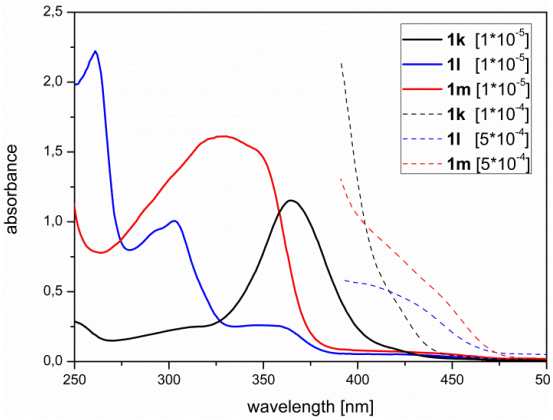

Figure 6. UV-Vis absorption spectra of **1k**-**m** (acetonitrile solution)

π /π* Transition. The π-π* bands of **1a-m** are more affected by the substitution at the aromatic ring than the n/σ - π * transition. This influence on π-π*-transitions was well described for organic compounds by Woodward and Fieser.[26] In general, substitution of an aromatic system with EWGs decreases the energy of the LUMO, whereas EDG substitution increases the energy of the HOMO leading to a bathochromic shift of the π-π* transition. Moreover, di-substitution with an EWG and EDG results in an intramolecular charge-transfer (ICT).[27] As acylgermanes carry an electron-withdrawing group (acyl) as well as an electron donating group (alkyl, alkoxy etc.) within one molecule this effect is even more pronounced. Figure 7 illustrates three selected examples, representing a strong electron-donating group (**1k**), a weak electron withdrawing group (**1j**) and the unsubstituted derivative.

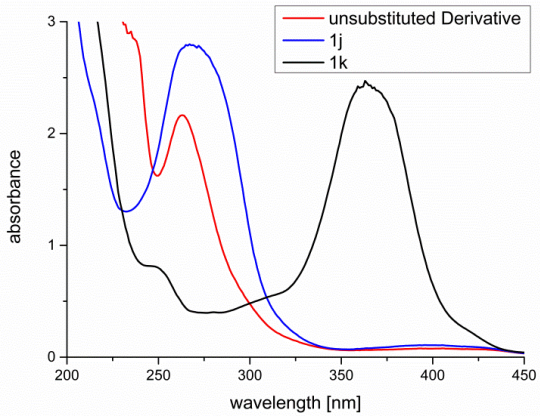

Figure 7. π-π*-Absorption bands of tetraacylgermanes **1j**, **1k** and the unsubstituted derivative (acetonitrile solution, c = 5•10^{-5} mol•L^{-1})

Table 2. Experimental and PCM(MeCN) TD-DFT CAM-B3LYP/def2-TZVP//B3LYP/6-31+G(d,p) calculated Wavelength Absorption Maxima λ [nm], Extinction Coefficients ϵ [$dm^2 \cdot mol^{-1}$] and Oscillator Strengths f for **1a**-**l** (acetonitrile) and **1m** (chloroform).

	λ_{max},exp (ϵ)	λ_{max},calc (f)	Assignment	$\lambda_{\pi\text{-}\pi^*}$,exp (ϵ)	$\lambda_{\pi\text{-}\pi^*}$,calc (f)[28]	Assignment
1a	407 (1266)	412 (0.0021)	n/σ-π*(CO/Aryl)	295 (12014), 262 (31340)	270 (0.0738), 247 (0.3057)	π(CO/Aryl)-π*(CO/Aryl)
1b	407 (1258)	415(0.0021)	n/σ-π*(CO/Aryl)	298 (17048), 263(42300)	271(0.0899), 248 (0.3010)	π(CO/Aryl)-π*(CO/Aryl)
1c	374 (1477), 403sh (954)	383 (0.0025)	n/σ-π*(CO/Aryl)	282 (12420), 234 (15180)	256 (0.0393), 249 (0.0155)	π(CO/Aryl)-π*(CO/Aryl)
1d	402 (1058)	407 (0.0022)	n/σ-π*(CO/Aryl)	299 (12014), 263 (43840)	272(0.0380), 252 (0.3367)	π(CO/Aryl)-π*(CO/Aryl)
1e	400 (1377), 422sh (1113)	402 (0.0023)	n/σ-π*(CO/Aryl)	272 (54720)	262 (0.0164), 259 (0.4668)	π(CO/Aryl)-π*(CO/Aryl)
1f	400 (1160)	413 (0.0022)	n/σ-π*(CO/Aryl)	318 (24760), 257 (48700)	294 (0.1841), 244 (0.1782)	π(CO/Aryl)-π*(CO/Aryl)
1g	395 (1897), 413sh (1556)	395 (0.0025)	n/σ-π*(CO/Aryl)	303 (51960); 228 (35800)	274 (0.5168), 259 (0.0071)	π(CO/Aryl)-π*(CO/Aryl)
1h	392 (1708), 415sh (1362)	393 (0.0025)	n/σ-π*(CO/Aryl)	304 (53900), 227 (34740)	272 (0.5635), 259 (0.0099)	π(CO/Aryl)-π*(CO/Aryl)
1i	393 (1765), 414sh (1396)	393 (0.0024)	n/σ-π*(CO/Aryl)	304 (56340), 227 (42460)	272(0.5784), 259 (0.0099)	π(CO/Aryl)-π*(CO/Aryl)
1j	400 (1262), 422sh (992)	405 (0.0023)	n/σ-π*(CO/Aryl)	268 (46600), 214 (56100)	263 (0.5666), 259 (0.0191)	π(CO/Aryl)-π*(CO/Aryl)
1k	*	385 (0.0026)	n/σ-π*(CO/Aryl)	364 (24940), 250 (115100)	310 (0.7111), 277 (0.0428)	π(CO/Aryl)-π*(CO/Aryl)
1l	*	415 (0.0021)	n/σ-π*(CO/Aryl)	346 (26130), 295 (99190), 250(220500)	322 (0.1089), 291(0.0917), 247 (1.2364)	π(CO/Aryl)-π*(CO/Aryl)
1m	*	419 (0.0020)	n/σ-π*(CO/Aryl)	327 (160700)	329 (1.3723), 275 (0.0171)	π(CO/Aryl)-π*(CO/Aryl)

* could not be detected because of overlap with π-π* transition

3.2.3.5 Time Resolved EPR Spectroscopy

We studied the photocleavage reactions of the new tetraacylgermane derivatives using time-resolved EPR (TR-EPR) spectroscopy. With its excellent time resolution (~ 50 ns) and rather high sensitivity based on the CIDEP effect (chemically induced dynamic electron polarization), TR-EPR allows the detection and characterization of primary radicals formed upon irradiation of **1a**-**m**.[1a,16,29] The TR-EPR spectrum (Figure 8) obtained upon laser-flash photolysis of **1g** reveals a germyl and a benzoyl-type radical (G• and B•). These radicals are formed upon intersystem crossing (ISC) from the excited singlet to the triplet-state followed by an *α*-cleavage (Norrish type I reaction, Scheme 2).

Scheme 2. Photocleavage of tetraacylgermanes 1 leading to the formation of benzoyl-type and germyl radicals.

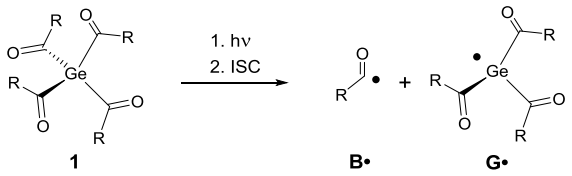

The spectrum shown in Figure 8 consists of two signals in absorption, assigned to the germyl radical **G**(**1g**)• (g = 2.001) and the *para*-methoxy benzoyl radical **B**(**1g**)• (g = 2.000). The signal of **B**(**1g**)• appears as a singlet shortly after the laser pulse (Figure 8). At later observation times (> 400 ns), this signal appears as a triplet with a hyperfine coupling constant of 0.1 mT, deriving from the two equivalent hydrogen atoms in *ortho*-position to the carbonyl radical center (see *Supporting Information*).

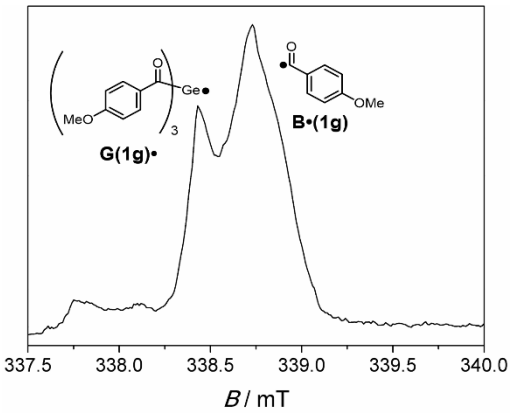

Figure 8. TR-EPR spectrum recorded 200-400 ns after laser-flash photolysis (355 nm) of an argon-saturated solution of **1g** in toluene (concentration: 10 mM).

An analogous photocleavage reaction has been observed for **1a** (compare *Supporting Information*).

3.2.4 Conclusion

In summary, we have reported the synthesis of several tetraacylgermanes **1a**-**m**. The robust reaction protocol allowed the preparation of differently substituted acylgermanes. These compounds were characterized by UV-Vis-, NMR spectroscopy, X-ray analysis and mass spectrometry. X-ray analysis of the prepared compounds highlighted the torsion angle γ as an important structural feature, as it influences the n/σ-π* transition. The combination of TD-DFT calculations and experimental data revealed that the absorption behavior is strongly influenced by the substitution pattern at the aromatic ring system. By TR-EPR measurements the formation of radicals upon photolysis could be detected. We could demonstrate that *ortho*-substitution induces a significant bathochromic shifted absorption edge, which is of major importance regarding the use as visible-light PIs. We will continue to investigate the photochemistry of these compounds and their applicability as promising photoinitiators for free-radical polymerization processes.

3.2.5 Experimental Section

3.2.5.1 General Considerations

All reagents were purchased from commercial sources and used as received. All air-sensitive compounds were prepared and handled using standard Schlenk techniques. Solvents were dried using a column solvent purification system.[30] ^{1}H (299.95 MHz), ^{13}C (75.43 MHz) were recorded on a Varian INOVA 300 spectrometer and referenced versus TMS using the internal ^{2}H-lock signal of the solvent. Tetrakis(trimethylsily)german and acid fluorides (avoid direct contact with skin) were synthesized according to published procedures.[31] HRMS spectra were run on a Kratos Profile mass spectrometer equipped with a solid probe inlet. Infrared spectra were obtained on a Bruker Alpha-P Diamond ATR spectrometer form the solid sample. Melting points were determined using a Büchi 535 apparatus and are uncorrected. Elemental analyses were conducted on a Hanau Vario Elementar EL apparatus, UV absorption spectra were recorded on a PerkinElmer Lambda 5 spectrometer.

3.2.5.2 Synthesis of 1a

1.94 g of tetrakis(trimethylsilyl)germane (5.31 mmol) and 0.66 g (5.84 mmol) of KO*t*Bu were dissolved in 20 mL DME. After stirring for 60 min, this solution was slowly added to a solution of 3.00 g (21.7 mmol) 2-methylbenzoyl fluoride in 10 mL DME. Subsequently, the mixture was stirred for a further 12h. After aqueous workup with 50 mL saturated NH_4Cl, the organic layer was separated, the aqueous layer three times extracted with dichloromethane. The combined organic phases were dried over Na_2SO_4, filtered and the volatile components removed *in vacuo*. The crude product was recrystallized from acetone yielding 2.4 g (4.35 mmol, 82%) of analytical pure **1a** as yellow crystals. Mp: 123-125°C. Anal. Calc. for $C_{32}H_{28}GeO_4$: C, 69.98; H, 5.14. Found: C, 69.94; H, 5.03. ^{13}C NMR ($CDCl_3$, TMS, ppm): 225.35 (GeC=O), 139.81, 137.24, 133.17, 132.07, 131.88, 125.89 (Aryl-C), 20.96 (*o*-Tol-CH_3). ^1H NMR ($CDCl_3$, TMS, ppm): 7.66 (d, 1H, *o*-Tol-H), 7.12 (d, 1H, *o*-Tol-H), 7.25 (m, 2H, *o*-Tol-H), 2.42 (s, 3H, *o*-Tol-CH_3). IR (neat): ν(C=O) 1635, 1595 (m) cm^{-1}. HRMS: calc. for $[C_{32}H_{28}GeO_4]^+$ (M^+) 550.1207; Found 550.1223. UV-vis: λ [nm] (ε [$L \cdot mol^{-1} \cdot cm^{-1}$]) = 407 (1266).

3.2.5.3 Synthesis of 1b

1b was prepared according to the synthetic protocol of **1a** with 2.34 g (6.40 mmol) tetrakis(trimethylsily)germane, 0.79 g (7.04 mmol) KO*t*Bu and 4.00 g (26.3 mmol) 2-ethyl-benzoyl fluoride. Yield: 3.45 g (5.70 mmol, 89%) of analytical pure **1b** as yellow crystals. Mp: 73-75°C. Anal. Calc. for $C_{36}H_{36}GeO_4$: C, 71.43; H, 5.99. Found: C, 71.64; H, 5.73. ^{13}C NMR ($CDCl_3$, TMS, ppm): 225.37 (GeC=O), 143.29, 139.64, 132.90, 132.08, 130.21, 125.86 (Aryl-C), 26.63 (*o*-CH_2CH_3), 15.65 (o-CH_2CH_3). ^1H NMR ($CDCl_3$, TMS, ppm): 7.64 (d, 1H, Aryl-H), 7.39 (t, 1H, Aryl-H), 7.28 (dd, 2H, Aryl-H), 2.87 (q, 2H, *o*-CH_2CH_3), 1.25 (t, 3H, *o*-CH_2CH_3). IR (neat): ν(C=O) 1637, 1598 (m) cm^{-1}. HRMS: calc. for $[C_{36}H_{36}GeO_4]^+$ (M^+) 606.1834; Found 606.1834. UV-vis: λ [nm] (ε [$L \cdot mol^{-1} \cdot cm^{-1}$]) = 407 (1258).

3.2.5.4 Synthesis of 1c

1c was prepared according to the synthetic protocol of **1a** with 3.00 g (8.21 mmol) tetrakis(trimethylsily)germane, 1.01 g (9.03 mmol) KO*t*Bu and 5.12 g (33.6 mmol) 2,6-dimethyl-benzoyl fluoride. Yield: 4.1 g (6.77 mmol, 82%) of analytical pure **1c** as yellow crystals. Mp: 142°C. Anal. Calc. for $C_{36}H_{36}GeO_4$: C, 71.43; H, 5.99. Found: C, 71.55; H, 6.20. ^{13}C NMR ($CDCl_3$, TMS, ppm): 233.05 (GeC=O), 144.03, 132.81, 129.54, 128.06 (Aryl-C), 19.00 (*o*-CH_3). ^1H NMR ($CDCl_3$, TMS, ppm): 7.07 (t, 1H, Aryl-H), 6.80 (d, 2H, Aryl-H), 2.07 (s, 6H, *o*-CH_3). IR (neat): ν(C=O) 1665, 1644 (m) cm^{-1}. HRMS: calc. for $[C_{36}H_{36}GeO_4]^+$ (M^+) 606.1834; Found 606.1853. UV-vis: λ [nm] (ε [$L \cdot mol^{-1} \cdot cm^{-1}$]) = 374 (1477), 403 (954).

3.2.5.5 Synthesis of 1d

1d was prepared according to the synthetic protocol of **1a** with 3.00 g (8.21 mmol) tetrakis(trimethylsily)germane, 1.01 g (9.03 mmol) KO*t*Bu and 4.55 g (32.9 mmol) 3-methyl-benzoyl fluoride. Yield: 3.79 g (6.90 mmol, 84%) of analytical pure **1d** as yellow powder. Mp: 92-94°C. Anal. Calc. for $C_{32}H_{28}GeO_4$: C, 69.98; H, 5.14. Found: C, 69.94; H, 5.13. ^{13}C NMR ($CDCl_3$, TMS, ppm): 222.23 (GeC=O), 140.45, 138.77, 134.92, 129.11, 128.78, 127.14 (Aryl-C), 21.18 (*m*-Tol-CH_3). ^{1}H NMR ($CDCl_3$, TMS, ppm): 7.59 (m, 3H, Aryl-H), 7.31 (s, 1H, Aryl-H), 2.30 (s, 3H, *m*-Tol-CH_3). IR (neat): ν(C=O) 1625, 1590 (m) cm^{-1}. HRMS: calc. for $[C_{32}H_{28}GeO_4]^+$ (M^+) 550.1207; Found 550.1200 . UV-vis: λ [nm] (ε [L·mol^{-1}·cm^{-1}]) = 402 (1058).

3.2.5.6 Synthesis of 1e

1e was prepared according to the synthetic protocol of **1a** with 3.23 g (8.84 mmol) tetrakis(trimethylsily)germane, 1.09 g (9.72 mmol) KO*t*Bu and 5.00 g (36.2 mmol) 4-methyl-benzoyl fluoride. Yield: 4.37 g (7.96 mmol, 90%) of analytical pure **1e** as yellow crystals. Mp: decomposition >230°C. Anal. Calc. for $C_{32}H_{28}GeO_4$: C, 69.98; H, 5.14. Found: C, 69.87; H, 5.08. ^{13}C NMR ($CDCl_3$, TMS, ppm): 221.45 (GeC=O), 145.34, 138.24, 129.61, 129.43 (Aryl-C), 21.77 (*p*-Tol-CH_3). ^{1}H NMR ($CDCl_3$, TMS, ppm): 7.68 (d, 2H, Aryl-H), 7.20 (d, 2H, Aryl-H), 2.34 (s, 3H, *p*-Tol-CH_3). IR (neat): ν(C=O) 1622, 1590 (m) cm^{-1}. HRMS: calc. for $[C_{32}H_{28}GeO_4]^+$ (M^+) 550.1207; Found 550.1221. UV-vis: λ [nm] (ε [L·mol^{-1}·cm^{-1}]) = 400 (1377), 422 (1113).

3.2.5.7 Synthesis of 1f

1f was prepared according to the synthetic protocol of **1a** with 1.16 g (3.17 mmol) tetrakis(trimethylsily)germane, 0.39 g (3.49 mmol) KO*t*Bu and 2.0 g (13.0 mmol) 2-methoxy-benzoyl fluoride. Yield: 1.81 g (2.95 mmol, 93%) of analytical pure **1f** as yellow crystals. Mp: 173°C. Anal. Calc. for $C_{32}H_{28}GeO_8$: C, 69.68; H, 4.60. Found: C, 69.64; H, 4.57. ^{13}C NMR ($CDCl_3$, TMS, ppm): 221.83 (GeC=O), 160.29, 134.58, 130.09, 126.58, 120.43, 111.55 (Aryl-C), 53.67 (*o*-OCH_3). ^{1}H NMR ($CDCl_3$, TMS, ppm): 7.63 (d, 1H, Aryl-H), 7.38 (t, 1H, Aryl-H), 6.94 (t, 1H, Aryl-H), 6.79 (d, 1H, Aryl-H), 3.48 (s, 3H, *o*-OCH_3). IR (neat): ν(C=O) 1614, 1583 (m) cm^{-1}. HRMS: calc. for $[C_{32}H_{28}GeO_8]^+$ (M^+) 614.1004; Found 614.0986. UV-vis: λ [nm] (ε [L·mol^{-1}·cm^{-1}]) = 400 (1160).

3.2.5.8 Synthesis of 1g

1g was prepared according to the synthetic protocol of **1a** with 5.23 g (14.3 mmol) tetrakis(trimethylsily)germane, 1.77 g (15.7 mmol) KO*t*Bu and 9.04 g (58.6 mmol) 4-methoxy-benzoyl fluoride. Yield: 7.99 g (13.0 mmol, 91%) of analytical pure **1g** as yellow crystals. Mp: decomposition > 221°C. Anal. Calc. for $C_{32}H_{28}GeO_8$: C, 69.68; H, 4.60. Found: C, 69.64; H, 4.77. ^{13}C NMR ($CDCl_3$, TMS, ppm): 220.06 (GeC=O), 164.49, 134.37, 131.95, 114.30 (Aryl-C), 55.67 (*p*-OCH_3). ^{1}H NMR ($CDCl_3$, TMS, ppm): 7.78 (d, 2H, Aryl-H), 6.89 (d, 2H, Aryl-H), 3.81 (s, 3H, *p*-OCH_3). IR (neat): ν(C=O) 1615, 1582 (m) cm^{-1}. HRMS: calc. for $[C_{32}H_{28}GeO_8]^+$ (M^+) 614.1004; Found 614.0991. UV-vis: λ [nm] (ε [L·mol^{-1}·cm^{-1}]) = 395 (1897), 413 (1556).

3.2.5.9 Synthesis of 1h

1h was prepared according to the synthetic protocol of **1a** with 1.32 g (3.61 mmol) tetrakis(trimethylsily)germane, 0.45 g (3.97 mmol) KO*t*Bu and 2.5 g (14.9 mmol) 4-ethoxy-benzoyl fluoride. Yield: 2.03 g (3.03 mmol, 84%) of analytical pure **1h** as yellow crystals. Mp: 145-148°C. Anal. Calc. for $C_{36}H_{36}GeO_8$: C, 64.60; H, 5.42. Found: C, 64.56; H, 5.40. ^{13}C NMR ($CDCl_3$, TMS, ppm): 220.03 (GeC=O), 163.88, 134.19, 131.92, 114.65 (Aryl-C), 63.96 (*p*-OCH_2CH_3), 14.72 (*p*-OCH_2CH_3). ^{1}H NMR ($CDCl_3$, TMS, ppm): 7.77 (d, 2H, Aryl-H), 6.86 (d, 2H, Aryl-H), 4.03 (q, 2H, *p*-O CH_2CH_3), 1.38 (t, 3H, *p*-OCH_2CH_3). IR (neat): ν(C=O) 1616, 1583 (m) cm^{-1}. HRMS: calc. for $[C_{36}H_{36}GeO_8]^+$ (M^+) 670.1631; Found 670.1622. UV-vis: λ [nm] (ε [L·mol^{-1}·cm^{-1}]) = 392 (1708), 415 (1362).

3.2.5.10 Synthesis of 1i

1i was prepared according to the synthetic protocol of **1a** with 2.00 g (5.47 mmol) tetrakis(trimethylsily)germane, 0.68 g (6.02 mmol) KO*t*Bu and 4.13 g (22.7 mmol) 4-propoxy-benzoyl fluoride. Yield: 3.30 g (4.55 mmol, 83%) of analytical pure **1i** as yellow crystals. Mp: 125-127°C. Anal. Calc. for $C_{40}H_{44}GeO_8$: C, 66.23; H, 6.11. Found: C, 66.12; H, 6.14. ^{13}C NMR ($CDCl_3$, TMS, ppm): 220.07 (GeC=O), 164.11, 134.19, 131.95, 114.70 (Aryl-C), 69.92 (*p*-$OCH_2CH_2CH_3$), 22.50 (*p*-$OCH_2CH_2CH_3$) 10.56 (*p*-$OCH_2CH_2CH_3$). ^{1}H NMR ($CDCl_3$, TMS, ppm): 7.77 (d, 2H, Aryl-H), 6.87 (d, 2H, Aryl-H), 3.92 (t, 2H, *p*-$OCH_2CH_2CH_3$), 1.78 (m, 2H, *p*-$OCH_2CH_2CH_3$), 1.00 (t, 3H, *p*-$OCH_2CH_2CH_3$). IR (neat): ν(C=O) 1638, 1619 (m) cm^{-1}. HRMS: calc. for $[C_{40}H_{44}GeO_8]^+$ (M^+) 726.2258; Found 726.2296. UV-vis: λ [nm] (ε [L·mol^{-1}·cm^{-1}]) = 393 (1765), 414 (1396).

3.2.5.11 Synthesis of 1j

1j was prepared according to the synthetic protocol of **1a** with 1.00 g (2.74 mmol) tetrakis(trimethylsily)germane, 0.34 g (3.03 mmol) KO*t*Bu and 2.04 g (11.2 mmol) 4-acetoxy-benzoyl fluoride. Yield: 1.59 g (2.19 mmol, 80%) of analytical pure **1j** as yellow powder. Mp: decomposition > 215°C. Anal. Calc. for $C_{36}H_{28}GeO_{12}$: C, 59.62; H, 3.89. Found: C, 59.60; H, 4.00. ^{13}C NMR ($CDCl_3$, TMS, ppm): 220.20 (GeC=O), 155.49, 137.78, 131.01, 122.45 (Aryl-C), 168.57 (*p*-OC(O)CH_3), 21.30 (*p*-OC(O)CH_3). ^{1}H NMR ($CDCl_3$, TMS, ppm): 7.81 (d, 2H, Aryl-H), 7.19 (d, 2H, Aryl-H), 2.29 (s, 3H, *p*-OC(O)CH_3). IR (neat): ν(C=O) 1627, 1577 (m) cm^{-1}. HRMS: calc. for $[C_{36}H_{28}GeO_{12}]^+$ (M^+) 726.0801; Found 726.0810. UV-vis: λ [nm] (ε [$L \cdot mol^{-1} \cdot cm^{-1}$]) = 400 (1262), 422 (992).

3.2.5.12 Synthesis of 1k

1k was prepared according to the synthetic protocol of **1a** with 2.22 g (6.08 mmol) tetrakis(trimethylsily)germane, 0.75 g (6.68 mmol) KO*t*Bu and 4.16 g (24.9 mmol) 4-dimethylamino-benzoyl fluoride. Yield: 3.50 g (5.26 mmol, 80%) of analytical pure **1k** as yellow crystals. Mp: decomposition > 233°C. Anal. Calc. for $C_{36}H_{40}GeN_4O_4$: C, 64.99; H, 6.06; N, 8.42. Found: C, 62.44; H, 5.92; N, 8.31. ^{13}C NMR ($CDCl_3$, TMS, ppm): 219.29 (GeC=O), 153.77, 131.81, 130.25, 110.75 (Aryl-C), 39.93 (*p*-N$(CH_3)_2$). ^{1}H NMR ($CDCl_3$, TMS, ppm): 7.74 (d, 2H, Aryl-H), 6.53 (d, 2H, Aryl-H), 2.91 (s, 3H, *p*-N$(CH_3)_2$). IR (neat): ν(C=O) 1609, 1566 (m) cm^{-1}. HRMS: calc. for $[C_{36}H_{40}N_4GeO_4]^+$ (M^+) 666.2269; Found 666.2270. UV-vis: λ [nm] (ε [$L \cdot mol^{-1} \cdot cm^{-1}$]) = could not be determined because of overlap with π-π* transition.

3.2.5.13 Synthesis of 1l

1l was prepared according to the synthetic protocol of **1a** with 0.5 g (1.37 mmol) tetrakis(trimethylsily)germane, 0.17 g (1.51 mmol) KO*t*Bu and 0.98 g (5.63 mmol) 2-naphthoyl fluoride. Yield: 0.77 g (1.11 mmol, 80%) of analytical pure **1l** as yellow crystals. Mp: 190-198°C. Anal. Calc. for $C_{44}H_{28}GeO_4$: C, 76.22; H, 4.07. Found: C, 76.25; H, 4.11. ^{13}C NMR ($CDCl_3$, TMS, ppm): 221.95 (GeC=O), 138.12, 136.29, 134.51, 132.73, 130.32, 129.39, 129.16, 127.90, 127.09, 122.86 (Aryl-C). ^{1}H NMR ($CDCl_3$, TMS, ppm): 8.48 (s, 1H, Aryl-H), 7.94 (d, 1H, Aryl-H), 7.83 (m, 3H, Aryl-H), 7.56 (t, 1H, Aryl-H), 7.47 (t, 1H, Aryl-H). IR (neat): ν(C=O) 1607, 1592 (m) cm^{-1}. HRMS: calc. for $[C_{44}H_{28}GeO_4]^+$ (M^+) 694.1207; Found 694.1212. UV-vis: λ [nm] (ε [$L \cdot mol^{-1} \cdot cm^{-1}$]) = could not be determined because of overlap with π-π* transition.

3.2.5.14 Synthesis of 1m

1m was prepared according to the synthetic protocol of **1a** with 0.3 g (0.82 mmol) tetrakis(trimethylsily)germane, 0.10 g (0.90 mmol) KO*t*Bu and 0.92 g (7.20 mmol) 4-phenylethynyl benzoyl fluoride. The crude product was dissolved in 5 mL acetone and filtered. The solvent was pumped down and the yellow solid suspended in 10 mL acetonitrile. The insoluble product was filtered off the solution and dried under reduced pressure. Yield: 0.60 g (0.67 mmol, 82%) of analytical pure **1m** as yellow powder. Mp: 114-117°C. Anal. Calc. for $C_{60}H_{36}GeO_4$: C, 80.65; H, 4.06. Found: C, 80.58; H, 4.01. ^{13}C NMR ($CDCl_3$, TMS, ppm): 220. (GeC=O), 139.09, 132.31, 131.94, 129.85, 129.31, 129.11, 128.58, 122.58 (Aryl-C) 94.14 (*p*-CCPh), 88.67 (*p*-CCPh). ^{1}H NMR ($CDCl_3$, TMS, ppm): 7.77 (d, 2H, Aryl-H), 7.56 (m, 4H, Aryl-H), 7.36 (s, 3H, Aryl-H). IR (neat): ν(C=O) 1630, 1581 (m) cm^{-1}. HRMS: calc. for $[C_{60}H_{36}GeO_4]^+$ (M^+) 894.1833; Found 894.1840. UV-vis: λ [nm] (ε [$L \cdot mol^{-1} \cdot cm^{-1}$]) = could not be determined because of overlap with π-π* transition.

3.2.5.15 X-ray Crystallography

All crystals suitable for single crystal X-ray diffractometry were removed from a vial and immediately covered with a layer of silicone oil. A single crystal was selected, mounted on a glass rod on a copper pin, and placed in the cold N_2 stream provided by an Oxford Cryosystems cryostream. XRD data collection was performed for all compounds on a Bruker APEX II diffractometer with use of an Incoatec microfocus sealed tube of Mo Kα radiation (λ = 0.71073 Å) and a CCD area detector. Empirical absorption corrections were applied using SADABS or TWINABS.[32] The structures were solved with use of the intrinsic phasing option in SHELXT and refined by the full-matrix least-squares procedures in SHELXL.[33] The space group assignments and structural solutions were evaluated using PLATON.[34]

Non-hydrogen atoms were refined anisotropically. Hydrogen atoms were located in calculated positions corresponding to standard bond lengths and angles. Disorder was handled by modeling the occupancies of the individual orientations using free variables to refine the respective occupancy of the affected fragments (PART).[35] In some cases, the constraints EXYZ and EADP were used in modelling disorder to make the ADP values of the disordered atoms more reasonable. In some cases, the distances between arbitrary atom pairs were restrained to possess the same value using the SADI instruction and in some cases distance restraints (DFIX) to certain target values were used. In some tough cases of disorder, anisotropic Uij-values of the atoms were restrained (ISOR) to behave more isotropically. Disordered positions for one of the substituents on **1g** were refined using 80/20 split positions. Disordered positions for the OPr group on one of the substituents on **1h** were refined using 50/50 split positions. Disordered positions for two **1h** substituent, one OEt group of a substituent, and ketone oxygens were refined using

55/45, 60/40, 50/50, 55/45, 50/50 split positions respectively. Disordered positions for the solvent of crystallization of acetone in **1k** were refined using 50/50 split positions. Disordered positions for the acetate group on one of the substituents on **1j** were refined using 70/30 split positions. Compound **1e** was twinned and was refined using the TWIN option in SHELXL. The main contributions of the two twin components refined to a BASF of 0.02.

CCDC 1557160-1557163 and 1557165-1557171 contain the supplementary crystallographic data for all compounds. These data can be obtained free of charge from The Cambridge Crystallographic Data Centre via www.ccdc.cam.ac.uk/data_request/cif. Table S1 contains crystallographic data and details of measurements and refinement for compounds **1a**-**c** and **1e**-**1l**.

3.2.5.16 TR-EPR Spectroscopy

Continuous-wave time-resolved (TR) EPR experiments were performed on a Bruker ESP 300E X- band spectrometer (unmodulated static magnetic field) equipped with a 125 MHz dual channel digital oscilloscope (Le Croy 9400). As the light source, the frequency triplet light of a Nd:YAG laser was used (InnoLas Spitlight 400, 355 nm, operating at 20 Hz, ca. 8 mJ/pulse, 8 ns). The setup is controlled by the fsc2 software developed by Dr. J. T. Toerring (Berlin). Spectra were recorded by acquiring the accumulated (50 accumulations) time responses to the incident laser pulses at each magnetic field value of the chosen field range (field steps: 0.1 G). Argon-saturated solutions of the photoinitiators in toluene ($\sim$ 10 mM in photoinitiator concentration) were pumped through a quartz flat cell positioned in the cavity of the EPR spectrometer using a flow system (flow rate: 2-3 mL min^{-1}).

3.2.5.17 Computational Section

All computational studies were executed on a computing cluster with blade architecture using the Gaussian09 software package.[36] Geometry optimizations were performed in the gas phase with B3LYP as hydride density functional[37] together with the 6-31G(d) split-valence basis set for all atoms.[38] Minimum structures were characterized by harmonic frequency calculations, yielding none imaginary frequency. Vertical excitations were calculated via time-dependent DFT (TD-DFT) at the CAM-B3LYP/def2-TZVP level of theory[39] and solvent effects were considered by applying the polarized continuum model (PCM).[40] Acetonitrile (MeCN) was used as a solvent with a dielectric constant of ε = 35.688. All gained vertical excitation energies were manually corrected by 3 %, as PCM(MeCN) TD-DFT CAM-B3LYP/def2-TZVP//B3LYP/6-31G(d) overestimated the excitation energies for this substance class systematically.[28] If not explicitly mentioned, all structures and molecular orbitals (isovalues of 0.025) were plotted using the Gabedit software package.[41]

3.2.6 References

[1] a) D. Neshchadin, A. Rosspeintner, M. Griesser, B. Lang, S. Mosquera-Vazquez, E. Vauthey, V. Gorelik, R. Liska, C. Hametner, B. Ganster, R. Saf, N. Moszner, G. Gescheidt, *J. Am. Chem. Soc.* **2013**, *135*, 17314; b) J. Lalevée, X. Allonas, J. P. Fouassier, *Chem. Phys. Lett* **2009**, *469*, 298; c) B. Ganster, U. K. Fischer, N. Moszner, R. Liska, *Macromolecules* **2008**, *41*, 2394.

[2] K. Mochida, K. Ichikawa, S. Okui, Sakaguchi Y., H. Hayashi, *Chem. Lett.* **1985**, 1433.

[3] a) M. B. Taraban, V. I. Maryasova, T. V. Leshina, L. I. Rybin, D. V. Gendin, N. S. Vyazankin, *J. Organomet. Chem.* **1987**, *326*, 347; b) A. G. Brook, S. A. Fieldhouse, *J. Organomet. Chem.* **1967**, *10*, 235.

[4] a) R. E. Bruns, P. Kuznesof, *J. Organomet. Chem.* **1973**, *56*, 131; b) M. Wakasa, K. Mochida, Y. Sakaguchi, J. Nakamura, H. Hayashi, *J. Phys. Chem.* **1991**, *95*, 2241; c) K. Mochida, K. Yamamoto, *Bull. Chem. Soc. Jpn.* **1988**, *61*, 2933; d) A. Alberti, G. Seconi, G. F. Pedulli, A. Degl'innocenti, *J. Organomet. Chem.* **1983**, *253*, 291.

[5] a) D. A. Nicholson, A. L. Allred, *Inorg. Chem.* **1965**, *4*, 1747; b) U. Iserloh, D. P. Curran, *J. Org. Chem.* **1998**, *63*, 4711; c) E. Piers, R. Lemieux, *Organometallics* **1995**, *14*, 5011; d) M. Nanjo, K. Matsudo, K. Mochida, *Chem. Lett.* **2001**, *30*, 1086.

[6] D. A. Bravo-Zhivotovskii, S.D. Pigarev, I. D. Kalikhman, O. A. Vyazankina, N. S. Vyazankin, *J. Organomet. Chem.* **1983**, *248*, 51.

[7] S. Kiyooka, A. Miyauchi, *Chem. Lett.* **1985**, *12*, 1829.

[8] A. G. Brook, M. A. Quigley, G. J. D. Peddle, N. V. Schwartz, C. M. Warner, *J. Am. Chem. Soc.* **1960**, *82*, 5102.

[9] A. G. Brook, J. M. Duff, P. F. Jones, N. R. Davis, *J. Am. Chem. Soc.* **1967**, *89*, 431.

[10] E. J. Corey, D. Seebach, *Angew. Chem. Int. Ed.* **1965**, *4*, 1075.

[11] K. Yamamoto, A. Hayashi, S. Suzuki, J. Tsuji, *Organometallics* **1987**, *6*, 974.

[12] a) J. A. Soderquist, A. Hassner, *Tetrahedron Lett.* **1988**, *29*, 1899; b) J. A. Soderquist, A. Hassner, *J. Am. Chem. Soc.* **1980**, *102*, 1577.

[13] A. Castel, P. Rivière, J. Satgé, H. Y. Ko, *Organometallics* **1990**, *9*, 205.

[14] A. Castel, P. Rivière, J. Satgé, D. Desor, *J. Organomet. Chem.* **1992**, *433*, 49.

[15] N. Moszner, F. Zeuner, I. Lamparth, U. K. Fischer, *Macromol. Mater. Eng.* **2009**, *294*, 877.

[16] J. Radebner, A. Eibel, M. Leypold, C. Gorsche, L. Schuh, R. Fischer, A. Torvisco, D. Neshchadin, R. Geier, N. Moszner, R. Liska, G. Gescheidt, M. Haas, H. Stueger, *Angew. Chem. Int. Ed.* **2017**, *56*, 3103.

[17] a) R. Fischer, J. Baumgartner, C. Marschner, F. Uhlig, *Inorg. Chim. Acta.* **2005**, *358*, 3174; b) J. Hlina, R. Zitz, H. Wagner, F. Stella, J. Baumgartner, C. Marschner, *Inorg. Chim. Acta.* **2014**, *422*, 120.

[18] J. Hlina, C. Mechtler, H. Wagner, J. Baumgartner, C. Marschner, *Organometallics* **2009**, *28*, 4065.

[19] J. E. Leffler, E. Grunwald in *Rates and equilibria of organic reactions*, Wiley (Dover reprint), **1963**.

[20] M. Haas, M. Leypold, D. Schnalzer, A. Torvisco, H. Stueger, *Organometallics* **2015**, *34*, 5291.

[21] M. Haas, M. Leypold, D. Schnalzer, A. Torvisco, H. Stueger, *Phosphorus, Sulfur, and Silicon Relat. Elem.* **2016**, *191*, 597.

[22] a) K. M. Baines, W. G. Stibbs, *Coord. Chem. Rev.* **1995**, *145*, 157; b) M. L. Amadoruge, C. S. Weinert, *Chem. Rev.* **2008**, *108*, 4253.

[23] A. F. Holleman, N. Wiberg in *Lehrbuch der anorganischen Chemie*, De Gruyter, Berlin, **2007**.

[24] a) F.G. A. Stone, R. West in *Advances in Organometallic Chemistry, 6*, Elsevier, Burlington, **1968**; b) M. L. Amadoruge, C. H. Yoder, J. Hope Conneywerdy, K. Heroux, A. L. Rheingold, C. S. Weinert, *Organometallics* **2009**, *28*, 3067; c) K. V. Zaitsev, A. A. Kapranov, A. V. Churakov, O. K. Poleshchuk, Y. F. Oprunenko, B. N. Tarasevich, G. S. Zaitseva, S. S. Karlov, *Organometallics* **2013**, *32*, 6500; d) K. V. Zaitsev, K. Lam, Z. Zhanabil, Y. Suleimen, A. V. Kharcheva, V. A. Tafeenko, Y. F. Oprunenko, O. K. Poleshchuk, E. K. Lermontova, A. V. Churakov, *Organometallics* **2017**, *36*, 298; e) M. L. Amadoruge, E. K. Short, C. Moore, A. L. Rheingold, C. S. Weinert, *J. Organomet. Chem.* **2010**, *695*, 1813.

[25] a) J. C. Dearden, W. F. Forbes, *Can. J. Chem.* **1958**, *36*, 1362; b) W. F. Forbes, W. A. Mueller, *Can. J. Chem.* **1955**, *33*, 1145; c) J. Tanaka, S. Nagakura, M. Kobayashi, *J. Chem. Phys.* **1956**, *24*, 311; d) M.M. Byrne, N. H. P. Smith, *Spectrochim Acta A* **1969**, *25*, 313.

[26] a) R. B. Woodward, *J. Am. Chem. Soc.* **1941**, *63*, 1123; b) L. F. Fieser, M. Fieser, S. Rajagoplan, *J. Org. Chem.* **1948**, *13*, 800.

[27] M. Hesse, H. Meier, B. Zeeh in *Spektroskopische Methoden in der organischen Chemie*. *100 Tabellen*, Thieme, Stuttgart [u.a.], **1995**.

[28] T. M. Maier, H. Bahmann, A. V. Arbuznikov, M. Kaupp, *J. Chem. Phys.* **2016**, *144*, 074106/1-074106/14.

[29] A. Yurkovskaya, O. Morozova, G. Gescheidt (Eds.) *Encyclopedia of Radicals in Chemistry, Biology and Materials*, John Wiley & Sons, Ltd, Chichester, UK, **2012**.

[30] A. B. Pangborn, M. A. Giardello, R. H. Grubbs, R. K. Rosen, F. J. Timmers, *Organometallics* **1996**, *15*, 1518.

[31] a) L. R. Subramanian, G. Siegemund (Eds.) *Houben-Weyl Methods of Organic Chemistry Supplement: Organo-Fluorine Compounds Fluorinating Agents and Their Application in Organic Synthesis*. Introduction of Fluorine with Alkali Metal Fluorides, Including Ammonium Fluoride and Tetraalkylammonium Fluorides (Including Special Methods of Fluorinations, e.g., Phase Transfer Catalysis, Activation by Crown Ethers, Reagents Bound to Polymers), Thieme, Stuttgart, **1998**; b) A. G. Brook, F. Abdesaken, H. Söllradl, *J. Organomet. Chem.* **1986**, *299*, 9.

[32] a) Bruker in *APEX2 and SAINT*. *version 5.03*. Bruker AXS Inc.:, Madison, Wisconsin, USA, **2012**; b) R. H. Blessing, *Acta Cryst.* **1995**, *51*, 33.

[33] a) G. M. Sheldrick, *Acta Crystallogr., Sect. A: Found. Crystallogr.* **2008**, *64*, 112; b) G. M. Sheldrick, *Acta Crystallogr., Sect. A: Found. Crystallogr.* **1990**, *A46*, 467; c) G. M. Sheldrick, *Acta Crystallogr., Sect. A: Found. Adv.* **2015**, *71*, 3.
[34] a) A. L. Spek, *J. Appl. Crystallogr.* **2003**, *36*, 7; b) A. L. Spek, *Acta Crystallogr., Sect. D: Biol. Crystallogr.* **2009**, *65*, 148.
[35] P. Müller, R. Herbst-Irmer, A. L. Spek, T. R. Schneider, M. R. Sawaya in *Crystal Structure Refinement: A Crystallographer's Guide to SHELXL*, Oxford University Press, **2006**.
[36] M. J. Frisch, G. W. Trucks, H. B. Schlegel, G. E. Scuseria, M. A. Robb, J. R. Cheeseman, G. Scalmani, V. Barone, B. Mennucci, G. A. Petersson, H. Nakatsuji, M. Caricato, X. Li, H. P. Hratchian, A. F. Izmaylov, J. Bloino, G. Zheng, J. L. Sonnenberg, M. Hada, M. Ehara, K. Toyota, R. Fukuda, J. Hasegawa, M. Ishida, T. Nakajima, Y. Honda, O. Kitao, H. Nakai, T. Vreven, Montgomery, Jr. J., A., J. E. Peralta, F. Ogliaro, M. Bearpark, J. J. Heyd, E. Brothers, K. N. Kudin, N. Staroverov, T. V. Keith, R. Kobayashi, J. Normand et al. in *Gaussian 09, Revision D.01, Gaussian, Inc.: Wallingford, CT*, **2013**.
[37] a) A. D. Becke, *J. Chem. Phys.* **1993**, *98*, 1372; b) C. Lee, W. Yang, R. G. Parr, *Phys. Rev. B: Condens. Matter Mater. Phys.* **1988**, *37*, 785.
[38] a) P. C. Hariharan, J. A. Pople, *Theoret. Chim. Acta* **1973**, *28*, 213; b) W. J. Hehre, R. Ditchfield, J. A. Pople, *J. Chem. Phys.* **1972**, *56*, 2257; c) R. Ditchfield, W. J. Hehre, J. A. Pople, *J. Chem. Phys.* **1971**, *54*, 724.
[39] a) T. Yanai, D. P. Tew, N. C. Handy, *Chem. Phys. Lett* **2004**, *393*, 51; b) F. Weigend, R. Ahlrichs, *Phys. Chem. Chem. Phys.* **2005**, *7*, 3297.
[40] J. Tomasi, B. Mennucci, R. Cammi, *Chem. Rev.* **2005**, *105*, 2999.
[41] A.-R. Allouche, *J. Comput. Chem.* **2011**, *32*, 174.

3.3 From Mono- to Tetraacylgermanes: Extending the Scope of Visible Light Photoinitiators

Anna Eibel,[a] Judith Radebner,[b] Michael Haas,[b] David E. Fast,[a] Hilde Freißmuth,[a] Eduard Stadler,[a] Paul Faschauner,[b] Ana Torvisco,[b] Iris Lamparth,[c] Norbert Moszner,[c] Harald Stueger[b] and Georg Gescheidt[a]*

[a] Institute of Physical and Theoretical Chemistry, NAWI Graz, Graz University of Technology, Stremayrgasse 9, 8010 Graz, Austria.

[b] Institute of Inorganic Chemistry, NAWI Graz, Graz University of Technology, Stremayrgasse 9, 8010 Graz, Austria.

[c] Ivoclar Vivadent AG, Bendererstrasse 2, 9494 Schaan, Liechtenstein.

published in *Polymer Chemistry*, **2018**, 9, 38.

Graphical Abstract:

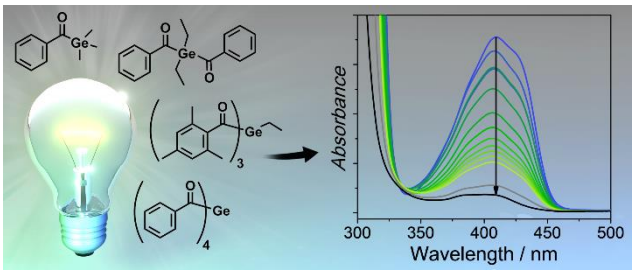

3.3.1 Abstract

We have investigated the inititiaton efficiency of carefully selected germanium-based photointiators for radical polymerization. To establish a systematic relationship between structure and reactivity, we have developed a convenient synthetic protocol for the preparation of a trisacylgermane, closing the gap from mono- to tetraacylgermane photoinitiators. The studied acylgermanes display distinct, wavelength-dependent photobleaching upon irradiation up to 470 nm. In particular, tetraacylgermanes featuring *ortho*-alkyl substituents reveal red-shifted n-π* bands, in line with excellent photobleaching upon visible light irradiation. Quantum yields of decomposition (determined at 385 nm) have been found to be highest for bisacylgermanes. Germyl radicals produced upon triplet-state α-cleavage of the acylgermanes react remarkably fast with monomers. Addition rate constants to (meth)acrylates range from 0.4 – 4.5 x 10^8 $M^{-1}s^{-1}$, depending on the substitution pattern. These values are clearly higher than those reported for related phosphorus-centered radicals derived from acylphosphane oxides. We have further established the nature of the products and side-products formed at initial stages of the polymerizations using chemically induced dynamic nuclear polarization (CIDNP) experiments.

3.3.2 Introduction

Shifting absorptions to specifically chosen wavelengths, particularly in the visible region, has been a major challenge in photoinitiator (PI) research. Additionally, a favorable quantum efficiency for the initiating process is highly desired. For medical applications such as dental fillings, low toxicity is another important issue. It has been shown that acylgermanes have the potential to meet these requirements.[1] Recently, we have introduced a straightforward synthetic route for the preparation of tetraacylgermanes, having the advantage of a simplified synthesis and red-shifted *n*-π* absorptions compared to mono- and bisacylgermanes.[2] In this contribution, we wish to systematically assess the photoinitiating efficiency of specifically modified tetraacylgermanes (**5**-**8**, Chart 1), and to provide a comparison with mono- to trisacylgermanes (**1**-**4**), as well as to the widely used mono- and bisacylphosphane oxide initiators **9** and **10**.[3]

Trisacylgermanes are very rarely known in literature[4] and have – to the best of our knowledge – not been investigated as photoinitiators yet. In order to complete the array of germanium-based photoinitiators displaying one to four acyl moieties, we have therefore developed a convenient synthetic protocol to obtain a trisacylgermane derivative (**4**).

Compounds **1**, **2** and **6** have been selected for this study, since they feature the same aromatic moiety (unsubstituted benzoyl group) one, two and four times, respectively. Similarly, bisacylgermane **3** and tetraacylgermane **7** allow studying the influence of the *p*-methoxy substituent on the photoreactivity. Additionally, we have decided to investigate tetraacylgermane **8** - an asymmetrically substituted derivative, providing good solubility in organic solvents and a strongly red-shifted absorption band.[2b] Trisacylgermane **4** and tetraacylgermane **5** both feature mesitoyl groups.

Chart 1. Chemical structures of acylgermanes **1**–**8** and acylphosphane oxides **9** and **10**.

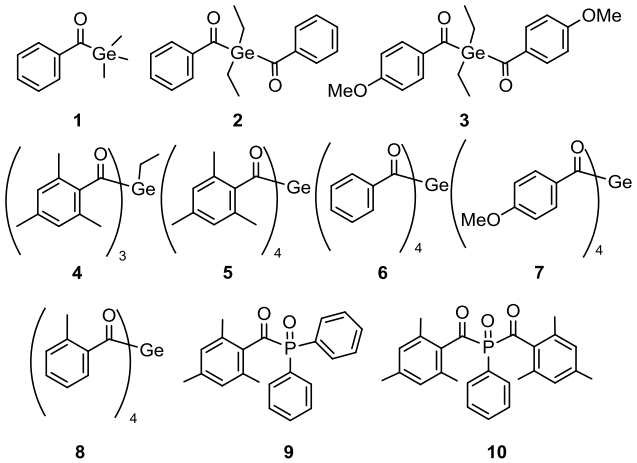

The goal of our work is to provide insights into structure-reactivity relationships, in order to promote further strategies for the development of tailor-made germanium-based initiators.

Generally, photolysis of acylgermanes (Scheme 1) leads to triplet-state *α*-cleavage of a Ge−C(O) bond, yielding a benzoyl-type and a germyl radical. We have investigated the α-cleavage reaction shown in Scheme 1 using time-resolved (TR) EPR spectroscopy. The photobleaching efficiency of acylgermanes **1**-**8** was analysed both qualitatively upon irradiation at different wavelengths, and quantitatively in terms of decomposition quantum yields. Moreover, we have studied the kinetics and reaction mechanisms of polymerizations utilizing laser-flash photolysis (LFP), and chemically induced dynamic nuclear polarization (CIDNP-NMR) spectroscopy.

Scheme 1. Photocleavage of acylgermanes, leading to the formation of a benzoyl-type radical **B•** and a germyl radical **G•**. R^1, R^2 and R^3 abbreviate the substituents displayed in the formulas in Chart 1.

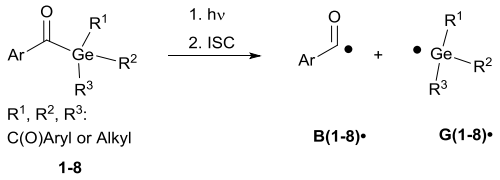

3.3.3 Results and Discussion

3.3.3.1 Ge-based Initiators

The systematic assessment of acylgermanes from mono- to tetraacyl-derivatives requires the preparation of trisacylgermanes such as **4**. The synthetic pathways leading to trisacylgermane **4** and to tetraacylgermanes **5**–**8** are summarized in Scheme 2. To obtain the desired germanide, the corresponding precursors, $(Me_3Si)_3GeEt$ or $(Me_3Si)_4Ge$, were treated with KOtBu. Upon addition of the respective acid fluoride the desired product was formed (**4**, yield: 71%).

Scheme 2. Synthesis of trisacylgermane **4** and tetraacylgermanes **5**–**8**

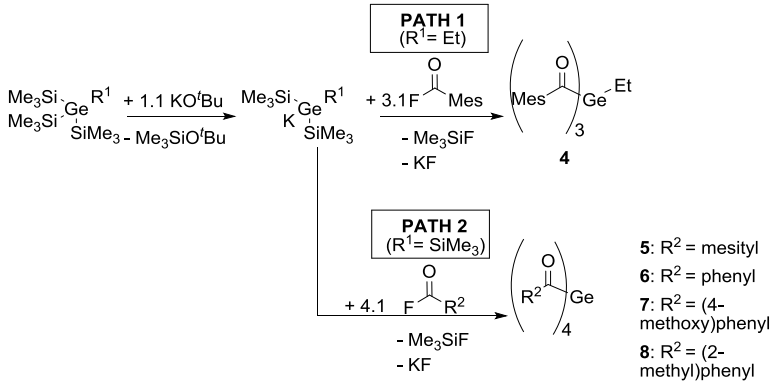

Concerning trisacylgermanes, a stable product could only be isolated in the case of compound **4**, featuring mesitoyl groups. We are currently working on the preparation of further functionalized derivatives. X-ray crystallography revealed the structure of **4** as shown in Fig. 1. Structural features such as bond lengths and angles (see Fig. 1) are compatible with previously reported values for tetraacylgermanes. For a more detailed discussion the reader is referred to the Supplementary Information and references [7] and [8].

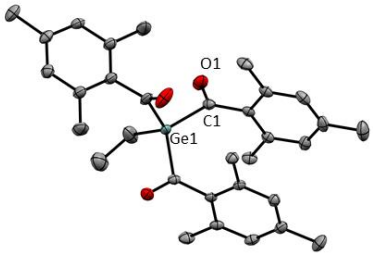

Figure 1. ORTEP representation of **4**. Thermal ellipsoids are depicted at the 50 % probability level. Hydrogen atoms are omitted for clarity. Selected bond lengths [Å] and angles [°]: Ge-C(mean) 2.031, C-O(mean) 1.214; C-Ge-C (mean) 109.45, O-C-C_{aryl}-C_{aryl} (mean) 90.1.

3.3.3.2 UV-Vis Absorption Spectra

Figure 2 depicts the UV-Vis absorption spectra of compounds **1–8** with intense π-π* absorption bands below 350 nm and weaker bands above 360 nm, attributable to n-π* transitions. Excitation of the latter ones is responsible for the photoinduced *α*-cleavage of the Ge–C(O) bond, leading to germyl and benzoyl-type radicals (Scheme 1). The extinction coefficients *ε* increase from mono- to tetraacylgermanes, in line with the extension of the π-system. The absorption bands of **1–8** are clearly influenced by the substituents at the aromatic rings.[2b] Compounds featuring a *p*-methoxy substituent (bisacylgermane **3** and tetraacylgermane **7**) show blue-shifted absorption spectra and higher extinction coefficients when compared to the corresponding unsubstituted acylgermanes **2** and **6** (benzoyl derivatives). For the mesitoylderivatives **4** (ethyltrismesitoylgermane) and **5** (tetramesitoylgermane), the strongest hypsochromic shifts are observed. The *o*-tolyl substituent of tetraacylgermane **8** induces a bathochromic shift, leading to the strongest absorbance among the studied initiators in the visible range above 450 nm. The UV-Vis spectra of phosphorus-based photoinitiators **9** and **10** are provided in the Supplementary Information, showing blue-shifted absorption spectra when compared to acylgermanes **1**-**8**. No absorbance is observed above 420 nm and 440 nm for compounds **9** and **10**, respectively, making these initiators unsuitable for long-wavelength curing applications.

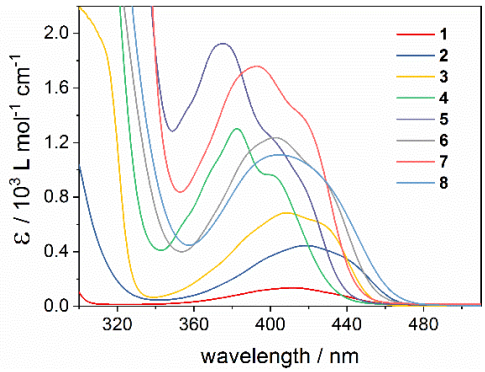

Figure 2. UV-Vis absorption spectra of mono-, bis- and tris- and tetraacylgermanes **1**-**8** recorded in acetonitrile.

3.3.3.3 Photobleaching Behavior

Efficient bleaching of the photoinitiator is an essential requirement to achieve high curing depth and to avoid colored polymers. Fast photobleaching at irradiation wavelengths in the visible range is particularly desirable for applications such as dental fillings. We have tested the photobleaching of **1**–**8** *via* steady-state-photolysis (SSP) at 385 nm and 470 nm. The LED operated at 385 nm was chosen as an example of shorter-wavelength irradiation, whereas LED light at 470 nm corresponds to the longest-wavelength emission band of typical dental lamps.[5]

Photobleaching experiments were performed in the presence of methyl methacrylate (MMA) monomer. The monomer acts as a radical trap, leading to the formation of photoproducts which do not absorb in the visible wavelength range. Further, samples were saturated with argon before the measurements to avoid side reactions of the excited photoinitiators and generated radicals with oxygen.

Fig. 3 depicts time-decays of the absorbance of mono- to tetraacylgermanes followed at the n-π* absorption maxima upon irradiation with LEDs at 385 nm and 470 nm. For a relative (qualitative) comparison of the photobleaching efficiency, these plots were normalized. The corresponding UV-Vis spectra are provided in the Supplementary Information. Photobleaching is more efficient upon irradiation with LED light at 385 nm than at 470 nm for all investigated compounds. Monoacylgermane **1** shows the least efficient bleaching at both wavelengths. Additionally, trisacylgermane **4** and tetraacylgermane **7** display rather inefficient photobleaching at 470 nm, despite their good bleaching performance at 385 nm. This might be due to low absorbance of these compounds at 470 nm (see the UV-Vis spectra, Fig. 2). In contrast, tetraacylgermane **8** exhibits remarkably fast photobleaching upon irradiation at 470 nm, indicating efficient initiation under high-wavelength visible light (Fig. 3b).

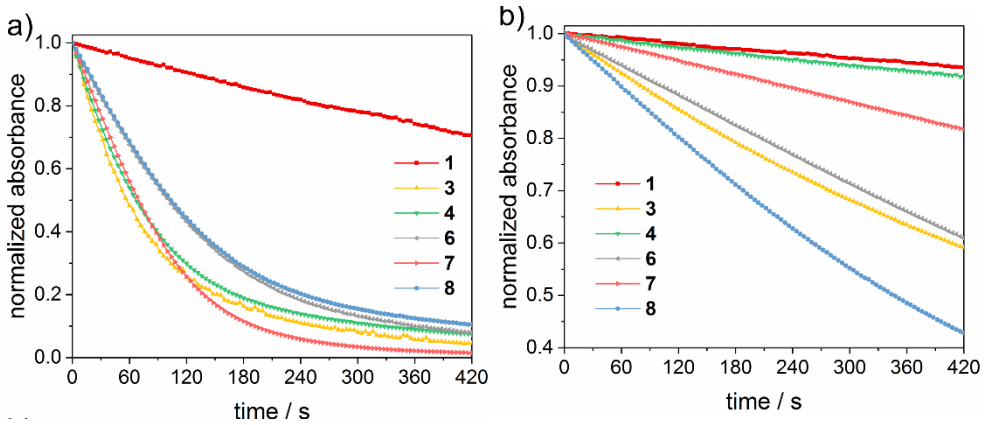

Figure 3. Steady-state photolysis of mono-, bis-, tris- and tetraacylgermanes in acetonitrile/MMA (1/1 v/v). Plots of normalized absorbance versus time for irradiation at a) 385 nm and b) 470 nm, monitored at the n-π* absorption maxima (**1**: 412.5 nm, **3**: 409 nm, **4**: 383 nm, **6**: 404 nm, **7**: 393 nm, **8**: 405.5 nm).

To further rationalize the wavelength-dependent photobleaching efficiency, we have utilized the Beer-Lambert law to calculate the amount of absorbed light and the penetration depth of the incident light at conditions similar to the SSP experiments. Plots of the absorbed light at an optical path length *l* of 1 cm as well as the path length at which 90% of the incident light is absorbed (penetration depth, $l_{90\%}$) are presented in Fig. 4 for compounds **1** and **8** (1 mM solutions). These calculations have been performed at wavelengths of 385 nm, 410 nm, 430 nm and 470 nm (see the Supplementary Information for the data for compounds **3**–**7**). Fig. 4 reflects the vast differences in the absorption properties between compounds **1** and **8**. The significantly lower molar extinction coefficients ε of **1** compared to **8** result in much lower amounts of absorbed light for **1**. The penetration depth of the incident light is inversely related to the amount of absorbed light, leading to a penetration depth approximately ten times higher for compound **1** than for **8** at 470 nm. Accordingly, the amount of absorbed light for irradiation at 470 nm is substantially higher for compound **8** than for **1**, in line with the significantly more efficient photobleaching of **8**.

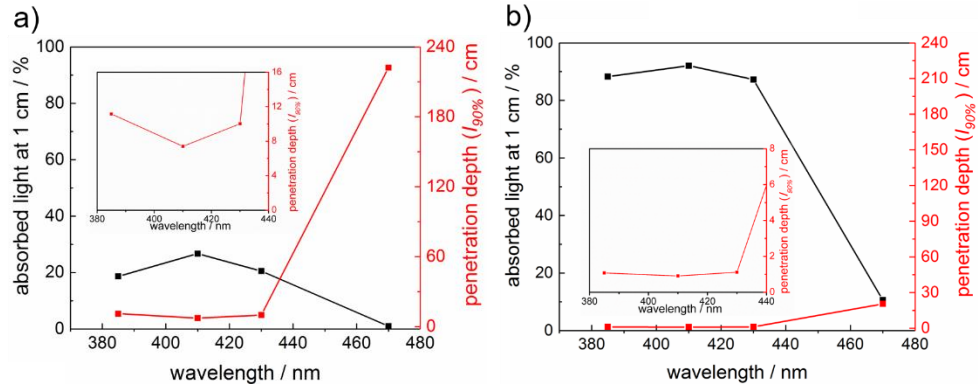

Figure 4. Plots of absorbed light at a path length *l* of 1 cm and calculated penetration depth $l_{90\%}$ for 1 mM solutions of a) compound **1** and b) compound **8**. The insets show a zoom into the lower penetration depth area. Lines are to guide the eye.

For practical applications, a good match between the absorption maxima and the applied irradiation wavelengths (corresponding to a high amount of absorbed light), as well as a high penetration depth of the incident light are desired, especially when curing thick layers.[6] The photobleaching effect leads to increasing penetration depths in the course of the polymerization. Therefore, photoinitiators with optimal bleaching efficiency at the irradiation wavelengths are beneficial, especially in cases where high curing depths are required. Further, high initial absorbance is advantageous, since this increases the probability of generating a sufficient amount of primary radicals which can effectively start the polymerization chain reactions, preventing that oxygen becomes dominant.[7] High initial absorbance can be achieved either by increasing the PI concentration and/or by choosing a PI with high extinction coefficients. Since the concentration of the photoinitiator in a formulation should be kept low (for reasons of reduced costs etc.), PIs with high extinction coefficients are particularly desired. These considerations suggest that tetraacylgermanes (highest extinction coefficients, good bleaching behavior) might be most suitable among the studied compounds for several curing applications.

3.3.3.4 Quantum Yields of Decomposition

Fig. 3 shows a relative comparison of the photobleaching behavior (the initial absorbance was normalized to 1 for all compounds). This represents a qualitative description of the photobleaching efficiency, but does not consider the differences in the extinction coefficients at the irradiation wavelengths. A quantitative evaluation has been achieved by measuring the photodecomposition quantum yields via on-line UV-Vis spectroscopy.[8]

As described for the photobleaching experiments above, we have determined these quantum yields in a solvent mixture of acetonitrile and MMA (1/1 v/v ratio), in order to evaluate the performance of the photoinitiators at conditions similar to the application in polymerization formulations. Furthermore, by adding the monomer as a radical trap, absorbing photoproducts in the n-π* region of the parent initiators, which may interfere with the evaluation, are avoided. As a light source, we have chosen the LED operated at 385 nm, since all compounds show sufficient absorbance at this wavelength, allowing for a precise evaluation. For good comparability, all samples were prepared to achieve equal initial light absorbance at the irradiation wavelength ($A_{385} \sim 0.6$, LED385 operated at 20 mA forward current). To account for solvent effects, the extinction coefficients of the investigated photoinitiators have been re-determined in the solvent mixture acetonitrile/MMA in order to allow exact determination of concentration changes.

Fig. 5 presents the kinetic trace (concentration versus time) obtained upon photolysis of bis(acyl)germane **3** at 385 nm, monitored at the n-π* absorption maximum (409.5 nm, ε = 763 L mol^{-1} cm$^{-1.}$, see the inset of

Fig. 5 for the corresponding UV-Vis spectra). As described in the experimental section, the initial reaction rate *k* is obtained from the first derivative of the exponential fit of this trace.[9] The quantum yield *Φ* is calculated via dividing -*k* by the photon flux I_0 ($1.89 \cdot 10^{-5}$ mol·L^{-1}·s^{-1}) and the factor *f* (determined from the initial absorbance at 385 nm, *f*=0.73).

The experimental data for compounds **1-2**, **6**-**8** and **10** are presented in the Supplementary Information. Table 1 summarizes the monitoring wavelengths, extinction coefficients, reaction rates *k* and the obtained decomposition quantum yields *Φ* for all investigated compounds and provides a comparison with previously published values, if available.

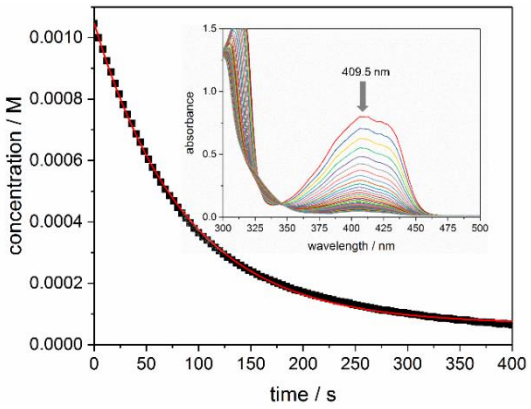

Figure 5. Decay of concentration versus irradiation time for compound **3**, monitored at 409.5 nm, together with the exponential fit of the data (red line). The inset shows the corresponding UV-Vis spectra recorded upon irradiation at 385 nm (time steps between each spectrum: 12 s, sample: 1.1 mM **3** in acetonitrile/MMA (1/1 v/v).)

Table 1. Summary of quantum yield experiments: observation wavelength λ together with extinction coefficients ε, initial reaction rates *k* and determined values for decomposition quantum yields *Φ*, as well as comparison with published values.

Compound	*λ* / nm (*ε* / M^{-1} cm^{-1})	*k* / 10^{-6} (M s^{-1})	*Φ* (measured)	*Φ* (published)
1	413 (136)	-2.91	0.21 ± 0.02	0.40[3]
2	420 (493)	-11.59	0.83 ± 0.01[a]	0.85[3]
3	409.5 (763)	-11.84	0.83 ± 0.01	–
6	403.5 (1224)	-5.50	0.38 ± 0.01	–
7	394 (1902)	-6.57	0.44 ± 0.02	–
8	405.5 (1370)	-4.72	0.34 ± 0.01	–
10	370 (996)	-8.95	0.64 ± 0.04[a]	0.6[9]

[a] Our work, see reference[8].

The decomposition quantum yield obtained for bisacylphosphane oxide **10** (Φ = 0.64 ± 0.04) is in good agreement with the published value of 0.6.[3a,3b] Moreover, for bisacylgermane **2** excellent agreement is obtained with the value determined previously via HPLC analysis ($\Phi_{measured}$ = 0.83, $\Phi_{published}$ = 0.85).[1c] In contrast, our value for compound **1** is lower than the published quantum yield ($\Phi_{published}$ = 0.40).[1c]

In general, bisacylgermanes **2** and **3** exhibit higher quantum yields of decomposition than the tetraacylgermanes **6**-**8**. This might however be compensated by the capability of tetraacylgermanes to undergo four subsequent photocleavage steps to produce in total four benzoyl radicals in a stepwise procedure.

Additionally, apart from the decomposition quantum yields, other factors contribute to the photoinitiating efficiency as well, including the match of the UV-Vis absorption spectra with the available light sources, the photobleaching efficiency (see also the discussion in the previous section), the reactivity of the generated radicals to monomers, and the probability of undergoing side-reactions, such as quenching by oxygen.

Time-resolved EPR Spectra of Primary Radicals

Time-resolved (TR) EPR spectroscopy allows the simultaneous observation of both radicals produced upon photolysis of acylgermanes **1**–**8** within short time scales (50 ns time regime).[1f,2a,3e,10] As the light source, a laser operated at 355 nm was used. This wavelength lies within the n-π* bands of the photoinitiators, as well as the wavelengths chosen for the photobleaching experiments (LED light up to 470 nm). Therefore, the photochemical reaction pathways are expected to be analogous for all light sources applied in this study (triplet-state α-cleavage). Performing photolysis experiments using tunable laser sources could however provide additional insights into bond cleavage efficiencies. This will be subject of future work.

Laser-flash photolysis of bisacylgermane **3** affords the TR-EPR spectrum shown in Fig. 6a. The spectrum is dominated by a quintet attributed to the germyl radical **G(3)•** (g = 2.006, hyperfine coupling constant (hfc) = 0.5 mT). The quintet (intensity ratio of 1:4:6:4:1) stems from the four equivalent methylene protons of the ethyl substituents at the Ge-center (β hydrogen atoms).[1f] This signal partly overlaps with the unresolved signal of the benzoyl-type radical **B(3)•** (g = 2.000). Fig. 6b depicts the TR-EPR spectrum of trisacylgermane **4**. Due to the two β hydrogen atoms, radical **G(4)•** exhibits a triplet (intensity ratio 1:2:1, g = 2.002, hfc = 0.44 mT), which partly overlaps with radical **B(4)•** (g = 2.000).

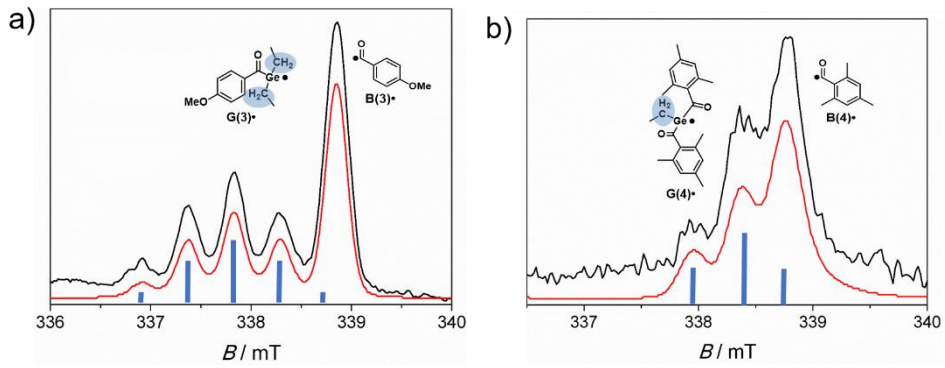

Figure 6. TR-EPR spectra recorded 300-400 ns after laser-flash photolysis (355 nm) of argon-saturated toluene solutions (10 mM) of a) **3** and b) **4**, together with their simulations (red lines). Blue bars indicate the splitting of the germyl radical signals due to β hydrogen atoms.

Similarly, the TR-EPR spectra of tetraacylgermane derivatives show two signals in absorption, being assigned to the germyl radicals **G•** and the benzoyl-type radicals **B•** (for the experimental spectra the reader is referred to references [2a] and [2b]). The TR-EPR spectrum of monoacylgermane **1** could not be obtained. This might be due to unfavorable triplet-polarization effects (magnetic field effects) and/or to inefficient α-cleavage, resulting in a radical concentration below the detection limit.[10]

3.3.3.5 Germanium-centered Radicals and their Reactivity

Laser-flash photolysis (LFP) is ideally suited for studying short lived species and their kinetics. A detailed overview is given by J.C. Scaiano.[11] Transient optical absorption spectra obtained upon LFP (355 nm excitation) of acylgermanes **2–8** reveal distinct absorption bands between 470 and 530 nm (see Fig. 7a and the Supplementary Information). These bands are attributed to the germyl radicals **G(2–8)•** (see Scheme 1).[1f,12] Benzoyl-derived radicals do not reveal distinct absorptions in the wavelength range of our LFP experiments, and can only be observed by time-resolved IR and EPR spectroscopy.[3d,13] In the case of monoacylgermane **1**, the Ge-centered radical was not distinguishable, which might be due to unfavorable absorption properties of the Me_3Ge• radical (**G(1)•**). Both Ge-centered and benzoyl-type radicals have been shown to add to the double bonds of monomers, the Ge-centered radicals being *ca.* two to three orders of magnitude faster.[1f,12,13] The distinct transient absorptions of the germyl radicals **G(2-8)•** allow to determine the rate constants for their addition to various monomers *via* pseudo-first-order analysis. Exponential fitting of the decay traces obtained at various quencher concentrations yielded the pseudo-first-order rate constants k_{exp}. The second order addition rate constants ($k_{monomer}$) are obtained from the slopes of their linear dependence on the monomer concentration $c_{monomer}$ (see equation 1).[1f,3a]

$$k_{exp} = k_0 + k_{monomer} \cdot c_{monomer} \qquad (1)$$

In equation 1, k_0 represents the estimated rate constant for the decay of the radicals in the absence of a quencher.

We have investigated the reactivity of **G(2–8)•** toward the monomers butyl acrylate (**BA**), methyl acrylate (**MA**) and methyl methacrylate (**MMA**) (Chart 2). The corresponding curves for radical **G(8)•** are shown in Fig. 7b (for **G(2–7)•** see the Supplementary Information).

The addition rate constants for **G(2–8)•** are summarized in Fig. 8 and Table 2. Generally, all Ge-centered radicals show higher reactivity toward methyl methacrylate than toward butyl acrylate and methyl acrylate. The higher reactivity toward methacrylates than to acrylates suggests that Ge-centered radicals prefer to react with electron rich double bonds. Analogous results have been obtained with phosphorus-centered radicals derived from bisacylphosphane oxide initiators.[14]

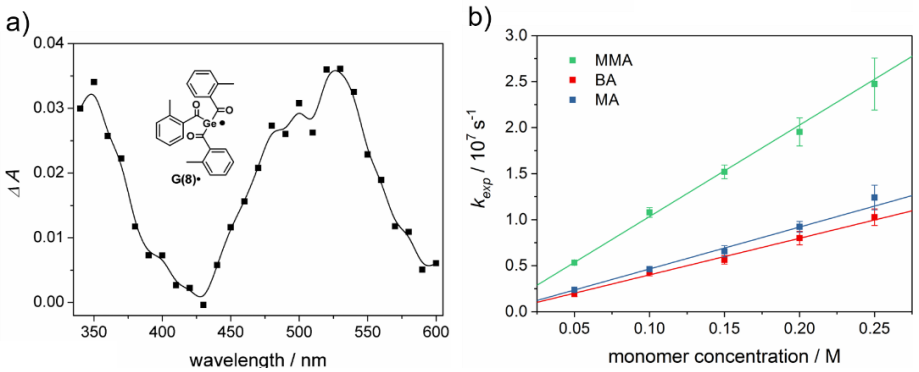

Figure 7. a) Transient optical absorption spectra (absorbance change ΔA versus wavelength) of radical **G(8)•** recorded 200–300 ns after laser excitation (355 nm, 8 ns) of **8** in argon-saturated acetonitrile solutions ($A_{355} \sim 0.3$). b) LFP of **8** in the presence of monomers: pseudo-first-order decay rate constant (k_{exp}) of radical **G(8)•** versus monomer concentration (excitation wavelength: 355 nm, monitoring wavelength: 530 nm).

Chart 2. Chemical structures of the investigated monomers.

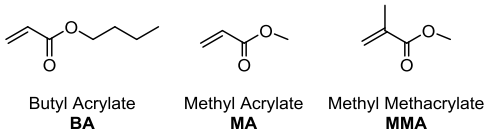

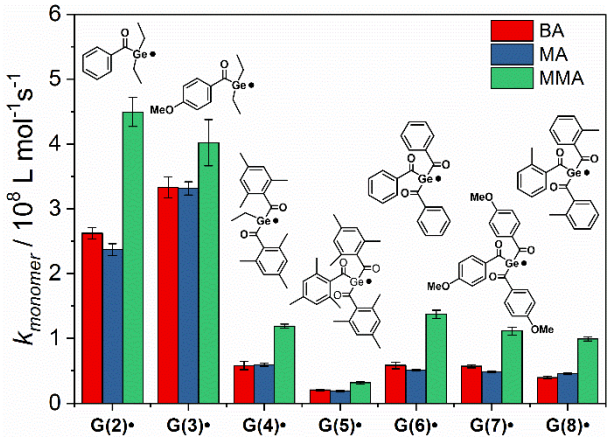

Figure 8. Second-order rate constants $k_{monomer}$ for the addition of **G(2-8)•** to butyl acrylate (**BA**), methyl acrylate (**MA**) and methyl methacrylate (**MMA**).

Table 2. Second-order rate constants $k_{monomer}$ for the addition of Ge-centered radicals **G(2–8)•** to monomers and comparison with phosphorus-centered radicals **P(9)•** and **P(10)•**. Errors are reported as twice the standard deviation from least squares analysis of the data.

	$k_{monomer}$ / 10^8 M^{-1}s^{-1}		
Radical	**BA**	**MA**	**MMA**
G(1)•	–	–	–
G(2)•	2.6 ± 0.1	2.4 ± 0.1	4.5 ± 0.3
G(3)•	3.2 ± 0.2	3.3 ± 0.1	4.0 ± 0.4
G(4)•	0.58 ± 0.06	0.59 ± 0.02	1.2 ± 0.05
G(5)•	0.20 ± 0.01	0.19 ± 0.01	0.32 ± 0.02
G(6)•	0.59 ± 0.05	0.51 ± 0.01	1.4 ± 0.07
G(7)•	0.57 ± 0.03	0.48 ± 0.02	1.1 ± 0.07
G(8)•	0.40 ± 0.01	0.45 ± 0.02	0.99 ± 0.03
P(9)•	0.32 ± 0.03 0.28[a]	–	–
P(10)•	0.12 ± 0.04 0.11[a]	–	–

[a] Value taken from reference[3a].

Addition rate constants toward butyl acrylate are higher for **G(2–8)•** than for phosphorus-centered radicals **P(9)•** and **P(10)•** (see Table 2).[3a,14] Table 2 shows excellent agreement of our measured rate constant with the published value for radical **P(10)•**. For radical **P(9)•**, our rate constant is slightly higher than the value reported by Turro and coworkers.[3a]

Germyl radicals derived from bisacylgermanes **2** and **3** display three to four times higher reactivity toward monomer double bonds than corresponding radicals derived from tris- and tetraacylgermanes **4**-**8**. Steric congestion by the bulky aromatic substituents around the radical center might be the reason for the lower reactivity of **G(4–8)•** when compared to **G(2–3)•**. In derivative **G(5)•**, where the radical center is substantially shielded by three mesitoyl groups, the addition rate constants are substantially lower than for the less sterically congested radicals **G(6–8)•**. The influence of steric factors is further evident by comparing the addition rate constants of **G(4)•** and **G(5)•**. Radical **G(4)•**, stemming from ethyltrismesitoylgermane **4** adds *ca.* three times faster to monomers than **G(5)•**, stemming from the more bulky tetramesitoylgermane **5**. Apart from the less reactive mesitoyl derivative (**5**), all derivatives within the group of tetraacylgermanes show similar reactivity toward monomers. Thus, substituents introduced on the aromatic rings do not interfere with the photoinitiating reactivity, while allowing to specifically tune solubility or absorption properties.

3.3.3.6 Radical Reaction Pathways

Photo-induced *α*-cleavage of **1**–**8** and the corresponding follow-up reactions can be conveniently followed by using ^{1}H CIDNP spectroscopy.[1f,3h,10,15] This NMR-based method reveals products formed exclusively *via* radical pairs (**B•/G•**). Fig. 9 compares the ^{1}H NMR and CIDNP spectra of **2** recorded in presence of butyl acrylate (**BA**). The signals of the methylene protons adjacent to the germanium center (marked with d) appear in strong enhanced absorption in the CIDNP spectrum due to a geminate (or cage) re-formation of **2** from **G•** and **B•**. The emissive quartet at δ = 3.03 ppm (J = 7.2 Hz) and the absorptive triplet at δ = 1.14 ppm (J = 7.2 Hz) are assigned to propiophenone **P**. This assignment is substantiated by an external reference NMR measurement of propiophenone, yielding the above-mentioned chemical shifts and J-couplings. We suggest that **P** is formed *via* recombination of **B•** and an ethyl radical Et•, which is produced in a second cleavage step at the stage of **G•** (Scheme 3). The singlet at δ = 10.01 ppm appearing in enhanced absorption corresponds to the aldehyde proton of the benzaldehyde derivative **BH**. Analogous signals have been observed in the CIDNP spectra of several photoinitiating systems containing a benzoyl moiety.[16] The formation of **BH** is usually attributed to a disproportionation reaction (*β*-hydrogen transfer) of a benzoyl-type radical and radicals, which are able to donate hydrogen atoms.[1f,16] In the absence of monomer, hydrogen atoms can be transferred from the ethyl group of **G•**, resulting in a weak aldehyde signal as described previously.[1f]

In the presence of a monomer, the aldehyde signal becomes significantly more pronounced since radicals from the growing polymer chain can serve as additional hydrogen donors, resulting in the formation of **BH** and chain termination products (*i.e*. species **GM=**, Scheme 3). Fig. 9 additionally shows two strongly

polarized signals consisting of an emissive triplet at δ = 4.59 ppm (J = 7.7 Hz) and an absorptive doublet at δ = 1.65 ppm (J = 7.7 Hz). These signals can potentially be assigned to species **GMB**, which is formed upon addition of benzoyl radical **B•** to a chain radical initiated by **G•** (Scheme 3). Photoinitiators **3**–**8** show analogous reactivity toward monomers, whereas aldehyde formation and radical-to-monomer addition products were not observed with monoacylgermane **1**, suggesting inefficient initiation (see the Supplementary Information).

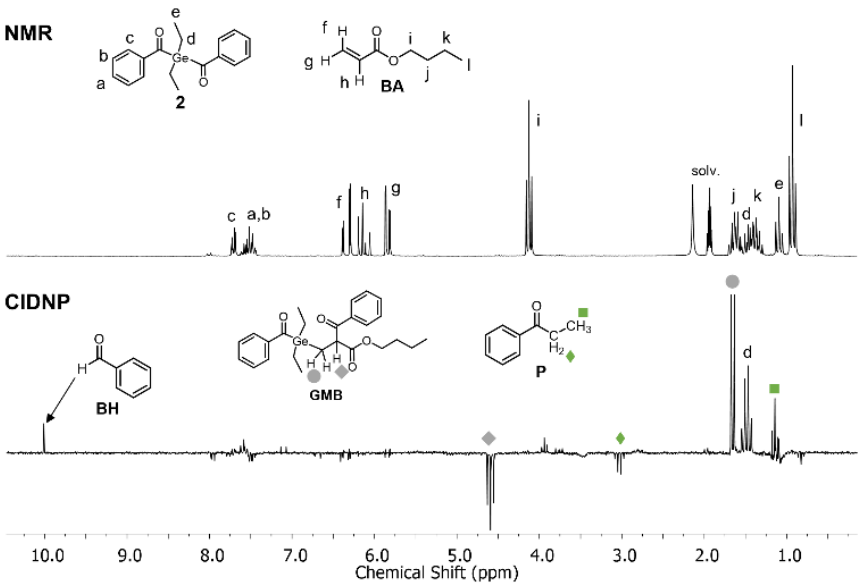

Figure 9. ^{1}H NMR and CIDNP spectra (excitation at λ = 355 nm, *ca.* 70 mJ/pulse) of **2** in the presence of butyl acrylate **BA** (10 mM **2**, 50 mM **BA** in acetonitrile-d_3).

Scheme 3. Proposed reaction scheme of initiator **2** in the presence of monomers.

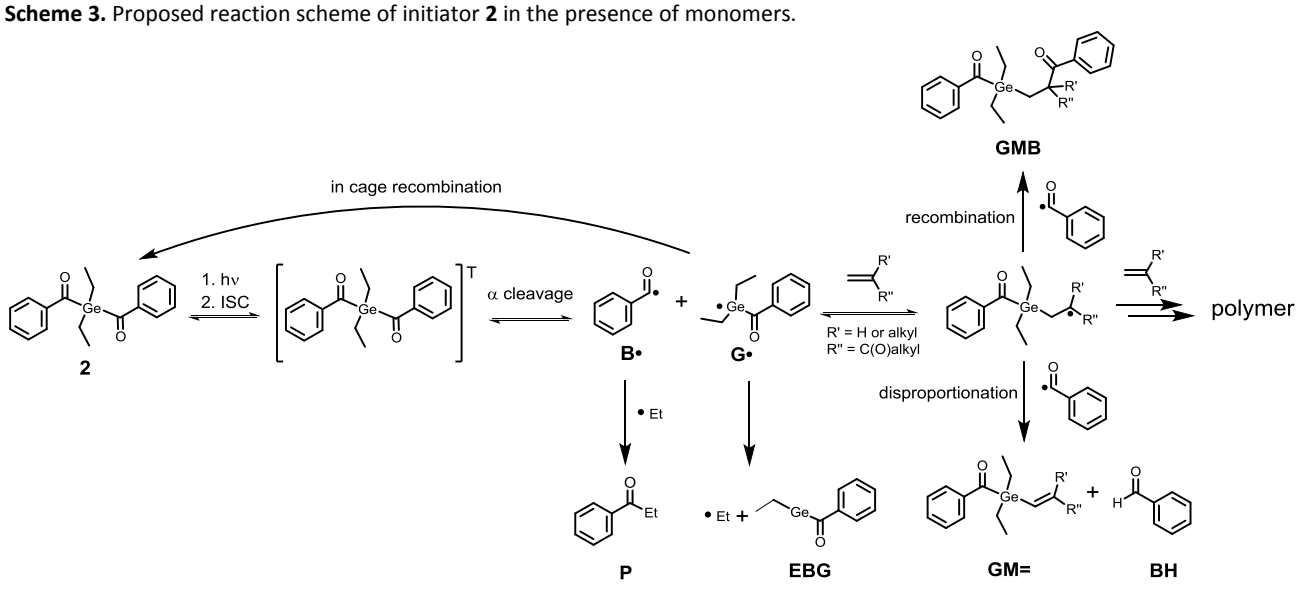

3.3.4 Conclusion

In this contribution, we present a detailed investigation of the photochemistry and photoinitiating properties of a series of mono-, to tetraacylgermanes. We additionally report on the synthesis and characterization of a trisacylgermane photoinitiator.

TR-EPR spectroscopy confirms the formation of germyl and benzoyl-type radicals (**G•** and **B•**) upon triplet-state *α*-cleavage of acylgermanes **1**–**8**. The reaction patterns of the primary radicals **G•** and **B•** in the presence of monomers have been established using CIDNP spectroscopy.

Tetraacylgermanes exhibit higher molar extinction coefficients than mono-, bis- and trisacylgermanes, especially in the long-wavelength region. This is particularly relevant for the application as visible light photoinitiators. Substituents on the aromatic rings lead to a shift of the n-π* absorption bands, with the *o*-tolyl derivative **8** showing the most red-shifted UV-Vis spectrum of all studied compounds. While shifting the absorption bands, substituents do not markedly influence the reactivity of the germanium-centered radicals toward monomers, as was shown using laser-flash photolysis experiments. The reactivity of these radicals toward monomer double bonds was found to be mostly influenced by the type of acylgermane. Germyl radicals derived from bisacylgermanes add faster to monomer double bonds than germyl radicals derived from tetraacylgermanes, both compound classes however being more reactive than related phosphorus-centered radicals.

Photobleaching experiments demonstrate the wavelength-dependent photobleaching behavior of **1**–**8**, with compound **8** displaying the most efficient bleaching upon irradiation with high-wavelength visible light (470 nm LED). Concerning quantum yields of decomposition, bisacylgermanes have been found to be most efficient. We have further discussed the interplay of several factors contributing to the efficiency of photoinitiators, including decomposition quantum yields, absorption spectra and their match with the desired irradiation wavelengths, photobleaching efficiency, amount and reactivity of generated radicals, side reactions, solubility and toxicity.

3.3.5 Experimental Section

3.3.5.1 General Considerations

All synthesis steps were performed under a nitrogen atmosphere using standard Schlenk techniques. Solvents were dried using a column solvent purification system.[17] Commercial KOtBu (97%) was used without further purification. Tetrakis(trimethylsilyl)germane ($(Me_3Si)_4Ge$)[18], ethyltris-(trimethylsilyl)germane ($(Me_3Si)_3GeEt$)[19] and the acid fluorides[20] were prepared according to published procedures. ^1H (299.95 MHz) and ^{13}C (75.43 MHz) NMR spectra were recorded on a Varian INOVA 300 spectrometer in $CDCl_3$ solution and referenced versus TMS using the internal ^2H-lock signal of the solvent. Tetraacylgermanes $Ge[C(O)R]_4$ (R=mesityl (5),[2a] R=phenyl (6),[2a] R=(4-methoxy)phenyl (7),[8] R = (2-methyl)phenyl (8)[8] were synthesized as described previously.[2]

3.3.5.2 Synthesis of Ethyltrismesitoylgermane (4)

A flask was charged with 1.25 g (3.9 mmol) of $(Me_3Si)_3GeEt$ and 0.48 g of KO*t*Bu (4.3 mmol). 10 mL of DME were added. The reaction mixture was stirred for one hour. In a second flask, 3.2 g (19.0 mmol) of mesitoyl fluoride were dissolved in 5 mL DME and the potassium germanide solution was slowly added via a syringe. After complete addition, the reaction mixture was stirred for another 12h. After aqueous work-up with saturated NH_4Cl the phases were separated and the aqueous phase was extracted with dichloromethane. The combined organic layers were dried over Na_2SO_4, filtered and the volatile components were evaporated. The crude product was recrystallized from acetone giving 1.5 g (2.8 mmol, 71%) of pure 4. Melting point: mp 100-103 °C. UV-Vis: λ_{max} (acetonitrile)/nm 382.5 (ε/L·mol^{-1}·cm^{-1} 1303). Elemental analysis: found C, 70.73; H, 7.07. Calc. for $C_{32}H_{38}GeO_3$: C, 70.75; H, 7.05%. ^1H NMR (300 MHz, $CDCl_3$, ppm): δ 6.66 (s, 2H, Aryl-H), 2.21 (s, 3H, *p*-CH_3), 2.09 (s, 6H, *o*-CH_3), 1.37 (q, 2H, Ge-CH_2-CH_3), 1.01 (t, 3H, Ge-CH_2-CH_3), ^{13}C NMR (75.43 MHz, $CDCl_3$, ppm): δ 237.24 (GeC=O), 142.13, 139.02, 132.30, 128.71 (Aryl-C), 21.04 (Mes-*p*-CH_3), 18.92 (Mes-*o*-CH_3), 10.31 ($GeCH_2$-CH_3), 8.62 ($GeCH_2$-CH_3). X-Ray crystallography: CCDC number 1561720.

3.3.5.3 Materials and Solvents for Spectroscopic Investigations

Photoinitiators **1**–**3** were kindly provided by Ivoclar Vivadent AG. The phosphorus-based initiators Irgacure® TPO (**9**) and Irgacure® 819 (**10**) were obtained from TCI. The monomers butyl acrylate (BA, purity ≥ 99.0 %), methyl methacrylate (MMA, purity ≥ 99.0 %) and methyl acrylate (MA, purity ≥ 99.5 %) were obtained from Fluka and freed from stabilizers by passing through a column of basic alumina before use. Propiophenone (99 %) was obtained from Sigma Aldrich and used as received. The solvents acetonitrile

(Sigma Aldrich, ≥ 99.9 %), acetonitrile-d_3 (Euriso-top) and toluene (Fluka, ≥ 99.8 %) were employed as received. All experiments were performed at ambient temperature.

3.3.5.4 UV-Vis Spectroscopy

UV-Vis spectra were recorded on a TIDAS UV-Vis spectrometer (J&M, Germany). For photobleaching experiments (steady state photolysis, SSP), samples were irradiated perpendicular to the light beam of the UV-Vis spectrometer in a fluorescence quartz cuvette (1 cm x 1 cm) while UV-Vis spectra were recorded. Irradiation was performed using low-power LEDs (Roithner Lasertechnik, Austria): LED470 (maximum at 462.5 nm, 30 nm half width, 0.013 W at 20 mA) and LED385 (maximum at 385 nm, 15 nm half width, 0.013W at 20 mA). A spectrophotometer (GL Spectis, GL Optics, Germany) was used to measure the output power of the LEDs and to ensure an equal photon flux for SSP experiments. All LEDs were operated at a photon flux of 0.05 µmol s^{-1}. Samples were prepared to achieve an absorbance within the linear range of the spectrometer during the course of the experiment (0.8–2 mM in a solvent mixture of acetonitrile and MMA (1/1 v/v ratio)). All samples were purged with argon for 5 minutes before the measurement and were magnetically stirred during the experiment to ensure sufficient mixing.

3.3.5.5 Quantum Yields of Decomposition

Quantum Yields of decomposition have been determined using the same setup as described for the photobleaching studies (see above). The evaluation procedure for determining photochemical quantum yields via on-line UV-Vis spectroscopy has been described in detail by our group recently.[8] We compute the quantum yield Φ by using the concentration change and the exact amount of absorbed light at the very beginning of the reaction. The quantum yield Φ is equal to the initial reaction rate divided by the product of the incident light intensity (photon flux I_0) and the fraction of absorbed light f. The initial reaction rate (k) corresponds to the first derivative of the exponential fit of concentration vs. time curves, obtained from the absorbance traces using the extinction coefficients of the photoinitiators.[8,9] For irradiation, the LED operated at 385 nm (LED385) was used. The photon flux I_0 was determined using the spectrophotometer. The factor f is easily calculated from the initial absorbance A of the sample at the irradiation wavelength ($f = 1\text{-}10^{-A}$).[9] All samples were prepared in a solvent mixture of acetonitrile and MMA (1/1 v/v ratio) to achieve an initial absorbance of ∼0.6 at 385 nm. Samples were purged with argon for 5 minutes before the measurement and magnetically stirred. Knowledge of the exact volume of the sample is required for calculating the photon flux of the LED in the unit ($mol \cdot L^{-1} \cdot s^{-1}$). Measuring single absorbance spectra before and after bubbling with argon allows to account for solvent evaporation during the bubbling procedure and to determine the correct sample volume.[8]

3.3.5.6 Laser Flash Photolysis (LFP)

The experiments were performed on a LKS80 Laser Flash Photolysis Spectrometer (Applied Photophysics, UK). Samples were excited with the frequency tripled light from a Spitlight Compact 100 (InnoLas, Germany) solid state Nd:YAG laser at 355 nm (∼10 mJ/pulse, 8 ns). Rate constants for the addition of the germyl radicals to the monomer double bonds were determined in pseudo-first-order experiments; solutions of the compounds in acetonitrile containing monomer concentrations in the range of 0.025 M to 0.5 M and providing absorbance of ∼0.3 at 355 nm were prepared. Static solutions were saturated with argon before the measurements. The decay of the germyl radicals was recorded at the absorption maximum determined from the transient absorption spectra.

3.3.5.7 TR-EPR Spectroscopy

Continuous-wave time-resolved (TR) EPR experiments were performed on a Bruker ESP 300E X-band spectrometer (unmodulated static magnetic field) equipped with a 125 MHz dual channel digital oscilloscope (Le Croy 9400). As the light source, the frequency tripled light of a Nd:YAG laser was used (InnoLas Spitlight 400, 355 nm, operating at 20 Hz, ∼7 mJ/pulse, 8 ns). The setup is controlled by the fsc2 software developed by Dr. J. T. Toerring (Berlin). Spectra were recorded by acquiring the accumulated (50 accumulations) time responses to the incident laser pulses at each magnetic field value of the chosen field range (field steps: 0.2 G). Argon-saturated solutions in toluene (∼15 mM in photoinitiator concentration) were pumped through a quartz flat cell positioned in the cavity of the EPR spectrometer using a flow system (flow rate: 2-3 mL min^{-1}).

3.3.5.8 ^{1}H CIDNP-NMR Spectroscopy

^{1}H NMR and CIDNP experiments were carried out on a 200 MHz Bruker AVANCE DPX spectrometer equipped by a custom-made CIDNP probe head. A Quantel Nd-YAG Brilliant B laser (355 nm, ∼70 mJ/pulse, pulse length 8−10 ns) operating at 20 Hz was employed as the light source. The timing sequence of the experiment consists of a series of 180° radiofrequency (RF) pulses (applied to suppress the NMR signals of the parent compounds), the laser flash, the 90° RF detection pulse and the acquisition of the FID. “Dummy” CIDNP spectra employing the same pulse sequence but without the laser pulse were always measured. Samples were prepared in deuterated acetonitrile and deoxygenated by bubbling with argon before the experiment. Chemical shifts (δ) are reported in ppm relative to tetramethylsilane (TMS) using the residual deuterated solvent signal as an internal reference (CD_3CN, δ_H = 1.94 ppm).

3.3.6 References

[1] a) N. Moszner, F. Zeuner, I. Lamparth, U. K. Fischer, *Macromol. Mater. Eng.* **2009**, *294*, 877; b) N. Moszner, U. K. Fischer, B. Ganster, R. Liska, V. Rheinberger, *Dent. Mater.* **2008**, *24*, 901; c) B. Ganster, U. K. Fischer, N. Moszner, R. Liska, *Macromolecules* **2008**, *41*, 2394; d) Y. Catel, U. Fischer, P. Faessler, N. Moszner, *Macromol. Chem. Phys.* **2016**, *217*, 2686; e) N. Moszner, I. Lamparth, J. Angermann, U. K. Fischer, F. Zeuner, T. Bock, R. Liska, V. Rheinberger, *Beilstein J Org Chem* **2010**, *6*, 26; f) D. Neshchadin, A. Rosspeintner, M. Griesser, B. Lang, S. Mosquera-Vazquez, E. Vauthey, V. Gorelik, R. Liska, C. Hametner, B. Ganster, R. Saf, N. Moszner, G. Gescheidt, *J. Am. Chem. Soc.* **2013**, *135*, 17314.

[2] a) J. Radebner, A. Eibel, M. Leypold, C. Gorsche, L. Schuh, R. Fischer, A. Torvisco, D. Neshchadin, R. Geier, N. Moszner, R. Liska, G. Gescheidt, M. Haas, H. Stueger, *Angew. Chem. Int. Ed.* **2017**, *56*, 3103; b) J. Radebner, M. Leypold, A. Eibel, J. Maier, L. Schuh, A. Torvisco, R. Fischer, N. Moszner, G. Gescheidt, H. Stueger, M. Haas, *Organometallics* **2017**, *36*, 3624.

[3] a) S. Jockusch, N. J. Turro, *J. Am. Chem. Soc.* **1998**, *120*, 11773; b) S. Jockusch, I. V. Koptyug, P. F. McGarry, G. W. Sluggett, N. J. Turro, D. M. Watkins, *J. Am. Chem. Soc.* **1997**, *119*, 11495; c) G. W. Sluggett, P. F. McGarry, I. V. Koptyug, N. J. Turro, *J. Am. Chem. Soc.* **1996**, *118*, 7367; d) G. W. Sluggett, C. Turro, M. W. George, I. V. Koptyug, N. J. Turro, *J. Am. Chem. Soc.* **1995**, *117*, 5148; e) I. Gatlik, P. Rzadek, G. Gescheidt, G. Rist, B. Hellrung, J. Wirz, K. Dietliker, G. Hug, M. Kunz, J.-P. Wolf, *J. Am. Chem. Soc.* **1999**, *121*, 8332; f) G. Müller, M. Zalibera, G. Gescheidt, A. Rosenthal, G. Santiso-Quinones, K. Dietliker, H. Grützmacher, *Macromol. Rapid Comm.* **2015**, *36*, 553; g) D. E. Fast, M. Zalibera, A. Lauer, A. Eibel, C. Schweigert, A.-M. Kelterer, M. Spichty, D. Neshchadin, D. Voll, H. Ernst, Y. Liang, K. Dietliker, A.-N. Unterreiner, C. Barner-Kowollik, H. Grützmacher, G. Gescheidt, *Chem. Commun. (Camb)* **2016**, *52*, 9917; h) M. Griesser, D. Neshchadin, K. Dietliker, N. Moszner, R. Liska, G. Gescheidt, *Angew. Chem. Int. Ed.* **2009**, *48*, 9359.

[4] A. Castel, P. Rivière, J. Satgé, D. Desor, *J. Organomet. Chem.* **1992**, *433*, 49.

[5] Scientific documentation bluephase(R) family - LED for every use, Ivoclar Vivadent (R).

[6] a) K. Dietliker, T. Jung, J. Benkhoff, H. Kura, A. Matsumoto, H. Oka, D. Hristova, G. Gescheidt, G. Rist, *Macromol. Symp.* **2004**, *217*, 77; b) D. E. Fast, A. Lauer, J. P. Menzel, A.-M. Kelterer, G. Gescheidt, C. Barner-Kowollik, *Macromolecules* **2017**, *50*, 1815; c) A. Lauer, D. E. Fast, J. Steinkoenig, A.-M. Kelterer, G. Gescheidt, C. Barner-Kowollik, *ACS Macro Lett.* **2017**, *6*, 952.

[7] S. C. Ligon, B. Husár, H. Wutzel, R. Holman, R. Liska, *Chem.Rev.* **2014**, *114*, 557.

[8] E. Stadler, A. Eibel, D. E. Fast, H. Freißmuth, C. Holly, M. Wiech, N. Moszner, G. Gescheidt, *Photochem. Photobiol. Sci.* **[under revision]**.

[9] K. L. Willett, R. A. Hites, *J. Chem. Educ.* **2000**, *77*, 900.

[10] A. Yurkovskaya, O. Morozova, G. Gescheidt in *Encyclopedia of Radicals in Chemistry, Biology, and Materials* (Eds.: C. Chatgilialoglu, A. Studer), John Wiley & Sons, Chichester, West Sussex, Hoboken, N.J., **2012**.

[11] J. C. Scaiano in *Reactive intermediate chemistry* (Eds.: R. A. Moss, M. Platz, M. Jones), Wiley-Interscience, Hoboken, N.J., **2004**.

[12] J. Lalevée, X. Allonas, J. P. Fouassier, *Chem. Phys. Lett* **2009**, *469*, 298.

[13] C. S. Colley, D. C. Grills, N. A. Besley, S. Jockusch, P. Matousek, A. W. Parker, M. Towrie, N. J. Turro, P. M. W. Gill, M. W. George, *J. Am. Chem. Soc.* **2002**, *124*, 14952.

[14] A. Eibel, M. Schmallegger, M. Zalibera, A. Huber, Y. Bürkl, H. Grützmacher, G. Gescheidt, *Eur. J. Inorg. Chem.* **2017**, *2017*, 2469.

[15] U. Kolczak, G. Rist, K. Dietliker, J. Wirz, *J. Am. Chem. Soc.* **1996**, *118*, 6477.

[16] A. Borer, R. Kirchmayr, G. Rist, *Helv. Chim. Acta* **1978**, *61*, 305.

[17] A. B. Pangborn, M. A. Giardello, R. H. Grubbs, R. K. Rosen, F. J. Timmers, *Organometallics* **1996**, *15*, 1518.

[18] A. G. Brook, F. Abdesaken, H. Söllradl, *J. Organomet. Chem.* **1986**, *299*, 9.

[19] J. Fischer, J. Baumgartner, C. Marschner, *Organometallics* **2005**, *24*, 1263.

[20] L. R. Subramanian, G. Siegemund (Eds.) *Houben-Weyl Methods of Organic Chemistry Supplement: Organo-Fluorine Compounds Fluorinating Agents and Their Application in Organic Synthesis*. Introduction of Fluorine with Alkali Metal Fluorides, Including Ammonium Fluoride and Tetraalkylammonium Fluorides (Including Special Methods of Fluorinations, e.g., Phase Transfer Catalysis, Activation by Crown Ethers, Reagents Bound to Polymers), Thieme, Stuttgart, **1998**.

3.4 Tetraacylgermanes as Highly Efficient Photoinitiators for Visible Light Cured Dimethacrylate Resins and Dental Composites

Norbert Moszner[a]*, Urs Karl Fischer[a], Iris Lamparth[a], Pascal Fässler[a], Judith Radebner[b], Anna Eibel[c], Michael Haas[b], Harald Stueger[b], and Georg Gescheidt[c]

[a]Ivoclar Vivadent AG, Bendererstrasse 2, FL-9494 Schaan, Liechtenstein

[b]Institute of Inorganic Chemistry, Technische Universität Graz, Stremayrgasse 9, A-8010 Graz

[c]Institute of Physical and Theoretical Chemistry, Technische Universität Graz, Stremayrgasse 9, A-8010 Graz

published in *Journal of Applied Polymer Science*, **2017**, 27, 46115.

Graphical Abstract:

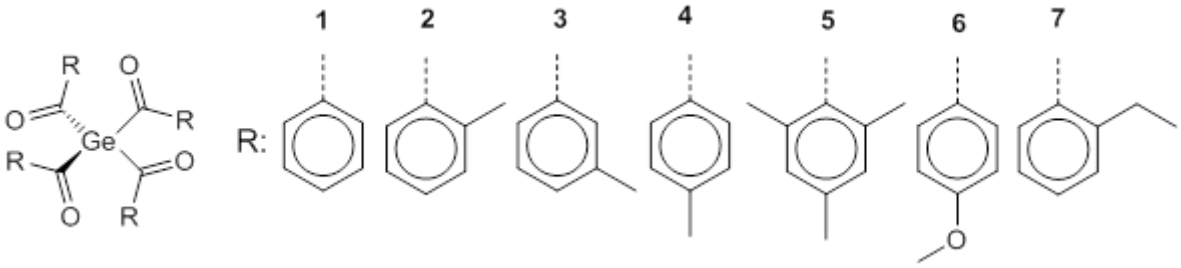

3.4.1 Abstract

Tetrabenzoylgermane **1** and various substituted tetrabenzoylgermanes **2**-**7** were investigated as visible light (VL) photoinitiators (PIs) for dental dimethacrylate resins and composites based thereon. The tetrabenzoylgermanes **1**-**7** show a very strong VL absorption between 400-450 nm. Substituents on the benzoyl chromophore strongly influence their properties such as melting point, solubility, absorption behavior or PI reactivity. A good photobleaching behavior and a very high reactivity as VL PI was found in photo-DSC experiments for selected tetrabenzoylgermanes. Composite pastes containing only ~0.1 wt% of Ge-PI exhibited a sufficient photocuring due to the high PI-reactivity of the tetraacylgermanes. Among the investigated germane PIs, tetrakis(2-methylbenzoyl)germane **2** shows the best performance as VL PI for restorative composites and enables photocuring using an LED with an emission maximum of 500 nm.

3.4.2 Introduction

Today, durable aesthetic tooth-colored resin-based filling composites in combination with efficient enamel-dentin adhesives are very popular and play an important role in modern dentistry. Resin-based dental composites are used as luting cements and restorative filling materials. Luting cements with a filler content between 55 and 70 wt% are used for the cementation of indirect restorations such as inlays, onlays, crowns or veneers and show high tensile and compressive strengths, and the lowest solubility compared to conventional cements, such as glass ionomer cements. Different resin-based direct filling composites are distinguished mainly by their viscosity in condensable/packable composites and flowable composites. Packable composites exhibit a higher viscosity and filler load (75-85 wt%), are condensable like amalgam and enable the formation of tight interproximal contacts. Flowable composites are characterized by a lower viscosity and filler load (65-75 wt%) and have the ability to be syringed into a cavity preparation with a needle tip.[1] Nowadays, so-called bulk–cure composites have been developed, distinguished by a shorter curing time and improved curing depth.[2] All these direct restorative composites are mainly based on mixtures of different fillers, crosslinking and functionalized methacrylates, and are mostly cured by visible light (VL) photoinitiators (PIs).[3] Most of the VL curable dental materials are still based on bimolecular PI systems, which are combinations of camphorquinone (CQ) with suitable tertiary amines (A) as coinitiator.[4] CQ-based PI systems allow fast curing of relatively thick layers, compared to UV curing. However, disadvantages of the CQ/A PIs concern the yellowing of the cured materials caused by oxidation of amine impurities and the relatively low quantum yield of radical formation. Furthermore, in CQ/A PIs as bimolecular photoinitiating systems, the interaction of the partners is strongly influenced by the viscosity of the medium and therefore such binary PIs tend to generate significant inhibition layers. Finally, in water-based acidic dental compositions, such as enamel-dentin adhesives, the acid-base reaction of the frequently used strongly acidic adhesive monomers with the amine coinitiator affects the initiating efficiency of the CQ/A PIs.[5] In this context, it could be shown that benzoyltrimethylgermane (**BTMGe**) and dibenzoyldiethylgermane can be used as VL PIs for the photopolymerization of dimethacrylate mixtures and thereon-based composites.[6] Further structure optimizations resulted in the development of the PI bis-(4-methoxybenzoyl)diethylgermane (**BMBDGe**), which was commercialized under the brand name Ivocerin®.[7] The bisacyldialkylgermanes are amine-free monomolecular PIs, which show very good solubility in dimethacrylate resins, strong absorption in the blue region of the VL spectrum, very high light sensitivity and reactivity as VL PI, very good storage stability at room temperature or elevated temperature and excellent bleaching behavior. Furthermore, it could be shown that **BMBDGe** is not only a very efficient PI for the photopolymerization of dimethacrylates, but also for bisacrylamides

or 2-vinylcyclopropanes.[8] Unfortunately, **BMBDGe** is a very expensive PI. The high price is due to the expensive starting compound dichlorodiethylgermane, the application of a dithiane-protecting group in the synthesis and the purification of **BMBDGe** by column chromatography. Recently, is was shown that tetraacylgermanes are available by a simplified synthetic approach starting from the less expensive tetrachlorogermane, without necessity of a protecting group and a purification procedure avoiding column chromatography.[9] Moreover, many tetraacylgermanes are crystalline solids and very reactive monomolecular VL PIs at very low PI concentration. Tetraacylgermanes form a Ge-centered radical and a benzoyl radical upon α-cleavage of the Ge-carbonyl bond (Scheme 1).

Scheme 1. α-Cleavage of the tetraacylgermane derivatives, leading to the formation of a Ge-centered radical and a benzoyl radical.

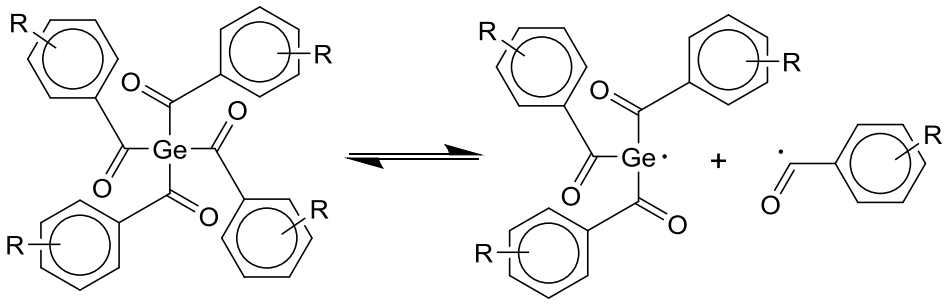

In this paper we report the use of tetrabenzoylgermane **1** and different tetrabenzoylgermane derivatives **2-7** as VL PIs in dimethacrylate resins or - dental composites based thereon.

Scheme 2. Structure of different tetraacylgermanes **1**-**7** used as PI

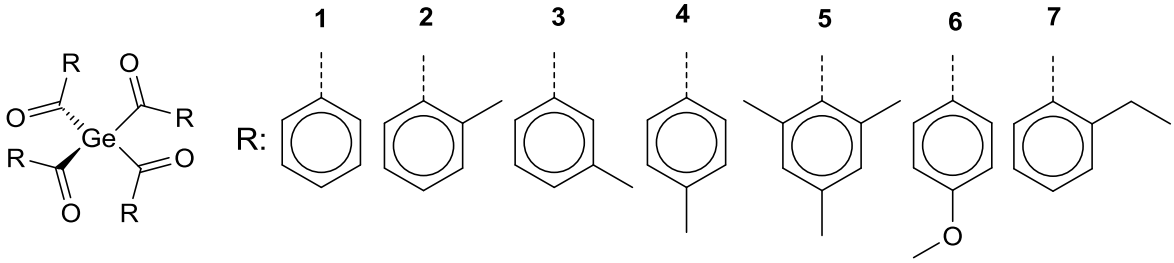

3.4.3 Results and Discussion

3.4.3.1 UV-Vis spectroscopy and Photo-DSC

The tetraacylgermanes **1**-**7** are deeply yellow colored crystalline solids featuring quite different melting points (Table 1), which are significantly higher compared to the bisacylgermane **BMBDGe** (47-50 °C). The unsubstituted compound **1** melts at 83 °C, while the monomethyl-substituted derivatives show higher melting points, for example 123-125 °C for the *ortho*-substituted compound **2**, and 92-94 °C for the *meta*-substituted derivative **3**. Surprisingly, the *para*-substituted compound does not melt below 230 °C and decomposes at higher temperatures. . The mesitoyl derivative **5** melts at 198-199 °C, whereas the *para*-CH_3O compound **6** decomposes above 221 °C. The lowest melting point was observed in the case of the *ortho*-ethyl-substituted tetraacylgermane **7** (73-75 °C). Compounds with high melting points can easily be crystallized upon synthesis, they show a significantly lower solubility in organic solvents, however. Therefore, compounds **1**, **2, 3** and **7** exhibit the highest solubilities in organic solvents and mono- or dimethacrylates, which is important for their use as photoinitiators in dental composites. In contrast to this, the tetraacylgermanes **4** and **6** show only poor solubility.

Table 1. Melting point, longest wavelength absorption maxima λ_{max} (acetonitrile solution) and extinction coefficient ε of the n/σ-π^* transition of tetraacylgermanes **1**-**7,** monoacylgermane **BTMGe**, bisacylgermane **BMBDG,** and trisacylgermane **ETMGe**

Acylgermane	Mp (°C)	λ_{max} (nm)	ε (L·mol^{-1}·cm^{-1})
1	83	403, 424sh	1063, 903
2	123-125	405	1403
3	92-94	403	1043
4	>230[1)]	399, 422sh	1450, 1213
5	198-199	376	1984
6	>221[1)]	393, 413sh	2010, 1738
7	73-75	405	1272
BTMGe	-[2)]	412	137
BMBDGe	47-50	408	724
ETMGe	100-103	381, 400sh	1336, 985

[1)] Decomposition, [2)] Liquid

The UV-Vis absorption spectra of **1** and of the monomethyl-substituted derivatives **2**, **3**, and **4** are depicted in Figure 1. The longest wavelength absorption bands, which are due to n(C=O)/σ(Ge-C)-π*(C=O/Aryl) transitions, are most important for the VL PI behavior of the compounds. **1** shows the longest-wavelength absorption maxima λ_{max} at 403 nm with a shoulder at 429 nm (Table 1). The absorption spectra of the monomethyl-substituted acylgermanes **2**-**4** are very similar with λ_{max} at 405 nm (**2**), 403 nm (**3**), and 399 nm with a shoulder at 422 nm (**4**). The extinction coefficients ε are between 1043 $L \cdot mol^{-1} \cdot cm^{-1}$ (**3**) and 1403 $L \cdot mol^{-1} \cdot cm^{-1}$ (**2**). In case of *para*-substituted benzoylgermanes, the longest wavelength absorption maximum depends on the substituent.[10] Compared to the unsubstituted compound, the electron-donating methoxy group exhibits a hypsochromic shift, whereas the electron-withdrawing nitro-group causes a bathochromic shift. Taking this into account, the substitution of tetraacylgermanes with methyl groups should not significantly change the longest wavelength absorption maximum. However, the absorption spectra of the mesitoyl derivative **5 (**λ_{max} at 376 nm) (Figure 2) shows a significant hypsochromic shift of the n/σ-π* transition. It could be shown that this hypsochromic shift is due to a steric effect resulting from an out-of-plane torsion of the phenyl ring and the C=O moiety induced by the *ortho*-methyl groups.[9a] The methoxy-substituted tetraacylgermane **6** shows the highest extinction coefficient and a slight hypsochromic shift compared to **1**. As mentioned above, the solubility of **6** in dimethacrylate resins is very poor. Furthermore, it can be seen that the extinction coefficients of the monoacylgermane **BTMGe** (137 L mol^{-1} cm^{-1}) or bisacylgermane **BMBDGe** (724 $L \cdot mol^{-1} \cdot cm^{-1}$) are significantly lower compared to the tetraacylgermanes, for example, compound **2** and **7** with an ε of 1403 and 1272 L mol^{-1} cm^{-1}.

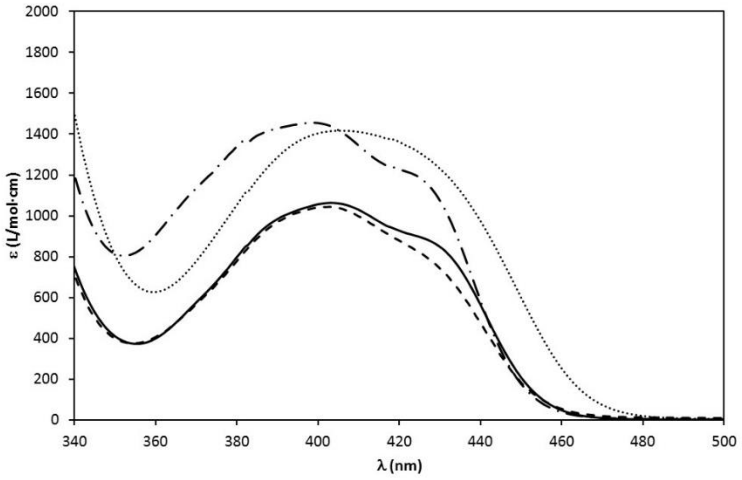

Figure 1. Absorption spectra of tetraacylgermane **1** (—) and monomethyl-substituted derivatives **2** (••••), **3** (---), and **4** (– • –).

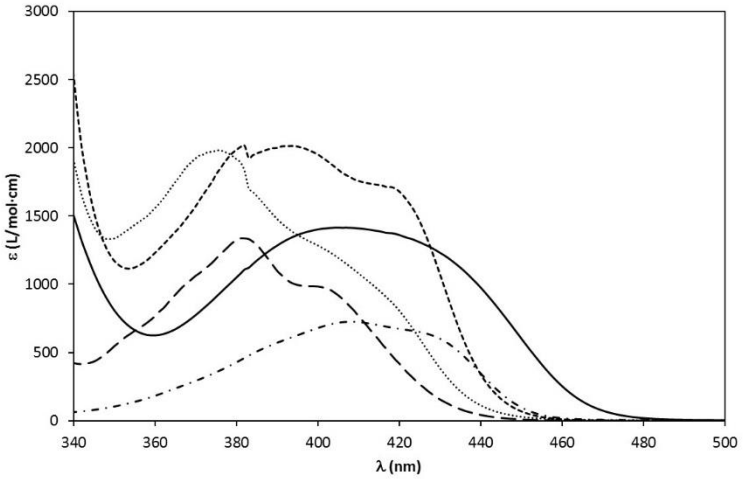

Figure 2. Absorption spectra of bisacylgermane BMBDGe (– • –), trisacylgermane ETMGe (– –), and tetraacylgermanes **2** (—), **5** (••••), and **6** (---)

This is based on the presence of four Ar-C=O chromophores in the tetraacylgermanes compared to one and two, chromophores in **BTMGe** and **BMBDG**, respectively, which results in a more efficient light absorption. The trisacylgermane **ETMGe (**λ_{max} at 381 nm with a shoulder at 400 nm) shows a moderate ε (1336 L mol^{-1} cm^{-1}, 985 L mol^{-1} cm^{-1}), however, it was shown that the monoacylgermane **BTMGe** and the trisacylgermane **ETMGe** exhibit a very unsatisfactory bleaching behavior compared to tetraacylgermanes **1** or **2**.[9c] Moreover, the *ortho*-methyl-substituted tetraacylgermane **2** shows a significant bathochromic shift of the absorption edge compared to other substituted tetraacylgermanes **3**-**6** (Figure 1 and 2). This may allow the use of LED curing lights with an emission spectrum shifted to longer wavelength, which possibly may improve the curing depth of VL-curable composites.

The polymerization initiating reactivity of different tetraacylgermanes **1**-**7** in comparison with the monoacylgermane **BTMGe,** the bisacylgermane **BMBDGe**, and the trisacylgermane **ETMGe** was investigated by photo-DSC using a ternary dimethacrylate mixture (BisGMA: 42%, UDMA: 38%, D_3MA: 20%). For this purpose, relatively low equivalent concentrations (0.82 mmol/L) of the germanium compounds were used as photoinitiators. The polymerization rates $R_{P,max}$ and double-bond conversions DBC of the dimethacrylate mixtures were determined. The relatively low DBC values were caused by the low PI concentration used. The highest $R_{P,max}$ values of 0.045 s^{-1} or 0.046 s^{-1} were found for the tetraacylgermanes **2** or **7** (Table 2). The $R_{P,max}$ values of other tetraacylgermanes were between 0.020 (**4** and **5**) and 0.039 s^{-1} (**1**). The monoacylgermane **BTMGe** (0.004 s^{-1}) showed a significantly lower polymerization initiating reactivity and the trisacylgermane **ETMGe** exhibited a moderate photoinitiator reactivity, which is in consistence with the poor bleaching behavior of the mono- or trisacylgermanes.

In contrast to this, the bisacylgermane **BMBDGe** showed a relatively high $R_{P,max}$ value of 0.033 s^{-1}, which is even higher than that of the methoxy-substituted tetraacylgermane **6**. Only a relatively small amount of 0.05-0.10 wt% of the photoinitiator **2** was necessary for a fast photopolymerization of a methacrylate resin (Figure 3). These results confirm that the tetraacylgermane **2** shows a better polymerization initiating reactivity compared to the best commercially available visible light PI **BMBDGe**.

Table 2. Polymerization rate $R_{P,max}$ and double-bond conversion DBC of a dimethacrylate mixture (BisGMA: 42%, UDMA: 38%, D_3MA: 20%) using tetraacylgermanes **1**-**7**, monoacylgermane **BTMGe**, bisacylgermane **BMBDGe**, or trisacylgermane **ETMGe** as photoinitiator (0.82 mmol/L), irradiation time 120 s.

Acylgermane	$R_{P,max}$ (s^{-1})	DBC (%)
1	0.039	46.6
2	0.046	52.3
3	0.036	47.6
4	0.020	41.7
5	0.020	42.0
6	0.031	49.5
7	0.045	49.1
BTMGe	0.004	15.7
BMBDGe	0.033	46.6
ETMGe	0.019	40.7

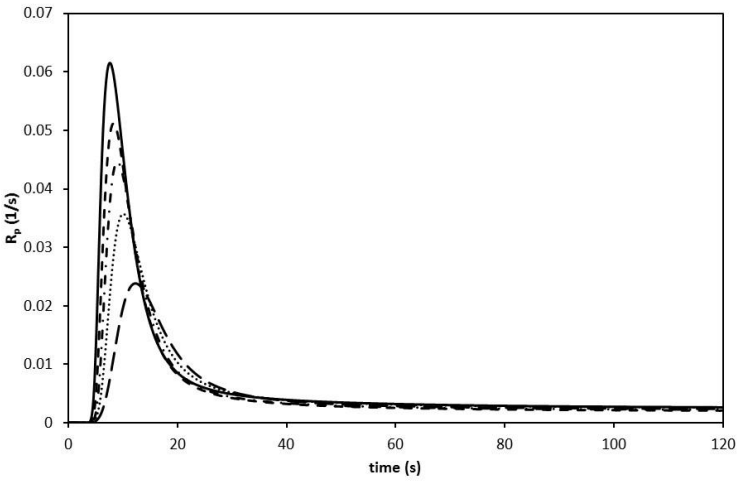

Figure 3. Polymerization rate $R_{P,max}$ of a dimethacrylate resin with different amounts (wt%: 0.01 (– – –), 0.05 (– • –), 0.10 (---), and 0.25 (—)) of tetraacylgermane **2** or **BMBDGe** (0.05 wt%:••••) as PI.

VL PIs used in direct restorative composites must show an excellent bleaching behavior, since residuals of the VL PI in the cured restorative may cause a yellowing, which impairs the aesthetics of the tooth-colored restoration, especially in the incisor region. Therefore, the bleaching behavior of the tetraacylgermane **2** was investigated compared to bisacylgermane **BMBDGe**, which presently shows the best photobleaching among VL PIs used in restorative composites. For this purpose, a 0.5 M solution of MMA in acetonitrile containing 1.0 mmol/L of the PIs was irradiated with the LED light Bluephase 20i. In these irradiation experiments, a monomer solution was used in order to inhibit the formation of recombination products of the formed benzoyl and germyl radicals. After an irradiation time of 1, 2, 3, 4, 5, 10 and 20 s, the UV-Vis spectra of the solutions were measured. The results (Figure 4) substantiate the excellent bleaching behavior of the **BMBDGe** solution, which was nearly completely discolored after 10 s. In comparison, a similar discoloration of the tetraacylgermane **2** solution took place after about 20 s (Figure 5). Nevertheless, the photobleaching of **2** occurs significantly faster compared to CQ, which is frequently used in dental composites.

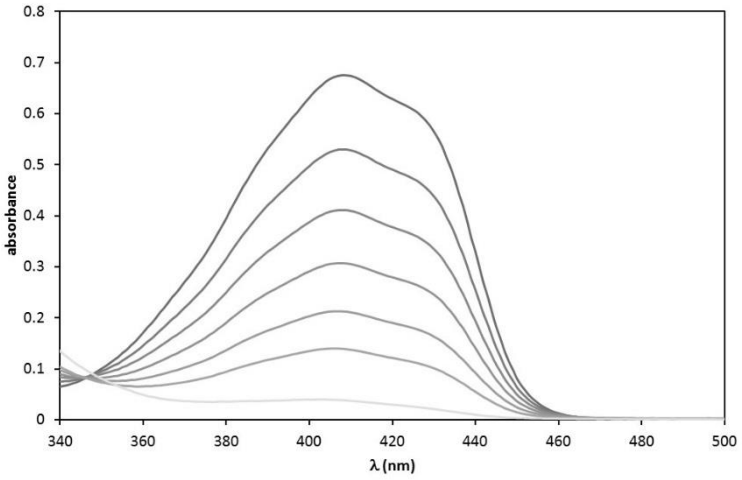

Figure 4. Absorption spectra of a solution of bisacylgermane **BMBDGe** (1.0 mmol/L) and MMA (0.5 mol/L) in acetonitrile after irradiation for 0, 1, 2, 3, 4, 5, and 10 s with the LED Bluephase 20i.

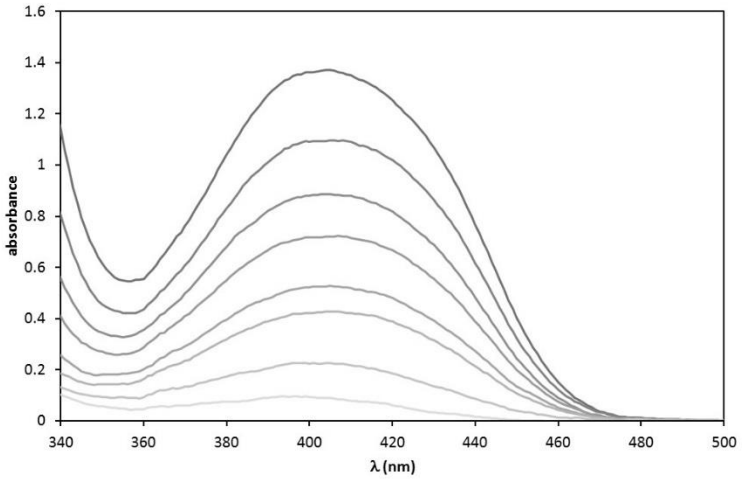

Figure 5. Absorption spectra of a solution of tetraacylgermane **2** (1.0 mmol/L) and MMA (0.5 mol/L) in acetonitrile after irradiation for 0, 1, 2, 3, 4, 5, 10, and 20 s with the LED Bluephase 20i.

3.4.3.2 Photopolymerization of composites

To evaluate the general curing behavior of the new tetraacylgermane PIs **1**-**3** and **5**-**7** in dental composite formulations, flowable composites FC1-6 were prepared based on a ternary dimethacrylate resin mixture of BisGMA, D_3MA, and UDMA with a total filler load of ~66 wt% (Table 3). Unfortunately, the solubility of the tetraacylgermane **4** was too low for the preparation of VL curable composites. For comparison, flowable composites based on bisacylgermane **BMBDGe** (FC7) and the trisacylgermane **ETMGe** (FC8) as PIs were used. For the flowable composite, a relatively low PI concentration (0.82 mmol/L) was used in order to find significant differences in the photoinitiating reactivity of the different PIs. The flowable composite specimens were cured for 6 min in a halogen lamp based light oven (400-500 nm). The flexural strength results (Tab. 3) confirm - similar to DSC results of the resins (Tab. 2) - the best curing performance for the composites based on the tetraacylgermanes **2** (118.9 MPa) and **7** (117.0 MPa). Moreover, also PI **5** resulted in composites with both, a high flexural strength (115.5 MPa) and high modulus of elasticity (6.24 GPa). In contrast to this, the flowable composite based on the high melting tetraacylgermane **6** showed only insufficient photocuring, which is probably due to the incomplete solution of PI **6** in the composite formulation.

Table 3. Flexural strength FS and flexural modulus of elasticity E of a flowable composite (FC) based on a dimethacrylate mixture of BisGMA (14.37 wt%), D_3MA (6.75 wt%), and UDMA (12.49 wt%) using different PIs (0.07 wt%) and a mixture of fillers (glass filler GM 27884: 56.23 wt% ,OX-50: 3.61 wt%, SiO_2-ZrO_2: 4.02 wt%, and YbF_3: 2.51 wt%), 6 min curing in a halogen lamp oven Spectramat.

Composite/PI	FS (MPa)	E (GPa)
FC1/**1**	103.6±6.7	5.74±0.29
FC2/**2**	118.9±4.8	6.59±0.58
FC3/**3**	101.1±6.0	4.90±0.18
FC4/**5**	115.5±8.5	6.24±0.30
FC5/**6**	45.6±6.1	2.23±0.21
FC6/**7**	117.0±9.1	5.85±0.11
FC7/**BMBDGe**	93.5±4.6	4.34±0.15
FC8/**ETMGe**	108.1±9.5	5.35±0.30

Compared to the tetraacylgermanes **2**, **5**, and **7** the bisacylgermane **BMBDGE** and the trisacylgermane **ETMGe** produced flowable composites with inferior mechanical properties. For a further evaluation of selected tetraacylgermanes, luting cements (LC) based on a binary dimethacrylate mixture of UDMA and TEGDMA with a filler load of 60 wt% were prepared. For this purpose, the tetraacylgermanes **1**, **2**, and **7**, which show the best solubilities in the diluent monomer TEGDMA, were selected. For comparison, luting cements based on bisacylgermane **BMBDGE** (LC5) and the binary mixture of CQ-EMBO (LC6) as VL PIs were used (Table 4). The molar concentration of the used germane-based PIs and CQ was equal (31.5 mmol/L) in all composite cements. This is a usual PI concentration in fast curing dental composites,[11] but this concentration is significantly higher compared to the PI concentration (0.82 mmol/L) in the flowable composites FC1-8. The luting cement specimens were cured similarly to the flowable composites. The luting cements based on the tetraacylgermanes **1**, **2**, and **7** confirm a superior photoinitiating performance compared to the binary CQ/amine photoinitiator, which presently is the most frequently used PI in dental composites. Surprisingly, the composite cement based on the bisacylgermane **BMBDGe** showed a significantly higher flexural strength.

Table 4. Flexural strength FS and flexural modulus of elasticity E of luting composite cements (LC) based on a dimethacrylate mixture of TEGDMA (7.8 wt%) with UDMA (31.7 wt%), and a mixture of fillers (OX-50 and YbF_3: 18.7 wt%) using different PIs, 6 min curing in a halogen lamp oven Spectramat.

Composite (PI/wt%)	OX-50 (wt%)	FS (MPa)	E (GPa)
LC1 (**1**/0.49)	41.31	134.0±17.0	6.63±0.53
LC2 (**2**/0.56)	41.24	132.2±8.1	5.78±0.25
LC3 (**7**/0.57)	41.23	127.9±13.2	5.91±0.30
LC4 (**BMBDGe**/1.01)	40.79	144.4±	6.31±
LC5 (**CQ**/0.30)[a)]	41.10	111.3±	5.38±

[a)] EMBO: 0.40 wt%

This result confirms that the optimal PI concentration of the tetraacylgermanes, which show a very strong VL absorption, is lower compared to the bisacylgermane **BMBDGe**.

Nowadays, LEDs are widely used for the curing of restorative composites instead of halogen lamps.[12] Currently used third generation blue LED curing lights, for example Bluephase 20i, are based on a combination of violet and blue LEDs arranged in an array within the curing light and therefore show a bimodal emission spectrum (Figure 6). These so-called multiwave curing LED lights permits the use of mixtures of different PIs, which may increase the depth of cure, especially for bulk-cure composites. Moreover, it is expected that the use of LEDs with a maximum of the emission spectrum at longer wavelength should further increase the curing depth of composites because of the reduced optical interaction of the long wavelength light with the composite filler particles. Therefore, the photocuring of flowable composites based on the tetraacylgermanes **1** and **2** was carried out using the multiwave LED Bluephase 20i (λ_{max} = 410 and 460 nm) and two monowave LEDs with λ_{max} = 480 and 500 nm, respectively (Figure 6). According to the ISO standard[13] the curing was performed by overlapping of irradiation zones 14 times, 20 s each. As comparison, a flowable composite based on the bisacylgermane **BMBDGe** was investigated.

Table 5. Flexural strength FS and flexural modulus of elasticity E of flowable composites based on a dimethacrylate mixture of BisGMA (14.37 wt%), D_3MA (6.75 wt%), and UDMA (12.49 wt%) with different PIs (0.03 wt%) and a mixture of fillers (glass filler GM 27884: 56.23 wt% ,OX-50: 3.61 wt%, SiO_2-ZrO_2: 4.02 wt%, and YbF_3: 2.51 wt%), each cured with the LED Bluephase 20i (λ_{max} = 410 and 460 nm) or LEDs with λ_{max} = 480 or 500 nm.

PI/Curing LED	FS, 24 h H_2O (MPa)	E, 24 h H_2O (GPa)
1/20i	104.4±5.9	5.40±0.35
1/BP 480 nm	97.5±7.3	3.49±0.26
1/BP 500 nm	60.5±4.9	1.66±0.11
2/20i	118.6±3.2	6.17±0.43
2/BP 480 nm	123.1±12.1	5.90±0.59
2/BP 500 nm	112.3±7.1	4.45±0.43
BMBDGe/20i	109.7±12.5	5.00±048
BMBDGe/BP 480 nm	82.6±5.2	3.18±0.17
BMBDGe/BP 500 nm	21.5	0.45±0.10

Table 6. Flexural strength FS and flexural modulus of elasticity E of bulk filled composites (BC) based on a dimethacrylate mixture of BisGMA (8.23 wt%), SR-348c (3.89 wt%), and UDMA (8.58 wt%), 0.1 wt% of the PIs, and a mixture of fillers (glass filler GM 27884: 47.50 wt% , prepolymer filler: 17.50 wt%, SiO_2-ZrO_2: 10.00 wt%, and YbF_3: 5.00 wt%), 6 min curing in a halogen lamp oven Spectramat.

BC/PI	FS, 24 h H_2O (MPa)	E, 24 h H_2O (GPa)
BC1/**2**	135.2±10.1	9.86±0.34
BC2/**7**	120±12.1	9.43±0.17
BC4/**BMBDGe**	102.6±21.7	9.67±0.36

The results shown in Table 5 confirm an excellent photocuring of the flowable composites based on the tetraacylgermane **2** for all curing LED lights, whereas the composites based on the tetraacylgermane **1** and the bisacylgermane **BMBDGe** experienced an insufficient photocuring by the LED with λ_{max} = 500 nm. This can be explained by the fact that in the contrast to **2**, the PIs **1** and especially **BMBDGe** do not show any relevant absorption at a wavelength higher than ~470 nm (see Figure 1 and 2). Furthermore, bulk-curable composites BC1-3 of a ternary dimethacrylate resin mixture of BisGMA, SR-348c, and UDMA with a total filler load of ~80 wt% were prepared based on the PIs **2**, **7** and **BMBDGe**, using only a small PI concentration of 0.1 wt%. The results (Table 6) showed an excellent photocuring behavior of composites BC 1 and BC2 based on the tetraacylgermanes **2** and **7**. Nevertheless, also **BMBDGe** resulted in a restorative composite with good mechanical properties. According to the ISO standard[14] intraorally cured restorative composites must have a flexural strength a least of 80 MPa.

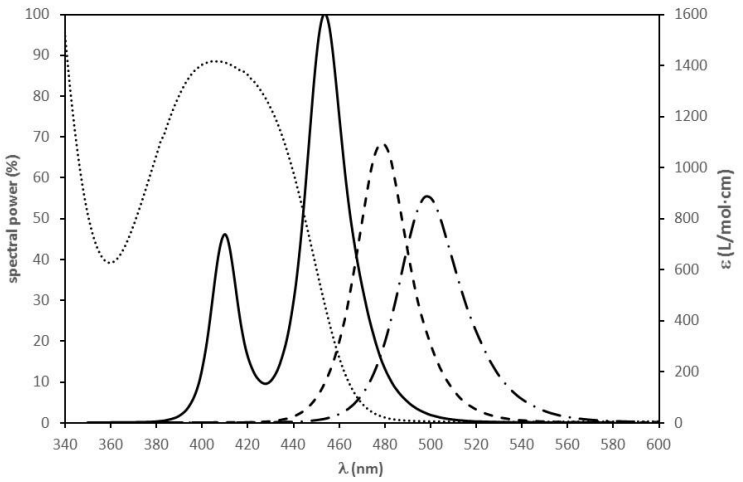

Figure 6. Absorption spectrum of the tetraacylgermane **2** (••••) and normalized spectral emission profiles of the dental multiwave LED Bluephase 20i (—) and of two monowave LEDs with λ_{max} = 480 (– – –) and 500 nm (– • –)

Finally, it should be mentioned that the investigated tetraacylgermanes and thereof based resinds or composites showed an excellent long-term thermal stability during storage at room temperature or 50°C, and the bacterial reverse mutation test (Ames test) proved that the tetraacylgermane **2** and **7** did not induce gene mutations.[15]

3.4.4 Conclusion

Tetrabenzoylgermane **1** and various substituted tetrabenzoylgermanes **2**-**8** are yellow solids, which synthetically are more easily accessible compared to the commercially available dibenzoylgermane **BMBDGe** The substitution on the benzoyl chromophore in the tetrabenzoylgermane strongly influences their properties such as melting point, solubility, absorption behavior or PI reactivity. The tetrabenzoylgermanes **1**-**7** show a very strong VL absorption. Upon VL irradiation, the tetraacylgermanes undergo α-cleavage under formation of a Ge-centered radical and a benzoyl radical. Selected tetrabenzoylgermanes displayed a very high reactivity as VL PIs in dental dimethacrylate resins and composites based thereon. Although the photobleaching behavior of **2** was not as excellent as that of dibenzoylgermane **BMBDGe**, it exceeded the photobleaching of CQ. Among the investigated acylgermane PIs tetrakis(2-methylbenzoyl)germane **2** showed the best VL PI performance at very low PI concentration. PI **2** enabled photocuring using a LED with an emission maximum of 500 nm, which is important for the development of bulk-curable restorative composites with increased curing depth. Based on the excellent PI properties and the relatively easy accessibility, PI **2** has great potential for additional applications such as photopolymerizable adhesives, coatings, or 3D-lithography techniques.

3.4.5 Experimental Section

3.4.5.1 Materials

2,2-Bis-[4-(2-hydroxy-3-methacryloyloxypropoxy)phenyl]propane (Bis-GMA) (DEGACRYL® 6662-0, Evonik), triethylene glycol dimethacrylate (TEGDMA) (Esschem), ethoxylated bisphenol-A dimethacrylate SR348C (Arkema), 1,6-bis-[2-methacryloyloxyethoxycarbonylamino]-2,4,4-trimethylhexane (UDMA), decanediol dimethacrylate (D_3MA), bis-(4-methoxybenzoyl)diethylgermane (**BMBDGe**) (Ivoclar Vivadent AG), DL-camphorquinone (CQ, Rahn, Switzerland), and ethyl *p*-dimethylaminobenzoate (EMBO, Sigma-Aldrich) were purchased from the suppliers indicated above and used without further purification. Benzoyltrimethylgermane (**BTMGe**) was synthesized according to a literature procedure.[6a] Tetrabenzoylgermane (**1**), tetrakis(2-methylbenzoyl)- (**2**), tetrakis(3-methylbenzoyl)- (**3**), tetrakis(4-methylbenzoyl)- (**4**), tetrakis(2,4,6-trimethylbenzoyl)- (**5**), tetrakis(4-methoxybenoyl)- (**6**), and tetrakis(2-ethylbenzoyl)germane (**7**) were synthesized as described previously,[9a,9b] as well as ethyltrismesitoylgermane (**ETMGe**).[9c]

Commercial products were used as fillers: fumed silica OX-50 (Degussa, Germany), YbF_3 (Sukgyung AT Co. Ltd., Korea), SiO_2-ZrO_2 mixed oxide Spherosil (Tokuyama Soda, Japan), and a barium-aluminum-borosilicate glass Ba-Al-B-SiO_2 (GM 27884, Schott, Germany). Before use, the silica, the mixed oxide, and the glass filler were modified with the silane coupling agent 3-methacryloyloxypropyltrimethoxysilane (MPTS, Union Carbide). The fillers, except YbF_3, were silanized by mixing them with 1.0 wt% of water and 5.0 wt% of MPTS at room temperature over a period of two hours. Subsequently, the modified fillers were dried at 50 °C for 4 days. The prepolymer filler was prepared from an initial microfilled composite (containing a mixture of dimethacrylates, a barium-aluminum-borosilicate glass, and YbF_3), which was thermally polymerized and then ground to a fine powder.

3.4.5.2 Methods

UV-VIS spectra were recorded with an UV/VIS spectrometer Evaluation 201 (Thermo Scientific) using acetonitrile as solvent.

3.4.5.3 Preparation and photopolymerization of resins and composites

The monomer mixtures, flowable composites, and luting cements were mixed in an Exakt three roll mill (Exakt Apparatebau, Germany), and the bulk-cure composites using a LPM 0.1 SP kneading machine (Linden, Germany). The photoinitiators were added to the monomer mixtures. The photopolymerization of most of the composites was carried out by irradiating the samples with a visible light oven (400-500 nm, Spectramat®, Ivoclar Vivadent AG). The exposure time of all test specimens was 6 minutes. Additionally, some of the composites were cured using the LED curing light Bluephase 20i (λ_{max} of 410 and 460 nm, Ivoclar Vivadent AG) or LEDs with λ_{max} of 480 and 500 nm (Lumileds, Philips).

3.4.5.4 Photopolymerization procedure with DSC

Photopolymerization was performed on a Perkin Elmer differential scanning calorimeter (DSC), Pyris Diamond. To each monomer mixture, a certain amount of photoinitiator was added. A sample (ca. 0.8-1.5 mg) of each monomer was placed in an uncovered aluminum DSC pan. The DSC chamber was purged with nitrogen for 5 min before polymerization. One minute after placement, the samples were irradiated for 2 min at 30 °C with a LED curing light Bluephase® (Ivoclar Vivadent AG). The incident light intensity was 20 $mW \cdot cm^{-2}$. Each experiment was repeated at least three times. The heat flux was monitored as a function of time using the DSC under isothermal conditions. Double-bond conversion (DBC) in % was calculated as the quotient of the overall enthalpy evolved [ΔH_P (kJ/mol)] and the theoretical enthalpy was obtained for 100% conversion of the monomer [ΔH_{0Pi} (kJ/mol)] (equation (1)).

$$DBC = 100 \cdot \frac{\Delta H_P}{\Delta H_{0Pi}} \qquad (1)$$

where ΔH_{0Pi} is the theoretical enthalpy of monomer i (i = dimethacrylate: ΔH_{0i} = 109.7 kJ/mol). From the height of the exothermic peak h (mW/mg), the polymerization rate $R_{P,max}$ (1/s) can be calculated using equation (2):

$$R_{P,max} = \frac{h}{\Delta H_{0Pi}} \qquad (2)$$

The flexural strength and flexural modulus were determined using dry samples (2x2x25 mm) after storage for 24 h at room temperature. The measurements were carried out in three-point bending tests (span: 20 mm) with a speed of 0.8 mm/min using a BZ2.5/TS1S universal testing machine (Zwick, Germany).

3.4.6 References

[1] a) J. L. Ferracane, *Dent. Mater.* **2011**, *27*, 29; b) P. Singh, N. Kumar, R. Sing, K. Kiran, S. Kumar, *Int. J. Sci. Study* **2015**, *3*, 169.

[2] J. Manhart, R. Hickel, *Swiss Dent. J.* **2014**, *124*, 19.

[3] N. Moszner, T. Hirt, *J. Polym. Sci. A Polym. Chem.* **2012**, *50*, 4369.

[4] N. Moszner, R. Liska in *Basics and applications of photopolymerization reactions* (Ed.: J.-P. Fouassier), Research Signpost, Kerala, India, **2010**, pp. 91–112.

[5] G. Ullrich, B. Ganster, U. Salz, N. Moszner, R. Liska, *J. Polym. Sci. A Polym. Chem.* **2006**, *44*, 1686.

[6] a) B. Ganster, U. K. Fischer, N. Moszner, R. Liska, *Macromol. Rapid Comm.* **2008**, *29*, 57; b) N. Moszner, U. K. Fischer, B. Ganster, R. Liska, V. Rheinberger, *Dent. Mater.* **2008**, *24*, 901; c) B. Ganster, U. K. Fischer, N. Moszner, R. Liska, *Macromolecules* **2008**, *41*, 2394; d) D. Neshchadin, A. Rosspeintner, M. Griesser, B. Lang, S. Mosquera-Vazquez, E. Vauthey, V. Gorelik, R. Liska, C. Hametner, B. Ganster, R. Saf, N. Moszner, G. Gescheidt, *J. Am. Chem. Soc.* **2013**, *135*, 17314.

[7] a) N. Moszner, F. Zeuner, I. Lamparth, U. K. Fischer, *Macromol. Mater. Eng.* **2009**, *294*, 877; b) Team of authors. Ivocerin - A Milestone in Composite Technology, Ivoclar Vivadent Report, No. 19, **2013**.

[8] a) N. Moszner, U. K. Fischer, J. Angermann, *Macromol. Mater. Eng.* **2016**, *301*, 750; b) Y. Catel, U. Fischer, P. Faessler, N. Moszner, *Macromol. Chem. Phys.* **2016**, *217*, 2686.

[9] a) J. Radebner, A. Eibel, M. Leypold, C. Gorsche, L. Schuh, R. Fischer, A. Torvisco, D. Neshchadin, R. Geier, N. Moszner, R. Liska, G. Gescheidt, M. Haas, H. Stueger, *Angew. Chem. Int. Ed.* **2017**, *56*, 3103; b) J. Radebner, M. Leypold, A. Eibel, J. Maier, L. Schuh, A. Torvisco, R. Fischer, N. Moszner, G. Gescheidt, H. Stueger, M. Haas, *Organometallics* **2017**, *36*, 3624; c) A. Eibel, J. Radebner, M. Haas, D. E. Fast, H. Freißmuth, E. Stadler, P. Faschauner, A. Torvisco, I. Lamparth, N. Moszner, H. Stueger, G. Gescheidt, *Polym. Chem.* **2018**, *9*, 38.

[10] W. Feuerstein, S. Höfener, W. Klopper, I. Lamparth, N. Moszner, C. Barner-Kowollik, A.-N. Unterreiner, *Chemphyschem* **2016**, *17*, 3460.

[11] N. B. Cramer, J. W. Stansbury, C. N. Bowman, *J. Dent. Res.* **2011**, *90*, 402.

[12] F. A. Rueggeberg, M. Giannini, C. A. G. Arrais, R. B. T. Price, *Braz. Or. Res.* **2017**, *31*, e61.

[13] International standard ISO/CD 16506: 2014. Filling and restorative materials, 2014.

[14] International standard ISO 4049: 2009. Dentistry - Polymer based restorative materials, 2009.

[15] a) Envigo-Report. Salmonella typhimurium and Escherichia coli Reverse Mutation Assay with K-174, 2016, p 1; b) Envigo-Report. Salmonella typhimurium and Escherichia coli Reverse Mutation Assay with K-201, 2017, p 1.

3.5 A Priori Prediction of Mass Spectrometric Product Patterns of Photoinitiated Polymerizations

Philipp Jöckle,[†,‡] Judith Radebner,[⊥] Michael Haas,[⊥] Iris Lamparth,[∥] Harald Stueger,[⊥] Norbert Moszner,[∥] Andreas-Neil Unterreiner,*[,‡] Christopher Barner-Kowollik*[,†,#]

[†]Macromolecular Architectures, Institut für Technische Chemie und Polymerchemie, Karlsruhe Institute of Techno-logy (KIT), Engesserstrasse 18, 76131 Karlsruhe (Germany) and Institut für Biologische Grenzflächen, Kalsruhe Institute of Technology (KIT), Hermann-von-Helmholtz-Platz 1, 76344 Eggenstein-Leopoldshafen (Germany).

[‡]Molekulare Physikalische Chemie, Institut für Physikalische Chemie, Karlsruhe Institute of Technology (KIT), Fritz-Haber-Weg 2,76131 Karlsruhe (Germany).

[⊥]Institut für Anorganische Chemie, Technische Universität Graz, Stremayrgasse 9/IV, 8010 Graz (Austria).

[∥]Ivoclar Vivadent AG, Bendererstrasse 2, 9494 Schaan (Liechtenstein).

[#]School of Chemistry, Physics and Mechanical Engineering, Queensland University of Technology (QUT), 2 George Street, Brisbane, QLD 4000 (Australia).

published in *ACS Macro Lett.*, **2018**, 7, 132-136.

Graphical Abstract:

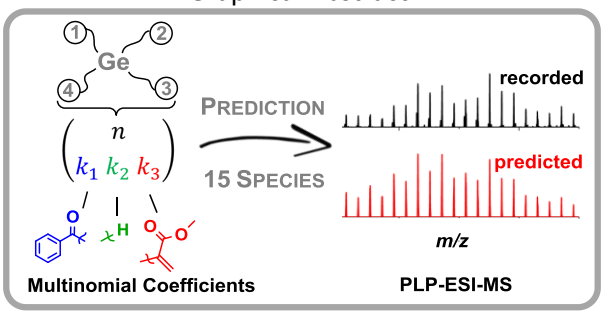

3.5.1 Abstract

We introduce a method for the *a priori* prediction of mass spectra of complex poly(methyl methacrylate)s initiated by photoinitiators featuring multiple cleavage points. The method is based on permutation mathematics using multinomial coefficients to predict the probability of each poly(methyl methacrylate) species' isotopic pattern contribution to the overall mass spectrum. The method assumes a statistical behavior for the cleavage of the photoinitiator. The excellent agreement of the predicted mass spectrum based on multinomial coefficients with the experimental mass spectrum confirms a multi-point cleavage mechanism of the assessed photoinitiators. We exemplify our method for the prediction of mass spectra of poly(methyl methacrylate)s initiated by four tetraacylgermane derivates and one bisacylgermane, recorded after visible light pulsed-laser polymerization by high resolution Orbitrap electrospray ionization mass spectrometry (ESI-MS). The excellent agreement of our approach with experimental data suggests that a wide array of polymer mass spectra of polymers initiated by initiators capable of multiple cleavage events can be quantitatively predicted.

3.5.2 Introduction

Visible light induced radical polymerization is of critical importance for advanced soft matter materials design, including curing technologies,[1] dental fillings,[2] or tissue engineering.[3] The development of visible light photoinitiators plays a key role in these fields due to the bioorthogonal nature of the wavelength.[4] Thus, it is critical to achieve an in-depth understanding of the mechanism of visible light induced radical formation that underpins the synthetic photoinitiator design. For example, mono-, and especially, bis-, and tetra-acylgermanes are potent visible light initiators, which have been shown to undergo an α-cleavage (Type I) leading to the formation of a benzoyl- and a germyl-based radical fragment,[5] without formation of further secondary radicals. In contrast, a secondary radical formation was postulated for bisacylphosphinoxides.[6] We have demonstrated – most recently with monoacylgermanes[5f] – that pulsed laser polymerization (PLP) with subsequent size exclusion chromatography (SEC) coupled with electrospray ionization mass spectrometry (ESI-MS) and evaluated by isotopic pattern simulations is a powerful tool to identify the key radical fragments responsible for inducing macromolecular growth.[7] In a PLP experiment, ns-laser pulses are exciting photoinitiator molecules, which cleave into radical fragments. These primary radicals can initiate or terminate polymerization reactions, whereby termination occurs either via combination or disproportionation. Thus, each laser pulse initiates chain propagation, while concomitantly inducing termination. Subsequent analysis of the PLP sample via (SEC-)ESI-MS affords a complex mass spectrum with several isotopic patterns of polymer species with different end groups within each repeat unit.

3.5.3 Results and Discussion

In the current study, we introduce a powerful and simple to apply statistical method to predict polymer mass spectra of multi-functional initiator species. The method is based on the assumption that radical termination reactions occur statistically for the star polymer species that are formed by multi-cleavable photoinitiators. A prediction for isotopic patterns of star polymers can be calculated by the use of multinomial coefficients. The method was developed on the mass spectrum of poly(methyl methacrylate)s (PMMA) initiated by tetraacylgermane THBG (**Scheme 1**).[5d] In addition, we assessed three tetraacylgermane derivates,[5e] i.e. ToMeBG, ToEtBG, TpPrOBG, and on one bisacylgermane BziG (**Scheme 1**),[5a] which are presented in the Supporting Information. We believe that the provision of a powerful yet

simple method for evaluating complex mass spectra stemming from multi-initiated core units is of critical importance to the community.

Scheme 1. Four tetraacylgermanes and one bisacyl-germane used as test systems in the current study.

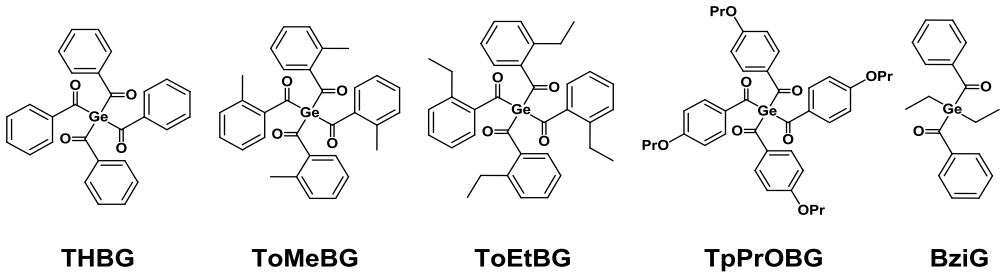

For tetraacylgermanes, only a primary cleavage into a benzoyl and tribenzoylgermyl radical fragment has been reported.[5d,5e] However, there are potentially three further benzoyl moieties available for subsequent radical formation. If all four benzoyl moieties are cleaved, one expects a high number of benzoyl initiated disproportionation and benzoyl terminated combination products. Further, various germanium-centered 4-armed star polymers are expected, with each chain individually terminated by disproportionation or combination. In line with these expectations, the recorded mass spectrum of PMMA initiated by THBG displays complex isotopic patterns with a repeating unit of MMA (*m/z*=100.0524) for example at ~ 1427 *m/z* (**Figure 1**), and a much weaker highly superimposed product distribution, for example at ~ 1405 *m/z* (refer to the inset of **Figure 1**).

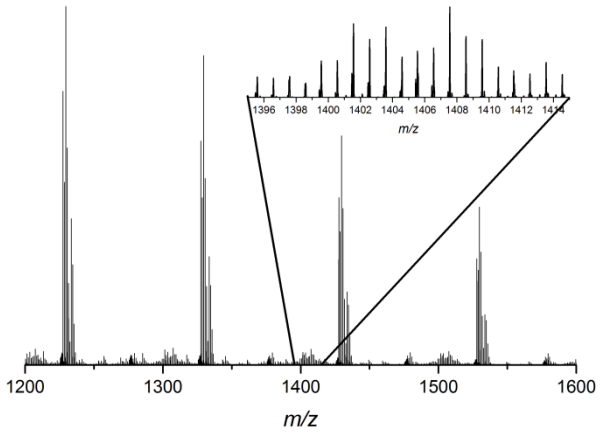

Figure 1. High resolution Orbitrap ESI-MS mass spectrum of several repeating units of PMMA initiated by THBG. Inset: Complex secondary PMMA isotopic pattern caused by multi-fragmentations.

These complex isotopic patterns, for example, near 1427 *m/z* can be assigned to disproportionation and combination PMMA products initiated and terminated by benzoyl radicals, respectively.[5f,7b] The quantitative evaluation of the obtained complex isotopic pattern as depicted in the inset within **Figure 1** is challenging, yet it contains critical information regarding the initiation mechanism of the photoinitiator. Highly superimposed mass spectra are in general challenging to predict or interpret, due to the complex addition of the individual peak to the overall isotopic pattern. Furthermore, the identical nature of isobaric structures with equal sum formulas is strongly reducing the validity of isotopic pattern simulations. This is highly problematic for the validation of star polymer products, because it cannot be safely differentiated between a single polymer chain with *a* repeating units initiated by a tribenzoylgermyl radical or an germanium centered 4-armed star polymer with *b+c+d+e=a* repeating units as illustrated in **Scheme S1**.

In the following, we demonstrate the mechanistic power of our a priori method for highly superimposed mass spectra, which is by definition a validation for star polymer chain growth with statistical termination behavior, independent of the problem of isobaric structures. Herein, it is assumed that all germanium carbonyl carbon bonds are cleaved during the photopolymerization and an *n*-armed star polymer with *n* equivalent ω-positions for termination are available. As a consequence, the termination with *s* different end groups has to occur statistically. Thus, depending on the number of positions *n* and end groups *s*, different classes of species with a certain probability within the *m/z*-range of the same repeating unit can be predicted by the use of multinomial coefficients. In general, a multinomial coefficient determines the permutation possibilities of an order of *n* objects from which *s* groups of $k_1,\ldots,k_s$ are identical (eq.1).

$$\binom{n}{k_1 \ldots k_s} = \frac{n!}{k_1! \cdot k_2! \cdot \ldots \cdot k_s!} \qquad (1)$$

Herein, *n* is the number of possible end group positions, while $k_1,\ldots,k_s$ is the number of 1,2,3,…,*s* different end groups experiencing termination. For tetraacylgermanes, *n*=4 end group positions, which can be occupied by four end groups selected from two disproportionation (= , H) and one benzoyl combination (B) patterns. By considering all possible end group arrangements, four statistical classes (A, B, C, D) of species occur, which are listed in the following. For each statistical class one coefficient is calculated.

Scheme 2. Fifteen germanium-centered 4-armed methyl methacrylate (MMA) star polymers divided into four statistical groups A,B,C,D. For isotopic pattern simulation and exact mass calculation, a Na^+-Ion is added to each structure.

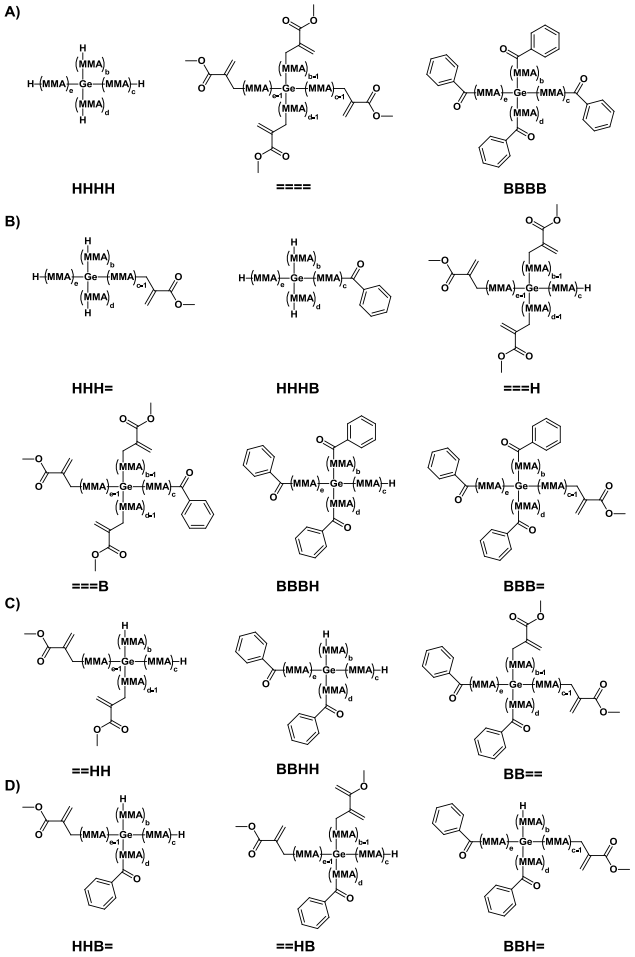

A. Four identical end groups, $\binom{4}{4\ 0\ 0} = 1$

B. Three identical and one different end group, $\binom{4}{3\ 1\ 0} = 4$

C. Two times two identical end groups, $\binom{4}{2\ 2\ 0} = 6$

D. Two identical and two different end groups, $\binom{4}{2\ 1\ 1} = 12$

Each statistical class and therewith multinomial coefficient is constituted of different species of germanium-centered 4-armed star polymers with appropriate end groups as depicted in **Scheme 2**.

A step by step instruction for the formulation of multinomial coefficients is given in **Scheme 3**.

Scheme 3. Step by step instruction for the formulation of multinomial coefficients used for the prediction of isotopic pattern distributions.

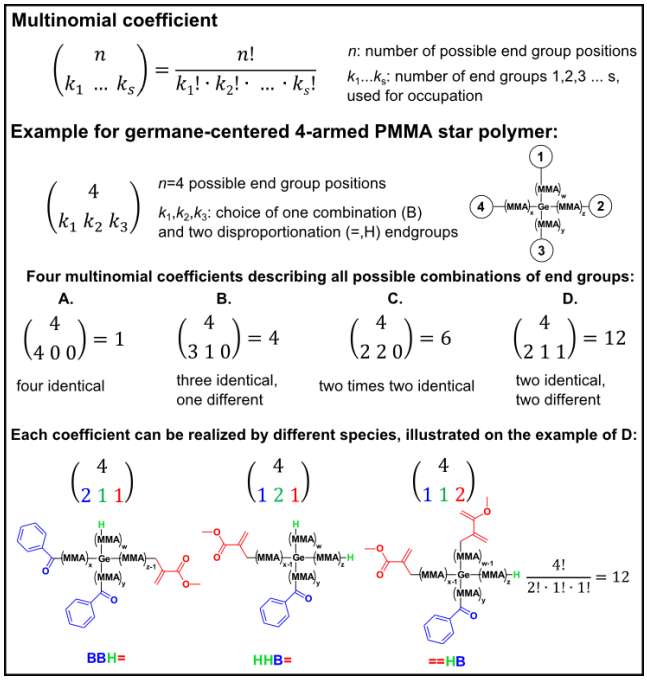

Normalization of the four coefficients in relation to each other leads to a ratio of 0.083 (A) : 0.33 (B) : 0.5 (C) : 1 (D), which can be directly used as the relative amounts of the fifteen germyl species in the isotopic pattern simulation (**Table S1**). Comparison of the peak heights of the recorded benzoyl (**Scheme S2**) and germyl species in **Figure 1** approximately leads to a fitted factor 6.7 (H, =), respectively 3.35 (B), higher relative amount for the predicted benzoyl species than for the statistical group D of the germyl species (**Table S2**). The resulting isotopic pattern simulation compared to the recorded mass spectrum is shown in **Figure 2**. Additional predictions and experimental results of the other test initiator systems (**Scheme 1**) are provided in the Supporting Information (**Figures S2-S5**).

Inspection of **Figure 2a)** indicates that the recorded (black) and predicted spectra (red) are in excellent agreement. A detailed view into the germyl species (**Figure 2b**) reveals good agreement of the peak height distribution of the predicted and recorded spectra. This agreement leads to the mechanistically important conclusion that 4-armed star polymers are generated.

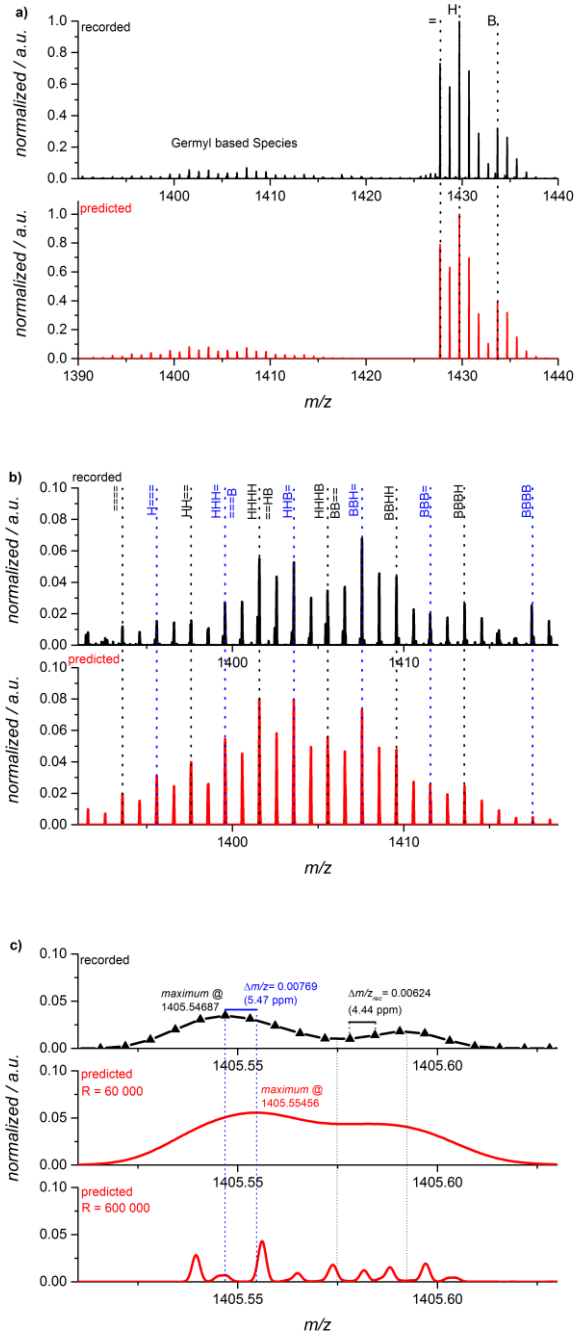

Figure 2. Predicted (red) and recorded mass (black) spectra of PMMA initiated by THBG. a) Overview of benzoyl and germyl species. b) Enlarged view of highly superimposed isotopic patterns of germanium-centered 4-armed star polymers. c) Enlarged view of recorded (black) and predicted (red) mass spectra simulated at two resolutions at ~1405.54 *m/z*.

Thus, unambiguously, the tetraacylgermanes photoinitiators are able to undergo multiple cleavages of the benzoyl moieties. By calculating the ratio of the integrated spectrum in the *m/z*-range of the simulation within a complete repeating unit, it is clear that nearly 89% of isotopic patterns can be explained with the

applied *a priori* prediction. The assignment of the residual 11% of species would need further investigations or a more complex prediction model.

To estimate possible errors in our method, a peak to peak comparison is carried out by calculating the differ-ence $\Delta m/z$ and the mass accuracy dm/m_{sim} in ppm be-tween each peak maximum of the recorded and predicted spectra (**Table 1**).

Table 1. Relative mass differences and mass accuracy of predicted and recorded mass spectra of germanium-centered 4-armed star polymers, according to Figure 2b).

Exact mass $(m/z)_{exp}$ (recorded)	Exact mass $(m/z)_{sim}$ (predicted)	$\Delta m/z = \lvert (m/z)_{exp} - (m/z)_{sim} \rvert$	$dm/m_{sim} = (\Delta m/z)/(m/z)_{sim} \cdot 10^6$ / ppm
1395.5860	1395.5884	0.0024	1.70
1396.5940	1396.5930	0.0011	0.75
1397.6031	1397.5931	0.0101	7.21
1398.6072	1398.5980	0.0092	6.58
1399.5626	1399.5709	0.0083	5.94
1400.5625	1400.5708	0.0083	5.93
1401.5697	1401.5714	0.0017	1.21
1402.5780	1402.5774	0.0006	0.43
1403.5873	1403.5806	0.0068	4.82
1404.5916	1404.5851	0.0065	4.61
1405.5469	1405.5546	0.0077	5.47
1406.5532	1406.5570	0.0038	2.68
1407.5543	1407.5577	0.0034	2.42
1408.5628	1408.5616	0.0013	0.89
1409.5724	1409.5661	0.0063	4.46
1410.5768	1410.5702	0.0066	4.66
1411.5319	1411.5368	0.0049	3.44
1412.5384	1412.5376	0.0008	0.59
1413.5459	1413.5443	0.0016	1.12
1414.5482	1414.5477	0.0005	0.36

Except for one value, all mass differences are smaller than 0.01 and can be averaged to 0.0046 (3.26 ppm). A value of 3.26 ppm is rather small in relation to the high number of fifteen superimposed species. In comparison, the simulation of the three benzoyl initiated species feature an averaged mass difference of 0.0017 (1.22 ppm, cf. **Table S3**). For illustration, the recorded (black) and predicted (red) spectra are presented enlarged near 1405.54 m/z at a (hypothetic) resolution of *R*= 600 000 and an experimentally accessible one at *R*= 60 000 of the simulated isotopic patterns (**Figure 2c)**). Independent of the resolution main and side peak are well represented by the predic-tion. At higher resolution (R= 600 000) nine broadened peaks of different species can be observed in a small mass range of 0.08 m/z (Figure 2c).

On the other hand, the envelope for the lower resolution is still sensitive enough to detect small differences in the peak height of each underlying species. Thus, small changes in the prod-uct height distribution can lead to noticeable mass shift of the envelope. One reason for deviations is the resolution limit of the mass spectrometric experiment. The shift between the recorded (m/z=1405.54687) and predicted maxima (m/z=1405.55456) of Δm/z=0.00769 is in the order of the distance between two measured points Δm/zrec=0.00624 (cf. triangles in Figure 2c)). A further reason is the limitation of the applied statistical model used for the isotopic pattern simulation, which assumes statistical behavior for all termination reactions. Only 4-armed star polymers with three end groups for termina-tion were assumed without any consideration of other reaction pathways.

3.5.4 Conclusion

Remarkably, the excellent overall agreement of the prediction and the experiment implies that all key reaction channels are considered in the pre-sented statistical model. Thus, our simple approach is able to capture a complex mechanistic situation well and provide unambiguous access to the cleavage products of the photoinitiator species. It goes without saying that one may assume a non-quantitative initiator cleavage result-ing in three- and two-armed star polymers, chain branch-ing of two or more polymers, and additional combina-tions of two or more germyl-based radicals, yet clearly these processes are of very minor importance. We thus submit that our prediction approach for complex polymer mass spectra is applicable to all systems where multiple initiation points exist, ranging from a plethora of photo-ini¬tiators to star polymer formation processes based on reversible deactivation radical polymerization protocols. We expect that all monomers which feature a linear chain-growth can be used within our approach. The evaluation procedure should be applicable to all polymer mass spec-tra which are recorded with soft mass spectrometric methods (e.g. matrix assisted laser desorption ionization with time-of-flight detection) without fragmentations during ionization. In the investigated case of several visible light multi-cleavable germyl-initiators, our approach unambiguously demonstrates that multi-cleavage is oper-ational and can be quantitatively predicted.

3.5.5 References

[1] a) K. Dietliker, R. Hüsler, J.-L. Birbaum, S. Ilg, S. Villeneuve, K. Studer, T. Jung, J. Benkhoff, H. Kura, A. Matsumoto, H. Oka, *Progress in Organic Coatings* **2007**, *58*, 146; b) F. Karasu, C. Croutxé-Barghorn, X. Allonas, L. G.J. van der Ven, *J. Polym. Sci. A Polym. Chem.* **2014**, *63*, 3597-3607.

[2] a) N. Moszner, U. K. Fischer, B. Ganster, R. Liska, V. Rheinberger, *Dent. Mater.* **2008**, *24*, 901; b) K. Ikemura, T. Endo, *Dent. Mater. J.* **2010**, *29*, 481.

[3] a) T. Billiet, M. Vandenhaute, J. Schelfhout, S. van Vlierberghe, P. Dubruel, *Biomaterials* **2012**, *33*, 6020; b) K. T. Nguyen, J. L. West, *Biomaterials* **2002**, *23*, 4307.

[4] B. T. Tuten, J. P. Menzel, K. Pahnke, J. P. Blinco, C. Barner-Kowollik, *Chem. Commun.* **2017**, *53*, 4501.

[5] a) B. Ganster, U. K. Fischer, N. Moszner, R. Liska, *Macromolecules* **2008**, *41*, 2394; b) J. Lalevée, X. Allonas, J. P. Fouassier, *Chem. Phys. Lett* **2009**, *469*, 298; c) D. Neshchadin, A. Rosspeintner, M. Griesser, B. Lang, S. Mosquera-Vazquez, E. Vauthey, V. Gorelik, R. Liska, C. Hametner, B. Ganster, R. Saf, N. Moszner, G. Gescheidt, *J. Am. Chem. Soc.* **2013**, *135*, 17314; d) J. Radebner, A. Eibel, M. Leypold, C. Gorsche, L. Schuh, R. Fischer, A. Torvisco, D. Neshchadin, R. Geier, N. Moszner, R. Liska, G. Gescheidt, M. Haas, H. Stueger, *Angew. Chem. Int. Ed.* **2017**, *56*, 3103; e) J. Radebner, M. Leypold, A. Eibel, J. Maier, L. Schuh, A. Torvisco, R. Fischer, N. Moszner, G. Gescheidt, H. Stueger, M. Haas, *Organometallics* **2017**, *36*, 3624; f) P. Jöckle, C. Schweigert, I. Lamparth, N. Moszner, A.-N. Unterreiner, C. Barner-Kowollik, *Macromolecules* **2017**, *50*, 8894.

[6] a) S. Jockusch, N. J. Turro, *J. Am. Chem. Soc.* **1998**, *120*, 11773; b) K. Dietliker, J.-L. Birbaum, R. Hüsler, G. Baudin, J.-P. Wolf, *Chimia* **2002**, *56*, 197; c) D. E. Fast, M. Zalibera, A. Lauer, A. Eibel, C. Schweigert, A.-M. Kelterer, M. Spichty, D. Neshchadin, D. Voll, H. Ernst, Y. Liang, K. Dietliker, A.-N. Unterreiner, C. Barner-Kowollik, H. Grützmacher, G. Gescheidt, *Chem. Commun. (Camb)* **2016**, *52*, 9917.

[7] a) D. E. Fast, A. Lauer, J. P. Menzel, A.-M. Kelterer, G. Gescheidt, C. Barner-Kowollik, *Macromolecules* **2017**, *50*, 1815; b) E. Frick, H. A. Ernst, D. Voll, T. J. A. Wolf, A.-N. Unterreiner, C. Barner-Kowollik, *Polym. Chem.* **2014**, *5*, 5053.

3.6 Recent Advances in Germanium-Based Photoinitiator Chemistry

Michael Haas,[a] Judith Radebner,[a] Anna Eibel,[b] Georg Gescheidt[b] and Harald Stueger*[a]

[a] Institute of Inorganic Chemistry and [b] Institute of Physical and Theoretical Chemistry, Technische Universität Graz, Austria

published in Chemistry – *A European Journal*, 2018, Ahead of Print.

Frontispiece:

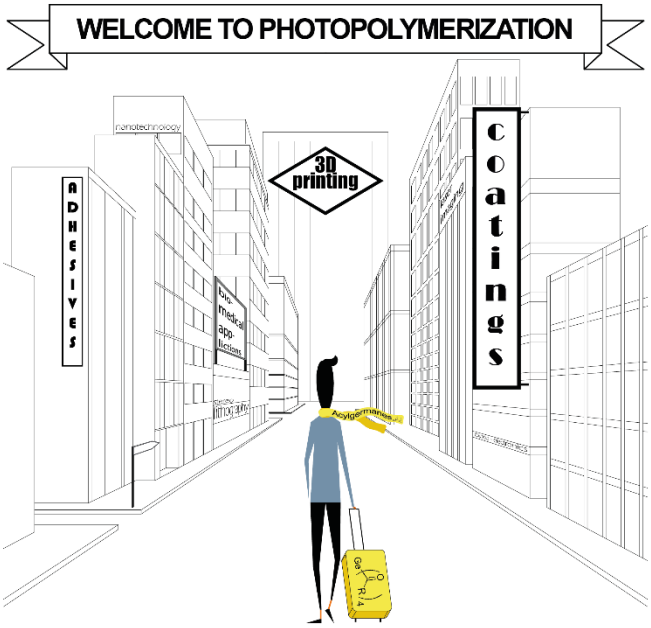

Graphical Abstract:

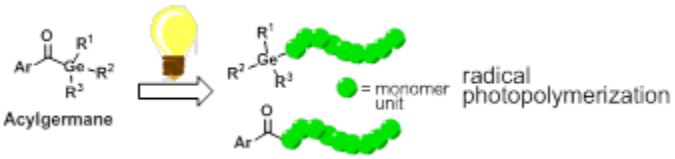

3.6.1 Abstract

Acylgermanes provide an outstanding photo-induced reactivity at highly useful absorption wavelengths. This encouraged multidisciplinary research groups to utilize them as highly effective and non-toxic photoinitiators for, particularly medical applications. In this minireview, we present the most recent breakthroughs to synthesize acylgermanes. We also outline mechanistic aspects of photo-induced reactions of several acylgermane derivatives based on fundamental spectroscopic insights. These studies may aid future developments for tailor-made photoinitiators.

3.6.2 Introduction

In the last decades the demand and application of high performance photochemically produced polymers has been immensely growing. Nowadays, their use is no longer restricted to the manufacture of micro-electronic devices, coatings, adhesives, inks, printing plates, optical waveguides but also emerges fields of medicine (dental filling materials, artificial tissue, heart valves etc.) and fabrication of 3D objects.[1] The world of photopolymerization is requiring high demands on performance of the related products. High functionality of the polymers faces prerequisites such as sustainable, economic and environmentally friendly production. To meet the strict qualifications, especially for medical applications, new types of non-toxic photoinitiating systems are necessary.

Upon absorption of light, the photoinitiating system (consisting of the photoinitiator and/or coinitiator and/or sensitizer) produces reactive species starting the polymerization process. These reactive species may be free radicals as well as ions (e.g. in cationic photopolymerization), generated from one-component (type I), two-component (type II) or multicomponent systems.[2] Type I photoinitiators (PIs) are molecules undergoing triplet-state homolytic bond cleavage, typically featuring a benzoyl moiety as the chromophore.[3] Examples include aryl ketones (e.g. benzoin ether or ester derivatives, α-hydroxy- and α-amino ketones), acylphosphane oxides as well as acylgermanes (Scheme 1).[4]

Scheme 1. Photocleavage of type I PIs on the example of acylgermanes. A benzoyl-type radical and a germyl-type radical are formed via α-cleavage from the excited triplet state following photoexcitation and intersystem crossing (ISC).

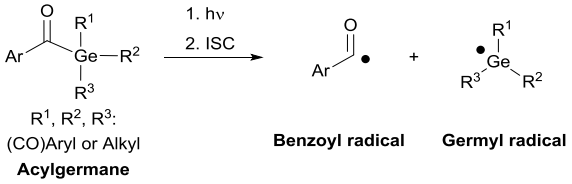

The photochemistry and photophysics of aryl ketones and acylphosphane oxides have been investigated in detail by Turro and coworkers[5] as well as by Wirtz, Dietliker, Gescheidt and coworkers (acylphosphane oxides).[6] Type II PIs, on the other hand, work in a bimolecular process together with a coinitiator. The initiating radicals are produced either by direct hydrogen abstraction between the excited PI and the coinitiator (a hydrogen donor) or by electron transfer followed by a proton transfer, which is more common. The light absorbing molecules in type II systems are usually based on benzophenone, thioxanthone, camphorquinone, anthraquinone, benzil or ketocumarin derivatives. Typical coinitators are amines, alcohols, or silanes serving as the electron donor and/or hydrogen source.[3] In addition, organogermanium hydrides have been described as efficient germanium-based coinitiators for type II PIs.[7]

Scheme 2 shows the type II initiation process with the champhorquinone/amine system serving as a paradigm which has been widely applied in the field of dental fillings.[8]

Scheme 2. Initiation mechanism of a type II initiator on the example of a campherquinone/amine system. Electron transfer is followed by proton transfer, producing the CQ ketyl radical and an α-aminoalkyl radical.

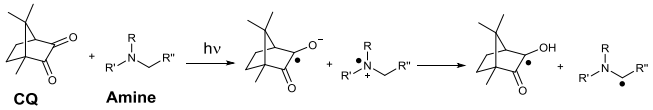

An efficient photoinitiator features a good match between its absorption lines and the emission spectrum of the utilized light source. A high quantum efficiency for radical formation and a high reactivity of the resulting radicals towards the monomers are additional important requirements. In general, type I PIs are most widely applied, due to higher efficiency and decomposition rates when compared to type II initiators.[9] However, type II initiators often show more favorable visible-light absorption properties.[9] Nowadays, visible light initiation systems are highly desired, for reasons of high penetration depth of the incident light, biocompatibility and cost-effective irradiation sources. An overview of various types of visible light sensitive photoinitiating systems is given by Lalevée and coworkers.[10]

The development of type I visible light PIs is thus of paramount importance and has become a growing field of research. Apart from the above-mentioned factors, good solubility in aqueous media, biocompatibility and storage stability are crucial for modern (biomedical) applications such as tissue engineering or the preparation of hydrogel-type materials. Concerning water solubility, immense progress has been made with functionalized acylphosphane oxides by Grützmacher and coworkers.[11]

Mainly, due to the high toxicity of most acylphosphane oxides, they are not suitable for applications such as dental fillings.[12] Compared to phosphoros-based PIs, acylgermanes offer the advantage of reduced toxicity as well as a significant red-shift of the longest-wavelength absorption bands.

Promoted by their outstanding absorption properties and their ability to efficiently produce reactive radicals (see Scheme 1), acylgermanes have become a promising class of photoinitiators.[13] Mono- and bisacylgermanes have first been reported as photoinitiators in 2008.[14] Since then, substantial efforts have been made by several working groups to elucidate the photoreactivity and preparation of acylgermanes.[13e,13d,15]

This minireview focuses on the synthetic aspects and the photoreactivity of mono- to tetraacylgermanes as a promising class of visible-light type I PIs.

3.6.3 The Beginning of Acylgermanium Chemistry

Acylgermanes were first synthesized by Brook and coworkers via hydrolysis of α,α-dibromoalkylgermanes (equation 1).[16]

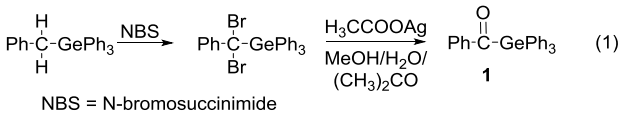

Concerning the synthetic methods towards mono-,[17] bis-, and trisacylgermanes,[18] several methods have been reported throughout the last decades. However, the compounds obtained were not investigated with respect to their photoinitiating properties. The resurgence of interest in acylgermanium chemistry lately is mainly based on the advantageous photo cleavage of the Ge-(CO) bond which has been overlooked for a long time. The development of novel and efficient synthetic strategies towards functionalized acylgermanes has evolved since then.

3.6.4 Synthesis of Germanium-Based PIs

3.6.4.1 Monoacylgermanes

The most common types of monoacylgermanes investigated as PIs are summarized in Scheme 3.

Scheme 3. Substitution patterns of acylgermanes investigated as PIs.

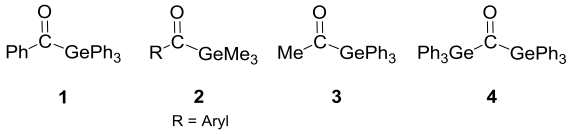

In 2008 and 2016 benzoyl germanium derivatives **2** were introduced as PIs for visible-light curing[1f,14b,13e] with excellent efficiency in dental composites. These monoacylgermanes were synthesized from hexamethyldigermane and the respective acid chlorides in the presence of a Pd-catalyst and triethyl phosphite (equation 2).[19]

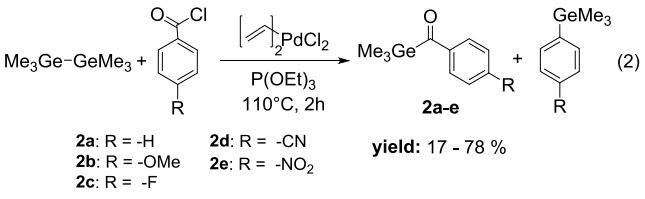

High photoinitiating ability was also reported for the acylgermanes **1** and **3**.[15c] Compounds **1** and **3** are most conveniently prepared from the reaction of Ph_3GeLi with the appropriate ester (equation 3)[17j] or from the corresponding germyl-1,3-dithiane (equation 4).[17k]

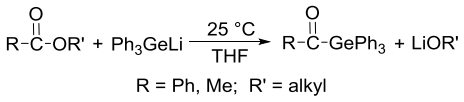

(3)

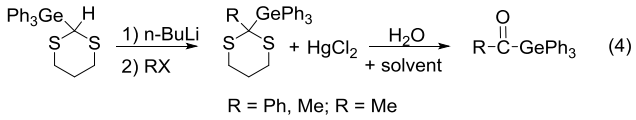

(4)

For the bisgermyl derivative **4** a substantial red-shifted absorption and a high polymerization ability under visible light irradiation was observed.[20] The synthesis of **4** was accomplished by the oxidation of bis(triphenylgermyl)methanol with dicyclohexylcarbodiimide/pyridinium trifluoroacetate in DMSO (equation 5).[21]

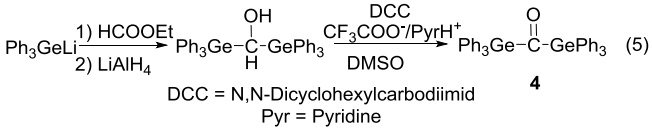

(5)

3.6.4.2 Bisacylgermanes

Almost concurrently with the introduction of monoacylgermanes as promising PIs, bisacylgermanes were studied. In this context, the bisacylgermanium derivatives **5a**-**g** were synthesized by a Corey-Seebach type reaction, which was adapted for higher homologues of carbon by A. Brook (equation 6).[14,17k,22]

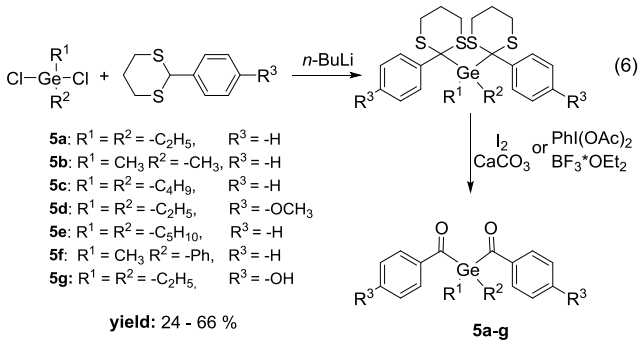

(6)

In the case of the sterically encumbered bisacylgermane **5h** the dithiane route failed. Thus, compound **5h** was alternatively prepared by the acylation of diphenylgermane though the low yield prevented complete characterization (equation 7).[22]

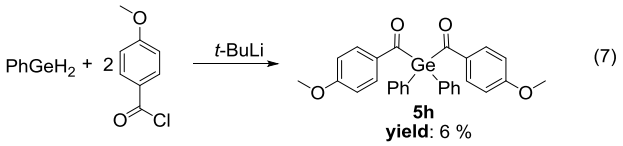

(7)

Based on the synthetic approach presented in equation 6 the first bisacylgermane was implemented as a commercially available photoinitiator [Bis(4-methoxybenzoyl)diethylgermane, Ivocerin®]. Ivocerin® and related bisacylgermanes show significantly enhanced extinction coefficients compared to monoacylgermanes resulting in reduced curing times and increased curing depth of the final composite material.[22,23,15a] Beside of these benefits, Ivocerin® still suffers from inefficient curing depths at wavelengths >450nm.[14a] Additionally, the multi-step synthesis and the tedious purification cause high production costs and prevents - so far - the application as PI apart from dental composites.

3.6.4.3 Tris- and Tetraacylgermanes

One trisacylgermane derivative was prepared from PhH_2GeLi and Cl-(CO)Mes and reported in 1992 (equation 8),[18a] however, without discussing its photo-induced reactions.

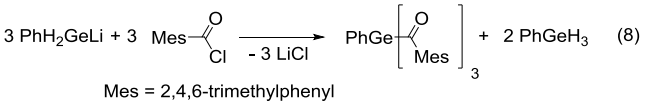

(8)

Recently, the chemistry of tris- and tetraacyl substituted germanes and their ability to serve as long-wavelength PIs was investigated.[16,23,24] In the course of these studies a synthetic protocol allowing a straightforward access to these highly desirable compounds was developed (equation 9).

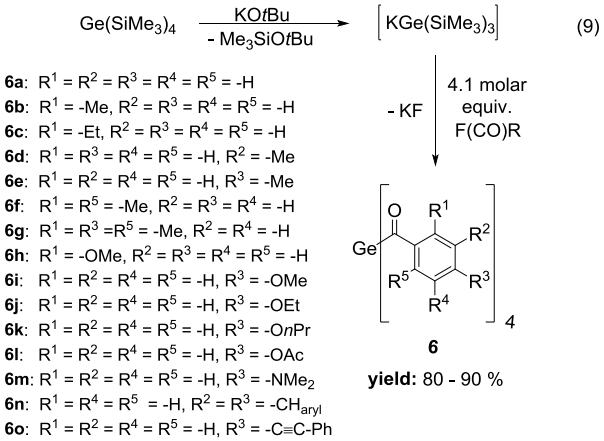

(9)

Based on the well-established multiple silyl group abstraction from $(Me_3Si)_3SiK$ by fluorinated reagents,[24] the reaction of $(Me_3Si)_3GeK$[25] with 4.1 molar equivalents of acid fluorides F-(CO)R (R = aryl) leads to the formation of tetraacylgermanes **6** in >85% yields (equation 9). Trisacylgermanes are formed *via* the same mechanism upon treatment of $(Me_3Si)_2EtGeK$ with the respective acid fluorides (equation 10).

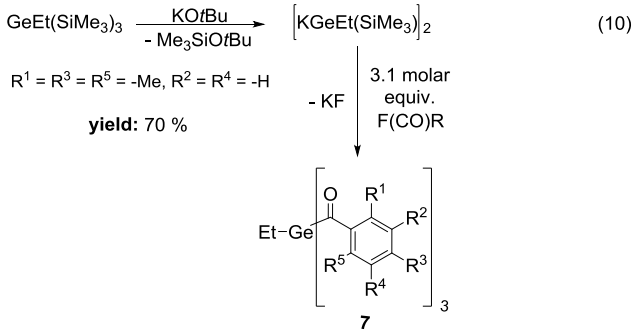

(10)

Contrary to the previously mentioned synthetic strategies towards acylgermanes, this protocol represents an easy-to-perform one-pot synthesis and the products can be isolated by simple recrystallization in excellent yields. Up to now, a variety of differently EDG-substituted tetraacylgermanes have been prepared.[13d,15e]

3.6.5 Spectroscopic Properties of Germanium-Based PIs

3.6.5.1 Absorption Behavior

A good match between the emission spectra of the lamp and the absorption bands of a photoinitiator is essential to achieve its preferential functionality. In this respect, aryl acylgermanes exhibit properties particularly suitable for long-wavelength visible-light curing processes. All aryl substituted acylgermanes show longest wavelength absorption bands with λ_{max} values between 363 and 419 nm, tailing well into the visible region. These bands are significantly red-shifted and intensified as compared to other common PI systems such as aryl ketones or the well-established acylphosphane oxides.[26,16,11a]

The longest wavelength absorption bands of acylgermanes were computationally assigned to the HOMO-LUMO transition and show considerable charge transfer character (compare Figure 1).[13d] Upon excitation, electron density is displaced from the n(C=O)/σ(Ge-C) bonding HOMO to the π*(C=O/Aryl) antibonding LUMO which results in the population of an orbital with antibonding character between the Ge-C bond. In analogy to related ketones, homolytic bond cleavage occurs upon intersystem crossing (ISC) *via* the excited triplet state.[5b]

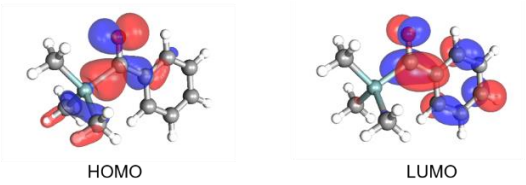

Figure 1. Frontier-orbitals of Me_3GeBz. Singlett excitations calculated at the PCM(MeCN) TD-DFT CAM-B3LYP/def2-TZVP//B3LYP/6-31+G(d,p) level of theory.

In line with literature data of simple aryl ketones, pronounced substituent effects on the absorption properties of aryl acylgermanes are observed. The introduction of electron withdrawing groups in ortho- or para positions at the aromatic ring induces a bathochromic shift of λ_{max} and decreases the extinction coefficients. The opposite behavior is observed when electron donating groups are attached.[13d,13e,22,15d] Figure 2 shows the effect of Me and OMe substitution on the absorption behavior of selected tetraacylgermanes. Detailed absorption data for aryl acylgermanes can be found in Table 1. Additionally, the extinction coefficients increase almost linearly according to the number of chromophores attached to the germanium center (Figure 3).

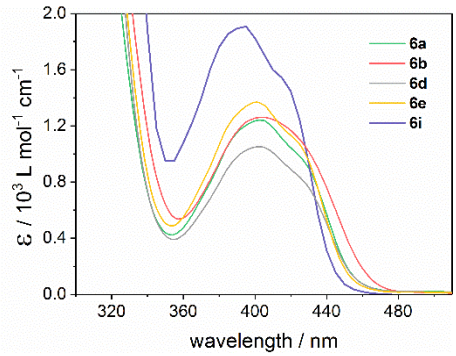

Figure 2. Absorption spectra of selected tetraacylgermanes (substituents at aromatic ring are stated in parentheses): **6a** (phenyl), **6b** (*o*-Me) **6d** (*m*-Me), **6e** (*p*-Me) and **6i** (*p*-OMe), (CH_3CN solution; c = 10^{-3} mol·l^{-1}).

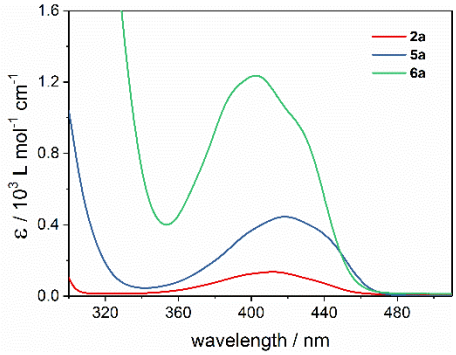

Figure 3. UV-Vis spectra of a monoacylgermane **2a**, bisacylgermane **5a**, and tetraacylgermane **6a** (CH_3CN solution; c= 10^{-3} mol·l^{-1}).

Di-*ortho*-substitution at the aromatic ring in aryl acylgermanes induces a significant hypsochromic shift of the longest wavelength absorption band. This hypsochromic shift roughly correlates with the twist (or dihedral) angle between the plane of the phenyl ring and the C=O moiety, which significantly deviates from a coplanar arrangement in the di-*ortho*-substituted derivatives caused by the steric repulsion between the *ortho*-substituents and the C=O group (compare Figure 4). This correlation is conclusive because larger values of the dihedral angle reduce phenyl/C=O π-π conjugation thus increasing the HOMO–LUMO gap and shifting the corresponding UV maximum to the blue.

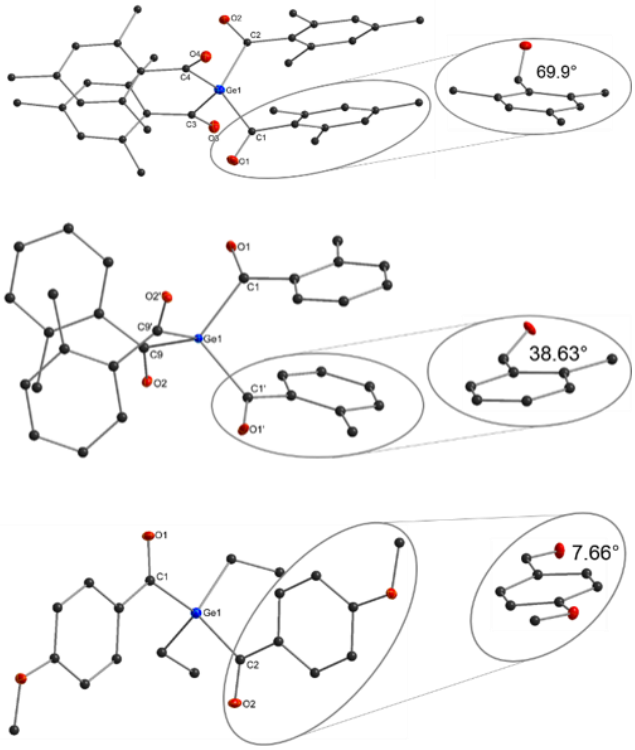

Figure 4. ORTEP representation of **6b**,**g** and **5d**. Thermal ellipsoids are drawn at the 50% probability level. Hydrogen atoms are omitted for clarity. Mean torsion angles [°] are shown in the magnified part.

Table 1 shows λ_{max} values and extinction coefficients for the longest wavelength absorption bands of all reported acylgermanes.

Table 1. λ_{max} values and extinction coefficients for the longest wavelength absorption bands of monoacylgermanes **2a**-**d**,[13e,14b] bisacylgermanes **5a**-**5f**,[22] trisacylgermane **7**,[15d] and tetraacylgermanes **6a**-**k**.[13d,15e]

	λ_{max}/ ε[L•mol^{-1}•cm^{-1}]		λ_{max}/ ε[L•mol^{-1}•cm^{-1}]		λ_{max}/ ε[L•mol^{-1}•cm^{-1}]
Monoacylgermanes					
2a	411.5/ 137	**2c**	405/ [a]	**2e**	429/ [a]
2b	397/ [a]	**2d**	425/ [a]		
Bisacylgermanes					
5a	418.5/ 490	**5d**	408.2/ 724	**5g**	406.2/ 686
5b	417.6/ 511	**5e**	418.1/ 568	**5h**	402.5/ 570
5c	418.5/ 529	**5f**	418.8/ 549		
Tris- and Tetraacylgermanes					
7	383/ 1226 402sh/ 903	**6f**	374/ 1477 403sh/ 954	**6l**	400/ 1262 422sh/ 992
6a	403/ 1240 419sh/ 1050	**6g**	376/ 1475	**6m**	[b]
6b	407/ 1266	**6h**	400/ 1160	**6n**	[b]
6c	407/ 1258	**6i**	395/ 1897 413sh/ 1556	**6o**	[b]
6d	402/ 1058	**6j**	392/ 1708 415sh/ 1362		
6e	400/ 1377 422sh/ 1113	**6k**	393/ 1765 414sh/ 1396		

[a] not published; sh = shoulder

[b] could not be detected due to overlapping of n-π* with π-π* bands

In summary, the substituent effects described above allow tuning of the absorption properties of aryl acylgermanes. The most intense absorption at wavelengths ≥ 450 nm is observed for the *ortho*-Me substituted tetraacylgermane **6b**. Hence, **6b** is of particular interest for applications with long-wavelength visible-light emitting sources.

3.6.6 PI Performance

3.6.6.1 Photochemistry of Acylgermanes

Whereas, the photochemistry of acylsilanes has been investigated in great detail by Brook and coworkers and Porter and coworkers in the 1970s and 1980s,[27,25a] only a few studies have been conducted concerning the photochemistry of acylgermanes. Their discovery serving as advantageous PIs has triggered extended mechanistic investigations.

Germyl radicals formed via photolysis of monoacylgermanes $Ph_3Ge(CO)Ph$ and $PhMe_2Ge(CO)Ph$ have been observed by Mochida and Hayashi in 1985 using laser-flash photolysis (LFP).[28] The assignment of the transient absorption bands to the Ge-centered radicals $Ph_3Ge\bullet$ and $PhMe_2Ge\bullet$ has been possible via comparison with the LFP spectra reported previously for Ge-centered radicals derived from germanium hydrides (1983 by Scaiano and Ingold as well as by Hayashi and Mochida).[29] Taraban and coworkers investigated the photocleavage of monoacylgermane $Et_3Ge(CO)Ph$ (benzoyltriethylgermane) via chemically-induced dynamic nuclear polarization (CIDNP) NMR spectroscopy in 1987, confirming the formation of $Et_3Ge\bullet$ and $\bullet(CO)Ph$ as the primary triplet radical pair.[30] The photochemical reaction pathways of acylgermanes in polar and non-polar media have been found to be analogous to those reported for acylsilanes.[30,31,27e]

Triplet-state α-cleavage of a Ge-(CO) bond has been confirmed as the major photochemical reaction pathway of bisacylgermane **5a** by Gescheidt and coworkers in 2013, as evident from time-resolved EPR (TR-EPR, CIDEP) spectroscopy as well as femto- and nanosecond transient absorption spectroscopy (see Scheme 1).[15b] TR-EPR spectra of a bis- and a tetraacylgermane are depicted in Figure 5.

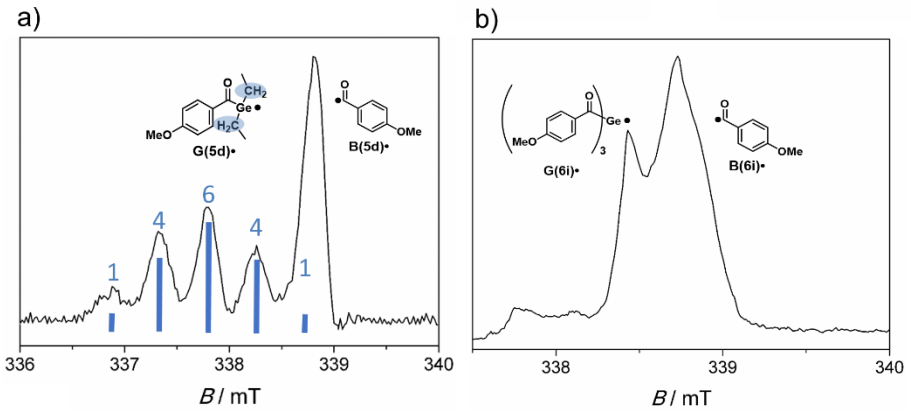

Figure 5. TR-EPR spectra recorded 300-400 ns after laser-flash photolysis (355 nm) of argon-saturated toluene solutions (10 mM) of a) **5d** and b) **6i**. Blue bars indicate the splitting of the germyl radical signal due to the four *β* hydrogen atoms in radical **G(5d)•**.

The follow-up reactions of the primary radicals have been elucidated by ^{1}H CIDNP spectroscopy.[32] Scheme 4 shows a summary of the radical reaction pathways proposed on the basis of CIDNP experiments of acylgermanes in absence and presence of monomers.[13d,15b,15d]

Scheme 4. Proposed reaction scheme of initiator **5a** in the presence of monomers, as established via CIDNP experiments.

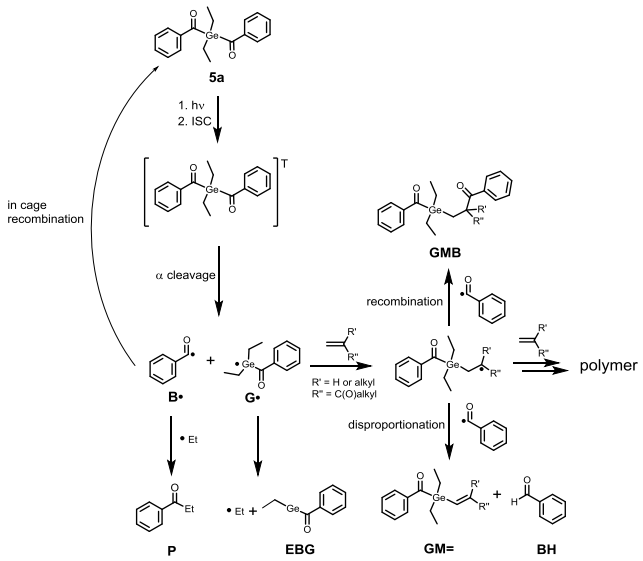

3.6.6.2 Initiation Efficiency

High quantum yields of decomposition are an important requirement for efficient photoinitiators. Quantum yields of mono- to tetraacylgermanes have been reported by our group recently, with values ranging from ~0.4 (tetraacylgermanes) to ~0.8-0.9 (bisacylgermanes).[15d]

To achieve high curing depth and to avoid colored polymers, fast photobleaching of the PI at the irradiation wavelength is equally crucial, especially upon irradiation with visible light. This is particularly relevant for (bio)medical applications such as dental composites. Various photobleaching studies of acylgermanes have been performed.[14a,33,15d]

Wavelength-dependent photobleaching curves are presented in Figure 6 for irradiation of mono- to tetraacylgermanes with LEDs at 385 nm and 470 nm in acetonitrile/monomer solutions. The monomer (methyl methacrylate, MMA) acts as a radical trap, leading to the formation of photoproducts, which do not absorb in the visible wavelength range. Generally, photobleaching is more efficient upon irradiation with LED light at 385 nm than at 470 nm for all investigated compounds. Tetraacylgermane **6b** exhibits remarkably fast photobleaching upon irradiation at 470 nm, indicating efficient initiation under high-wavelength visible light.[15d]

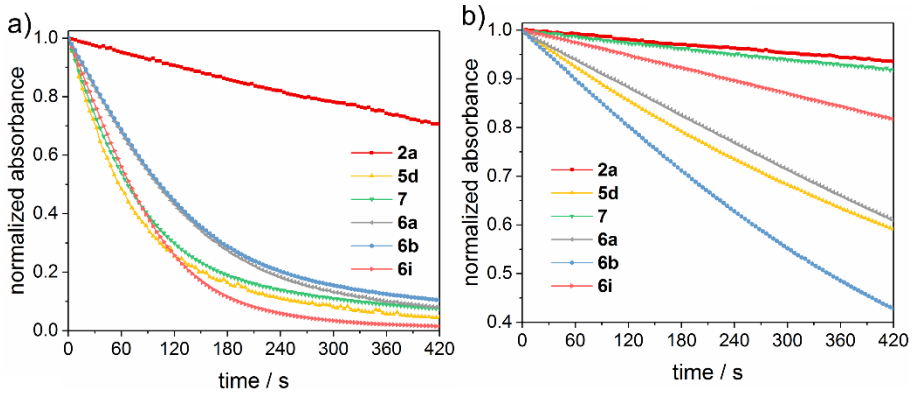

Figure 6. Steady-state photolysis of mono-, bis-, tris- and tetraacylgermanes in acetonitrile/MMA solutions. Plots of normalized absorbance versus time for irradiation at a) 385 nm and b) 470 nm, monitored at the n-π* absorption maxima (**2a**: 412.5 nm, **5d**: 409 nm, **7**: 383 nm, **6a**: 404 nm, **6b**: 405.5 nm, **6i**: 393 nm).

Apart from high decomposition quantum yields and efficient photobleaching, fast addition of the primary radicals to monomers is essential for an efficient photoinitiator. Laser-flash photolysis (LFP) is a powerful method for the analysis of radical-to-monomer addition kinetics. Lalevée and coworkers reinvestigated the transient absorption properties of the $Ph_3Ge•$ radical in 2009, showing remarkably fast reactivity of this radical toward monomer double bonds (rate constants in the order of 10^8 $M^{-1}s^{-1}$).[15c]

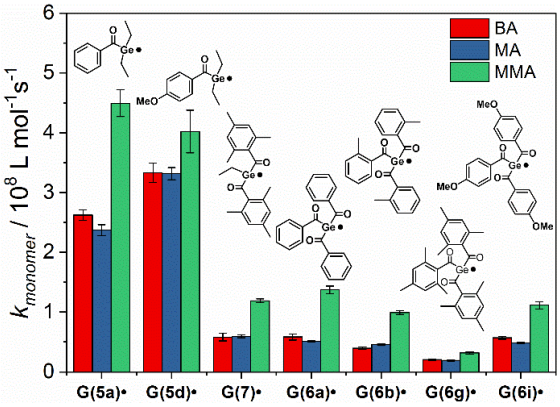

Figure 7. Second-order rate constants $k_{monomer}$ for the addition of **G•** to butyl acrylate (**BA**), methyl acrylate **(MA)** and methyl methacrylate **(MMA).**

We studied the kinetics of various Ge-centered radicals derived from mono- to tetraacylgermanes toward a series of monomers.[15b,15d] A summary of the addition rate constants is given in Figure 7. Notably, Ge-centered radicals show significantly higher reactivity toward monomers than related phosphorus-based radicals derived from acylphosphane oxides.[11e] Further efficiency studies of acylgermanes have been performed using photo-DSC, showing particularly high reactivity for bisacylgermane **5d** and tetraacylgermane **6b**.[33,13d]

3.6.7 Conclusion

Acylgermanes have been shown to be highly efficient, non-toxic visible-light photoinitiators for radical polymerization. Recently, novel straight-forward synthetic protocols have led to the preparation of tris- and tetraacylgermanes, completing the spectrum from mono- to tetrasubstituted derivatives. Functionalization on the aromatic rings allows fine-tuning the absorption properties and shifting the absorption bands towards the long-wavelength region. Fast photobleaching and high reactivity of the germanium-centered radicals towards monomer double bonds substantiate their high potential for various applications including photopolymerizable adhesives, coatings, or 3D-lithography techniques.

3.6.8 Outlook

In the future, the development of acylgermane derivatives with improved solubility in aqueous media will become a major challenge, broadening the range of potential applications. Further insights into the photoreactivity of acylgermanes will remain of great interest, in order to fully elucidate structure-reactivity relationships and to enable the design of derivatives with tailor-made absorption bands and initiation efficiency.

3.6.9 References

[1] a) J. P. Fouassier in *Photoinitiation, Photopolymerization, and Photocuring*. *Fundamentals and Applications*, Hanser, New York, **1995**; b) R. S. Davidson in *Exploring the science, technology and applications of U.V. and E.B. curing*, SITA Technology, London, **1999**; c) C. G. Roffey in *Photopolymerization of surface coatings*, Wiley, Chichester, **1982**; d) J. G. Kloosterboer, *Adv. Polym. Sci.* **1988**, *84*, 1; e) T. J. Bunning, L. V. Natarajan, V. P. Tondiglia, R. L. Sutherland, *Annu. Rev. Mater. Sci.* **2000**, *30*, 83; f) B. Ganster, U. K. Fischer, N. Moszner, R. Liska, *Macromol. Rapid Comm.* **2008**, *29*, 57; g) K. S. Anseth, S. M. Newman, C. N. Bowman, *Adv. Polym. Sci.* **1995**, *122*, 177; h) H.-B. Sun, S. Kawata, *Adv. Polym. Sci.* **2004**, *170*, 169.

[2] N. S. Allen (Ed.) *Photochemistry and Photophysics of Polymer Materials*, John Wiley & Sons, Inc, Hoboken, NJ, USA, **2010**.

[3] J. P. Fouassier, X. Allonas, J. Laleve, C. Dietlin in *Photochemistry and Photophysics of Polymer Materials* (Ed.: N. S. Allen), John Wiley & Sons, Inc, Hoboken, NJ, USA, **2010**, pp. 351–419.

[4] a) W. Rutsch, K. Dietliker, D. Leppard, M. Köhler, L. Misev, U. Kolczak, G. Rist, *Progress in Organic Coatings* **1996**, *27*, 227; b) K. Dietliker, T. Jung, J. Benkhoff, H. Kura, A. Matsumoto, H. Oka, D. Hristova, G. Gescheidt, G. Rist, *Macromol. Symp.* **2004**, *217*, 77.

[5] a) C. S. Colley, D. C. Grills, N. A. Besley, S. Jockusch, P. Matousek, A. W. Parker, M. Towrie, N. J. Turro, P. M. W. Gill, M. W. George, *J. Am. Chem. Soc.* **2002**, *124*, 14952; b) S. Jockusch, M. S. Landis, B. Freiermuth, N. J. Turro, *Macromolecules* **2001**, *34*, 1619; c) S. Jockusch, N. J. Turro, *J. Am. Chem. Soc.* **1998**, *120*, 11773; d) S. Jockusch, I. V. Koptyug, P. F. McGarry, G. W. Sluggett, N. J. Turro, D. M. Watkins, *J. Am. Chem. Soc.* **1997**, *119*, 11495; e) G. W. Sluggett, C. Turro, M. W. George, I. V. Koptyug, N. J. Turro, *J. Am. Chem. Soc.* **1995**, *117*, 5148.

[6] a) M. Griesser, D. Neshchadin, K. Dietliker, N. Moszner, R. Liska, G. Gescheidt, *Angew. Chem. Int. Ed.* **2009**, *48*, 9359; b) D. Hristova, I. Gatlik, G. Rist, K. Dietliker, J.-P. Wolf, J.-L. Birbaum, A. Savitsky, K. Möbius, G. Gescheidt, *Macromolecules* **2005**, *38*, 7714; c) I. Gatlik, P. Rzadek, G. Gescheidt, G. Rist, B. Hellrung, J. Wirz, K. Dietliker, G. Hug, M. Kunz, J.-P. Wolf, *J. Am. Chem. Soc.* **1999**, *121*, 8332; d) U. Kolczak, G. Rist, K. Dietliker, J. Wirz, *J. Am. Chem. Soc.* **1996**, *118*, 6477.

[7] J. Lalevée, A. Dirani, M. El-Roz, X. Allonas, J. P. Fouassier, *J. Polym. Sci. A Polym. Chem.* **2008**, *46*, 3042.

[8] K. IKEMURA, T. ENDO, *Dent. Mater. J.* **2010**, *29*, 481.

[9] S. C. Ligon, B. Husár, H. Wutzel, R. Holman, R. Liska, *Chem. Rev.* **2014**, *114*, 557.

[10] P. Xiao, J. Zhang, F. Dumur, M. A. Tehfe, F. Morlet-Savary, B. Graff, D. Gigmes, J. P. Fouassier, J. Lalevée, *Progress in Polymer Science* **2015**, *41*, 32.

[11] a) A. Huber, A. Kuschel, T. Ott, G. Santiso-Quinones, D. Stein, J. Bräuer, R. Kissner, F. Krumeich, H. Schönberg, J. Levalois-Grützmacher, H. Grützmacher, *Angew. Chem. Int. Ed.* **2012**, *51*, 4648; b) G. Müller, M. Zalibera, G. Gescheidt, A. Rosenthal, G. Santiso-Quinones, K. Dietliker, H. Grützmacher, *Macromol. Rapid Comm.* **2015**, *36*, 553; c) J. Wang, G. Siqueira, G. Müller, D. Rentsch, A. Huch, P. Tingaut, J. Levalois-Grützmacher, H. Grützmacher, *Chem. Commun.* **2016**, *52*, 2823; d) S. Benedikt, J. Wang, M. Markovic, N. Moszner, K. Dietliker, A. Ovsianikov, H. Grützmacher, R. Liska, *J. Polym. Sci. A Polym. Chem.* **2016**, *54*, 473; e) A. Eibel, M. Schmallegger, M. Zalibera, A. Huber, Y. Bürkl, H. Grützmacher, G. Gescheidt, *Eur. J. Inorg. Chem.* **2017**, *2017*, 2469.

[12] Safety Data sheet of Phenylbis(2,4,6-trimethylbenzoyl)phosphine oxide.

[13] a) H. Grützmacher, J. Geier, D. Stein, T. Ott, H. Schönberg, R. H. Sommerlade, S. Boulmaaz, J.-P. Wolf, P. Murer, T. Ulrich, *Chimia* **2008**, *62*, 18; b) L. Gonsalvi, M. Peruzzini, *Angew. Chem. Int. Ed.* **2012**, *51*, 7895; c) R. Appel, G. Haubrich, F. Knoch, *Chem. Ber.* **1984**, *117*, 2063; d) J. Radebner, A. Eibel, M. Leypold, C. Gorsche, L. Schuh, R. Fischer, A. Torvisco, D. Neshchadin, R. Geier, N. Moszner, R. Liska, G. Gescheidt, M. Haas, H. Stueger, *Angew. Chem. Int. Ed.* **2017**, *56*, 3103; e) W. Feuerstein, S. Höfener, W. Klopper, I. Lamparth, N. Moszner, C. Barner-Kowollik, A.-N. Unterreiner, *Chemphyschem* **2016**, *17*, 3460; f) Safety Data sheet of Bis(4-methoxybenzoyl)diethylgermane.

[14] a) B. Ganster, U. K. Fischer, N. Moszner, R. Liska, *Macromolecules* **2008**, *41*, 2394; b) N. Moszner, U. K. Fischer, B. Ganster, R. Liska, V. Rheinberger, *Dent. Mater.* **2008**, *24*, 901.

[15] a) Y. Catel, U. Fischer, P. Faessler, N. Moszner, *Macromol. Chem. Phys.* **2016**, *217*, 2686; b) D. Neshchadin, A. Rosspeintner, M. Griesser, B. Lang, S. Mosquera-Vazquez, E. Vauthey, V. Gorelik, R. Liska, C. Hametner, B. Ganster, R. Saf, N. Moszner, G. Gescheidt, *J. Am. Chem. Soc.* **2013**, *135*, 17314; c) J. Lalevée, X. Allonas, J. P. Fouassier, *Chem. Phys. Lett* **2009**, *469*, 298; d) A. Eibel, J. Radebner, M. Haas, E. D. Fast, P. Faschauner, A. Torvisco, I. Lamparth, N. Moszner, H. Stueger, G. Gescheidt, *Polymer Chemistry* **2017**, *submitted*; e) J. Radebner, M. Leypold, A. Eibel, J. Maier, L. Schuh, A. Torvisco, R. Fischer, N. Moszner, G. Gescheidt, H. Stueger, M. Haas, *Organometallics* **2017**, *36*, 3624.

[16] A. G. Brook, M. A. Quigley, G. J. D. Peddle, N. V. Schwartz, C. M. Warner, *J. Am. Chem. Soc.* **1960**, *82*, 5102.

[17] a) R. E. Bruns, P. Kuznesof, *J. Organomet. Chem.* **1973**, *56*, 131; b) M. Wakasa, K. Mochida, Y. Sakaguchi, J. Nakamura, H. Hayashi, *J. Phys. Chem.* **1991**, *95*, 2241; c) K. Mochida, K. Yamamoto, *Bull. Chem. Soc. Jpn.* **1988**, *61*, 2933; d) A. Alberti, G. Seconi, G. F. Pedulli, A. Degl'innocenti, *J. Organomet. Chem.* **1983**, *253*, 291; e) D. A. Nicholson, A. L. Allred, *Inorg. Chem.* **1965**, *4*, 1747; f) U. Iserloh, D. P. Curran, *J. Org. Chem.* **1998**, *63*, 4711; g) E. Piers, R. Lemieux, *Organometallics* **1995**, *14*, 5011; h) M. Nanjo, K. Matsudo, K. Mochida, *Chem. Lett.* **2001**, *30*, 1086; i) D. A. Bravo-Zhivotovskii, S.D. Pigarev, I. D. Kalikhman, O. A. Vyazankina, N. S. Vyazankin, *J. Organomet. Chem.* **1983**, *248*, 51; j) S. Kiyooka, A. Miyauchi, *Chem. Lett.*

1985, *12*, 1829; k) A. G. Brook, J. M. Duff, P. F. Jones, N. R. Davis, *J. Am. Chem. Soc.* **1967**, *89*, 431; l) J. A. Soderquist, A. Hassner, *J. Am. Chem. Soc.* **1980**, *102*, 1577; m) J. A. Soderquist, A. Hassner, *Tetrahedron Lett.* **1988**, *29*, 1899.

[18] a) A. Castel, P. Rivière, J. Satgé, D. Desor, *J. Organomet. Chem.* **1992**, *433*, 49; b) A. Castel, P. Rivière, J. Satgé, H. Y. Ko, *Organometallics* **1990**, *9*, 205.

[19] K. Yamamoto, A. Hayashi, S. Suzuki, J. Tsuji, *Organometallics* **1987**, *6*, 974.

[20] M.-A. Tehfe, N. Blanchard, C. Fries, J. Lalevée, X. Allonas, J. P. Fouassier, *Macromol. Rapid Comm.* **2010**, *31*, 473.

[21] A. G. Brook, P. F. Jones, G. J. D. Peddle, *Can. J. Chem.* **1968**, *46*, 2119.

[22] N. Moszner, F. Zeuner, I. Lamparth, U. K. Fischer, *Macromol. Mater. Eng.* **2009**, *294*, 877.

[23] Y. Catel, P. Fässler, U. Fischer, C. Pesch, C. Pruvost, S. Tauscher, N. Moszner, *Polym. Int* **2017**, *27*, 29.

[24] J. Hlina, C. Mechtler, H. Wagner, J. Baumgartner, C. Marschner, *Organometallics* **2009**, *28*, 4065.

[25] a) A. G. Brook, F. Abdesaken, H. Söllradl, *J. Organomet. Chem.* **1986**, *299*, 9; b) J. Fischer, J. Baumgartner, C. Marschner, *Organometallics* **2005**, *24*, 1263.

[26] a) J. Tanaka, S. Nagakura, M. Kobayashi, *J. Chem. Phys.* **1956**, *24*, 311; b) M.M. Byrne, N. H. P. Smith, *Spectrochim Acta A* **1969**, *25*, 313; c) W. F. Forbes, W. A. Mueller, *Can. J. Chem.* **1955**, *33*, 1145; d) J. C. Dearden, W. F. Forbes, *Can. J. Chem.* **1958**, *36*, 1362.

[27] a) A. G. Brook, J. M. Duff, *J. Am. Chem. Soc.* **1967**, *89*, 454; b) N. A. Porter, P. M. Iloff, *J. Am. Chem. Soc.* **1974**, *96*, 6200; c) A. G. Brook, P. J. Dillon, R. Pearce, *Can. J. Chem.* **1971**, *49*, 133; d) J. M. Duff, A. G. Brook, *Can. J. Chem.* **1973**, *51*, 2869; e) A. G. Brook, J. M. Duff, *Can. J. Chem.* **1973**, *51*, 352.

[28] K. Mochida, K. Ichikawa, S. Okui, Y. Sakaguchi, H. Hayashi, *Chem. Lett.* **1985**, *14*, 1433.

[29] a) C. Chatgilialoglu, K. U. Ingold, J. Lusztyk, A. S. Nazran, J. C. Scaiano, *Organometallics* **1983**, *2*, 1332; b) H. Hayashi, K. Mochida, *Chem. Phys. Lett* **1983**, *101*, 307.

[30] M. B. Taraban, V. I. Maryasova, T. V. Leshina, L. I. Rybin, D. V. Gendin, N. S. Vyazankin, *J. Organomet. Chem.* **1987**, *326*, 347.

[31] M. B. Taraban, O. S. Volkova, A. I. Kruppa, T. V. Leshina (Eds.) *The Chemistry of Functional Groups*, *Vol. 2*, John Wiley & Sons, Ltd, Chichester, UK, **2002**.

[32] A. Yurkovskaya, O. Morozova, G. Gescheidt in *Encyclopedia of Radicals in Chemistry, Biology, and Materials* (Eds.: C. Chatgilialoglu, A. Studer), John Wiley & Sons, Chichester, West Sussex, Hoboken, N.J., **2012**.

[33] N. Moszner, U. K. Fischer, I. Lamparth, P. Fässler, J. Radebner, A. Eibel, M. Haas, G. Gescheidt, H. Stueger, *J. Appl. Polym. Sci.,* DOI 10.1002/app.46115.

3.7 Breaking Borders: Tetraacylstannanes as Long-Wavelength Visible-Light Photoinitiators with Intriguing Low Toxicity

Judith Radebner,*[,†] Anna Eibel,[‡] Mario Leypold,[†] Nina Jungwirth,[†] Thomas Pickl,[†] Ana Torvisco,[†] Roland Fischer,[†] Urs Karl Fischer,[§] Norbert Moszner,[§] Georg Gescheidt,[‡] Harald Stueger[†] and Michael Haas*[,†]

[†]Institute of Inorganic Chemistry and [‡] Institute of Physical and Theoretical Chemistry, Graz University of Technology, Stremayrgasse 9, 8010 Graz, Austria

[§]Ivoclar Vivadent AG, Bendererstraße 2, 9494 Schaan, Liechtenstein

submitted to Journal of American Chemical Society

Graphical Abstract:

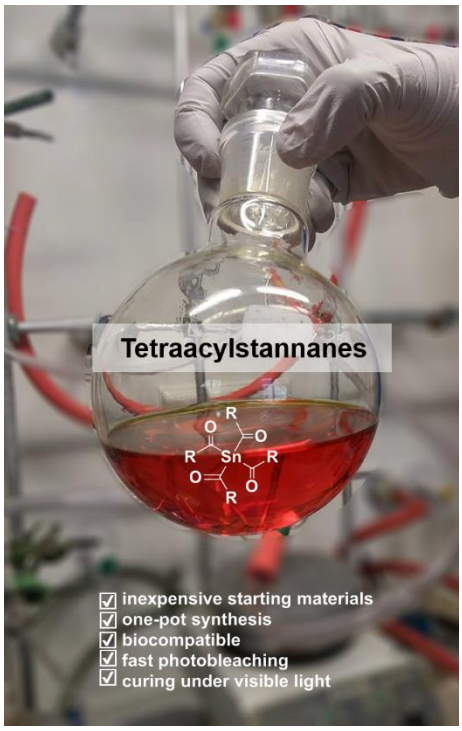

3.7.1 Abstract

The first tetraacylstannanes $Sn[(CO)R]_4$ (R = 2,4,6-trimethylphenyl (**1a**) and 2,6-dimethylphenyl (**1b**)), a class of highly efficient Sn-based photoinitiators, were synthesized. The formation of these derivatives was confirmed by NMR spectroscopy, mass spectrometry, and X-ray crystallography. The UV-Vis absorption spectra of **1a**,**b** reveal a significant red shift of the longest wavelength absorption compared to the corresponding germanium compounds. In contrast to the well-known toxicity of organo-tin derivatives, the AMES test and cytotoxicity studies reveal intriguing low toxicity. The excellent performance of **1** as photoinitiators is demonstrated in photobleaching (UV-Vis) and NMR/CIDNP investigations as well as by photo-DSC studies.

3.7.2 Introduction

From the Bronze Age (3500 BC) onward, tin has been a highly appreciated metal and raw material for further processing. Its acquisition marks an important part in the evolution of mankind. Pioneering works in organometallic tin chemistry by Frankland,[1] Cadet[2] or Zeise[3] sparked the interest into organic tin derivatives. Advances in analytical techniques including Sn-NMR, X-ray diffraction or appropriate computational methods aided organotin chemistry to be a thriving field of research. Besides being used as fungicides, insecticides or stabilizers in PVC, organostannanes are widely used in chemical synthesis. However, due to the acute toxicity of organotin compounds their use in synthetic chemistry has been connoted quite negatively and gradually diminished related research activities. Hitherto, the interest in acylstannane-chemistry remained modest because of a lack of suitable synthetic methods towards such. For a long time they were virtually unknown and believed to be extremely labile. For the sake of completeness, the acylated tin derivatives were mentioned as a side note when reporting on acylsilanes and acylgermanes.[4] Recent years have witnessed intense scientific efforts in the chemistry of keto derivatives of main group IV organometalloids (mainly Ge-based) and their application as long-wavelength visible light photoinitiators.[5] The search for new photoinitiators (PIs) for radical polymerization exhibiting enhanced reactivity remains of great interest.[6]. So far, phosphoros-based initiators (mono- and bisacylphosphane oxides) are well established, although UV-light is required for sufficient photocuring and the parent compounds as well as their photoproducts are in most cases highly toxic.[7] Thus, germanium-centered PI systems have emerged over the past view years as promising alternatives due to their low toxicity and the bathochromic shift of their longest-wavelength absorption bands.[8,5b] However, a significant drawback of the latter is the low abundance of germanium in the earth crust, resulting in high prices of germanium-based PIs. Therefore, this system cannot fully meet the requirements for photoinitiators in high-throughput polymer synthesis. To overcome the above-mentioned restrictions, we investigated the implementation of other central atoms. The replacement of germanium by silicon leads to the formation of tetraacylsilanes. But these derivatives appeared to be ineffective for free-radical photopolymerization.[9] Herein, we pioneer the use of tin as the central atom in metallo-acyl based photoinitiators, tremendously extending the scope of previously established systems in terms of long-wavelength absorption in combination with cost-effective synthesis and outstanding biocompatibility.

3.7.3 Results and Discussion

We report the outstanding potential of tetraacylstannanes **1a**,**b** as a unique class of long-wavelength visible light PIs for free-radical polymerization. Tetraacylstannanes **1a**,**b** are accessible in a remarkably easy-to-perform one-pot reaction (see Scheme 1). Notably, this novel PI system shows very low cytotoxicity (XTT_{50} value of 108.53 µg·mL^{-1}), in line with its low water-solubility.[10] Moreover, the bacterial reverse mutation test, the so-called Ames test, proved that **1** does not induce gene mutations, which is remarkable for organo-tin compounds.[11] Structurally related acylgermanes show similar low cytotoxicity (e.g. benzoyltrimethylgermane: XTT_{50} value of 215 µg·mL^{-1}.[5d,8b] In contrast, for the widely applied phosphorus-based PIs (e.g. Irgacure 819) barely any reports on cytotox and AMES tests are available.[12,7e] However, a similar acylphosphine oxide[13] was reported to show a higher cytotox (XTT_{50} value of 69.1µg·mL^{-1})[14] than Sn- or Ge- compounds. Additionally, photoproducts of P-based PIs are known to be highly toxic.[15] In this context, acylgermanes and acylstannanes are promising PIs for applications requiring biocompatibility.

Scheme 1. Synthesis of Tetraacylstannanes **1a**,**b**

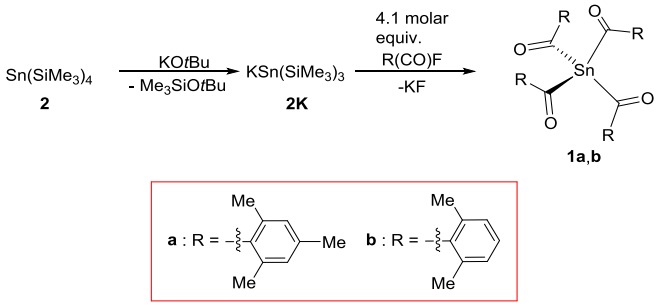

Recently, our group published a series of papers on previously unknown acylgermanes.[5b,16] Exploiting the multiple silyl abstraction enabled the targeted synthesis of these highly efficient PIs in high yields. Moreover, the strength of this reaction sequence lies in its high functional-group tolerance.[16a,16b] Following the results obtained for tetraacylgermanes, we discovered that the reaction of potassium stannide **2K**[17] with 4.1 molar equiv. of acid fluorides F-(CO)R (R = aryl) leads to the formation of tetraacylstannanes **1**. Mechanistically speaking, **2K** undergoes a salt metathesis reaction with the respective acid fluoride where KF and tris(trimethylsilyl)acylstannane **3** are formed. The consecutive nucleophilic attack of the fluoride ion on **4**, originating from the formation of **2K**, *in situ* generates Me_3SiF **5** and *t*BuO$^-$, which further reacts with **3** to form the stannenolate **6**. Accordingly, **4** and **5** could be detected by NMR spectroscopy in the reaction mixture (δ^{29}Si = 30.3 ppm and 6.92 ppm, respectively).[18] Subsequently the applied excess of acid fluoride immediately reacts with **6** to the respective bisacylstannane **7** releasing again KF and **4**. Acylation

proceeds until all trimethylsilyl-groups are abstracted and the final product **1** is formed (Scheme 2). It appears that di-*ortho* substitution at the phenyl ring is necessary for the successful preparation of tetraacylstannanes. So far, no derivatives with a different substitution pattern were isolated. We assume that the di-*ortho* substitution prevents the nucleophilic attack of any reactive anionic intermediate formed (F^- or tBuO$^-$). A characteristic feature of tetraacylstannanes **1** is the ^{13}C resonance for the carbonyl group, which appear between 243 ppm and 244 ppm. A similar tendency was found for tetraacylgermanes and -silanes.[5b,9a]

Scheme 2. Proposed Mechanism for the Synthesis of Tetraacylstannanes.

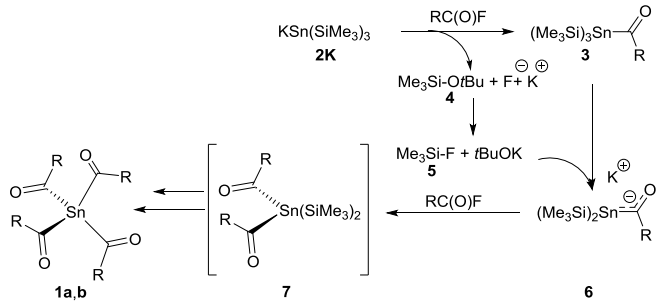

The analytical data for **1a**,**b** (see *Supporting Information*) are consistent with the proposed structures. As a representative example, the structure of **1a** is depicted in Figure 1. The structural features of these tin derivatives correlate with the results obtained for acylgermanes. Di-*ortho* substitution induces a significant torsion between the carbonyl group and the aromatic ring plane. The Sn-C bond length is similar to the values found for other Sn-C single bonds.[19]

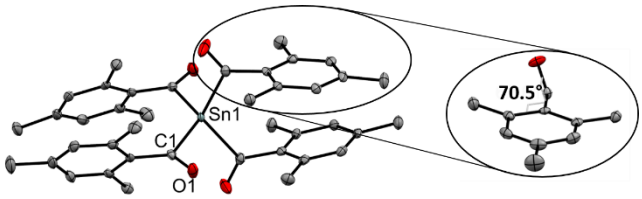

Figure 1. ORTEP representation of **1a**. Thermal ellipsoids are drawn at the 50% probability level. Hydrogen atoms are omitted for clarity. Selected bond lengths [Å] and angles [°] with estimated standard deviations: Sn(1)-C(1) 2.244(2), Sn(1)-C(11) 2.247(2), Sn(1)-C(21) 2.247(2), Sn(1)-C(31) 2.256(2), C-O (mean) 1.208; C-Ge-C (mean) 111.7; O-C-C_{aryl}-C_{aryl} (mean) 70.5.

Photopolymerization of biocompatible materials requires non-toxic PIs and non-toxic irradiation sources (visible light). Therefore, free radical photoinitiators with long-wavelength absorption are highly desired. In the course of our studies we found that the absorption maximum of non-toxic tetraacylgermanes show values between 363 and 422 nm.[16a] However, tetraacylgermanes lack of sufficient curing efficiency upon

irradiation with light sources operating above 450 nm. Nevertheless, this Type I PI system represents the most bathochromic shifted absorption bands so far. This border was shattered by the introduction of tetraacylstannanes **1**. Figure 2 illustrates the longest-wavelength absorption bands, which were computationally assigned to the HOMO-LUMO transition and show considerable charge transfer character. Upon excitation, electron density is displaced from the n(C=O)/σ(Sn-C) bonding HOMO to the π*(C=O/Aryl) antibonding LUMO (compare Figure 3), which results in the population of an orbital with antibonding character between the Sn-C bond.

Chart 1. Reference Compounds: Tetraacylgermanes **2a**,**b** and **3**.

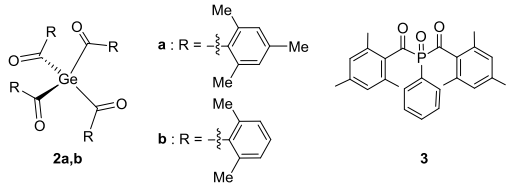

In comparison to the respective germanium analogues **2a**,**b** (Chart 1) the extinction coefficient of **1a**,**b** are significantly increased. The bathochromic shifted λ_{max} as well as the increased extinction coefficient induce a more pronounced tailing into the visible-light region > 450 nm enabling α-cleavage upon irradiation with light sources operating > 450 nm. Hence, **1** represents a radical source with most promising absorption properties for a visible light (VL) applications.

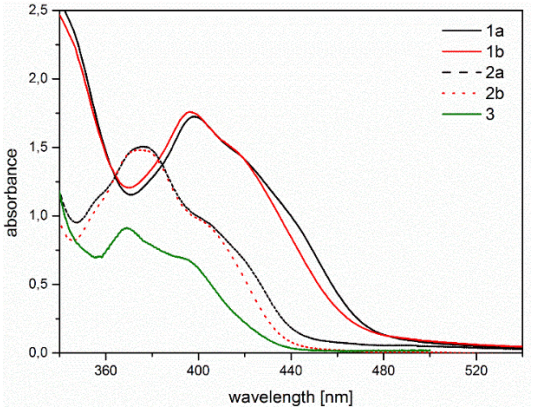

Figure 2. UV-Vis absorption spectra of **1a**,**b**, **2a**,**b** (the respective germanium-analogues) and **3** (bisacylphosphane oxide ®Irgacure 819)(chloroform solution, c = 10^{-3} mol L^{-1})

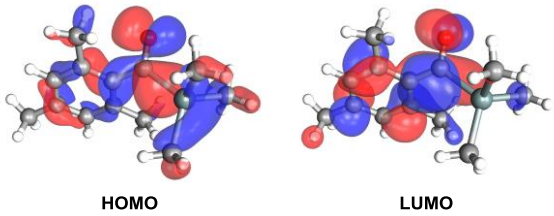

Figure 3. HOMO (left) and LUMO (right) of mesitoyltrimethylstannane, a simplified version of **1a**, to illustrate the Frontier orbitals of tetraacylstannanes **1a**,**b**.

Table 1. Experimental and PCM($CHCl_3$) TD-DFT CAM-B3LYP/LANL2DZdp-ECP(Sn),def2-TZVP(H,C,O)//B3LYP/LANL2DZdp-ECP(Sn),6-31+G(d)(H,C,O) calculated Wavelength Absorption Maxima λ [nm], Extinction Coefficients ϵ [$dm^2 \bullet mol^{-1}$] and Oscillator Strengths f for **1a**,**b** ($CHCl_3$).

	λ_{max},exp (ϵ)	λ_{max},calc (f)	Absorption Edge	Assignment
1a	398 (1776)	416, 409, 389 (0.0221, 0.0051, 0.0137)	480	n/σ-π*(CO/Aryl)
1b	396 (1735)	417, 409, 389 (0.0167, 0.0053, 0.0131)	480	n/σ-π*(CO/Aryl)

To assess the efficiency of **1a**,**b** as radical photoinitiators, we have performed photobleaching experiments.[5c,5b] Steady-state photolysis (SSP) upon irradiation with an LED operated at 470 nm reveals remarkably fast bleaching of **1a**,**b** when compared to phosphorus-[7b,20] and germanium-based[8c,5a,5c,5b] photoinitiators **2** and **3** (see Figure 4 and Scheme 3). The superior photobleaching performance of tetraacylstannanes **1** over the reference initiators **2**, **3** upon irradiation with high wavelength visible light (470 nm) is consistent with the bathochromically shifted absorption spectra (see the Supporting Information for a comparison of the UV-Vis spectra). Fast photobleaching of the initiator is an indication for efficient radical formation and is moreover crucial for achieving high curing depths and colourless polymers[21]. Compound **1b** exhibits the fastest photobleaching, while bisacylphosphane oxide **3** shows almost no bleaching, being unsuitable for curing applications in this wavelength region.

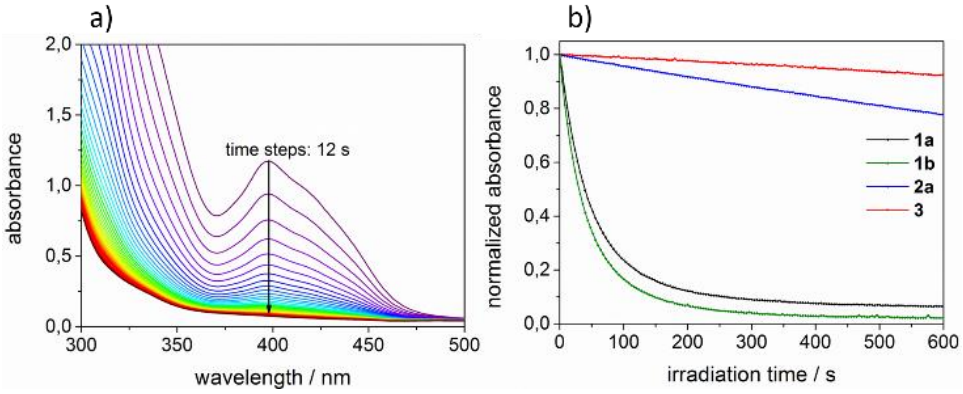

Figure 4. a) Photobleaching of **1a** upon irradiation at 470 nm, b) Plots of normalized absorbance versus time for compounds **1a,b**, **2a** and **3**, monitored at absorption maxima (**1a**: 398 nm, **1b**: 396.5 nm, **2a**: 375 nm **3**: 369.5 nm, **3**: 409 nm). Samples: 0.6 mM PI in acetonitrile.

We have investigated the radical reaction pathways upon irradiation of **1a**,**b** in presence of monomers using chemically induced dynamic nuclear polarization (CIDNP) NMR spectroscopy. This method allows following the *α*-cleavage of the photoinitiators **1a**,**b** and provides information about reaction products formed *via* radical pairs (**Sn•**/**B•**, see Scheme 3). Radical-pair-based phenomena lead to enhanced absorptive or emissive NMR signals of reaction products, caused by a non-Boltzmann population of magnetic energy levels. [15,22,5a] Figure 5 compares the ^{1}H NMR and CIDNP spectra of **1a** recorded in presence of butyl acrylate **BA** (see the Supporting Information for the corresponding spectra of **1b**). Polarized signals of the hydrogen atoms of the parent compound (at δ = 2.25 ppm (1), δ = 6.67 ppm (2) and δ = 1.99 ppm (3)) can be attributed to the (cage) re-formation of **1a**, indicating a partly reversible *α*-cleavage. The characteristic singlet at δ = 10.5 ppm appearing in enhanced absorption corresponds to the aldehyde proton of the benzaldehyde derivative **BH**, clearly indicating *α*-cleavage of **1a** (Scheme 3 and Figure 5). Analogous signals have been observed in the CIDNP spectra of several photoinitiating systems containing a benzoyl moiety.[23] The formation of **BH** is attributed to a disproportionation reaction (*β*-hydrogen transfer) between a benzoyl-type radical and radicals, which are able to donate hydrogen atoms (growing polymer chain).[23,24] Figure 5 additionally shows a strongly polarized emissive multiplet at δ = 4.49 ppm and an absorptive multiplet at δ = 3.37 ppm. These signals are tentatively assigned to the methylene protons of species **SnBAB**, which is formed upon addition of benzoyl radical **B•** to a chain radical initiated by **Sn•**. The analogous photoproduct has been observed for tetraacylgermanes.[5b] We assume that rotation around the C-C bond derived from **BA** (marked in pink in the structure of **SnBAB**, Figure 5) is sterically hindered by the adjacent bulky mesitoyl group, making the signal at δ = 4.49 ppm appear as a doublet of doublets, instead of a triplet.

Scheme 3. *α*-Cleavage of tetraacylstannane derivatives **1a**,**b**, leading to the formation of a tin-centered radical **Sn•** and a benzoyl-type radical **B•**.

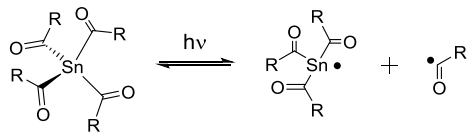

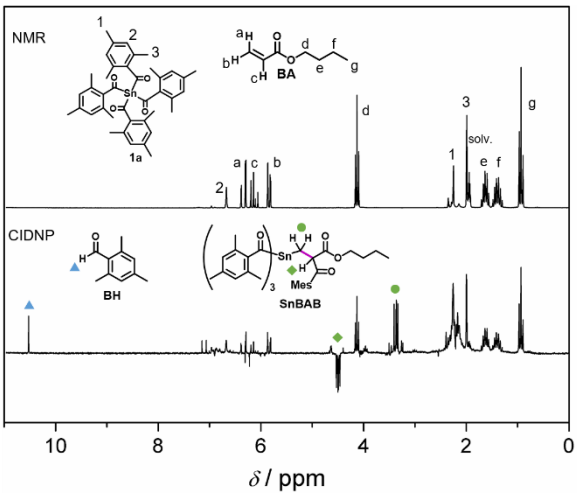

Figure 5. ^{1}H NMR and CIDNP spectra of **1a** (10 mM solution in acetonitrile-d_3), recorded in the presence of butyl acrylate monomer (**BA**, 50 mM).

The prepared compounds were also investigated by means of photo-DSC measurements in order to get fast and accurate information on their activity. With a single measurement, various significant parameters are accessible. From the height of the exothermic peak, the rate of polymerization R_P (mol L^{-1} s^{-1}) can be calculated.[25] The overall heat evolved (ΔH_P) gives information on the final double conversion (DBC). Furthermore, the time to reach the maximum heat flow (t_{max}) can be derived from the photo-DSC plots. Here, the photocuring of the crosslinking monomer 1,6-hexandiol diacrylate (HDDA) with **1a** was investigated (**1a:** $t_{max} \sim 4.5$ s, $R_{P,max} > 0.31$ mol L^{-1} s^{-1}, DBC ~ 59%). The previously reported tetraacylgermane **2a** was used as reference compound, showing comparable reactivity to **1a** under the chosen experimental conditions (**2a:** $t_{max} \sim 5.1$s, $R_{P,max} > 0.25$ mol L^{-1} s^{-1}, DBC ~ 57%). Photo-DSC and conversion plots are depicted in Figure 6. A summary of the DSC parameters can be found in the Supporting Information.

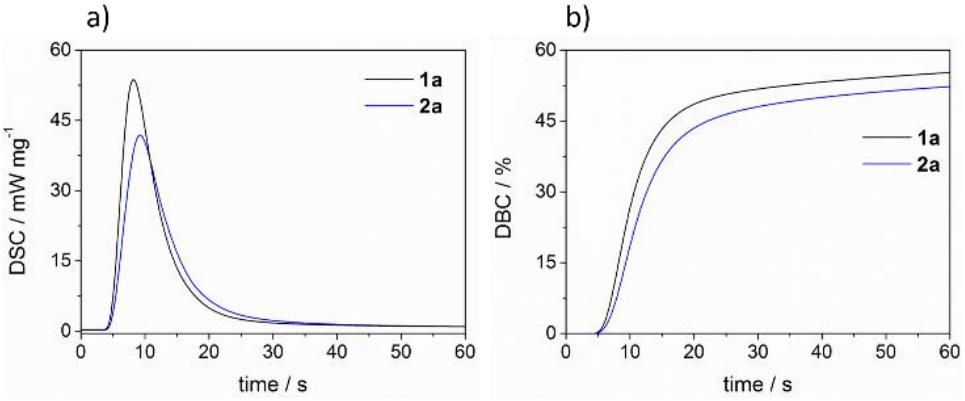

Figure 6. Photo-DSC (a) and conversion plots (b) for the photo- polymerization of HDDA with 0.3 w% photoinitiator. Samples were stabilized with 1000 ppm BHT prior to the measurement to prevent spontaneous polymerization.

3.7.4 Conclusion

In summary, we could synthesize and fully characterize the first examples of tetraacylstannanes, representing a class of highly efficient VL PIs. Unprecedentedly, the found photo-physical properties are beneficial over those known for Ge- or P-based PIs. Additionally, the low toxicity gives rise to any application where biocompatibility and costs are an issue. SSP experiments show that the tetraacylstannanes **1a**,**b** are promising initiators for high-wavelength visible-light curing. CIDNP experiments confirm α-cleavage of **1a**,**b** and efficient addition of tin-centered radicals and benzoyl radicals to monomer double bonds. High activity as photoinitiator was further verified by photo-DSC experiments.

3.7.5 Experimental Section

3.7.5.1 General Considerations

All experiments were performed under a nitrogen atmosphere using standard Schlenk techniques. Solvents were dried using a column solvent purification system.[26] Commercial KOtBu (97%), 2,4,6-Trimethylbenzoyl chloride (99%) and 2,6-Dimethylbenzoic acid (97%) were used without any further purification.

^{1}H (299.95 MHz), ^{13}C (75.43 MHz) and ^{29}Si (59.59 MHz) NMR spectra were recorded on a Varian INOVA 300 spectrometer in C_6D_6 or $CDCl_3$ solution and referenced versus TMS using the internal ^{2}H-lock signal of the solvent. Tetrakis(trimethylsilyl)stannane, 2,4,6-Trimethylbenzoyl fluoride and 2,6-Dimethylbenzoyl fluoride were prepared according to published procedures.[27]

HRMS spectra were run on a Kratos Profile mass spectrometer. Infrared spectra were obtained on a Bruker Alpha-P Diamond ATR Spectrometer from the solid sample. Melting points were determined using Stuart SMP50 apparatus and are uncorrected. Elemental analyses were carried out on a Hanau Vario Elementar EL apparatus.

CIDNP experiments were carried out on a 200 MHz Bruker AVANCE DPX spectrometer equipped with a custom-made CIDNP probe head. A Hg-Xe UV lamp (Hamamatsu Lightningcure LC4, 3500 mW/cm², λ_{max} = 365 nm) served as the light source. The typical CIDNP timing sequence consists of the following parts: composite pulse presaturation, lamp flash, 90° radiofrequency detection pulse (2.2 µs), and FID. "Dummy" CIDNP spectra employing the same pulse sequence but without the lamp pulse were always measured and subtracted from the CIDNP spectra. Samples were prepared in deuterated acetonitrile and deoxygenated by bubbling with argon before the experiment. Chemical shifts (δ) are reported in ppm relative to tetramethylsilane (TMS) using the residual deuterated solvent signals as an internal reference (CD_3CN, δ_H = 1.94 ppm).

UV absorption spectra were recorded on a Perkin Elmer Lambda 5 spectrometer. Photobleaching experiments (steady state photolysis, SSP) were performed on a TIDAS UV- VIS spectrometer (J&M, Germany). Samples (0.6 mM photoinitiator in acetonitrile) were irradiated in a quartz cuvette (1 cm x 1 cm) from the side with a 470 nm LED (Roithner Lasertechnik, Vienna) while UV-Vis spectra were recorded. A spectroradiometer (GL Spectis, GL Optics, Germany) was used to measure the output power of the LED and to ensure an equal photon flux for SSP experiments (13.1 mW, photon flux: 0.05 µmol s^{-1} at 20 mA, peak wavelength: 462.5 nm).

Materials and Solvents for Spectroscopic Investigations. Bis(acyl)phosphane oxide BAPO Irgacure 819 (**3**) was obtained from TCI. Tetraacylgermanes **2a** and **2b** were synthesized as described previously.[5b] The monomer butyl acrylate (BA, purity ≥ 99.0 %) was obtained from Fluka and freed from stabilizers by passing through a column of basic alumina before use. The solvents acetonitrile (MeCN, Sigma Aldrich, ≥ 99.9 %), and CD_2Cl_2 (Sigma Aldrich, 99.9 %) were employed as received. All experiments were performed at ambient temperature.

Photo-DSC. Experiments were performed on a photo-DSC instrument from Perkin Elmer (DSC 7). All formulations were analyzed in triplicate. After an equilibration phase (4 min) the samples were irradiated for 3 min with blue LED light (Bluephase Lamp, 1200 mW·cm^{-2}, Ivoclar Vivadent AG) at 30°C under constant nitrogen flow (20 mL min^{-1}).

The heat flow of the polymerization reaction was recorded as a function of time. From the theoretical heat of polymerization of the monomer HDDA ($\Delta H_{0,HDDA}$ = 761.92 J g^{-1} or 172.4 kJ mol^{-1} determined from 86.2 kJ mol^{-1} per acrylate unit)[28]. The double bond conversion (DBC) was calculated by dividing the measured heat of polymerization ΔH through $\Delta H_{0,HDDA}$. The maximum rate of polymerization $R_{P,max}$ was determined using equation 1, with h as the height of the exothermic polymerization signal in mW mg^{-1} and ρ = 1010 g L^{-1} as the density for HDDA at 25 °C.[25,29]

$$R_{P,max} = \frac{h \cdot \rho}{\Delta H_{0,HDDA}} \qquad (1)$$

3.7.5.2 Synthesis of 1a

A solution of $(Me_3Si)_3SnK$ in 10 mL of DME was freshly prepared from 1.00 g $Sn(SiMe_3)_4$ (2.43 mmol) and 0.30 g KOtBu (2.67 mmol) and slowly added to a solution of 1.66 g (9.96 mmol) 2,4,6-trimethylbenzoyl fluoride in 15 mL DME at 0°C. The mixture was stirred for another 10 min. For the work up the volatile components were evaporated under reduced pressure. The solid residue was extracted with pentane/toluene and filtered. The filtrate was pumped down. The obtained crude product was recrystallized from toluene, giving orange crystals of **1a**. Yield: 0.86 g (50%) of analytically pure **1a** as orange crystals.

mp: 122-125°C. Anal. Calc.: C, 67.91; H, 6.27 % Found: C, 67.24; H, 5.99 %. ^{119}Sn-NMR ($CDCl_3$, TMS, ppm): -499.02. ^{13}C-NMR ($CDCl_3$, TMS, ppm): 243.88 (C=O); 143.71, 139.53, 131.95, 128.99 (Mes-C); 21.33, 18.84 (Mes-CH_3).^{1}H-NMR ($CDCl_3$, TMS, ppm): 6.61 (s, 2H, Mes-H); 2.24 (s, 3H, Mes-CH_3); 2.05 (s, 6H, Mes-CH_3). IR (neat): ν(C=O) = 1662, 1622 cm^{-1}. HRMS: Calc. 561.1458 for (M^+-Acyl) Found: 561.1450. UV-VIS: λ [nm] (ε [L mol^{-1} cm^{-1}]) = 399 (1727).

3.7.5.3 Synthesis of 1b

A solution of $(Me_3Si)_3SnK$ in 10 mL of DME was freshly prepared from 1.00 g $Sn(SiMe_3)_4$ (2.43 mmol) and 0.30 g KOtBu (2.67 mmol) and slowly added to a solution of 1.52 g (9.96 mmol) 2,6-dimethylbenzoyl fluoride in 15 mL DME at 0°C. The mixture was stirred for another 10 min. For the work up the volatile components were evaporated under reduced pressure. The solid residue was extracted with pentane/toluene and filtered. The filtrate was pumped down. The obtained crude product was recrystallized from toluene, giving orange crystals of **1b**. Yield: 0.98 g (62%) of analytically pure **1b**.

mp: 130-135°C. Anal. Calc.: C, 66.38; H, 5.57 % Found: C, 66.03; H, 5.81 %. ^{119}Sn-NMR (C_6D_6, TMS, ppm): -505.88. ^{13}C-NMR (C_6D_6, TMS, ppm): 243.18 (C=O); 146.99, 131.88, 129.66, 128.66 (Aryl-C); 18.82 (Aryl-*o*CH_3).^{1}H-NMR (C_6D_6, TMS, ppm): 7.05 (t, 1H, Aryl-H); 6.84 (s, 2H, Aryl-H); 2.04 (s, 6H, Aryl-*o*CH_3). IR (neat): ν(C=O) = 1669, 1633 cm^{-1}. HRMS: Calc. 519.1027 for (M^+-Acyl) Found: 519.0988 UV-VIS: λ [nm] (ε [L mol^{-1} cm^{-1}]) = 396 (1758).

3.7.5.4 Steady-State Photolysis (SSP) / UV-Vis Spectroscopy

Figure S1. Comparison of the UV-Vis absorption spectra of compounds **1a,b** and **2–5** (samples: 0.6 mM solutions in acetonitrile).

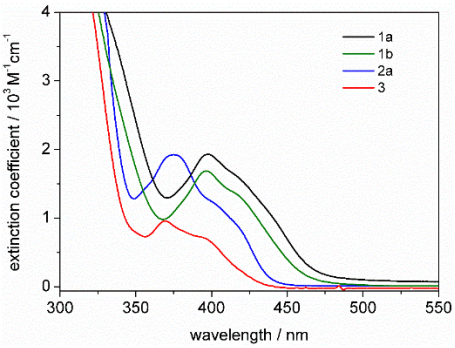

3.7.5.5 CIDNP Spectroscopy

Figure S2. ^{1}H NMR and CIDNP spectra of **1b** (10 mM solution in acetonitrile-d_3) recorded in presence of butyl acrylate **BA** (50 mM).

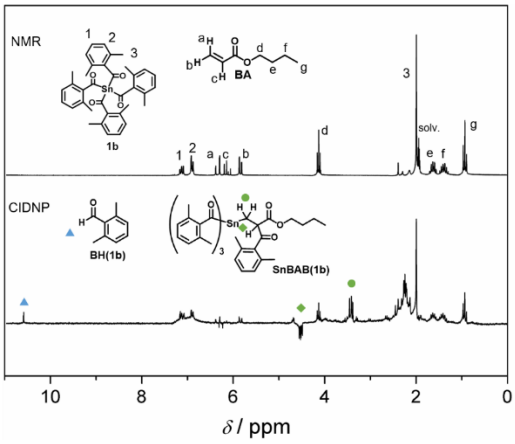

3.7.5.6 X-ray Crystallography

All crystals suitable for single crystal X-ray diffractometry were removed from a vial and immediately covered with a layer of silicone oil. A single crystal was selected, mounted on a glass rod on a copper pin, and placed in the cold N_2 stream provided by an Oxford Cryosystems cryostream. XRD data collection was performed for all compounds on a Bruker APEX II diffractometer with use of an Incoatec microfocus sealed tube of Mo Kα radiation (λ= 0.71073 Å) and a CCD area detector. Empirical absorption corrections were applied using SADABS or TWINABS.[30] The structures were solved with use of the intrinsic phasing option in SHELXT and refined by the full-matrix least-squares procedures in SHELXL.[31] The space group assignments and structural solutions were evaluated using PLATON.[32] Non-hydrogen atoms were refined anisotropically. Hydrogen atoms were located in calculated positions corresponding to standard bond lengths and angles. CCDC 1824373 and 1824374 contain the supplementary crystallographic data for all compounds. These data can be obtained free of charge from The Cambridge Crystallographic Data Centre *via* www.ccdc.cam.ac.uk/data_request/cif. Table S1 contains crystallographic data and details of measurements and refinement for compounds **1a**,**b**.

Table S1. Crystallographic data and details of measurements for compounds **1a**,**b** Mo Kα (λ=0.71073Å). $R_1 = \Sigma / |F_o| - |F_c| / |\Sigma| F_d$; $wR2 = [\Sigma_w(F_o^2-F_2^2)^2/\Sigma_w(F_o^2)^2]^{1/2}$

Compound	**1a**	**1b**
Formula	$C_{40}H_{44}O_4Sn$	$C_{36}H_{36}O_4Sn$
Fw (g mol^{-1})	707.44	651.34
***a* (Å)**	10.8064(4)	15.062(3)
***b* (Å)**	12.0573(4)	11.477(2)
***c* (Å)**	14.7267(6)	17.674(3)
***α* (°)**	112.379(2)	90
***β* (°)**	96.797(2)	90
***γ* (°)**	94.499(2)	90
***V* (Å^3)**	1745.83(11)	3055.2(10)
Z	2	4
Crystal size (mm)	0.15 × 0.13 × 0.12	0.16 × 0.13 × 0.09
Crystal habit	Block, yellow	Block, orange
Crystal system	Triclinic	Orthorhombic
Space group	*P*-1	$Pca2_1$
d_{calc} (mg/m^3)	1.346	1.416
μ (mm^{-1})	0.77	0.87
***T* (K)**	100(2)	100(2)
2ϑ range (°)	2.6–27.7	2.3–33.1
***F*(000)**	732	1336
R_{int}	0.107	0.084
independent reflns	6143	11687
No. of params	418	378
R1, wR2 (all data)	R1 = 0.0337 wR2 = 0.0744	R1 = 0.0390 wR2 = 0.0588
R1, wR2 (>2σ)	R1 = 0.0240 wR2 = 0.0516	R1 = 0.0297 wR2 = 0.0714

3.7.5.7 Photo-DSC

Table S2. Time to peak maximum t_{max}, maximum rate of photopolymerization $R_{P,max}$ and final double bond conversion DBC acquired from photo-DSC.

	PI [w%]	t_{max} [s]	$R_{P,max}$ [mol L^{-1} s^{-1}]	DBC [%]
1a	0.30	4.5	0.31	59 ± 1
2a	0.30	5.1	0.25	57 ± 1

3.7.5.8 Computational Section

All computational studies were executed on a computing cluster with blade architecture using the Gaussian09 software package.[33] Geometry optimizations were performed in the gas phase with B3LYP as hydride density functional[34] together with the LANL2DZdp-ECP for Sn[35] as well as 6-31+G(d,p) split-valence basis set for H, C and O.[36] Minimum structures were characterized by harmonic frequency calculations, yielding none imaginary frequency. Vertical excitations were calculated via time-dependent DFT (TD-DFT) at the LANL2DZdp-ECP(Sn),def2-TZVP(H,C,O) level of theory[37] and solvent effects were considered by applying the polarized continuum model (PCM).[38] Chloroform ($CHCl_3$) was used as a solvent with a dielectric constant of ε = 4.7113. All structures and the simulated UV-Vis spectra were plotted using the Gabedit software package.[39]

Table S3. Experimental and PCM($CHCl_3$) TD-DFT CAM-B3LYP/LANL2DZdp-ECP(Sn),def2-TZVP(H,C,O)//B3LYP/LANL2DZdp-ECP(Sn),6-31+G(d)(H,C,O) calculated Wavelength Absorption Maxima λ [nm], Extinction Coefficients ϵ [$dm^2 \bullet mol^{-1}$] and Oscillator Strengths f for **1a**,**b** as well as the corresponding trimethylstannane derivatives.

	λ_{max},exp (ϵ)	Tetra λ_{max},calc (f)	Mono λ_{max},calc (f)	Absorption Edge	Assignment
1a	398 (1776)	416, 409, 389 (0.0221, 0.0051, 0.0137)	414 (0.0038)	480	n/σ-π*(CO/Aryl)
1b	396 (1735)	417, 409, 389 (0.0167, 0.0053, 0.0131)	415 (0.0036)	480	n/σ-π*(CO/Aryl)

3.7.6 References

[1] E. von Frankland, *Ann. Chem. Pharm.* **1849**, *71*, 171.
[2] D. Seyferth, *Organometallics* **2001**, *20*, 1488.
[3] W. C. Zeise, *Ann. Phys. Chem.* **1831**, *97*, 497.
[4] a) G.J.D. Peddle, *J. Organomet. Chem.* **1968**, *14*, 139; b) A. Capperucci, A. Degl'innocenti, C. Faggi, G. Reginato, A. Ricci, *J. Org. Chem.*, *54*, 2966; c) M. Kosugi, H. Naka, H. Sano, T. Migita, *Bull. Chem. Soc. Jpn.* **1987**, *60*, 3462.
[5] a) D. Neshchadin, A. Rosspeintner, M. Griesser, B. Lang, S. Mosquera-Vazquez, E. Vauthey, V. Gorelik, R. Liska, C. Hametner, B. Ganster, R. Saf, N. Moszner, G. Gescheidt, *J. Am. Chem. Soc.* **2013**, *135*, 17314; b) J. Radebner, A. Eibel, M. Leypold, C. Gorsche, L. Schuh, R. Fischer, A. Torvisco, D. Neshchadin, R. Geier, N. Moszner, R. Liska, G. Gescheidt, M. Haas, H. Stueger, *Angew. Chem. Int. Ed.* **2017**, *56*, 3103; c) B. Ganster, U. K. Fischer, N. Moszner, R. Liska, *Macromolecules* **2008**, *41*, 2394; d) B. Ganster, U. K. Fischer, N. Moszner, R. Liska, *Macromol. Rapid Comm.* **2008**, *29*, 57.
[6] a) J. P. Fouassier, J. F. Rabek in *Radiation curing in polymer science and technology*, Elsevier Applied Science, London, **1993**; b) S. P. Pappas in *Radiation Curing*. *Science and Technology*, Springer US; Imprint; Springer, Boston, MA, **1992**.
[7] a) W. Feuerstein, S. Höfener, W. Klopper, I. Lamparth, N. Moszner, C. Barner-Kowollik, A.-N. Unterreiner, *Chemphyschem* **2016**, *17*, 3460; b) H. Grützmacher, J. Geier, D. Stein, T. Ott, H. Schönberg, R. H. Sommerlade, S. Boulmaaz, J.-P. Wolf, P. Murer, T. Ulrich, *Chimia* **2008**, *62*, 18; c) R. Appel, G. Haubrich, F. Knoch, *Chem. Ber.* **1984**, *117*, 2063; d) L. Gonsalvi, M. Peruzzini, *Angew. Chem. Int. Ed.* **2012**, *51*, 7895; e) Safety Data sheet of Phenylbis(2,4,6-trimethylbenzoyl)phosphine oxide.
[8] a) Safety Data sheet of Bis(4-methoxybenzoyl)diethylgermane.; b) N. Moszner, F. Zeuner, I. Lamparth, U. K. Fischer, *Macromol. Mater. Eng.* **2009**, *294*, 877; c) N. Moszner, U. K. Fischer, B. Ganster, R. Liska, V. Rheinberger, *Dent. Mater.* **2008**, *24*, 901.
[9] a) J. Ohshita, Y. Tokunaga, H. Sakurai, A. Kunai, *J. Am. Chem. Soc.* **1999**, *121*, 6080; b) M. Mitterbauer, M. Haas, H. Stüger, N. Moszner, R. Liska, *Macromol. Mater. Eng.* **2017**, *302*, 1600536.
[10] *Cytotoxicity assay in vitro: Evaluation of test items in the XTT-Test with K-203, RCC-CCR Study, March 2017, 1-20 (Study number: 1818710, Cytotest Envigo CRS GmbH)*.
[11] *RCC-Report, Salmonella Typhimurium and Escherichia Coli Reverse Mutation Assay with K-203, 2017, 1-32 (Study number: 1818710, Cytotest Envigo CRS GmbH)*.
[12] NICNAS Full Public Report, Phenylbis(2,4,6-trimethylbenzoyl)phosphine oxide, May 1998, Study Number: NA599FR (Australia).
[13] N. Moszner, I. Lamparth, J. Angermann, U. K. Fischer, F. Zeuner, T. Bock, R. Liska, V. Rheinberger, *Beilstein J Org Chem* **2010**, *6*, 26.
[14] RCC-Report, in vitro single cell gel electrphoresis (comet assay) in chinese hamster V79 cells with PH-77, 2008, 1-14 (Study number: 1182000, Cytotest Cell Research GmbH).
[15] U. Kolczak, G. Rist, K. Dietliker, J. Wirz, *J. Am. Chem. Soc.* **1996**, *118*, 6477.
[16] a) J. Radebner, M. Leypold, A. Eibel, J. Maier, L. Schuh, A. Torvisco, R. Fischer, N. Moszner, G. Gescheidt, H. Stueger, M. Haas, *Organometallics* **2017**, *36*, 3624; b) A. Eibel, J. Radebner, M. Haas, D. E. Fast, H. Freißmuth, E. Stadler, P. Faschauner, A. Torvisco, I. Lamparth, N. Moszner, H. Stueger, G. Gescheidt, *Polym. Chem.* **2018**, *9*, 38; c) N. Moszner, U. K. Fischer, I. Lamparth, P. Fässler, J. Radebner, A. Eibel, M. Haas, G. Gescheidt, H. Stueger, *J. Appl. Polym. Sci.* **2017**, *27*, 46115.
[17] R. Fischer, J. Baumgartner, C. Marschner, F. Uhlig, *Inorg. Chim. Acta.* **2005**, *358*, 3174.
[18] a) B. K. Hunter, L. W. Reeves, *Can. J. Chem.* **1968**, *46*, 1399; b) J. Schraml, V. Chvalovsky, H. Jancke, G. Engelhardt, *Org. Magn. Reson.* **1977**, *9*, 237.
[19] Z. Rappoport in *The chemistry of organo-germanium, tin and lead compounds. Vol. 2*, Wiley, Chichester, **2002**.
[20] A. Huber, A. Kuschel, T. Ott, G. Santiso-Quinones, D. Stein, J. Bräuer, R. Kissner, F. Krumeich, H. Schönberg, J. Levalois-Grützmacher, H. Grützmacher, *Angew. Chem. Int. Ed.* **2012**, *51*, 4648.
[21] K. Dietliker, T. Jung, J. Benkhoff, H. Kura, A. Matsumoto, H. Oka, D. Hristova, G. Gescheidt, G. Rist, *Macromol. Symp.* **2004**, *217*, 77.
[22] A. Yurkovskaya, O. Morozova, G. Gescheidt in *Encyclopedia of Radicals in Chemistry, Biology and Materials*.
[23] A. Borer, R. Kirchmayr, G. Rist, *Helv. Chim. Acta* **1978**, *61*, 305.
[24] M. Griesser, D. Neshchadin, K. Dietliker, N. Moszner, R. Liska, G. Gescheidt, *Angew. Chem. Int. Ed.* **2009**, *48*, 9359.
[25] G. Ullrich, B. Ganster, U. Salz, N. Moszner, R. Liska, *J. Polym. Sci. A Polym. Chem.* **2006**, *44*, 1686.
[26] A. B. Pangborn, M. A. Giardello, R. H. Grubbs, R. K. Rosen, F. J. Timmers, *Organometallics* **1996**, *15*, 1518.
[27] a) L. R. Subramanian, G. Siegemund (Eds.) *Houben-Weyl Methods of Organic Chemistry Supplement: Organo-Fluorine Compounds Fluorinating Agents and Their Application in Organic Synthesis*. Introduction of Fluorine with Alkali Metal Fluorides, Including Ammonium Fluoride and Tetraalkylammonium Fluorides (Including Special Methods of Fluorinations, e.g., Phase Transfer Catalysis, Activation by Crown Ethers, Reagents Bound to Polymers), Thieme, Stuttgart, **1998**; b) U. G. H. Buerger, *Angew. Chem. Int. Ed.* **1968**, *7*, 212.
[28] K. S. Anseth, C. M. Wang, C. N. Bowman, *Macromolecules* **1994**, *27*, 650.

[29] M. K. Mishra, Y. Yagci, M. K. H. o. r. v. p. Mishra in *Handbook of vinyl polymers*. *Radical polymerization, process, and technology / editors, Munmaya Mishra and Yusuf Yagci*, Taylor & Francis, Boca Raton, FL, **2008**.
[30] a) Bruker in *APEX2 and SAINT*. *version 5.03*. Bruker AXS Inc.:, Madison, Wisconsin, USA, **2012**; b) R. H. Blessing, *Acta Cryst.* **1995**, *51*, 33.
[31] a) G. M. Sheldrick, *Acta Crystallogr., Sect. A: Found. Crystallogr.* **1990**, *A46*, 467; b) G. M. Sheldrick, *Acta Crystallogr., Sect. A: Found. Crystallogr.* **2008**, *64*, 112; c) G. M. Sheldrick, *Acta Crystallogr., Sect. A: Found. Adv.* **2015**, *71*, 3.
[32] a) A. L. Spek, *J. Appl. Crystallogr.* **2003**, *36*, 7; b) A. L. Spek, *Acta Crystallogr., Sect. D: Biol. Crystallogr.* **2009**, *65*, 148.
[33] M. J. Frisch, G. W. Trucks, H. B. Schlegel, G. E. Scuseria, M. A. Robb, J. R. Cheeseman, G. Scalmani, V. Barone, B. Mennucci, G. A. Petersson, H. Nakatsuji, M. Caricato, X. Li, H. P. Hratchian, A. F. Izmaylov, J. Bloino, G. Zheng, J. L. Sonnenberg, M. Hada, M. Ehara, K. Toyota, R. Fukuda, J. Hasegawa, M. Ishida, T. Nakajima, Y. Honda, O. Kitao, H. Nakai, T. Vreven, Montgomery, Jr. J., A., J. E. Peralta, F. Ogliaro, M. Bearpark, J. J. Heyd, E. Brothers, K. N. Kudin, N. Staroverov, T. V. Keith, R. Kobayashi, J. Normand et al. in *Gaussian 09, Revision D.01, Gaussian, Inc.: Wallingford, CT*, **2013**.
[34] a) A. D. Becke, *J. Chem. Phys.* **1993**, *98*, 1372; b) C. Lee, W. Yang, R. G. Parr, *Phys. Rev. B: Condens. Matter Mater. Phys.* **1988**, *37*, 785.
[35] a) P. J. Hay, W. R. Wadt, *J. Chem. Phys.* **1985**, *82*, 270; b) W. R. Wadt, P. J. Hay, *J. Chem. Phys.* **1985**, *82*, 284; c) P. J. Hay, W. R. Wadt, *J. Chem. Phys.* **1985**, *82*, 299; d) C. E. Check, T. O. Faust, J. M. Bailey, B. J. Wright, T. M. Gilbert, L. S. Sunderlin, *J. Phys. Chem. A* **2001**, *105*, 8111.
[36] P. C. Hariharan, J. A. Pople, *Theoret. Chim. Acta* **1973**, *28*, 213.
[37] a) T. Yanai, D. P. Tew, N. C. Handy, *Chem. Phys. Lett* **2004**, *393*, 51; b) F. Weigend, R. Ahlrichs, *Phys. Chem. Chem. Phys.* **2005**, *7*, 3297.
[38] J. Tomasi, B. Mennucci, R. Cammi, *Chem. Rev.* **2005**, *105*, 2999.
[39] A.-R. Allouche, *J. Comput. Chem.* **2011**, *32*, 174.

4 CONCLUSION AND OUTLOOK

To conclude, the synthesis of the long sought-after tetra substituted acylgermanes which have been predicted to act as advantageous photoinitiators for the radical polymerization under visible-light irradiation was achieved. The outlined one-pot reaction protocol is a landmark in the field of organometallic synthesis, as the preparation of acyl substituted group 14 compounds still depends on the use of protection group chemistry (Corey Seebach reaction). For the first time, we could demonstrate how to overcome current synthetic limitations and to generate tetraacylgermanes even in high yields (equation 1).

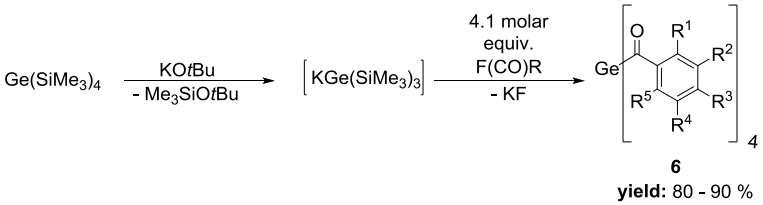

6a: $R^1 = R^2 = R^3 = R^4 = R^5 = -H$
6b: $R^1 = -Me, R^2 = R^3 = R^4 = R^5 = -H$
6c: $R^1 = -Et, R^2 = R^3 = R^4 = R^5 = -H$
6d: $R^1 = R^3 = R^4 = R^5 = -H, R^2 = -Me$
6e: $R^1 = R^2 = R^4 = R^5 = -H, R^3 = -Me$
6f: $R^1 = R^5 = -Me, R^2 = R^3 = R^4 = -H$
6g: $R^1 = R^3 = R^5 = -Me, R^2 = R^4 = -H$
6h: $R^1 = -OMe, R^2 = R^3 = R^4 = R^5 = -H$
6i: $R^1 = R^2 = R^4 = R^5 = -H, R^3 = -OMe$
6j: $R^1 = R^2 = R^4 = R^5 = -H, R^3 = -OEt$
6k: $R^1 = R^2 = R^4 = R^5 = -H, R^3 = -O\mathit{n}Pr$
6l: $R^1 = R^2 = R^4 = R^5 = -H, R^3 = -OAc$
6m: $R^1 = R^2 = R^4 = R^5 = -H, R^3 = -NMe_2$
6n: $R^1 = R^4 = R^5 = -H, R^2 = R^3 = -CH_{aryl}$
6o: $R^1 = R^2 = R^4 = R^5 = -H, R^3 = -C{\equiv}C\text{-}Ph$

(1)

Moreover, the robust reaction protocol allowed the preparation of a variety of derivatized acylgermanes (equation 1). We could show that functionalization on the aromatic ring system allows fine-tuning the absorption properties and shifting the absorption bands towards the long-wavelength region (Figure 1).

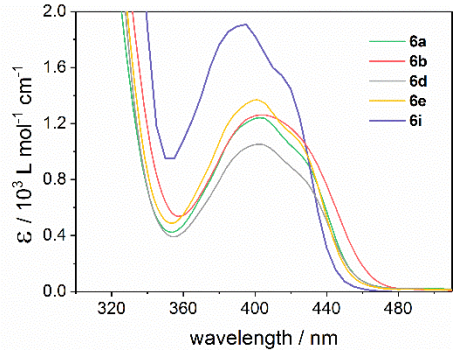

Figure 1. Absorption Spectra of Selected Tetraacylgermanes (Substituents at Aromatic Ring Are Stated in Parentheses): **6a** (phenyl), **6b** (*o*-Me) **6d** (*m*-Me), **6e** (*p*-Me) and **6i** (*p*-OMe), (CH_3CN Solution; c = 10^{-3} mol·l^{-1}).

Additionally, we could show that the extinction coefficients increase almost linearly according to the number of chromophores attached to the germanium center (Figure 2).

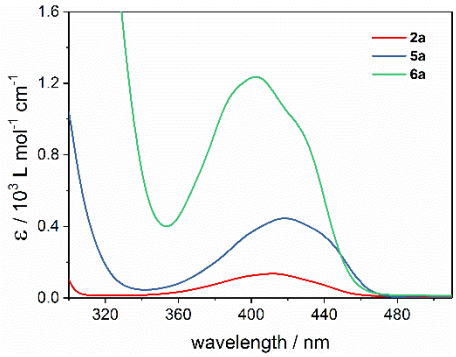

Figure 2. UV-Vis spectra of a monoacylgermane **2a**, bisacylgermane **5a**, and tetraacylgermane **6a** (CH_3CN solution; c= 10^{-3} mol·l^{-1}).

From the obtained X-ray structures we could observe that di-*ortho*-substitution at the aromatic ring in aryl acylgermanes induces a significant hypsochromic shift of the longest wavelength absorption band. This hypsochromic shift roughly correlates with the twist (or dihedral) angle between the plane of the phenyl ring and the C=O moiety, which significantly deviates from a coplanar arrangement in the di-*ortho*-substituted derivatives caused by the steric repulsion between the *ortho*-substituents and the C=O group (compare Figure 3). This correlation is conclusive as larger values of the dihedral angle reduce phenyl/C=O π-π conjugation thus increasing the HOMO–LUMO gap and shifting the corresponding UV maximum to larger energies.

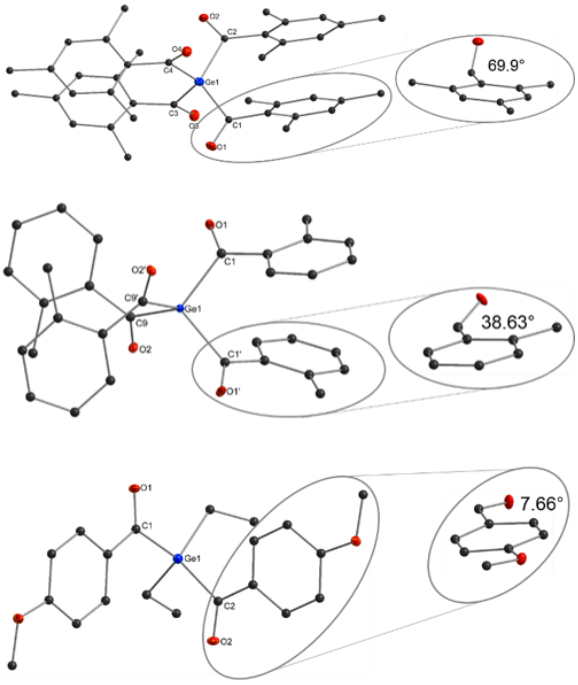

Figure 3. ORTEP Representation of **6b**,**g** and **5d**. Thermal Ellipsoids Are Drawn at the 50% Probability Level. Hydrogen Atoms Are Omitted for Clarity. Mean Torsion Angles [°] Are Shown in the Magnified Part.

In cooperation with Prof. Gescheidt and Anna Eibel of the Institute of Physical and Theoretical Chemistry in Graz we investigated the properties of the Ge-based radicals via sophisticated physico-chemical measurements. The results of collaborative work are summarized below.

The formation of the primary germyl-centered radical via photolysis was observed by time-resolved EPR-spectroscopy and has be confirmed as the major photochemical reaction pathway upon irradiation with UV-light. Moreover, we obtained insights in the follow-up reactions of the primary formed radicals in presence of monomer by performing ^{1}H CIDNP spectroscopy (Scheme 1).

Scheme 1. Proposed Reaction Scheme of Initiator **5a** in the Presence of Monomers, as Established via CIDNP Experiments.

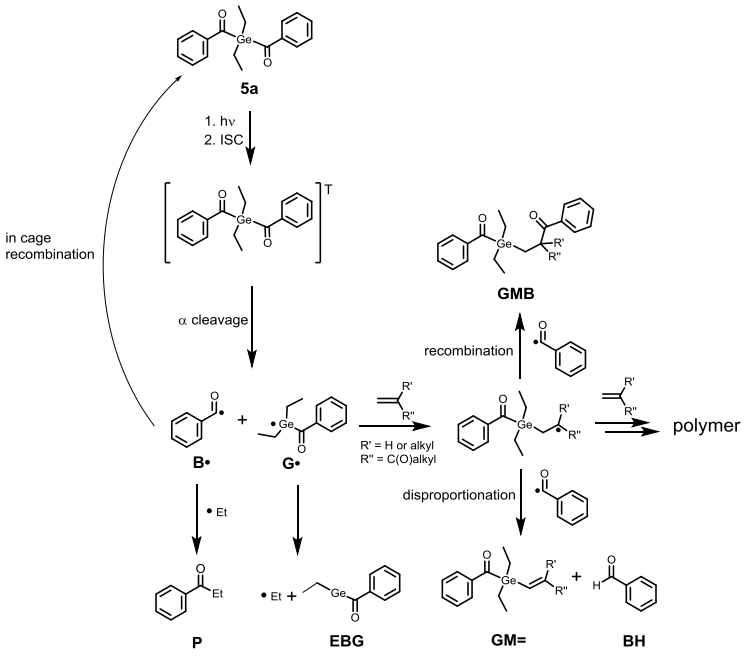

High quantum yields of decomposition are an important requirement for efficient photoinitiators. Quantum yields of ~0.8-0.9 for mono- and bisacylgermanes have been reported by Moszner and coworkers. In cooperation with Prof. Gescheidt and Anna Eibel we could also determine the quantum yield of decomposition for tetraacylgermanes (~0.4).

To achieve high curing depth and to avoid colored polymers, fast photobleaching of the PI at the irradiation wavelength is equally crucial, especially upon irradiation with visible light, which is particularly relevant for (bio)medical applications such as dental composites. Therefore, various photobleaching studies of acylgermanes have been performed.

The wavelength-dependent photobleaching curves are presented in Figure 4 for irradiation of mono- to tetraacylgermanes with LEDs at 385 nm and 470 nm in acetonitrile/monomer solutions. The monomer (methyl methacrylate, MMA) acts as a radical trap, leading to the formation of photoproducts, which do not absorb in the visible wavelength range. We observed that photobleaching is more efficient upon irradiation with LED light at 385 nm than at 470 nm for all investigated compounds. Tetraacylgermane **6b** exhibits remarkably fast photobleaching upon irradiation at 470 nm, indicating efficient initiation under high-wavelength visible light.

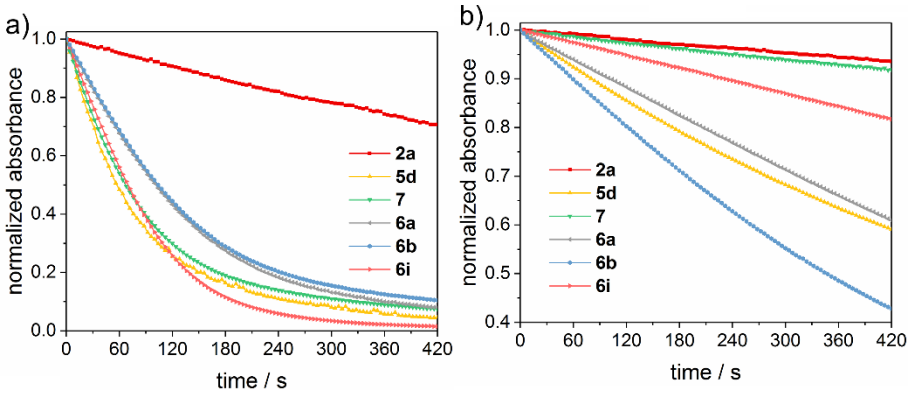

Figure 4. Steady-State Photolysis of Mono-, Bis-, Tris- and Tetraacylgermanes in Acetonitrile/MMA Solutions. Plots of Normalized Absorbance versus Time for Irradiation at a) 385 nm and b) 470 nm, Monitored at the n-π* Absorption Maxima (**2a**: 412.5 nm, **5d**: 409 nm, **7**: 383 nm, **6a**: 404 nm, **6b**: 405.5 nm, **6i**: 393 nm).

Apart from high decomposition quantum yields and efficient photobleaching, fast addition of the primary radicals to monomers is essential for an efficient photoinitiator. Thus, LFP experiments were conducted to determine the radical-to-monomer addition kinetics. A series of different acrylate monomers was tested (cf. Figure 5).

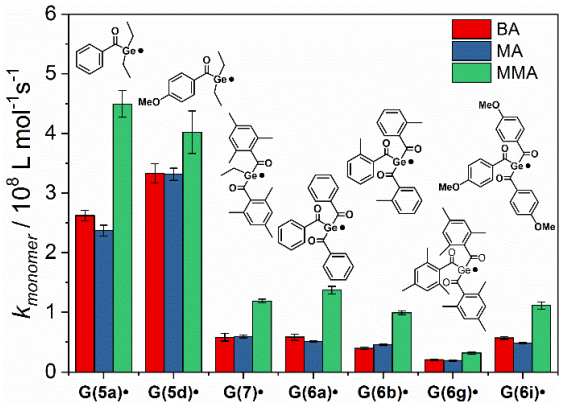

Figure 5. Second-Order Rate Constants $k_{monomer}$ for the Addition of **G•** to Butyl Acrylate (**BA**), Methyl Acrylate **(MA)** and Methyl Methacrylate **(MMA).**

Notably, Ge-centered radicals show significantly higher reactivity toward monomers than related phosphorus-based radicals derived from acylphosphane oxides.

Together with our cooperation partner Ivoclar Vivadent AG and Prof. Moszner we performed further efficiency studies of tetraacylgermanes. The obtained results of the cooperation are summarized below.

We investigated the toxicity of tetraacylstannanes. The cytotoxicity tests appeared to be negative as well as the AMES test proved that tetraacylgermanes do not induce gene mutation. Thus, enabling the implementation of tetraacylgermanes in (bio)medical applications.

Additionally, we have been performed photo-DSC studies to evaluate the PI performance, showing particularly high reactivity for tetraacylgermane **6b** ($R_{P,max}$ value of 0.046 s^{-1}, DBC = 52.3). The obtained results highlighted that tetraacylgermanes show better polymerization initiating reactivity than the best commercially available visible-light PI **5d** (Ivocerin). In comparison to bisacylgermane **5d** (0.05 w%) a fifth of the PI load of **6b** (0.01 w%) was used, still achieving similar results.

Speaking of dental application, together with Prof. Moszner we were able to photo-cure a composite using a LED with an emission maximum of 500 nm, which is important for the development of bulk-curable restorative composites with an increased curing depth. Currently applied PI systems (Ivocerin, **5d**) fail to photo-cure monomers under this irradiation conditions. The prepared composites were also investigated towards their mechanical properties. According to the ISO standard intraorally cured restorative composites must have a flexural strength a least of 80 MPa. As a representative example, composites prepared with tetraacylgermane **6b** showed a flexural strength of 135.2 ± 10.1 MPa.

Together with Ivoclar Vivadent AG we were testing the storage stability of the novel PIs and thereof based resins or composites. The PIs themselves and all prepared resins and composites showed an excellent long-term thermal stability during storage at room temperature or 50°C.

A central topic of discussion throughout this thesis was, whether tetraacylgermanes, carrying the highest number of photo-cleavable bonds per molecule, undergo multiple cleavage upon irradiation. Through the collaboration with Prof. Barner-Kowollik we examined this issue by combining permutation mathematics and electronspray ionization mass spectrometry. The obtained results displayed that tetraacylgermanes undergo multiple photo-cleavage.

Eventually, we were able to extend the scope of the developed synthetic strategy and prepare tetraacylstannanes for the first time (equation 2).

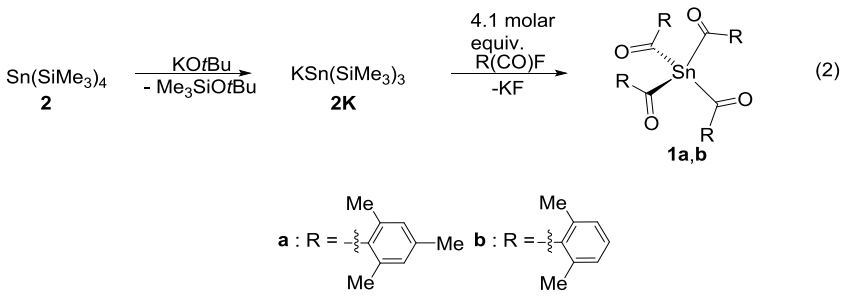

The isolated orange compounds show unexpectedly high stability under ambient conditions. Their absorption properties indicate promising PI properties and performance (Figure 6).

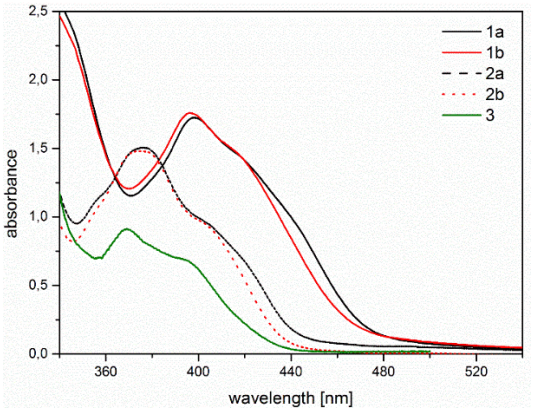

Figure 6. UV-Vis Absorption Spectra of **1a**,**b**, **2a**,**b** (the Respective Germanium-Analogues) and **3** (Bisacylphosphane Oxide ®Irgacure 819)(Chloroform Solution, c = 10^{-3} mol L^{-1})

Through the collaboration with Prof. Gescheidt we found similar PI properties for tetraacylstannanes when compared to tetraacylgermanes. Likewise, we found the same photoproducts when we performed CIDNP experiments.

The LFP studies revealed that tetraacylstannanes undergo even faster photobleaching than tetraacylgermanes (Figure 7).

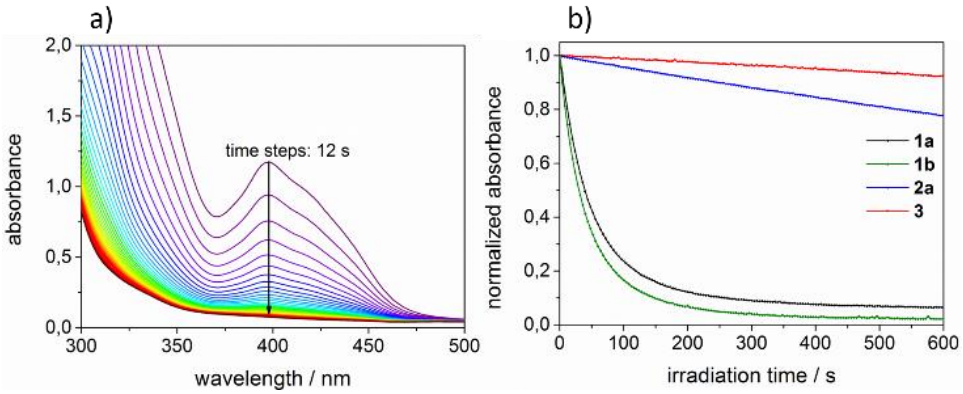

Figure 7. a) Photobleaching of **1a** Upon Irradiation at 470 nm, b) Plots of Normalized Absorbance Versus Time for Compounds **1a,b**, **2a** and **3**, Monitored at Absorption Maxima (**1a**: 398 nm, **1b**: 396.5 nm, **2a**: 375 nm **3**: 369.5 nm, **3**: 409 nm). Samples: 0.6 mM PI in Acetonitrile.

Together with Prof. Moszner we conducted photo-DSC studies to evaluate the PI performance. First investigations showed relatively good double bond conversions and polymerization rates for tetraacylstannanes when compared to the performance of tetraacylgermanes (Figure 8).

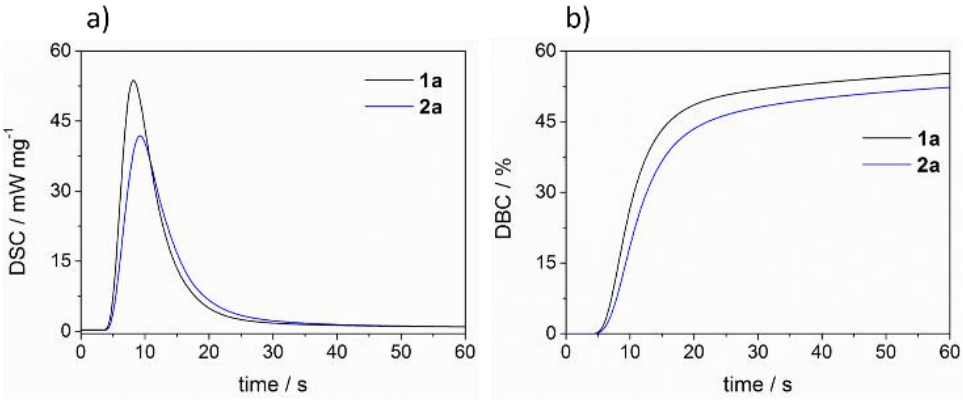

Figure 8. Photo-DSC (a) and conversion plots (b) for the photo- polymerization of HDDA with 0.3 w% photoinitiator. Samples were stabilized with 1000 ppm BHT prior to the measurement to prevent spontaneous polymerization.

The results obtained in the course of this thesis provide an excellent basis for further investigations. Moreover, until now we only investigated the application of tetraacylgermanes in dental filling materials.

Further investigations need to be done to expand the application of Ge- and Sn-based PI to other fields apart from the dental industry. Their outstanding properties and performance open up the possibility to enter other areas of photopolymerization (3D-printing, inks, coatings etc.).

The easy accessibility of tetraacylgermanes and their superior PI performance prompted our cooperation partner Ivoclar Vivadent AG to initiate the scale-up tests for the production of tetraacylgermanes. The commercialization and implementation of tetraacylgermanes into dental restorative filling materials by Ivoclar Vivadent AG is foreseeable.

CURRICULUM VITAE

Name:	**Judith Radebner**, MSc.
Address:	Moserhofgasse 36/16
	8010 Graz
	Austria
Mobile:	+43660 1674246
Email:	j.radebner@tugraz.at
Date of Birth:	05.10.1990

EDUCATION

09/2015 – 05/2018	**PhD Student**, TU Graz, Institute of Inorganic Chemistry, Field of Research: Germanium-and Tin-Based Photoinitiators (cooperating with Ivoclar Vivadent AG)
10/2012 – 03/2015	**Master of Science** in Technical Chemistry, Graz University of Technology (in cooperation with the University of Graz as part of the NAWI-Graz program)
	Master's Thesis, TU Graz, Institute of Inorganic Chemistry, Title: *„Polymer precursor synthesis and characterization of functionalized 1-naphthylsilanes"* (Prof. Frank Uhlig)
10/2009 – 07/2012	**Bachelor of Science** in Chemistry, Graz University of Technology (in cooperation with the University of Graz as part of the NAWI-Graz program) **Bachelor's Thesis**, TU Graz, Institute of Inorganic Chemistry, Title: "*Vorversuche zur Synthese von Sn-Sn Polymeren*" (Prof. Frank Uhlig)

INTERNATIONAL EXPERIENCE

08/2012 – 05/2013	**Erasmus Program**, Helsingin yliopisto (University of Helsinki), Helsinki, Finnland

WORK EXPERIENCE

09/2015 – ongoing	**PhD Project** cooperating with Ivoclar Vivadent AG
07/2013 – 08/2013	**Project-Assistant**, TU Graz, Institute for Chemistry and Technology of Materials, *Topic of Research „Nanocomposite solar cells"* (Prof. Gregor Trimmel)
10/2013 – 12/2013	**Project-Assistant**, TU Graz, Institute of Chemical Engineering and Environmental Technology, *Topic of Research „DuraPEM - Stabilisierte aktive Platin-Übergangsmetallkatalysatoren für die Sauerstoffreduktion in Hochtemperatur-PEM-Brennstoffzellen"* (Prof. Viktor Hacker)

PUBLICATIONS

2017	Haas, Michael; **Radebner, Judith**; Winkler, Christoph; Fischer, Roland; Torvisco, Ana and Stueger, Harald*; Journal of Organometallic Chemistry* **2017**, 830, 131-140.
	Radebner, Judith; Leypold, Mario; Eibel, Anna; Maier, Janine; Schuh, Lukas; Torvisco, Ana; Fischer, Roland; Moszner, Norbert; Gescheidt, Georg; Stueger, Harald and Haas, Michael; *Organometallics* **2017**, 36, 3624-3632.
	Radebner, Judith; Eibel, Anna; Leypold, Mario; Gorsche, Christian; Schuh, Lukas; Fischer, Roland; Torvisco, Ana; Neshchadin, Dmytro; Geier, Roman; Moszner, Norbert; Liska, Robert; Gescheidt, Georg; Haas, Michael and Stueger, Harald, *Angewandte Chemie, International Edition* **2017**, 56, 3103-3107.
	Haas, Michael; Christopoulos, Viktor; **Radebner, Judith**; Holthausen, Michael; Lainer, Thomas; Schuh, Lukas; Fitzek, Harald; Kothleitner, Gerald; Torvisco, Ana; Fischer, Roland; Wunnicke, Odo; Stueger, Harald; *Angewandte Chemie, International Edition* **2017**, 56, 14071-14074.
2018	Eibel, Anna; **Radebner, Judith**; Haas, Michael; Fast, David E.; Freissmuth, Hilde; Stadler, Eduard; Faschauner, Paul; Torvisco, Ana; Lamparth, Iris; Moszner, Norbert; Stueger, Harald; Gescheidt, Georg; *Polymer Chemistry* **2018**, 9, 38-47.
	Moszner, Norbert; Fischer, Urs Karl; Lamparth, Iris; Faessler, Pascal; **Radebner, Judith**; Eibel, Anna; Haas, Michael; Gescheidt, Georg; Stueger, Harald; *Journal of Applied Polymer Science* **2018**, DOI: 10.1002/app.46115.
	Joeckle, Philipp; **Radebner, Judith**; Haas, Michael; Lamparth, Iris; Stueger, Harald; Moszner, Norbert; Unterreiner, Andreas-Neil; Barner-Kowollik, Christopher; *ACS Macro Letters* **2018**, 7, 132-136.
	Haas, Michael; **Radebner, Judith**; Eibel, Anna; Gescheidt, Georg; Stueger, Harald; *Chem. Eur. J.* **2018**, DOI: 10.1002/chem.201705567.

ADDITIONAL INFORMATION

Awards	**Paul Dufour Award** (RadTech Conference, 2017) **Start-Up Idea Competition** (Science Park Graz, 2017) **Houska-Preis** (B&C Industrieholding, 2018)
Languages	German (mother-tongue), English (C2), French and Italian (B1), Russian and Finnish (A2), Latin
Workshops/Seminars	**"**Exploitation strategies and market research to maximize success." with Lance Leverette, Feb. 2018
IT- Skills	ECDL, MS-Office, SciFinder, ChemOffice, SciDex CLAKS, VNMRJ, MestReNova/ MestReC
Interests and Hobbies	Travelling, Sports, Languages